Catalytic secondary methods for the removal of tar derived from biomass gasification: use of low-cost materials and study of the effect of sulfur species on the steam reforming activity of the catalysts

PhD candidate
Asbel David Hernandez

Supervisor
Marco Scarsella

SAPIENZA
UNIVERSITÀ DI ROMA

Abstract

Biomass gasification could potentially mitigate the actual dependency on fossil fuels. The practical application of this technology still faces many challenges to be considered a sustainable and profitable energy production source. One of the drawbacks of this technology is the production of undesirable by-products such as high molecular weight hydrocarbons collectively known as "tar" and sulfur compounds. These unwanted compounds must be removed before syngas end-use applications as they can foul pipes and reduced the performance of equipment downstream the gasifier as well as poison the catalyst used for upgrading the syngas. Catalytic steam reforming stands as an appealing tar removal technology in the small and medium sized gasification plants where heat management is crucial and recovery of the energy content within the tar compounds is desirable avoiding wastewater effluents and disposal of adsorbents. Nickel based catalysts have been the preferred choice in industrial applications for the reforming reactor. However, deactivation by carbon deposition is at present an unresolved problem which must be addressed before commercial application of biomass gasification technology. Moreover, the presence of sulfur compounds even at the low concentration found in most biomass feedstocks is deleterious for the steam reforming activity of the catalyst. This thesis comprises four experimental studies, each of them deal with a specific arguments of the hot gas cleanup technology of biomass syngas. The main focus was on the steam reforming activity of nickel-based catalyst and the effect of sulfur and the potassium-sulfur interactions on the steam reforming performance of the catalyst.

The main contributions from these studies are; 1) the development of a less time and energy consuming synthesis procedure for the production of a mayenite-supported nickel catalyst using low-cost precursors. This new method involves the addition of the nickel precursor during the mayenite synthesis procedure. Compared to the "wet impregnation" technique the developed method showed slightly lower toluene steam reforming activity but greater stability, which was ascribed to a higher carbon deposition tolerance. 2) Better understanding on the sulfur poisoning of catalysts under steam reforming conditions at

laboratory scale. The results evidenced that for a deeper knowledge of the sulfur poisoning, the calculation of the sulfur coverage should be more accurate and new methods for its measurement are required. 3) Comprehension of the mechanism of interaction between potassium and sulfur on a sulfur passivated commercial nickel catalyst under reforming conditions using real biomass syngas. The preferential adsorption site for sulfur and potassium was determined for the applied experimental conditions and catalyst and a mechanism involving the interaction of potassium with the sulfur chemisorbed on the active sites was proposed.

List of figures

List of tables

Table of contents

1 Setting the scene

Currently, roughly 80 % of the world total primary energy supply is from fossil fuel sources such as oil, natural gas and coal [1]. Concerns exist regarding access to adequate, affordable, and reliable energy supplies and accelerated rates of climate change caused by greenhouse gas emissions from fossil fuel combustion are driving interest in renewable energy sources such as solar, wind, biomass, and geothermal [2]. The transition from fossil fuels towards the integration of more and more renewable energy requires rethinking and redesigning the energy system both on the generation and consumption side [3]. This process requires alternative production chains of renewable substitutes, as well as combined actions such as changes in behavior, changes in vehicle technology and development of public transportation [4]. The purpose of introducing more and more renewable energy into the energy system is to save fuels, which in the short term are fossil fuels (and nuclear in some contexts). In the longer-term bioenergy will become the key concern, as biomass is a limited resource that cannot be expected to replace all fossil fuels used today, in other words, it is equally important to limit the use of energy by recycling, reusing and reducing wastes and using more efficient technologies [3]. Bioenergy can be converted from biomass via two main types of processes: thermochemical and biochemical/biological processes [5]. Generally, thermochemical processes have higher efficiencies and the superior ability to destroy most of the organic compounds. [5]. Regardless of the technology applied, biomass conversion to energy could provide a sustainable waste management practice [6].

Potential thermochemical processes to produce bioenergy are gasification and pyrolysis. Biomass gasification has attracted the most attention because it offers high carbon conversion efficiency and high flexibility in using different kind of feedstock materials as well as in the generation of different intermediate products for upgrading to high-value end products such as hydrogen and biofuels e.g. methanol, dimethyl ether, Fischer-Tropsch and synthetic natural gas (SNG) [7]. Globally, 52 countries have set targets and mandates for biofuels [8]. However, the commercialization of advanced biofuels have experienced

financing gaps due to high specific investment costs, uncertainty about the stability of policies and lack of knowhow in sourcing and conversion of biomass [8]. Regarding the conversion of biomass through the gasification technology, formation of heavy hydrocarbons (referred to as tar) and release of inorganic species such as potassium and sulfur represent the main obstacle for the efficiency and profitability of the process and it needs to be addressed. A promising way to mitigate tars is the catalytic reforming of the raw gas from the biomass gasifier at temperatures close to the former operating temperature, which allow a more efficient performance and the conversion of the tar species to useful permanent gases i.e. H_2, CO, CO_2 [9]. The presence of small amounts of sulfur in the biomass feedstock will negatively affect the performance of the catalyst in the reformer reactor, this effect has been known for many years and several countermeasures have been proposed such as promotion of the catalyst of changes in the operating conditions of the reformer [10]–[12]. Moreover, formation of carbon deposits on the catalyst surface along with the production of permanent gases during the reforming reactions can have detrimental consequences of the overall performance and profitability of the process [13].

Therefore, the need for a better understanding of the biomass tar reforming process focusing on the stability of the catalyst and its tolerance against sulfur and carbon formation is fundamental to improve the utilization of biomass and boosted the production of biofuels

1.1 Scope of the thesis

The scope of this thesis is the experimental study of secondary hot gas cleaning measurements, specifically, adsorption and conversion of high molecular aromatic species and the catalytic steam reforming of tar species produced from the gasification of biomass. Additionally, the impact of sulfur and K-S interaction on the steam reforming performance of the catalyst was assessed. The objective, problem, methodology and expected outcome are depicted in **Figure 1.1**

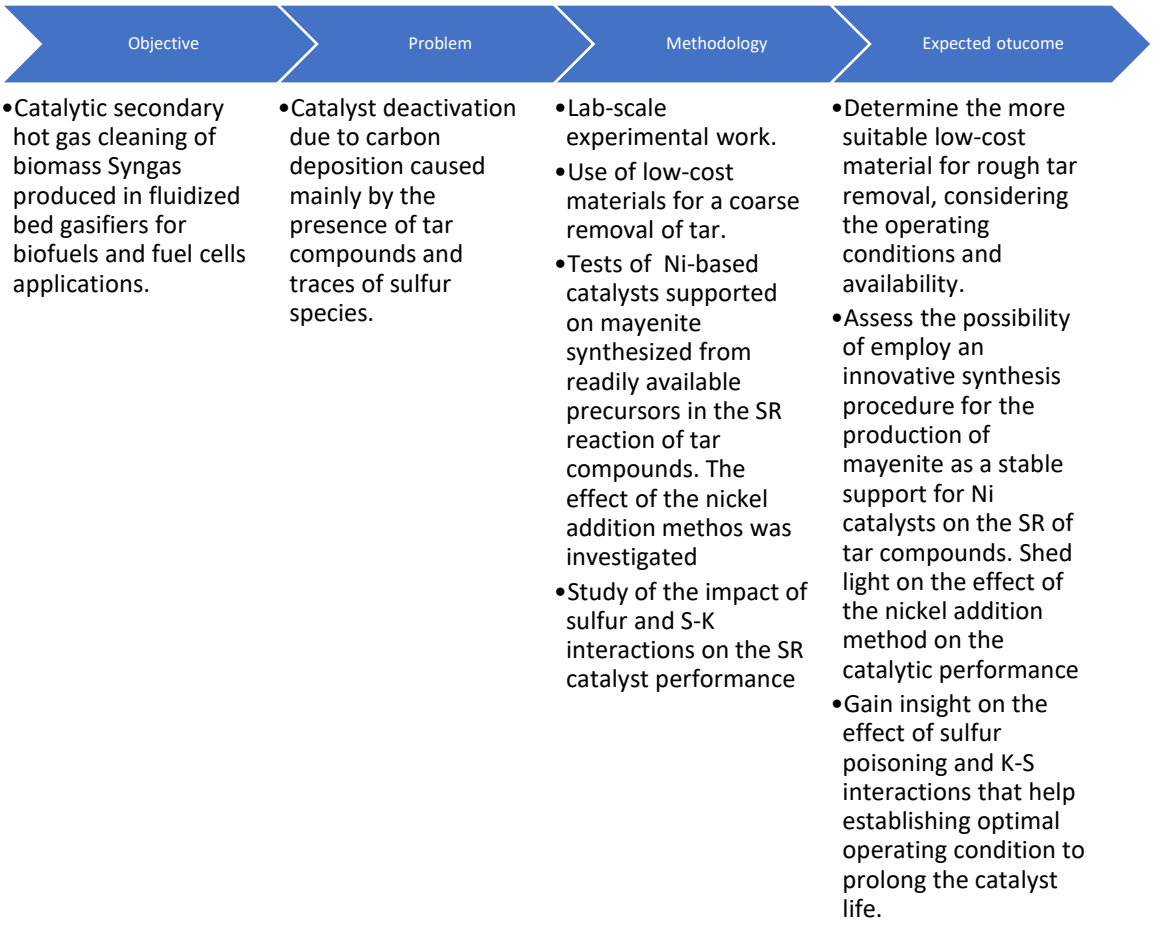

Figure 1.1 Objective, problem, methodology and expected outcome of the present study.

1.2 Summary of the experimental studies

The first study concerns the evaluation of different low-cost readily available materials for the initial coarse removal of tar that can be used as a guard bed to extend the life of the nickel catalyst in the downstream reformer. In this study the low-cost material tested namely char from olive residue, commercial activated carbon (Aquacarb 207 EA), γ-Al_2O_3 (Sigma Aldrich) and pumice stone (JT Baker), were exposed to the raw gas from the pyrolysis of olive residue. Measurements of H_2, CO, CO_2, CH_4 and dry gas volume along with gravimetric analysis of the unconverted tar after condensation were carried out to examined the removal performance of the materials. Evaluation of the extent of endothermic reaction occurring on the materials was indirectly performed by measuring the temperature at the middle of the bed. Deactivation of the materials tar removal capacity

was explored. The limitations of the experimental set-up were identified. A graphical abstract of this study is shown in **Figure 1.2 A**.

The second study of the thesis refers to the assessment of the activity and stability of different nickel-based catalysts on the steam reforming of toluene as model tar compound. The catalysts are constituted of nickel as the active metal supported of mayenite. It was shown in a previous work carried out in the same setup that Ni/mayenite [14] has high activity for the steam reforming of hydrocarbons as well a good stability towards the coke formation. Four nickel/mayenite catalysts were prepared starting from two methods consisting in the use of different precursors, namely boehmite + $CaNO_3$ and gibbsite + $Ca(OH)_2$. The effect of the Ni addition method was also evaluated, comparing wet impregnation on the mayenite and direct inclusion of nickel precursor during the mayenite synthesis. The as synthesized catalysts were evaluated based on activity and stability for the steam reforming of toluene. A simplified first order kinetic model was used to obtain the kinetic parameters. Characterization of the fresh and spent catalysts (XRD, BET, SEM/EDS and TGA) was conducted to examined structural and morphological properties of the materials and related them to the steam reforming activity results. **Figure 1.2 B** illustrates a graphical abstract of this study.

The third study of this thesis was conducted at VTT Technical Research Centre of Finland and deals with the sulfur poisoning of three catalysts, namely Ni/Al_2O_3, Ni/mayenite and Rh/Al_2O_3 on the steam reforming of benzene and methane present in a H_2-rich feed stream using H_2S concentrations typically found in syngas from biomass gasification. Sulfur poisoning of the catalyst on the benzene steam reforming reaction were carried out at the same temperature as in sulfur-free experiments and the effect of the temperature on the benzene conversion of the poisoned catalyst was closely related to the sulfur chemisorption equilibrium and free active sites since already at the lowest temperature investigated the benzene conversion was close to 100 %. Sulfur coverage (θ_s) was calculated and correlated with benzene conversion at different temperatures. Regeneration tests in a sulfur-free H_2-rich feed stream were performed. Water-gas shift poisoning, and regeneration was studied

as function of temperature in a hydrocarbon-free feed stream. The total sulfur capacity of the bed was calculated based on the H_2-chemisorption analysis and it was used to have a rough approximation for the timeframe of total deactivation of the bed.

The fourth study was carried out at KTH Royal Institute of Technology and was a follow up of a detailed experimental work started by Pouya H. Moud [15] on the investigation of the effect of dosing potassium in the gas phase on the reforming activity of a pre-sulfided commercial $Ni/MgAl_2O_4$ HT-25934 Haldor Topsoe A/S catalyst steam reforming activity. The feed was obtained from the gasification of pine pellets in an oxygen blown bubbling fluidized bed (BFB) gasifier. Before the reaction the catalyst and the support of support i.e. $MgAl_2O_4$ Haldor Topsoe A/S were mixed with an inert material and pre-treated in a sequence involving; reduction, ageing and sulfidation using a H_2S/H_2 ratio similar to the one present in the producer gas from the gasifier following the procedure developed by Pouya H. Moud [15]. Subsequently, the catalyst and support were exposed, simultaneously, to the producer gas and a KCl aqueous solution fed with an aerosol generator, during this period naphthalene was measured along with the non-condensable gases e.g. H_2, CO, CO_2, CH_4, C_2H_4 and N_2. Afterward, the catalyst and support were separated, and the reaction was carried out again for the catalyst and the support without the KCl addition. Characterization of the catalyst and support were conducted during all the phases of the experimental work. Based on the results a model of the interaction mechanism of potassium on the sulfided catalyst during the steam reforming reaction was proposed.

A graphical abstract of the third and four parts of the present study is presented in **Figure 1.2¡Error! No se encuentra el origen de la referencia. C** and **Figure 1.2 D.**

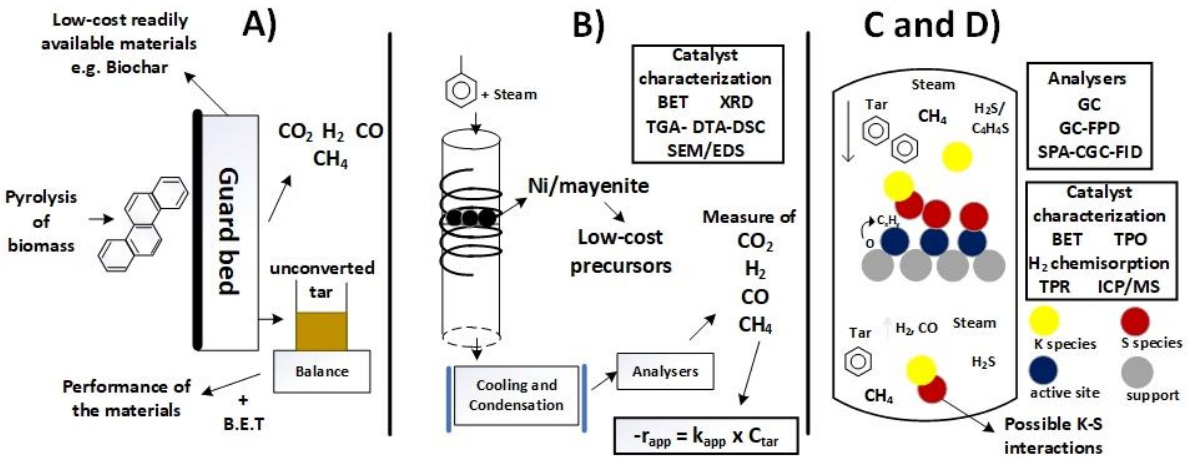

Figure 1.2 Scope of the thesis. A) Study of low-cost materials for the removal of tar. B) Evaluation of the activity and stability of Ni/mayenite catalysts synthesized from different precursors. C and D) Study of the sulfur poisoning of nickel and rhodium and the K-S interactions

In conclusion the general scope of the thesis is to a have a better understanding of the tar compounds removal and conversion at temperatures close to the exit temperature of state-of-the-art fluidized bed biomass gasifiers using catalytic steam reforming technologies, focusing on the role of sulfur and potassium-sulfur interactions on the steam reforming activity of nickel-based catalysts. The contribution of this work is an insightful study of the sulfur poisoning on the catalyst steam reforming performance under conditions i.e. concentrations and temperatures, similar as those encountered in real biomass producer-gas streams. Evaluation of the temperature effect of the sulfur poisoning was isolated from temperature effect on the steam reforming activity under sulfur-free conditions. Sulfur tolerance of the steam reforming and water-gas shift reaction were examined together to shed light on the extent of poisoning of both reactions under the same conditions. Moreover, the impact of gas-phase addition of potassium on an aged and sulfided commercial catalyst have been reported only by Pouya. Moud [16] before and a deep understanding thereof can have significant implications on commercial applications. The latter study forms the foundation for a detailed in-situ dynamic investigation of the potassium desorption kinetics from an aged and sulfided nickel catalyst under steam reforming conditions that will result in a clearer picture of the role of gas-phase potassium and therefore an accurate interpretation of the possible implications on commercial applications. Preferential adsorption sites for sulfur and potassium were examined. The role of the support and the

effect of gas-phase reactions caused by the presence of K species on the overall hydrocarbon conversion was evaluated.

1.3 Thesis outline

As described above the thesis consists of four experimental studies conducted during the three years of career. First an introduction part (chapter 2) is given to review the biomass gasification technology, focusing on the gas conditioning steps, the sulfur poisoning on nickel steam reforming catalyst and the effect of potassium addition of the catalyst as well as the sulfur-potassium interactions under steam reforming conditions. In chapter 3 a description of the experimental setup, materials, methodology as well as the data treatment is provided. This chapter is divided in four sections, each for every study. For the sake of readability and also considering the different arguments dealt on each study the results and discussion part of these studies is presented in dedicated chapters (from chapter 4 to 7). Finally, in chapter 8 final conclusions and recommendations are given based on the discussion of the results and also on the experience gained throughout the career.

2 Introduction

2.2 Biomass and biofuels

Biomass is contemporaneous (non-fossil) and complex biogenic organic–inorganic solid product generated by natural and anthropogenic (technogenic) processes, and comprises: (1) natural constituents originated from growing land- and water-based vegetation via photosynthesis or generated via animal and human food digestion; and (2) technogenic products derived via processing of the above natural constituents [17]. The general classification of biomass varieties as fuel resources can be divided preliminary and roughly into several groups, which are depicted in **Figure 2.1**

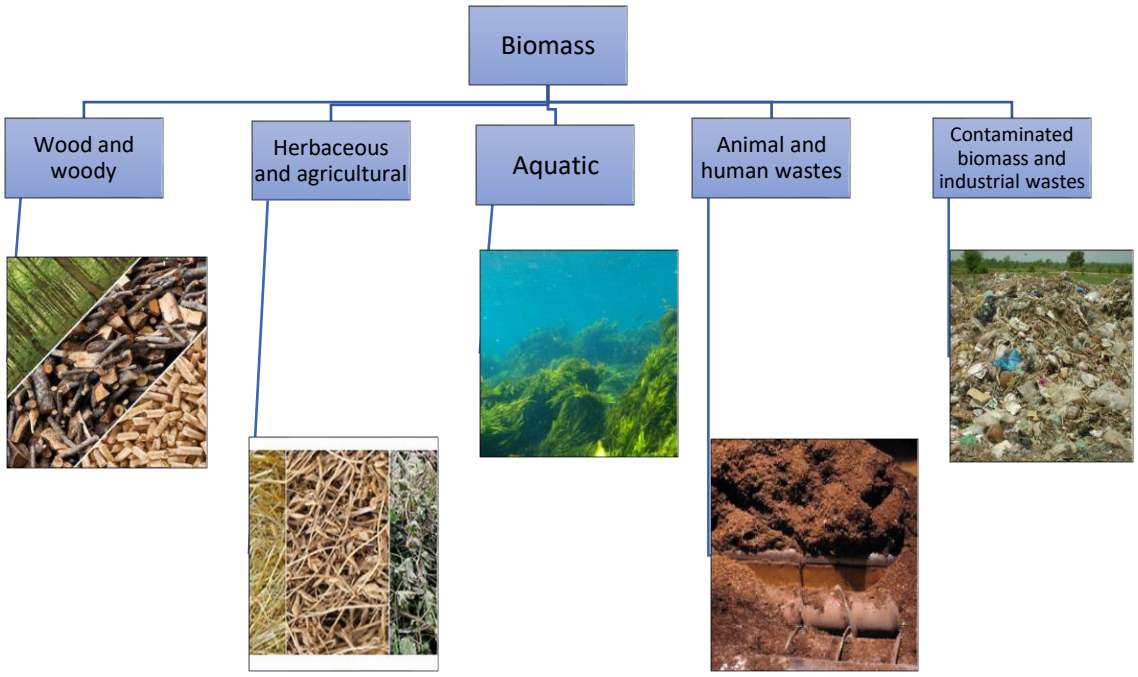

Figure 2.1 General classification of biomass varieties as solid fuel resources according to their biological diversity, source and origin. Adapted from [1].

Biomass fuels or biofuels are technogenic solid, liquid or gaseous fuels generated from natural biomass resources via some processing. Respectively, the bioenergy is the energy produced from biomass fuels [17].

Unfortunately, most of the biomass wastes is used very inefficiently with adverse impacts on public health, therefore, a significant longstanding need for improved bioenergy technologies in the developing world is needed. Recently, there has been renewed interest in the industrialized world in the potential for bioenergy to mitigate global climate change and for liquid biofuels to substitute for expensive imported oil [18].

In terms of biofuels technologies, the most important areas for research, in terms of sustainability, are those that enable the use of lignocellulosic as well as aquatic, animal-, human- and industrial-waste feedstocks i.e. second-generation biomass, and yield high-quality liquid fuels, such as bio-based hydrocarbons. However, the use of aquatic, animal-, human- and industrial-waste biomass feedstocks it is challenging due to the presence of high quantities of contaminants such as heavy metals, sulfur and alkali metals and volatile matter with respect to softwood.

The chemical composition of biomass is highly variable as determined by proximate, ultimate and particularly ash analyses. When the proximate and ultimate data are recalculated respectively on dry and dry ash-free basis, the characteristics show quite narrow ranges. This is due to the extremely high variations of moisture, bulk ash yield and different genetic types of inorganic matter in biomass [17]. In **¡Error! No se encuentra el origen de la referencia.** the proximate and ultimate analyses are presented for some types of biomass. It should be noted that the numbers listed in **¡Error! No se encuentra el origen de la referencia.** are average values, the standard deviation can be very large due to use of unsuitable scientific approaches, incomplete data or unusual and sometimes inappropriate terms that lead to inaccurate interpretations and misunderstandings about the biomass and biomass fuels [9], [17].

Table 2.1 Proximate and Ultimate analyses of biomass and coal [18]

Feedstock	Proximate analysis, wt. %				Ultimate analysis, wt. % (daf)					Net calorific value, MJ kg^{-1}
	Moisture	Ash, (dry)	FC (daf)	VM (daf)	C	H	N	S	O	
Black liquor	6.7	36.5	16.4	83.6	40.9	7.9	0.2	6.9	56.5	20
Softwood	4.7	1.7	25.7	74.3	53.4	5.8	0.4	0.03	40.3	18.4
MSW	6.1	16.8	12.7	87.3	59.2	9.8	2.2	0.3	28.5	22.5
Bituminous coal	3.0	9.6	62.1	37.9	82.0	5.3	1.4	0.4	10.9	31.2

In general, biomass has higher oxygen content and thus has a lower net calorific value than coal. In addition, the higher volatile matter content in biomass compare to coal translates in the formation of high quantities of organic condensable compounds under gasification conditions.

Improved policies, detailed cycle-assessments and techno-economic analysis and increased knowledge in technologies that permits the use of second-generation biomass to produce energy could render the gasification of biomass a sustainable and competitive way to produce electricity, heat, biofuels and biochemicals, in the short-to-middle term.

2.3 Biomass gasification for fuel cells and biofuel applications

The first step of the gasification of biomass is called *pyrolysis* and consists in the conversion of biomass by the action of heat in an inert atmosphere into char, gas and a liquid composed of a mixture of hundreds of oxygenated organic compounds [19]. According to the Waterloo mechanism the pyrolysis of biomass is most frequently considered as the superposition of three main primary mechanisms, namely char formation (dehydration), depolymerization and fragmentation [20]. The proportion of products formed is strongly dependent on the reaction temperature and time, and on the heating rate [21]. In general, low process

temperature e.g. 350 °C, and long vapor residence time increase the char yield, whereas high temperature e.g. 750 °C, and long residence time increase the gas yield. Moderate temperature e.g. 550 °C and short vapor residence time e.g. tenths of seconds, favors production of liquids.

Biomass gasification is a complex combination of pyrolysis and partial oxidation of carbonaceous materials in the condensed and vapor phases in the presence of an oxidizing agent that may be pure oxygen, steam, air or combinations of these [22]. The interest in biomass gasification arises from the fact that H_2 and CO carries more than 70 % of the energy stored in the biomass feedstock [23]. Historically, It appears that interest in gasification research correlates closely with the relative cost and availability of liquid and gaseous fossil fuels [24].

The result of the gasification is a fuel gas - the so-called syngas - consisting mainly of carbon monoxide (CO), hydrogen (H_2), carbon dioxide (CO_2), water vapor (H_2O), methane (CH_4), nitrogen (N_2) C_2 hydrocarbons in relatively low amounts and contaminants, such as carbon particles, tar and ash [24]. The original chemical composition of the biomass feedstock along with the design, gasifying agent and operating conditions of the gasification reactor determine the relative amounts of the by-products and contaminants in the raw gasifier gas [23]. The term "**tar**" does not have a generally accepted definition [22]. According to Devi et al [25], **Tar** *is a complex mixture of condensable hydrocarbons produced under thermal or partial oxidation regimes, comprising single-ring to 5-ring aromatic compounds plus other oxygen-containing hydrocarbons and complex polycyclic aromatic hydrocarbons (PAHs).*

The main chemical reactions taking place during the thermochemical conversion in a biomass gasifier can be summarized as follows [26]:

Pyrolysis process

$$\text{Biomass} \rightarrow \text{Char(C)} + \text{CO} + \text{CO}_2 + \text{H}_2\text{O} + \text{H}_2 + \text{tar} + \text{light hydrocarbons} \qquad \Delta H_r^0 < 0 \text{ at high heating rates [6]} \qquad \textbf{Eq. 2.1}$$

Oxidation process

$$C + \frac{1}{2}O_2 \rightarrow CO \qquad \Delta H_r^0 = -109\ KJ/mol \qquad \textbf{Eq. 2.2}$$

$$H_2 + \frac{1}{2}O_2 \rightarrow H_2O \qquad \Delta H_r^0 = -242\frac{KJ}{mol} \qquad \textbf{Eq. 2.3}$$

241 Reduction process

$$C + CO_2 \leftrightarrow 2CO \quad \text{(Reverse Boudouard)} \qquad \Delta H_r^0 = 172\ KJ/mol \qquad \textbf{Eq. 2.3}$$

$$C + H_2O \rightarrow CO + H_2 \quad \text{(Water gas reaction)} \qquad \Delta H_r^0 = 131\ KJ/mol \qquad \textbf{Eq. 2.4}$$

$$CH_4 + H_2O \rightarrow CO + 3H_2 \quad \text{(Steam reforming)} \qquad \Delta H_r^0 = 159\ KJ/mol \qquad \textbf{Eq. 2.5}$$

$$CO + H_2O \rightarrow CO_2 + H_2 \quad \text{(Water-gas shift)} \qquad \Delta H_r^0 = -42\ KJ/mol \qquad \textbf{Eq. 2.6}$$

$$CO + 3H_2 \rightarrow CH_4 + H_2O \quad \text{(Methanation)} \qquad \Delta H_r^0 = -206\ KJ/mol \qquad \textbf{Eq.2.7}$$

242

243 The application of biomass gasification technology strongly depends on syngas quality
244 requirements for the end-use application and economic factors such as intended production
245 scale and subsidies.

246 The schematic in **Figure 2.2** illustrates the different possible applicable processes in a
247 gasification system depending on fuel selected, gasification technology as well as
248 downstream application.

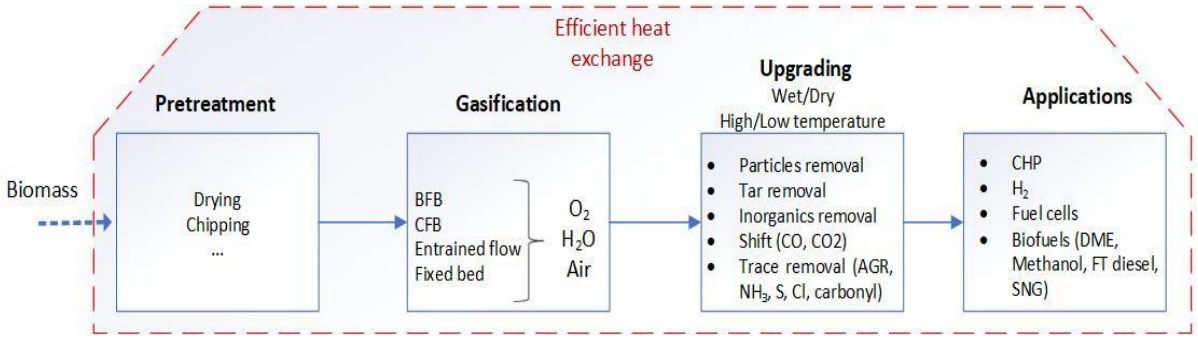

249

250 **Figure 2.2** Schematic of the different steps and processes included in a gasification system. Adapted from [3]

There are generally two gasification technologies suitable for production of high calorific syngas from biomass, either by using an entrained flow gasifier at a high temperature of 1300 °C, or using a fluidized bed gasifier together with a downstream catalytic reformer, both operating at around 900 °C [27]. The two technologies have different degree of maturity. Entrained flow gasifiers are a proven concept in case of coal as a fuel, but biomass is not suitable to be directly injected to the reactor and therefore pre-treatments, such as torrefaction or pyrolysis are needed. In case of fluidized bed gasification, the technology is developed and already demonstrated with biomass to produce heat and/or electricity [9]. Heat needed for the endothermic reactions may be supplied internally in the gasifier by controlled partial combustion as expressed in ¡Error! No se encuentra el origen de la referencia.. Heat can also be provided externally by superheated steam, heated bed materials or by burning some of the char or gases separately [27]. Examples of large-scale fluidized bed biomass gasifiers, which have demonstrated a prolonged period of operation and have been delivering a raw gas that has been conditioned into a pure synthesis gas, are the Repotec gasifier in Güssing, Austria, and the Andritz Carbona gasifier in Skive, Denmark. However, the lower gasification temperature in the fluidized bed case results in a syngas still containing significant amounts of tar that first needs to be removed or converted to syngas before additional gas conditioning, purification, and conversion to chemicals or fuels. If the tarry raw syngas is left untreated, condensation of tar at low temperatures i.e. 400 °C, may occur downstream the gasifier, leading to plugging and fouling issues [28]. Even at very low concentrations, tars in the syngas may result in coking of catalysts in downstream gas upgrading processes [29].

Figure 2.3 shows the transition as a function of process temperature from primary products to phenolic compounds to aromatic hydrocarbons. The description of process changes should be a function of reaction severity, which combines both temperature and time. Another important factor is the importance of gas-phase reactions leading to "tar" synthesis. Hydrocarbon chemistry, based on free radical processes, occurs in this thermal regime where olefins react to give aromatics. This process occurs while dehydration and decarbonylation reactions cause the transformations shown in **Figure 2.3**.

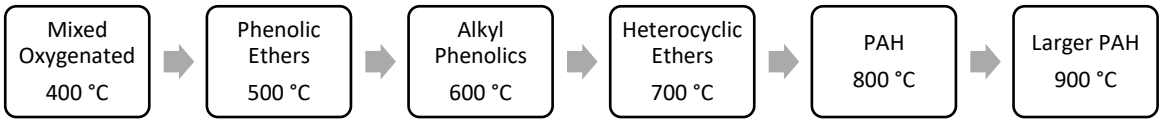

Figure 2.3 Tar maturation scheme. Adapted from [22]

In fluidized bed gasifiers air/oxygen/steam levitate the incoming particles which recirculate through the bed. Some of the oxidant contacts biomass and burns the tars as they are produced as in a downdraft gasifier; some of the oxidant contacts charcoal as in an updraft gasifier. Thus, the tar level is intermediate between updraft and downdraft i.e. -10-100 g Nm^{-3}, depending on the temperature, oxidizing agent, the point of introduction of feed, the thoroughness of circulation, the properties of bed material; the feed particle size distribution, the geometry of the bed and the tar analysis [22]. According to Baker et al. [30] the produced tar in an oxygen/steam atmospheric fluidized bed gasifier at 850 °C is almost completely aromatic and is not very soluble in water.

Generally, the H_2S concentration in the raw syngas, produced by gasification of most biomass fuels, is of the order of 100 ppm(v); with an exceptional case sulfur species of 2000 to 3000 ppm(v) are obtained from the gasification of the black liquor from pulp and paper manufacturing [31]. Even though the concentrations of sulfur species in product gas are quite low, for certain important applications a deep desulfurization is required to meet stringent standards. Moreover, alkali metals, primarily potassium and to a lesser extent sodium, are also present in the raw syngas. Alkali content in the biomass feedstock is both reactive and volatile. Some reactions of alkali with other ash components of biomass yield non-volatile compounds that remain as bottom ash in the gasifier [32]. However, some alkali compounds melt or even vaporize above 600 °C and can leave the reactor as aerosols and vapors, respectively. Alkali compounds transported out of the reactor, usually in the form of chlorides, hydroxides, and sulphates, can cause substantial fouling and corrosion in downstream processes [32]. Gas-phase K-species levels are ca. 0.01-53 ppm(w) (db) and have a complex dependence of particle size, temperature, bed additives, residence time and

the method used to carried out the measurement [8], [33], [34]. According to thermodynamic calculations [35], [36] the potassium species in the raw syngas from an air and steam blown gasifiers will be distributed between KOH, elemental K and KCl (in high-chlorine content feedstocks) in the temperature range 750-1000 °C

2.4 The dual fluidized bed gasifier (DFB)

The basic idea of the gasifier concept is to divide the fluidized bed into two zones, a gasification zone and a combustion zone [37]. Between these two zones a circulation loop of bed material is created and loop seals prevent gas leakage between the reactors [37], [38]. The circulating bed material acts as heat carrier from the combustion to the gasification zone. A dedicated chamber for the combustion and heating supply for the gasification reactions creates additional options for controlling the air-to-fuel ratio (ARF) for the heat-generating reactor without affecting the quality of the raw gas. In this manner, stable gas quality and high heating value of the gas are ensured [38]. In addition, by choosing a DFB configuration the economic burden of an air separation unit can be avoided, which is normally necessary for the production of a high heating value producer gas. This leads to a technology suitable for medium sized gasification plants and is therefore most suitable for biomass gasification profitable capacity [39]. Both bubbling and circulating fluidized bed are available and its selection should be done after an exhaustive thermoeconomic analysis. **Figure 2.4** shows the principle of the DFB steam gasification process [38]. The configuration and coupling between the chambers can be done in several ways e.g. co-current, counter-current, downflow, upflow etc. An innovative configuration was proposed by Murakami et al. [40] the setup comprise a bubbling fluidized bed (BFB) gasifier is coupled to a pneumatic transported riser (PTR) char combustor. The lower end of the PTR combustor is immersed into the particle bed (or particle bulk) of the BFB gasifier, and the riser itself is seated around the central vertical line of the BFB gasifier. To prevent intermixing of gases between the riser and gasifier, the gasifier had a specially designed bed structure, called reactor siphon [41].

The use of catalytic bed materials such as olivine [39], [42], [43], promoting char gasification, water-gas-shift and steam reforming reactions, and reduce the tar yield can simplify downstream cleaning methods. In this case the attrition of the material must be evaluated [44].

Through Aspen® simulations and practical considerations Murakami et al. [40] suggested that to achieved a cold gas efficiency higher than 75 % the water content of the feedstock should be ≤ 10 wt. %. Heat balance calculations lead Larsson et al. [38] to concluded that in order to increase the overall efficiency of the DFB system the internal heat demand should be decreased. To accomplish the latter, effective measures such as steam, fuel and combustion air preheating together with reduction in the amount of steam for fluidization were proposed [38].

A review done by Corella et al. [45] collected evidence to be less enthusiastic with the DFB technology. According to the authors [45] the low steam conversion ≤ 10 % and the frequent external supply of energy are the main constrains for the economic feasibility of the DFB technology. Furthermore, autothermal conditions were seldom reached using pilot-scale FBG, hence the use of external heater was mandatory thereby causing an efficiency penalty.

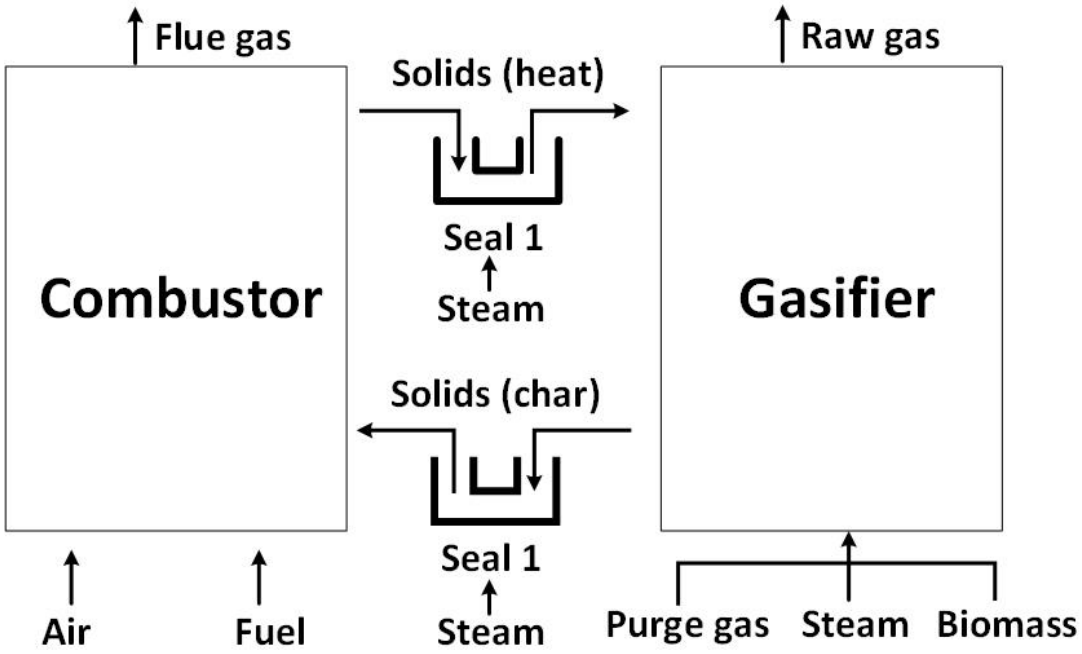

Figure 2.4 Schematic of a Dual Fluidized Bed (DFB) gasifier. Adapted from [38]

The dual fluidized bed gasifier (DFB)

The DFB technology is still the preferred choice for many practical and economic reasons. **Table 2.2** Compares some specifications, requirements and average values of tar present in the obtained syngas from the downdraft, updraft, entrained flow and the DFB gasifiers.

Table 2.2 Specifications and average values of tar of the main type of gasifiers [46], [47]

	Downdraft	Updraft	Entrained flow	DFB
Maximum fuel moisture (%)	25	60	≤ 15	11-25
Gas lower heating value LHV (MJ m^{-3})	4.5 – 5	5 – 6	4 – 6	5.6 – 6.3
Tar (g Nm^{-3})	0.02 – 3	30 – 150	0.01 - 4	0.2 - 2
Ash and particles in syngas	Low	High	Low	High
Process flexibility	Good turndown. Difficult to handle fast changes of fuels that differed in their calorific values	Limited turndown. Difficult to handle fast changes of fuels that differed in their calorific values	Limited turndown. Size and energy content of the feedstock must be in a narrow range	Turndown is limited by fluidization requirements.
Temperature profile	High gradients. Presence of hot-spots. Low degree of automation	High gradients. Presence of hot-spots. Low degree of automation	Flat profile. Special attention to the ash melting temperature is required	Flat profile. Reduced formation of hot-spots.

2.5 Formation of polycyclic aromatic hydrocarbons (PAH)

A comprehensive study conducted by Jarvis et al. [48] on the elucidation of biomass pyrolysis products using a laminar entrained flow reactor reported a convincing global mechanism for the formation of PAHs during gasification. The authors used white oak as biomass source. The temperature and residence time range studied was 450-950 °C and 0.2-1 s, respectively. Accordingly, pyrolysis vapors are produced from the biopolymers when the biomass is rapidly heated. Products from hemicellulose and lignin were observed at the lowest temperatures and thus those are likely the first products evolved during gasification. Cellulose products are evolved at a slightly higher temperature. The hemicellulose and cellulose products evolved over a small temperature range and are probable rapidly formed during gasification. Lignin, on the other hand, evolves over a longer temperature (and time) range. The carbohydrates readily crack into smaller molecular fragments such as furans, aldehydes, ketones, and acids, while forming hydrogen, carbon dioxide, and carbon monoxide. Eventually, these products further crack into hydrocarbons and radicals [48]. The formed hydrocarbons are then involved in reduction reactions, hence, the oxygen in these molecules is liberated as carbon dioxide and carbon monoxide. Likewise, the lignin products expel carbon dioxide and carbon monoxide to form less oxygenated and smaller molecular species and radicals. Finally, as the temperature (or the residence time) is increased (≤ 750 °C), the radicals and small molecules combine to produce aromatic compounds by molecular weight growth reactions similar to what is seen in sooting flames. Shukla and Koshi [49], [50] examined the efficiency of three growth mechanisms of PAH, namely, phenyl addition/cyclization (PAC), methyl addition/cyclization (MAC) and hydrogen abstraction/acetylene addition (HACA). The authors [49], [50] suggested that a collaboration of the three radical-neutral mechanism is useful for constructing a general mechanism capable of covering a wide range of combustion conditions. A schematic of the proposed model for PAH formation during gasification is illustrated in **Figure 2.5**.

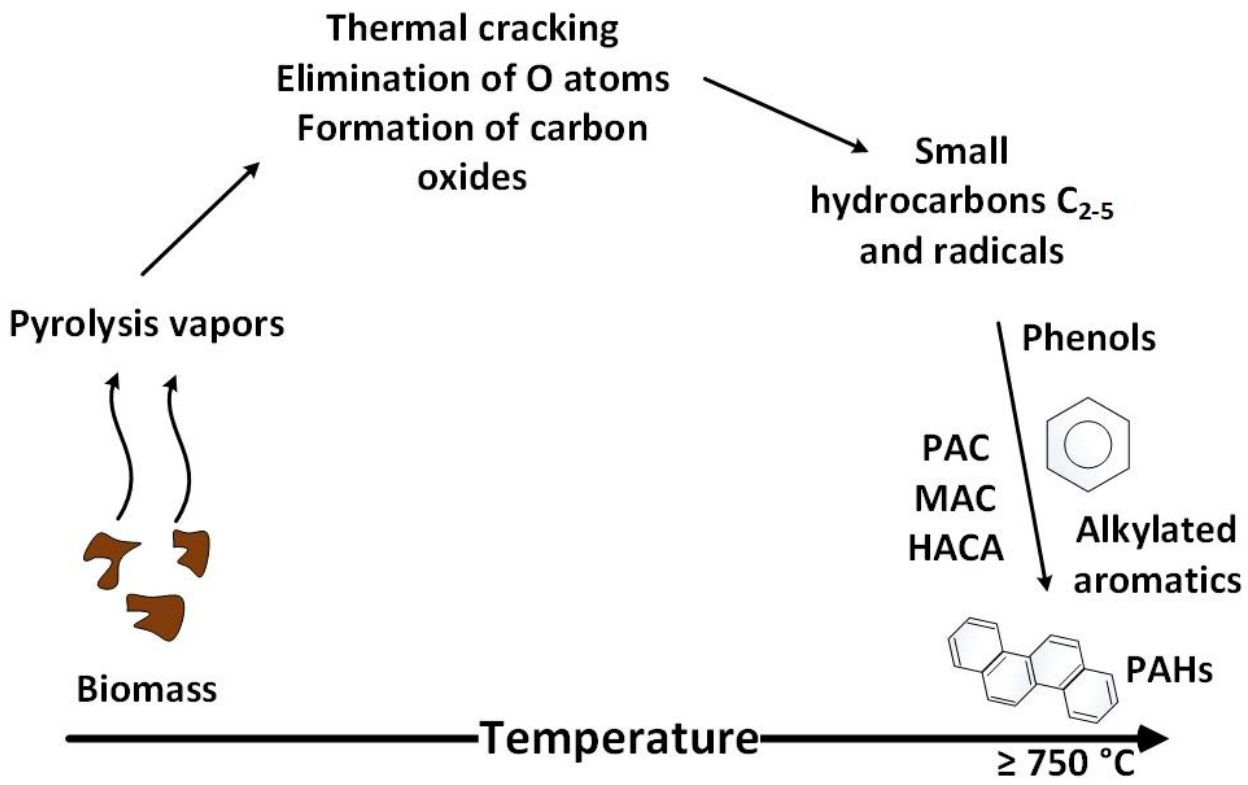

Figure 2.5 Schematic of the proposed model for PAH formation during gasification. Adapted from [48].

2.6 Syngas conditioning

Gas conditioning is a general term for removing the unwanted impurities from biomass gasification product gas and generally involves an integrated, multi-step approach that depends on the end use of the product gas [29]. Considering treatment systems for product gas cleaning and tar removal used in biomass gasification industrial plants, it can be observed that a combination of physical, thermal and catalytic technologies is usually required, not only to achieve high removal efficiencies of impurities, but also aiming to produce valuable gas by the catalytic transformation of tar into hydrogen and CO or any other high-added-value gaseous compound; this option could render a clean product gas, free of tar or at acceptable levels, with higher energetic content and consequently with higher economic profile. Although there are numerous laboratory studies and experimental developments for tar removal and reduction, only alternatives like oxidation reactors, electrostatic precipitators, bag filters, cyclones and scrubbers have been the technologies

401 frequently used in biomass gasification industrial plants, while thermal and catalytic
402 cracking reactors correspond to less commonly used alternatives for the same industrial
403 scale purpose [51]. Hence, it is evident that a better understanding of the technologies that
404 enable the simultaneous removal and transformation of tar and other impurities at
405 temperatures close to the exit temperature of the gasifier avoiding the accumulation and
406 treatment of liquid solvents is essential for the optimization and feasibility of medium-to-
407 large scale biomass gasification processes. A promising hot gas conditioning method
408 complying with the above features is the catalytic steam reforming [27], [29], [52], [53].

409 **¡Error! No se encuentra el origen de la referencia.** shows indicative syngas specifications
410 that have been adapted from Fischer-Tropsch and methanol catalysis processes. It must be
411 realized that there is an economic trade-off between gas cleaning and catalyst performance.
412 Cleaning well below the specifications as mentioned below, might be economically
413 attractive for synthesis processes that use sensitive and expensive catalytic materials [27].

414 **Table 2.3** Maximum allowable levels of impurities in syngas for chemical synthesis. Adapted from [27].

Impurity	Specification
$H_2S + COS + CS_2$	< 1 ppmv
NH_3 + HCN	< 1 ppmv
HCl + HBr + HF	< 10 ppbv
Na + K	< 10 ppbv
Particles (soot, ash)	"almost completely removed"
Tar	Not condensing: below dew point
Hetero organic components (incl. S, N, O)	< 1 ppmv

415

416 To achieve the stringent syngas quality requirements presented in **¡Error! No se encuentra**
417 **el origen de la referencia.**, primary mitigations, such as optimization of operational
418 conditions, catalytic bed materials or additives, combined with secondary hot gas cleaning
419 in the form of filtering of particulates, removal of impurities and catalytic cracking may be
420 needed [51].

In this section the focus will be on secondary hot gas cleaning techniques i.e. downstream of the gasifier, for particulate removal and tar mitigation. **Figure 2.6** illustrate a simplified schematic of the hot gas cleaning and conditioning process proposed by Kurkela et al. [54] (Hot gas filtration route) and an innovative and promising but still not proven technology proposed by Tuomi et al. [55] (High-T hot has filtration route) and studied by Pouya H. Moud [15].

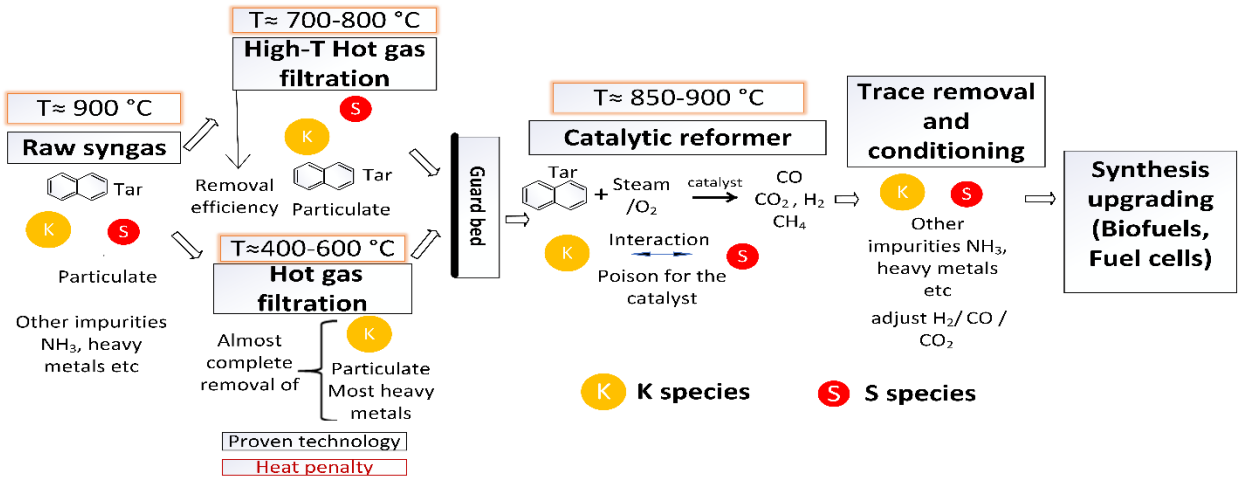

Figure 2.6 Simplified schematic of the hot gas cleaning and conditioning process for fuel cell and biofuels applications.

2.6.1 Hot gas filtration

Kurkela et al. [54] performed hot gas filtration experiments using a ceramic filter at 550 °C, a temperature high enough to avoid tar condensation in the dust cake or inside the filter pores which would lead to stickiness of dust and blocking of the filter pores. Higher temperatures were found to result in a rapidly increasing filter pressure drop caused by the thermal soot formation reactions of tars and ethene i.e. blinding effect, this effect was amplified when the dust content was low, and the concentration of heavy tars was high [54]. Stable and unproblematic filter operation i.e. dust concentration below the detection limit of 5 mg/m^{3}n, was achieved throughout a 215-hour test run, during which the filter elements were pulse cleaned at one hour intervals in order to remove dust cake from the candle filter surfaces [54]. According to the authors [54] fine calcined dolomite particles appeared to

441 protect the filter cake from sticky particles containing tar and soot. Moreover, potassium,
442 sodium and chorine species were completely removed in the hot filter unit.

443 Although, the economic benefits and process efficiency gain of elevating the filtration
444 temperature close to the gasifier temperature, around 800-900 °C have been acknowledged
445 the practical operation is challenging due to corrosion and material fatigue issues and only
446 few researcher have dealt with this topic [55], [56]. Simeone et al. [56] have performed
447 filtration tests at around 800 °C in steam-O_2 gasification conditions with different bed
448 material (magnesite, olivine) and biomass feedstock (wood, miscanthus, straw)
449 combinations. From the authors [56] results it can be deduce that the selection of bed
450 material/fuel combination plays an important role in filter performance as they influence
451 the gas quality, especially tars, and dust load in the gas as well as the carry-over of bed
452 material to the filter. Complete removal of alkali species is hardly feasible, especially with
453 high alkali content feedstock [56]. Furthermore, contradictory results about the removal of
454 heavy tars and formation of light tars and naphthalene during high temperature filtration
455 hot gas filtration [55] expose the need for improvements in this field.

456 It is important to mention that the gradual build-up of the cake on the filter can have a
457 complex sorption effects that influence the levels of impurities reaching downstream units
458 [54]–[56].

459 ### 2.6.2 The use of a guard bed before the catalytic reformer

460

461 The use of a guard bed before the catalytic reformer can increase the lifetime of the catalyst.
462 The most reactive and unstable species of the tar content in the raw syngas will removed or
463 converted to light (C_{1-2}) hydrocarbons, H_2, carbon oxides and more stable, usually aromatic
464 compounds with 1-3 rings e.g. benzene and naphthalene.

465 The use of low-cost materials as well as by-products of the gasification/pyrolysis process
466 will benefit the overall efficiency and profit of the biomass to biofuels or fuel cell technology.
467 In this regard, the use of char (biochar) derived from biomass pyrolysis/gasification as a tar
468 removal in a guard bed is considered a promising alternative [57]–[62]. Compared with

other catalysts, the biochar catalysts would be simply gasified to recover energy from char after deactivation. However, at the temperatures used in the hot cleaning gas technology biochar could be consumed by steam or CO_2 in the producer gas, to address this problem continuous external char supply is needed (or withdrawal depending on the balance of char consumption and production in the gasification system) [62]. Additionally, by using this approach the biochar properties can neither be fixed nor tailored because they depend on biomass feedstock and process conditions.

Matsuhara et al. [60] carried out experiments to study the in-situ reforming of tar over char from the rapid pyrolysis of a brown coal: they concluded that tar was reformed in a sequence of coking and steam gasification of the coke rather than for direct steam reforming over the char, furthermore, they reported that in order to have a negative coke yield due to faster progress of coke/char gasification with respect to coke deposition, the reforming should be carried out at 900°C. Moreover, the authors state that the specific surface area and pore volume of the char were not straightforwardly related to its tar reforming activity.

According to Shen. Y [63] the surface area and functional group content of biochar are key factors in determining the tar removal capacity of this material. High surface area and the presence of -OH, C-O and C=O groups are required features on a biochar to have enhanced tar removal [64]. Illustrated in **Figure 2.7**. is a simplified scheme of the mechanism of tar removal over a carbonaceous surface. The tar compounds initially meet a fresh char with a certain number of active sites distributed over the surface. The tar is adsorbed on the char matrix and undergoes polymerization reactions, producing hydrogen and soot, the latter staying over the char surface as solid deposits. This soot blocks the active sites, hindering the interaction of the active sites with the gaseous tar. If the carbon deposition rate is higher than the carbon consumption rate, soot accumulation over the surface will occur, decreasing the number of active sites available for reaction with tar molecules and then the biochar activity. The active sites could be attributed to the presence of alkali and alkaline earth metallic species in the fresh biochar, since these species are known to be active during steam gasification of soot generated after tar deposition on biochar surfaces [63], [65].

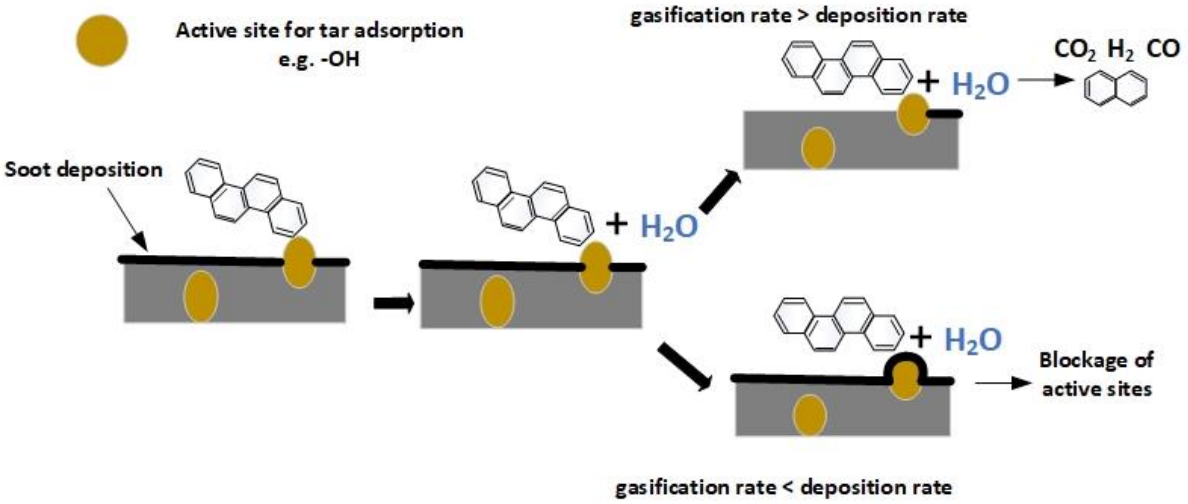

Figure 2.7 Mechanism of tar removal over a carbonaceous surface. Adapted from [63].

Narváez et al. [66] used dolomite as a tar cracking material in a guard bed downstream of an air-blown bubbling fluidized bed gasifier to protect the catalyst in the subsequent reformer. The authors obtained a tar reduction of ca. 90 % and the activity and stability of the catalytic was increased.

Biomass pyrolysis and gasification in a fluidized bed of porous alumina particles was conducted by Matsuoka et al. [67], the alumina particles showed a very promising ability to capture the formed tar. Furthermore, the yield of H_2 in the case of alumina was slightly increased by the presence of steam at 973 K, the authors ascribed this result to the reforming of the coke deposited on the surface of the alumina. Similar results were obtained by Erkiaga et al. [68] using γ-alumina and olivine as a primary catalyst in the steam gasification of biomass in a conical spouted bed reactor, the higher H_2 and CO concentration obtained with alumina was related to the acid sites on the γ-alumina.

Mun et al. [69] studied the tar reduction performance of a commercial activated carbon in a two-stage air gasifier using sewage sludge as feedstock. The authors achieved a 6-fold reduction in the tar amount as well a considerable increased in H_2 concentration.

An interesting material but surprisingly not tested yet on the tar removal at high temperatures is the pumice stone. Pumice is a light, porous, volcanic stone with a large surface area. It is easily and cheaply found in nature or some kinds of waste. This volcanic

stone is commonly pale in color, ranging from white, cream, blue, or grey, to green-brown or black. It is formed when volcanic gases exsolving from viscous magma nucleate bubbles, which cannot readily decouple from the viscous magma prior to chilling to glass [70]. Pumice particles, resembling a sponge, consist of a network of irregular or oval shape internal voids/pores or vesicles, some of which are interconnected and open to the external surface, while others are isolated inside the particle. Moreover, since most internal pores, especially micropores, are not connected pumice has a low permeability, providing very high isolation for heat and sound. Additionally, pumice can exhibit acidic or basic character and has a high silica content (60–75 %) [71]. Pumice stone has been tested and used in various environmental applications mainly as an adsorbent, filtration media, biofilm or catalyst support, similar to the uses of sand [70]–[76].

2.6.3 Catalytic tar reforming

The catalytic tar reforming process involves oxidation of the tar components using steam/CO_2/O_2 to produce hydrogen and carbon oxides and it is usually carried out with supported transition metal (group VIII) catalysts at temperatures of between 650 and 900 °C [77]. The reactions, which are highly endothermic can be described as follows [51]:

$$C_nH_m + nH_2O \rightarrow nCO + \left(n + \frac{m}{2}\right)H_2 \quad \text{(Steam reforming)} \qquad \Delta H > 0 \qquad \textbf{Eq. 2.8}$$

$$C_nH_m + nCO_2 \rightarrow nCO + \left(\frac{m}{2}\right)H_2 \quad \text{(Dry reforming)} \qquad \Delta H > 0 \qquad \textbf{Eq. 2.9}$$

The chemistry involved in catalytic tar decomposition of producer gas is a complex mix of hydrocarbon decomposition and equilibrium reactions [51]. In fact, along with the steam and dry reforming reactions **Eq. 2.6** and **Eq.2.7** occur concurrently in the catalytic reformer. The extent of the reactions taken place in the reformer are dependent on the operating conditions.

It is assumed that the mechanism for the steam reforming of hydrocarbons involves the chemisorption of the hydrocarbons on a dual site followed by successive α-scission of the

carbon-carbon bonds. The resulting C_1-species react at the interface of the metal and support with adsorbed oxygen species adsorbed on the support or on the metal forming carbon oxides and H_2 [78].

According to Bartolomew et al. [79] the composition of heterogeneous catalysts can be divided into three primary components: (1) an active catalytic phase or metal, (2) a promoter, which increases activity and/or stability, and (3) a high surface area support that facilitates dispersion of the active phase. The catalyst properties are dictated by the severe operating conditions, including temperatures of 450-950°C and steam partial pressures of up to 30 bar [80]. Therefore, chemical and mechanical stability are two fundamental features of a tar reforming catalyst.

The main limitation for hot gas catalytic tar cracking is catalyst deactivation. Deactivation occurs from both physical and chemical processes associated with the harsh reaction conditions and impurities in the feed stream. Attrition, coking, sintering and sulfur poisoning are the primary deactivation mechanisms that affect the efficient catalytic conditioning of biomass-derived syngas, although the cumulative effects of the other trace inorganic species that are present in biomass (e.g., Si, Al, Ti, Fe, Ca, Mg, Na, K, P, S, and Cl) must also be considered [81].

2.6.4 Steam reforming of tar compounds using nickel-based catalysts

Among the transition metals (group VIII), nickel is the most widely used in the industry for steam and dry reforming reactions. An excellent trade-off of commercial availability, relatively low costs and high activity are the reasons behind the preferential use of this metal among other transition metals [23], [29], [62], [82].

A detailed DFT study conducted by Bengaard et al [83] on the steam reforming of methane on two different nickel surfaces namely Ni(111) and Ni (211) provided a consistent picture of the process. The authors [83] concluded that the steam reforming reaction on nickel catalysts is structure sensitive and certain step sites are considerable more reactive than close-packed facets. Moreover, all intermediates were also much more strongly bound at

570 the steps than on the terrace [83]. Therefore, on a supported nickel catalyst it is possible to
571 have (at least) two different reaction channels, one with a low activation barrier, which is
572 associated with steps, and another associated with terraces. The latter channel is
573 characterized by a higher barrier, but there will be freer active sites in this channel, both
574 because there will usually be more terrace sites than step sites and because the coverage
575 with intermediates is smaller on the terrace sites [80]. This statement is in agreement with
576 the universality in heterogeneous catalysis which state that the optimum catalyst is one in
577 which activation energy and heats of adsorption form a carefully balanced compromise [84].

578 The main challenges of nickel catalysts in steam reforming that negatively affect the activity
579 and stability have been recognized to be sulfur poisoning, coke formation and sintering, all
580 of which are interconnected are represent the principal hindrance for the commercialization
581 of the biomass to fuel cells an biofuels technology [85], [86].

582 ***Coke formation****:* Coke forms may vary from high molecular weight hydrocarbons to
583 primarily carbons such as graphite, depending upon the conditions under which the coke
584 was formed and aged [87]. According to Menon [88] and Bartholomew [87] the structure,
585 location and mechanism of formation of coke are more important than its quantity in
586 affecting catalytic activity. Carbon may (1) chemisorb strongly as a monolayer or physically
587 adsorb in multilayers and in either case block access of reactants to metal surface sites, (2)
588 totally encapsulate a metal particle and thereby completely deactivate that particle, and (3)
589 plug micro- and mesopores such that access of reactants is denied to many crystallites inside
590 these pores. Finally, in extreme cases, strong carbon filaments may build up in pores to the
591 extent that they stress and fracture the support material, ultimately causing the
592 disintegration of catalyst pellets and plugging of reactor voids [87]. The latter case is referred
593 as whisker carbon and under steam reforming condition is one of the most destructive type
594 of carbon. The bond strength of carbon to the metals is a crucial factor which determines
595 whether the coverages of carbon are enough for nucleation of graphene. In addition, the use
596 of catalysts with small metal particle size (high dispersion) tend to decrease the carbon
597 deposition on the catalysts [89].

The risk for coke formation is increased by high adsorption rates on the surface of the active metal, as for alkenes, and low hydrocracking rates as in the case of aromatics. On the other hand, a strong adsorption and/or an enhanced dissociation of steam on the catalyst will depress the coke formation [90]. Another measure for limiting/retarding the coke formation is the addition of H_2 which reduce the formation of olefin intermediates [91]. Nonetheless, there is a balance between the coke retarding effect of hydrogen and the increased rate for hydrocracking with low molecular hydrocarbon products as a result of a high hydrogen partial pressure [91]

The coke build-up will affect not only the activity of the catalysts but also the overall performance and efficiency of the reformer reactor. For instance, coke formation from pyrolysis of hydrocarbons at temperatures ≥ 650 °C results in dense polyaromatic deposits on the tube walls which causes poor heat transfer of the latter [91]. The problem could be even worse in the case of high alloy steel tubes which are susceptible to carburization due to pyrolytic coke deposited on the its surface [91], [92].

2.6.5 Role of the support and metal-support interactions

To withstand the harsh environment at which tar reforming catalysts are exposed, most industrial catalysts for tubular reforming are based on ceramic oxides or oxides stabilized by a hydraulic cement. Typical ceramic supports are α-alumina, magnesia, magnesium aluminum spinel, and zirconia fired at temperatures well above 1270 K [80].

Many efforts for suppressing coke formation on nickel catalysts have been undertaken, from those studies it has been showed that the use of thermal-stable supports featuring high amount of “free” oxygen species related to the presence of hydroxide, peroxide and superoxide radicals can enhance the resistance of coke of nickel catalysts [93]–[95]. The effectiveness of the use of this kind of supports depend upon the so-called strong metal support interactions (SMSI) in which the metal surface is partially covered by reduced moieties of the support or promoter. This covering effect can significantly influence chemisorption and reaction properties of the metal catalyst [96]. In addition, the SMSI could

potentially minimize the sintering of the metal particles, an anchoring effect of support-O-M (M for metal) has been proposed [97] to suppress or decrease the sintering of the metal. In this context, mayenite have been identified as a thermal-mechanical stable support which at high temperatures i.e. 700 °C, shows a high mobility of oxygen species capable of interacting the carbon species adsorbed on the nickel active sites [98]–[100].

Mayenite consists of an aluminate framework with a heavily disordered extra-framework comprised by oxygen and calcium [101]. It has a unique cubic crystal structure composed of 3-dimensionally connected sub-nanometer-sized cages with 2 out of 12 cages are statistically occupied by O^{2-} and O^{-} ions to compensate the positive charge of the cage framework having the chemical composition of $[Ca_{24}Al_{28}O_{64}]^{4+}$ [102]. These anions feature a nearly free mobility within the cage. Boysen et al. [101] carried out a high-temperature neutron powder diffraction study and concluded that at high temperatures (≥ 973 K) the density of the "free" oxygen is extremely spread out and its diffusion within the mayenite structure proceeds *via* a jump-like process involving exchange of the "free" oxygen with framework oxygen. Based on these findings it is believed that during the steam reforming reaction the "free" oxygen in the cages will transfer to nickel site to gasify the surface carbon on nickel metal to CO, thus reducing the carbon deposition on the nickel active sites [93]. Furthermore, Li et al. [93] demonstrated that mayenite can adsorb sulfur, hence, it could protect the active nickel during the steam reforming in the presence of sulfur compounds. However, upon hydration immobilization of oxygen interstitial due to hydroxide formation and thereby decrease in the ionic conductivity was observed [103], [104]. In addition conversion from a solid electrolyte to an electride was noticed when the oxygen activity was zero (reducing conditions) [103]. A simplified scheme of the possible path of the steam reforming reaction of a metal supported on mayenite in illustrate in **Figure 2.8**.

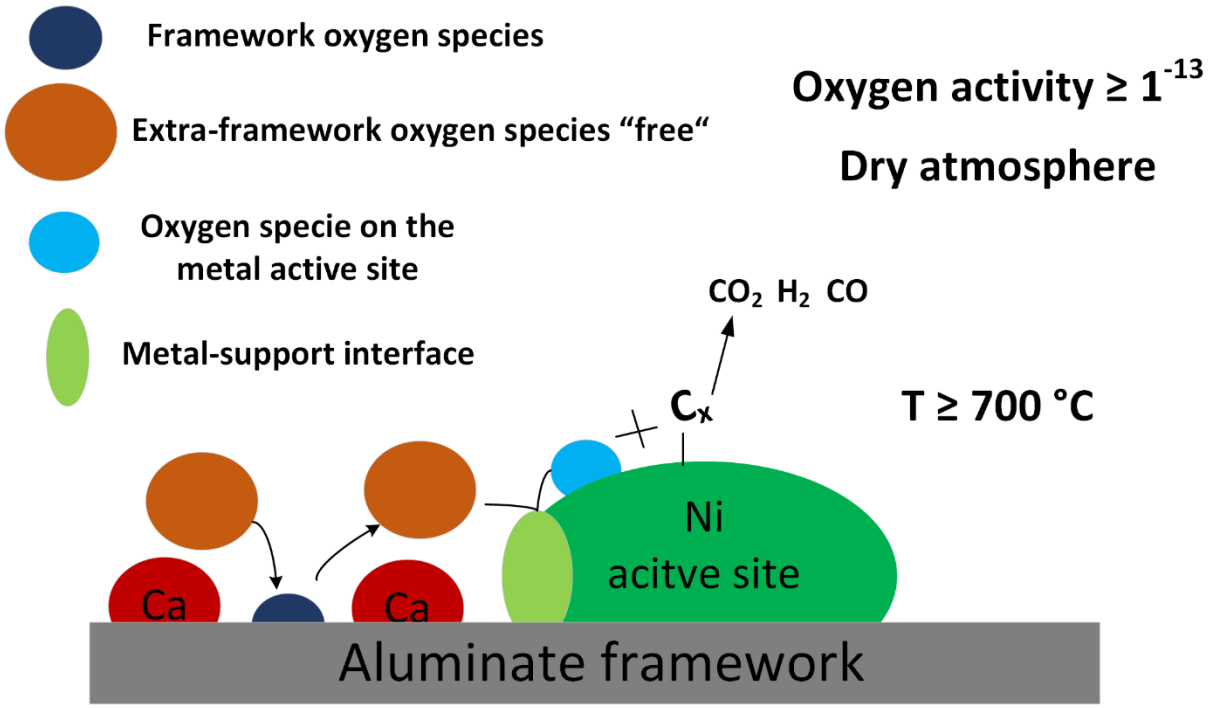

Figure 2.8 Simplified scheme of the possible path of the steam reforming reaction of a metal supported on mayenite according to [101], [93] and [103].

2.7 Poisoning of nickel steam reforming catalyst by sulfur species

Sulfur poisoning is considered the most severe poison for nickel catalysts used in steam reforming of hydrocarbons [105]. Despite the lower sulfur concentration present in the raw syngas produced from the gasification of some biomass feedstocks compared to the sulfur present in coal, the sulfur poisoning problem is still significant due to the strong bonding of the sulfur to nickel and the high isosteric heat of adsorption, at low sulfur concentrations, which was calculated to be ca. 40 kJ/mol energetically more stable than the bulk Ni_3S_2 [106].

In the context of hot cleaning technologies for gas condition the sulfur poisoning problem on the nickel catalysts in the reformer will commonly happen because the lack of a robust and completely reliable technology for sulfur capture/removal at temperatures ≥ 600 °C [31].

The poisoning effect of sulfur involves covalent bonding between S and the Ni surface accompanied by a small transfer of electronic charge towards the S atoms (site blocking and deactivation of the surface) as well as direct interactions between S and adjacent molecules e.g. reactants [107]. The sulfur surface overlayer causes a significant reduction in the

emission of the Ni d-bands [108], hence, it reduces the interaction of the metal with other species [109].

The interaction of H_2S with nickel surfaces involves a number of steps including molecular adsorption, dissociative chemisorption, surface diffusion and reconstruction of the sulfur adlayer into a two-dimensional nickel/sulfur compound [110]. Moreover, the structure and stoichiometry of sulfur adsorbed on nickel are complex functions of temperature, H_2S concentration, sulfur coverage and pretreatment, phenomena that account at least in part for the complex nature of nickel poisoning by sulfur [87].

Eq. 2.10 represents the exothermic and reversible sulfur chemisorption reaction on transition and noble metals.

$$nH_2S(g) + \text{Metal Surface} \leftrightarrow nH_2(g) + nS - \text{Metal Surface(a)} \qquad \textbf{Eq. 2.10}$$

Due to the exothermic nature of this reaction an increment of the temperature of the catalyst will shift the chemisorption equilibrium to the left-hand side of **Eq. 2.10¡Error! No se encuentra el origen de la referencia.** and from a thermodynamic point of view, it is possible to regenerate or avoid the poisoning effect of sulfur on the catalyst by increasing the temperature. This approach has been adopted in many studies dealing with H_2S poisoning of active metal for the steam reforming reactions[111]–[113]. Conclusions about the regenerabilty of the active sites of the catalyst on lab-scale reactors by increasing the temperature cannot be straightforward extrapolated to industrial-scale processes due to diffusion restrictions[12]. According to Rostrup-nielsen [105] a significant radial gradient of sulfur is present in the catalysts used in industrial tubular reformers, on the other hand, no front of sulfur moving through the bed i.e. no axial sulfur gradient, was found.

In an effort to improve the efficiency of a steam reformer by reducing the amount of steam without affecting the catalyst's stability, which will be threat due to deactivation by coke formation, Rostrup-nielsen [114] studied the steam methane reforming activity and carbon formation of a sulfur-passivated nickel catalyst. The author [114] found that above a certain sulfur coverage threshold (ca. 70 %) the rate of methane steam reforming is less affected than the rate of whisker carbon formation. The effects were explained by assuming that a

large ensemble of active sites is involved in the nucleation of whisker carbon whereas the reforming reaction can proceed on the small ensembles left at high (but not complete) sulfur coverage. The ensemble requirement was defined as the minimum required number of contiguous surface atoms of the element able to form bonds with the end adsorbate [115]. The results were developed into an industrial practice called SPARG [105].

An alternative explanation for why sulfur passivation retards whisker carbon formation was presented by Bengaard et al. [116] and Helveg et al. [89] using DFT calculations. Both research groups concluded that step sites act as preferential growth centers for graphene and also sulfur binds preferentially on these sites, hence, the passivated effect involves the blockage of step sites for nucleation of carbon, while the steam reforming reaction can proceed at the terrace sites, which are known to be less active but represents the vast majority of sites in the catalysts and at high temperatures e.g. 900 °C may controlled the rate of the steam reforming reaction [116]. It should be pointed out, that the presence of pyrolytic carbon can still deactivate the sulfur-passivated catalyst.

From the beginning of the 70's to the mid-80's an extensive research on the sulfur poisoning of the metals commonly use as reforming and/or methanation catalyst, with a particular focus on nickel, was performed prompted by the commercial impact of catalytic processes involving sour petroleum feedstocks and coal -derived synthesis gas which contain significant concentrations of H_2S and organic sulfides [117]. Exhaustive experimental studies conducted by two important research groups, namely the group led by Bartholomew C.H and the group led by Rostrup-Nielsen J.R, combined with surface science studies of well-defined metal structures [108], [118]–[121] established the basis for the most suited experimental procedure for the sulfur poisoning studies, the interaction of sulfur with the metal surface and equations for the calculation of sulfur surface coverage for nickel catalysts and the free nickel active sites of a sulfur poisoned nickel catalyst [122], [123]. Rostrup-Nielsen [105] proposed to deal the poisoning of catalysts by separating the effects into three groups i.e. the influence on the intrinsic activity, on the activity of the single pellet, and on the performance of the whole reactor. Bartholomew's group focused on the intrinsic

723 activity effect of the sulfur poisoning using a gradientless quartz continuous-flow stirred-
724 tank reactor [124] while Rostrup-Nielsen's group concentrated on the performance of the
725 whole reactor, therefore, they stated that the rate of poisoning should be evaluated in terms
726 of fixed bed adsorption whereas poisoning models neglecting the pore diffusion are of less
727 relevance for industrial conditions [105].Evidently, the study of the influence of sulfur
728 compounds on the intrinsic activity of the catalyst requires Bartholomew's research group
729 approach and together with surface science and DFT studies a significant improvement on
730 the sulfur tolerance of the catalysts can be achieved. Moreover, the use of catalysts with
731 improved sulfur tolerance and stability will translate in lower operation temperatures in the
732 steam reformer with long term benefits in the reformer life and in the profitability of the
733 process [90].

734 A summary of the different aspects involved in the study of the effect of sulfur poisoning
735 on steam reforming nickel-based catalysts is illustrated in **Figure** . It is important to mention,
736 that the sulfur-passivated technology is dynamic and as the sulfur chemisorption will
737 depend on the temperature and the P_{H2s}/P_{H2} ratio on the particles.

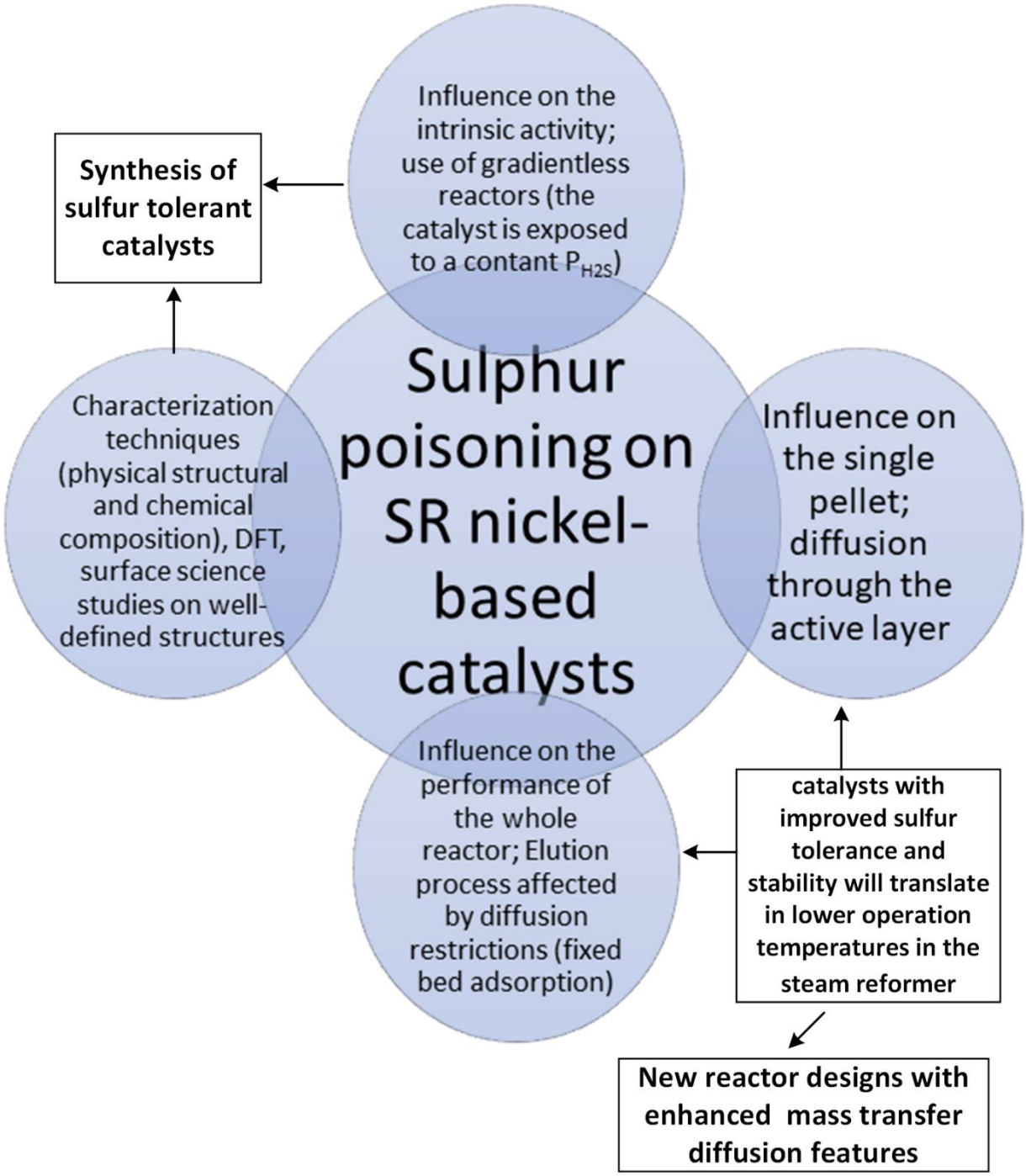

738

739 **Figure 2.9** A summary of the different aspects involved in the study of the effect of sulfur poisoning on steam reforming
740 nickel-based catalysts.

741

742

2.8 Potassium interaction with nickel-based steam reforming catalysts

Potassium is considered an electronic promotor and thus it could potentially enhance the catalyst activity by modifying its surface [84]. Generally, K becomes strongly polarized when adsorbed on the surface, setting up a dipole field on the surface that will interact with other adsorbates and may, for example, help in dissociation and adsorption of other adsorbates, but only if the latter have an opposite dipole field in the transition state such as methane on Ni(100) [125], since this will lower the activation energy [84].

The electron donor nature of potassium is believed to be the reason for the enhanced chemisorption of electron acceptor species such as carbon monoxide and oxygen on the metal active sites and also on the supports [126].

Hadden et al. [127] observed a reduced accumulation of coke on the surface on an K-impregnated (5 wt. %) Ni/Al_2O_3 compared to the undoped catalyst using temperature programmed reaction analyses of propane as well as TPD of the formed coke. The temperature range studied was 100-500 °C. A decreasing rate of hydrocarbon decomposition together with an increasing of the rate of steam gasification of filamentary carbon from the catalysts were obtained with the alkali-promoted catalyst. Moreover, increased molecular water surface coverage was found on the $K\text{-}Ni/Al_2O_3$ catalyst. However, decomposition of water on the surface of the alkali doped catalyst was deemed to require more energy compared to the unpromoted one.

Even in the absence of a nickel-base catalyst the impregnation of wood with K_2CO_3 significantly reduced the tar production after gasification of the biomass, although it was not possible to determine if its catalytic effect is related to primary reaction steps or secondary reactions of the initial products [128]. The same researcher group also observed that the impregnated alkali carbonates behaved also as water-gas shift catalysts with higher activity than the nickel catalyst used in a secondary fluidized bed reactor [129].

Commonly, potassium is introduced to supported nickel catalysts in the form of aqueous solution of KOH, K_2CO_3 or KNO_3. Therefore, after standard calcinations and reduction, potassium appears in the catalysts in the form of K^{1+} ion. On the contrary, the surface science studies of the effect of potassium on nickel are usually performed on well-defined Ni planes with metallic potassium evaporated on them so the deposited potassium appears in the form of $K^{\delta+}$ ions. The difference between the state of potassium in supported catalysts and model objects implies that the effect of potassium on chemical/catalytic properties of supported nickel may be different from the effect observed for the basic Ni planes [130]. Therefore, extrapolation of the results obtained from the surface science studies to the application with supported catalyst must be done cautiously.

After K_2CO_3 incipient wetness impregnation of a Ni/Al_2O_3 Bailey et al [131] found that much of the potassium was on the Al_2O_3 surface and thus the number of adsorption sites on nickel did not change significantly. Moreover, potassium decreased the steady-state rate of CO hydrogenation on Ni/ Al_2O_3 catalysts as well as the concentration of sites that can form H-CO complexes on Al_2O_3. The authors [131] also found that the transfer rate of CO from nickel to Al_2O_3 to form a H-CO complex was severely decreased. Juan-Juan et al. [132] investigated the effect of potassium in a K-promoted Ni/ Al_2O_3 catalyst, prepared using the incipient wet impregnation, on the dry reforming of methane. The results showed that potassium migrates from the support to the Ni surface, neutralizes a fraction of the active sites and suppressed the coke formation on the catalyst.

Li et al. [133] investigated the effect of potassium on the steam methane reforming activity of a Ni_4/Al_2O_3 model catalyst surface using density functional theory (DFT) calculations. According to the authors [133] the atomic K could promote the reactivity of the SMR reaction by lowering the barrier of the dissociative methane adsorption step. The increased overlapping orbitals of Ni and carbon from CH_x was ascribed to the donation of electrons from the neighboring K to the nickel active site. Moreover, from the DFT study the authors [133] concluded that K could hardly get adsorbed on the Ni_4 cluster due to the large radius (2.34 Å) and will locate onto the bridge site of the lattice oxygen on the Al_2O_3 support. This

797 statement is consistent with the Kotarba et al. [134] who using the surface ionization
798 technique found that the potassium stability was markedly higher on the oxidized surface
799 of the iron ammonia catalyst compared to the reduced one.

800 However, at the high temperatures condition of steam reformers desorption and
801 volatilization of potassium from the K-impregnated catalysts is still an unresolved problem
802 which not only causes loss of the desired promoting effects but can negatively affect
803 downstream processes e.g. plugging of heat exchangers and poisoning of synthesis catalysts
804 [126], [135]–[138].

805 ### 2.8.1 Potassium-Sulfur interaction on nickel-based steam reforming catalysts
806

807 The addition of SO_2, ammonium sulfate and/or the use of high potassium content biomass
808 have been applied in the field of emission control for combustion processes to reduce the
809 SO_x and/or the KCl and chlorine emissions [139]–[145].

810 To mitigate the corrosion and deposition on heat exchangers and turbines caused by the
811 release of KCl and chlorine from the combustion of biomass feedstocks the addition of
812 ammonium sulfate and co-combustion with coal has shown to be a suitable solution, the
813 formation of K_2SO_4, a less corrosive compound, has been identified [139], [140], [145].
814 Evidence of the interaction between potassium and sulfur in a duel fluidized bed
815 gasification system was observed by Marinkovic et al [43].

816 Formation of K_2SO_4 aerosol under oxidizing atmosphere e.g. biomass-fired boilers, was
817 proposed to take place by sulfation of gas-phase KCL [146]. Combination of SO_3 with KCL
818 to yield a stable complex i.e. an alkali oxysulfur chloride KSO_3Cl, the latter was found to act
819 as a precursor for the K_2SO_4. The transformation of the KCl to K_2SO_4 were believed to
820 proceed by a number of molecule–molecule reactions, which could be anticipated to exhibit
821 ionic behavior [146].

822 Papageorgopoulus and Kamaratos [147] studied the K and S coadsorption on Ni(100)
823 surfaces by means of Auger electron spectroscopy (AES), thermal desorption spectroscopy

824 (TDS) and WF (work-function) measurements in UHV and found that the K overlayer on S-
825 covered Ni(100) weakens the S–Ni bond, and forms a compound with S. Additionally, at S
826 coverages higher than 0.5 ML a KS peak was observed in the AES spectra.

827 The influence of potassium-impregnated catalysts on the tolerance to sulfur (H_2S and
828 thiophene) poisoning on the hydrogenation reaction have been studied by Díaz et al. [148].
829 The increased sulfur poisoning tolerance of the Ni/SiO_2 was attributed to the presence of
830 potassium decoration that blocked part of the nickel surface hindering the adsorption of
831 thiophene and H_2S.

832 Ferrandon et al. [149] found that the addition (impregnation) of potassium to a Rh/La-Al_2O_3
833 catalyst led to a higher H_2 yield and a lower number of hydrocarbons during the
834 autothermal reforming reaction (ATR) of low-sulfur gasoline compared to the same catalyst
835 without K. As a possible explanation the authors [149] pointed out as both an increase in
836 reaction temperature and by blockage of Rh sites preventing H_2S adsorption and coke
837 formation.

838 The improved sulfur tolerance of the potassium-impregnated Ni/ Al_2O_3 for the
839 hydrodesulfurization reaction of thiophene observed by Chen and Shiue [150] was related
840 to the weakening of the nickel sulfide bond caused by release and transfer of electrons from
841 the potassium to the nickel crystallite.

842 The reaction between adsorbed sulfur and alkali promoter followed by a migration of the
843 formed compound e.g. K_2S and/or KSH, from the active surface was considered by
844 Arabczyk et al [151] and was linked with the increased sulfur tolerance of the potassium-
845 impregnated industrial iron catalyst for ammonia synthesis. A similar result and
846 explanation was given by Anderson et al. [152] using a potassium-impregnated commercial
847 iron catalyst for the Fischer-Tropsch synthesis.

848 A survey on the literature revealed that the study of the potassium-sulfur interaction of a
849 pre-sulfided nickel steam reforming catalyst without previous potassium impregnation is
850 lacking. An important contribution to this topic was made by Pouya. M. [15] who performed

851 experimental studies on a Ni/$MgAl_2O_4$ steam reforming catalyst to investigate the
852 interactions between gas-phase potassium species and the surface of the pre-sulfided nickel
853 catalyst. The most interesting outcome of this study was that the addition of ca. 2 ppm(v) of
854 KCl as fine aerosol particles to the steam reforming reactor appears to lower the surface
855 sulfur coverage at active nickel sites and increase methane as well as tar reforming
856 conversion

3 Experimental part

In this chapter the experimental set-up, experimental conditions, materials and methodology used as well as the data treatment and data analysis are described for each of the four studies presented in the summary of the experimental studies section.

3.1 Coarse tar removal using readily available low-cost materials

3.1.1 Experimental set-up and experimental conditions

Experimental set-up

The experimental set-up is reported in **¡Error! No se encuentra el origen de la referencia.**. Two stainless steel reactors (i.d.= 4 cm; L=50 cm), heated by external electrical resistances were placed in series vertically. In the first reactor, where the pyrolysis process takes place, the biomass is fed from the top continuously by means of a piston feeding system. The produced tar and gas flowed to the second reactor and passed through a fixed bed of the selected material placed in the second reactor. The char produced from the biomass pyrolysis is accumulated and collected on a quartz wool bed in the first reactor. The second reactor is equipped with a thermocouple placed perpendicularly in the middle of the bed to track the temperature profile when the tar removal reactions take place. The bed height was set at 8 cm and kept constant for all the materials tested. In the experimental runs, the pyrolysis reactor was heated at 700 °C and the measured internal temperature was ca. 660 °C. In all the tests, a nitrogen flow was fed at the top of the pyrolysis reactor. To condense the tar downstream of the tar removal reactor, the outlet stream from the reactor flowed through four empty water-cooled glass traps and then the non-condensable gases were measured by an on-line non-dispersive Infrared (NDIR) analyzer (Simens Ultramat 23) and an online mass spectrometer (Hiden QGA) to measure the concentration of CO, CH_4, CO_2 and H_2. After removal of the condensed water present together with the tar compounds in the glass traps by the help of a rotavapor (R II BUCHI) the condensed tar was then

884 quantified gravimetrically using a lab scale balance (GX-4000-EC A & D instruments) with
885 a precision of 0.01 g. Loss of some of the condensed tar is predicted during the removal of
886 water. But the amount of heavier and less volatile tar compounds which are the main target
887 for this process should not change noticeably. The tar condensed within the portion of line
888 connecting the exit of the reactor to the first trap was rinsed with acetone and measured
889 using the same lab-scale balance.

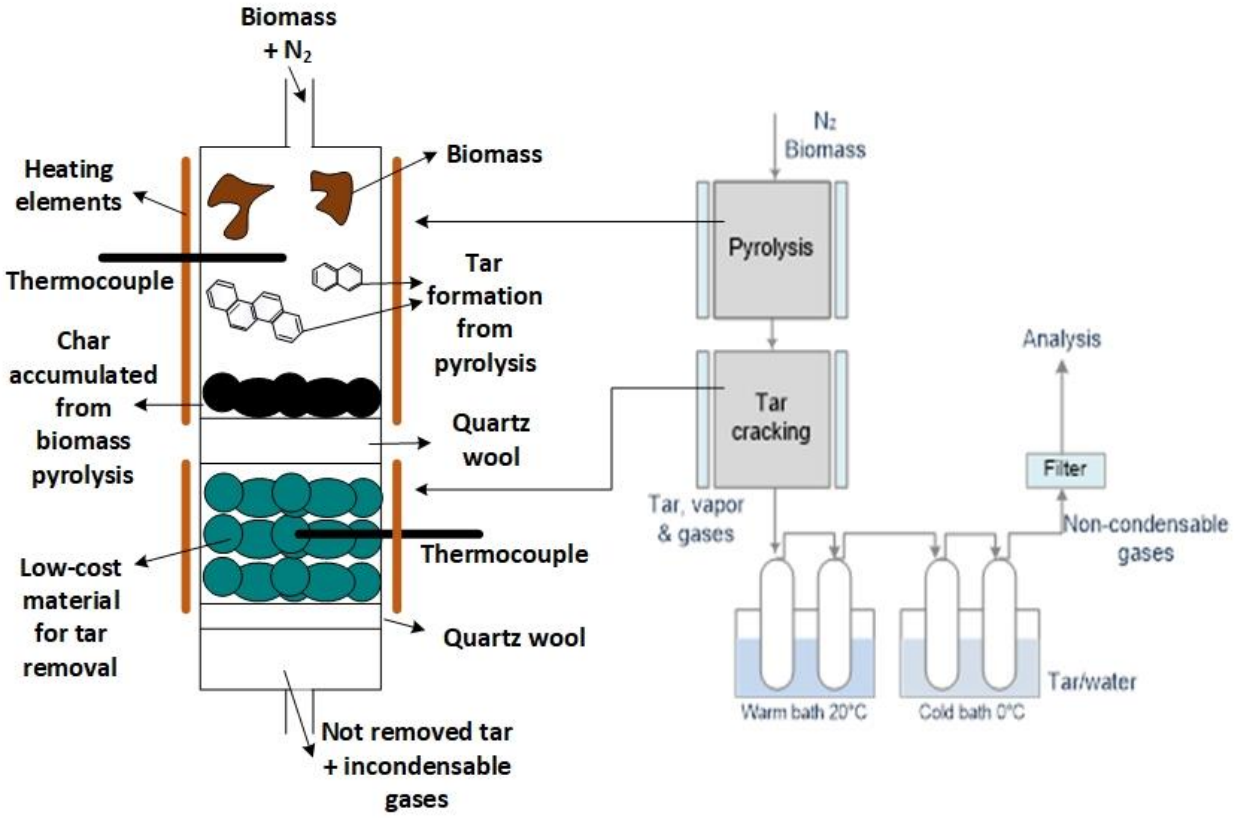

890

891 **Figure 3.1** Experimental set-up used in the study of tar removal using low-cost materials.

892 To assess the amount of tar species produced during the pyrolysis of olive pomace, blank
893 tests were conducted using the same experimental set-up but loading only the quartz wool
894 in both reactors. Three runs were performed using 50 g of biomass each, at identical
895 experimental conditions as during the evaluation of the tar removal performance of the
896 selected materials. The average measured tar was 16 wt. % of the fed biomass, this average
897 value considers the effect on the amount of tar produced caused by the accumulation of char
898 at the bottom of the pyrolysis reactor during the experiment and the effect of the quartz
899 wool.

Operating conditions

In **Table 3.1** the list of the operative conditions is reported. The absence of added oxidizing agents was proposed to simulate the situation in real secondary guard bed reactors in biomass gasification cleaning technologies [153], [154].

Table 3.1 Experimental conditions in the study of tar removal using low-cost materials.

N_2 flow rate (Nl min^{-1})	0.4
Average biomass flow rate (g min^{-1})	2.3
Pyrolysis bed temperature (°C)	660
Tar removal bed temperature (°C)	650-700-780
Tar removal bed height (cm)	8
Residence time of gas in bed ((s) at 700 °C)[a]	5-8

a Based on the dry gas flow rate measured during the blank experiments

3.1.2 Materials and methodology

Materials

The biomass used in all the tests was olive pomace purchased from olive oil producer farms in the region of Lazio Italy. This material was chosen because constitutes an abundant and readily available source of organic residue in Italy.

The materials used in the fixed bed to enhance the removal of tar are: char from the same olive pomace used in the pyrolysis reactor, commercial activated carbon (Aquacarb 207 EA), γ-Al_2O_3 in pellets (Sigma Aldrich) and pumice stone (JT Baker). All the commercial materials were used as received without any pre-treatment with the exception of γ-Al_2O_3 that were calcined at 900 °C for 5 h to stabilize its chemical and physical properties. Changes in the

surface area of surface area after the calcination treatment were not considered because the lack of an appropriate equipment to measure it.

The olive residue char was produced by pyrolysis at 800 °C with a heating rate of 100 °C/min and 0.3 Nl/h of N_2, keeping constant the maximum temperature for 30 min.

Characterization of the materials

Proximate composition was determined using a thermogravimetric (TG) method according to the ASTM D5142/02. The ultimate analysis was carried out with a EA3000 (Eurovector) elemental analyzer.

Table 3.2 shows the proximate and ultimate analysis of the olive pomace used in the experimental study.

Table 3.2 Proximate and ultimate analysis of the olive pomace used in the study.

Proximate analysis, wt. %				Ultimate analysis, wt. % (daf)					Net calorific value, MJ kg^{-1}
Moisture (wt. %)	Ash, (dry)	FC (daf)	VM (daf)	C	H	N	S	O By difference	
15	5.4	29.6	65.0	44.2	5.8	1.8	0.5	48.2	17.6

The surface area and pore volume measurements for the produced char was performed by N_2 adsorption/desorption (Micromeritics, ASAP 2000) and Brunauer–Emmett–Teller (BET)method with data collected at relative pressures between 0.06 and 0.2. The samples were outgassed under vacuum at 250◦C for 4 h prior to analysis. Data were collected at liquid nitrogen boiling temperature i.e. -196 °C. For the remaining three materials the information was provided by the supplier. The specific surface area, pore volume and particle dimension values of the materials are listed in

Table *3.3*. It is important to keep in mind that the measurement of the specific surface area of biochar using N_2 adsorption/desorption at -196 °C can lead to erroneous values because

of the low diffusion into the pores and equilibration rates [155]. The use of CO_2 as adsorbent gas at 0 °C is recommended to obtain reliable values [155]

Table 3.3 Properties of the materials used in the study of tar removal using low-cost materials.

	Specific surface area ($m^2\ g^{-1}$)	Pore volume (cm^3 100 g of sample^{-1})	Particle dimension (mm)
Activated carbon[a]	950-1100	75.6	1-2
γ-Al_2O_3[a]	230	63.4	1-3
Char[b]	150	24.5	1-2
Pumice stone[a]	15	41.1	1-3

a Data from the suppliers

[b] Measured values

3.1.3 Data treatment and analysis

Effect of temperature on the tar removal performance

The impact of temperature on the tar removal performance of the used materials was evaluated feeding 50 g of biomass to the pyrolysis reactor. The experiments were carried out in duplicate and the average value is presented in the figures of the result section.

The tar removal was calculated using **Eq. 3.1**

$$TR_i = \frac{x_o - x}{weight\ of\ bed\ material} \qquad \textbf{Eq. 3.1}$$

where TR_i is the tar removal capacity of the tested material i (g of tar removed g of material^{-1}), x_o is the amount of tar fed to the second reactor and x is the amount of tar measured at the end of each experiment.

Deactivation of the materials and measurement of deposited coke

961 To study and compare the deactivation of the used materials a series of experiments were
962 performed at 700 °C. The total amount of fed biomass was 150 g divided into three runs in
963 which 50 g of biomass was fed. After each run, the amount of tar and gas produced were
964 evaluated. The effect of the accumulated char during the second and third run on the tar fed
965 to the second reactor was estimated during blank tests (including the quartz wool) in which
966 the measured tar was 14 wt.% and 9 wt.% of the fed biomass, respectively. These later tests
967 take into account the effect of the progressive accumulation of tar and its effect on the tar
968 formation and removal. It is predicted that tar composition will vary due to the presence of
969 char. Aznar et al. [154] suggested to split the concept of tar as a whole lump into sub-lumps
970 related to tar termed "soft"(easy-to-destroy) and "hard" tars (difficult-to-destroy). In the
971 present experimental set-up the accumulation of char in the first reactor it is conjectured to
972 have a significant influence on the removal of the soft tars, such as phenol derivatives [154].
973 The possibility of more complex reactions caused by the presence of char such as cyclization,
974 condensation and polymerization cannot be ruled out. However, these reactions are
975 expected to occur in a similar fashion for all the material tested and a comparison of the
976 performance of the materials under similar conditions was the objective of the study.

977 At the end of each deactivation test the heating elements of both reactors were switch off
978 and the reactors were cooled down to room temperature under N_2 flow. Afterwards, the
979 materials were collected to measure the deposited coke. In the case of the pumice stone and
980 γ-Al_2O_3 the weight difference at the beginning of the test and after treatment in a muffle at
981 600 °C under static air for 4 h was used to estimate the coke deposited. As regard for the
982 char and activated carbon the weight at the beginning and the end of the deactivation
983 experiment were used for the deposited coke calculation. Underestimation of the coke
984 deposited using the latter method is foreseen as gasification reactions of the carbonaceous
985 materials as well as difficulties in collecting all the sample from the reactor are likely to
986 occur.

3.2 Steam reforming of toluene as tar model compound on Ni/mayenite synthesized using innovative procedures.

3.2.1 Experimental set-up and experimental conditions

Experimental set-up and reactants

The experimental setup used is depicted in **Figure 3.2**. The detailed description of the set-up is reported in [95]. The reactor was a stainless steel cylindrical (ID= 10 mm, h= 50 mm). The materials used in this study were deionized water and toluene (Sigma-Aldrich ≥ 99.5 %) which were fed separately with a steam to carbon ratio S/C=5. N_2 was employed as carrier gas and was mixed with the water and toluene in a three-way valve before entering to an evaporator held at 300°C to vaporize the feed before it entered to the reactor. The catalysts were held by a small piece of quartz wool placed on top of a stainless-steel grid. In each experiment 0.1 g of catalyst (grain size 0.1-0.3 mm) diluted with 1 g of SiO_2 (grain size 0.1-0.3 mm) was used. The height of the bed was 15 mm. Before the beginning of the tests the catalysts were activated with a H_2 flow rate of 0.5 NL/min (16 % in N_2) at 750°C for 30 min. At the end of each tests the heating system was turn off and the catalyst was cool down to room temperature under N_2, then it was collected and kept in a glass sealed container

At the reactor exit the unreacted reactants and condensable products were removed in a counter-current condenser using water maintained at 5 °C by means of a chiller. The produced gas flow was measured with a volumetric flow meter. A fixed bed of small Al_2O_3 sticks were placed before the on-line analyzers to adsorb any residual steam content present in the gas. CO, CO_2 and CH_4 were measured by an online analyzer (Siemens Ultramat 21). The concentration of H_2 and possible traces of C_2H_4 were quantified by a GC mass spectrometer (Hiden QGA).

To evaluate the activity of the SiO_2 filler material on the conversion of the tar model compounds a pure SiO_2 bed was used in the reactor and experiments with the model tar

compounds were performed at 750 °C keeping constant all the operative conditions used for the catalytic tests. The concentration values of CO and H_2 measured at the reactor exit were negligible and hence the catalytic/thermal effect of the reactor and the SiO_2 particles was neglected.

The occurrence of deactivation was evaluated conducting 6-hour long tests at 700 °C

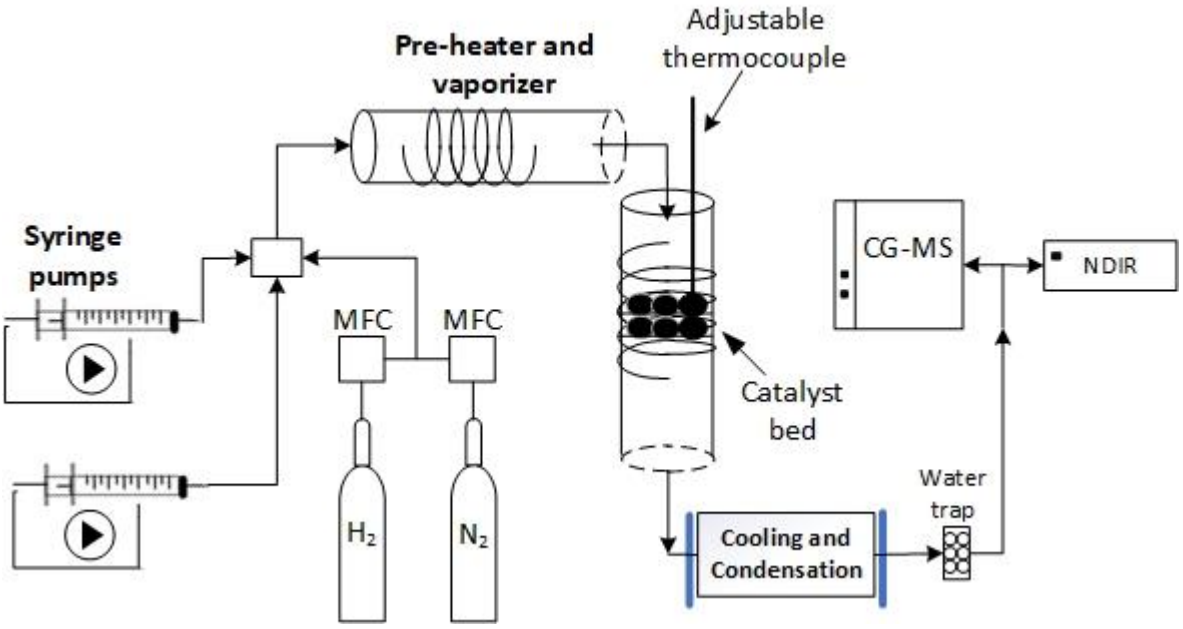

Figure 3.2 Experimental set-up used in the study of the activity of different Ni-based catalysts supported on mayenite on the steam reforming of tar model compounds.

Operating conditions

The experimental conditions used in the study of the activity of different Ni-based catalysts supported on mayenite on the steam reforming of toluene (STR) are listed in **Table 3.4**

In the present work severe conditions with respect to the inlet tar concentration were used as can be seen in **Table 3.4**, these conditions are comparable with the tar concentration measured in atmospheric bubbling fluidized bed biomass gasifiers with steam as gasifier agent [156]. The chosen S/C ratio was based on reported values of syngas composition obtained in air [157] and steam/oxygen [156] fluidized bed gasifiers. In addition, the relatively high S/C value was applied to prevent a fast deactivation of the catalysts due to carbon deposition during the tests conducted to obtain the kinetics parameters

Steam ageing of the catalysts was not performed before the experiments. Nevertheless, XRD and BET specific surface area analyses of the fresh catalysts and after the 6 hour-long experiments were performed to assess the change in their physical structure.

Table 3.4 Experimental conditions used in the study of the activity of different Ni-based catalysts supported on mayenite on the steam reforming of tar model compounds.

	STR
Temperature (°C)	670-750
Total gas inlet flow (NL min^{-1})	0.41
N_2 flow rate (NL min^{-1})	0.24
tar concentration (g Nm^{-3})	47
GHSV (h^{-1} at 700 °C)	73750
Space-time, $w_{cat}/F_{toluene}$ (kg_{cat} h Nm^{-3})	0.33
S/C	5

3.2.2 Materials and methodology

Catalysts synthesis

Mayenite, used as support in all the catalysts, was obtained starting from different precursors: from boehmite (AlO(OH)) and $Ca(NO_3)_2{\cdot}4H_2O$ (mayenite B) and from gibbsite ($Al(OH)_3$) and $Ca(OH)_2$ (mayenite H).

Mayenite B was synthetized starting from a stable dispersion of boehmite [158]. First a dispersion was prepared adding commercial aluminum oxide hydroxide powder (Sigma Aldrich ≥ 99 %) to a 0.4 % (w/w) HNO_3 aqueous solution and then $Ca(NO_3)_2.4H_2O$ was added to the dispersion under vigorous stirring. The used amount of $Ca(NO_3)_2.4H_2O$ was determined based on the stoichiometric ratio in the mayenite (Ca/Al molar ratio = 12/14). The dispersion was kept under stirring for 24 h at room temperature till a gel was obtained. The gel was then dried overnight at 100 °C and the resultant solid was grinded and calcined at 950 °C for 16h under static air.

For the synthesis of mayenite H, $Al(OH)_3$ and $Ca(OH)_2$ were stoichiometrically mixed in solid state, then water was added till a homogeneous paste was obtained. The paste was dried for 24 h at 105 °C, then the obtained solid was grinded and calcined at 1250 °C for 16 hours under static air.

Both calcination temperatures for mayenite B and H were determined relying on TGA-DSC analysis (SDTQ600, TA instrument) performed on the precursors, where the exothermic peak of the phase transformation is recorded at 940 °C and 1250 °C for boehmite and hydroxides precursors, respectively (**Figure 3.3**)

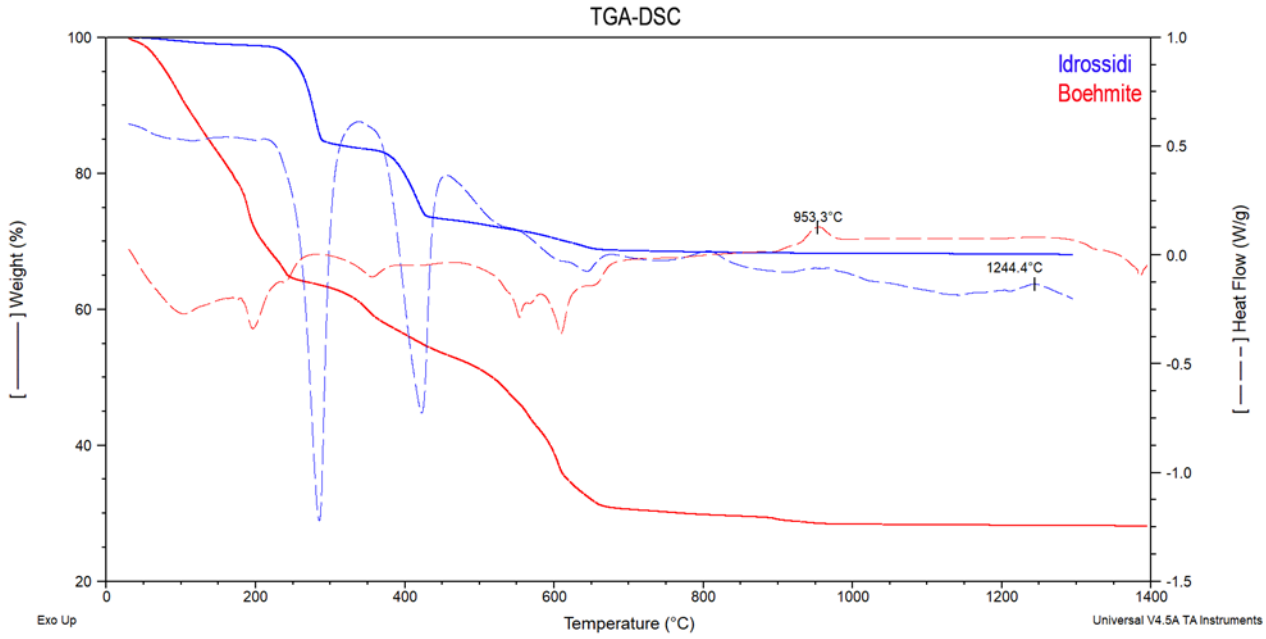

Figure 3.3 TGA-DSC corresponding to the calcination of the precursors of mayenite B and mayenite H

Four nickel supported catalysts were prepared with two different routes for the metal addition on mayenite B and H. The first route was by wet impregnation (wi) on the previously obtained supports (Ni/mayenite B-wi and Ni/mayenite H-wi) sieved between 0.1-0.3 mm. These solids were mixed under stirring with the aqueous solution of Ni precursor and then dried for 24 h at 105 °C. The powders obtained were calcined at 900 °C for 6 h under static air atmosphere.

The second route was by a "one step" (os) procedure consisting in adding the Ni precursor directly during the mayenite preparation described above. In the case of Ni/mayenite B-os

the Ni precursor was added to the dispersion together with calcium precursor, while to prepare Ni/mayenite H-os the Ni precursor was dissolved in the water added to the mixture of solid precursor to obtain a paste.

In all the cases $Ni(NO_3)_2 \cdot 6H_2O$ (Sigma Aldrich 99.99 %)was used as precursor and its amount was calculated to produce a catalyst having 10 wt% of nickel.

Figure 3.4 and **Figure 3.5** Depicts a scheme with the synthesis procedure followed for Ni/mayenite B (wi and os) and Ni/mayenite H (wi and os) respectively.

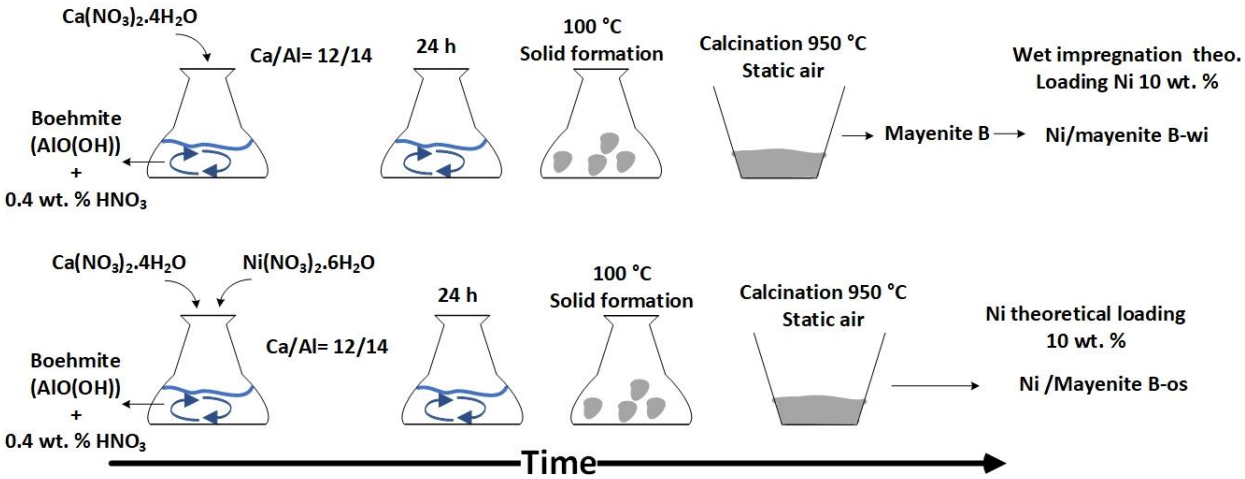

Figure 3.4 Steps for the synthesis of mayenite B, Ni/mayenite B-wi and Ni/mayenite B-os

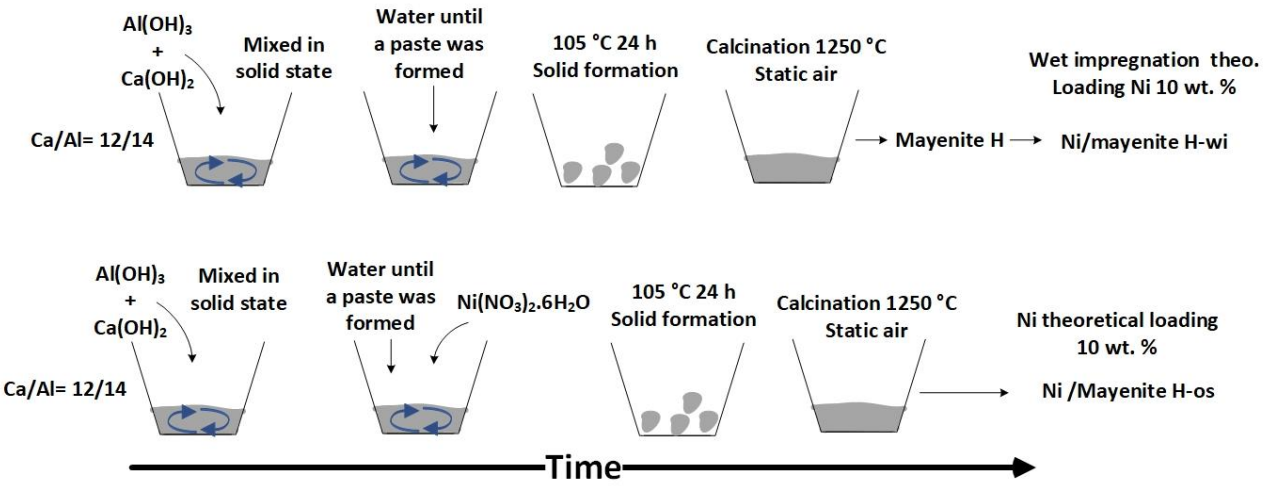

Figure 3.5 Steps for the synthesis of mayenite H, Ni/mayenite H-wi and Ni/mayenite H-os

Catalysts characterization

The synthesized catalysts and supports were analyzed by X-ray powder diffraction (XRPD) (Philips Analytical PW1830), Brunauer-Emmett-Teller (BET) and Barrett-Joyner-Halenda (BJH) analyses. XRD patterns were acquired using a Philips Analytical PW1830 X-ray diffractometer, equipped with Cu Kα (1.54056 Å) radiation, in the 2θ range from 15 to 70° with a step size of 0.02° and a time for step of 3.5 s. The data were collected with an acceleration voltage and applied current of 40 kV and 30 mA, respectively. The crystalline phases in the resulting diffractograms were identified through the COD database (Crystallography Open Database – an open-access collection of crystal structures) [159].The average nickel crystallite sizes were calculated with the Scherrer's equation on the most intense Ni peak plane. The constant related to crystallite shape (K) was taken as 0.9 [160]

BET analyses were determined by N2 adsorption–desorption isotherms acquired at −196°C using a Micromeritics Triflex analyzer (Micromeritics Instrument Corp.). The adsorption-desorption isotherms were acquired in a p/p^0 range from 0.01 to 0.99. Isotherm analyses were performed using the 3Flex Version 4.05 software. Samples were previously outgassed at 300 °C for 3 h at least. The BET and BJH methods were used to calculate the specific surface area, pore volume and average pore diameter, respectively.

To obtain morphologic and topologic information, SEM/EDS (Scanning Electron Microscopy combined with Energy Dispersive X-ray Spectrometry) analysis were performed on the obtained catalysts. Backscattered electron (BSE) images were recorded with a High Resolution-Field Emission Scanning Electron Microscope (HR-FESEM, AURIGA Zeiss) operated at 15 kV. The samples were prior sputter-coated with 10 nm thin layer of chromium using a Quorumteach Q150T sputter coater. For elemental analyses EDS maps were acquired with QUANTAX EDS XFlash® 6 detector (Bruker Nano GmbH), providing elemental topography of zones of external surfaces. The coke content was determined by Thermogravimetric (TG) analysis using an SDTQ600 simultaneous TGA-DTA-DSC analyzer (TA Instruments, USA) under a gas mixture of 20 % O_2 in nitrogen mixture and with a flux rate of 100 mL min^{-1}. The samples of the fresh and spent catalysts

were prior heated under nitrogen in an open ceramic pan up to 800 °C with a ramp rate of 20 °C min^{-1} to strip away volatile organic compounds physically absorbed. The samples were then equilibrated to 31 °C and the O_2/N_2 gas mixture was introduced. Specimens were afterward subjected to the following thermal program: heating up to 230 °C, 30 min hold, heating to 800 °C and 30 min hold, all ramps were set to 10 °C min^{-1}. Differences from the curves of the fresh and spent catalysts were used to individuate the peaks corresponding to oxidation of carbon and the troughs related to nickel oxidation. This was done to correct the peaks whenever overlapping occurred.

Temperature programmed reduction (TPR) analysis on the fresh catalysts was performed using a thermogravimetric analyzer SDTQ600 (TA Instruments, USA). The samples were pre-treated under Ar flow at 150 °C for 60 min to remove adsorbed moisture and air. Then the TPR profiles were recorded by heating the sample from 40 °C to 900 °C at 5 °C min^{-1} under a H_2 flow (5.0 % H_2 in Ar, 50 mL min^{-1}).

3.2.3 Data treatment and analysis

Carbon conversion and H_2 selectivity

Due to the complexity of the reactions occurring during the steam reforming of tar model compounds a simplified reaction scheme which takes into consideration only the reforming and the water gas shift (WGS)reactions was adopted [161]

SRT: $C_7H_8 + 7H_2O \rightarrow 7CO + 11H_2$ **Eq. 3.2**

WGS: $CO + H_2O \rightarrow CO_2 + H_2$ **Eq. 3.3**

The conversion of the tar model compounds was calculated as the carbon conversion X_C:

$$X_C = \frac{n_{CO_{OUT}} + n_{CO2_{OUT}} + n_{CH4_{OUT}}}{molar\ flow\ of\ carbon\ in\ the\ feed} \quad \textbf{Eq. 3.4}$$

where n_{COout}, n_{CO2out}, and n_{CH4out} are the molar flow of gas containing carbon at the reactor exit i.e. CO, CO_2 and CH_4, respectively. Reactions leading to carbon formation on the catalyst such as toluene decomposition and the Boudouard reaction procced concurrently with the steam reforming and WGS reactions and need to be considered.

Hydrogen selectivity was defined according to the work of Polychronopoulou et al. [162]:

$$S_{H_2} = \frac{y_{H_2}}{1.6 \times y_{CO} + 2.6 \times y_{CO_2}} \quad \textbf{Eq. 3.5}$$

S_{H_2} was used to identify whether reactions other than those described in the selected reaction network occurred [162]**.** y_{H_2}, y_{CO} and y_{CO_2} are the measured mole fraction of hydrogen, CO and CO_2 at the exit of the reactor. In **Eq. 3.5** the coefficients 1.6 and 2.6 represent the stoichiometric correlation of 1 mol of hydrogen to that of the produced CO and CO_2, respectively, based on **Eq. 3.2** and **Eq. 3.3**

Elemental balance calculations

Carbon mass balance was calculated for Ni/mayenite B-wi and Ni/mayenite H-wi during the initial period of the deactivation tests i.e. when the carbon conversion was close to 1, considering the measured carbon species in the exit gas. In both cases it was closed within 5 %. Hydrogen and oxygen atomic balances were used to calculate the unreacted mass of water during the same initial period. The latter value was checked and confirmed weighting the collected condense. The measured exit volumetric dry flow rate was verified using the N_2 atomic balance.

Equilibrium calculations

Thermodynamic equilibrium calculations were done using Aspen plus V8.8®. The Gibbs reactor was chosen to calculate the equilibrium composition of the simulated gas. The SRKKD thermodynamic method was set for all the calculations. The input for the simulation was the molar flow rate of C_7H_8, water and N_2.

3.2.4 Kinetic modelling

Evaluation of mass transfer limitations

Axial isothermal conditions were verified and confirmed by moving the thermocouple inside the bed throughout the catalytic bed length during the steam reforming of the model tar compounds whereas radial temperature gradients were not measured. Temperature gradients within the particles were assumed to be negligible when mayenite was used as support because of the low surface area of the used catalyst as shown in **Table 5.1** in section 5.1 of the chapter 5 [163]. Moreover, the pressure drop in the packed bed was neglected. For the kinetic study conversion values ≤ 0.9 were used to fulfil the mears'criterion

The Mears'criterion [164] (**Eq. 3.6**) was used to evaluate the occurrence of external mass transfer limitations within the experimental set-up during the steam reforming reactions. Spherical particle geometry was assumed

$$\frac{-r_{A,obs} \times R \times n}{k_c \times C_{Ab}} \leq 0.15 \qquad \textbf{Eq. 3.6}$$

where, $-r_{A,obs}$ is the measured rate of reaction (mol grams of catalyst^{-1} s^{-1})), R is the catalyst particle radius (m), n is the reaction order, k_c is the mass transfer coefficient (m s^{-1}) and C_{Ab} is the bulk concentration of the model tar compound (mol m^{-3}). The molecular diffusivity of toluene in air at 700 °C [165] was used in the k_c calculation i.e. 8.5 x 10^{-6} m^2 s^{-1}. **Eq. 3.6** should

be used with caution because at the low Reynolds numbers encountered in laboratory reactors, the mass and heat transfer coefficients are quite insensitive to changes in flow rates and this could disguise the validity of the criterion [166]. Furthermore on evaluating $-r_{A,obs}$ it is essential the use of the most suitable rate equation i.e. the rate equation that takes into account the rate determining step(s) at the experimental conditions and possibly the mechanism of reaction. Failing in use the proper rate equation can lead to biased results and the inability to detect the presence of transfer limitations [166]. In the present study a pseudo first-order reaction have been applied in which it was hypothesized that the obtained apparent kinetic constant takes into account the rate determining step e.g. the reaction between adsorbed CHO with adsorbed O to produce adsorbed CO_2 and adsorbed H_2 [167], in the overall reaction network of the steam reforming of the tar model compounds at the experimental conditions applied.

Reactor model

A selected number of experiments were dedicated to obtaining kinetic parameter in which fresh catalyst was used in every experiment. Four different temperatures were set in each test. The same catalyst was used for the whole duration of the test. The tests were performed starting from the lowest temperature. Each selected temperature was maintained until the concentration of the main gases reached steady state conditions, usually 20 min, after which the temperature was increased.

The plug flow condition was confirmed using the criteria proposed by Froment et al. [166]. The ratio of the height of the bed to the particle size was larger than the criterion for axial dispersion i.e. catalyst bed height/particle diameter ≥ 50. The ratio of the internal diameter of the reactor and the catalyst particle was higher than 30 and hence the channeling criterion was fulfilled. Plug flow conditions were further verified using the criterion proposed by Kapteijn. F and Moulijn. J. A. [168]:

$$\frac{L_b}{d_p} \geq \frac{8 \times n}{Pe_p} \times \ln\left(\frac{1}{1-x}\right) \quad \textbf{Eq. 3.7}$$

where Lb is the bed height (0.015 m), dp is the particle diameter ($2.5 * 10^{-4}$), n is the reaction order, Pe_p is the Peclet number of the particle, calculated as the Reynolds number of the particle (651.2) times the Schmidt number ($2.5 * 10^{-3}$) and x is the conversion, which was equal to 0.9 for the calculation. The obtained value was 11.4 which was lower than the used bed height to particle diameter ratio. From this result the plug flow conditions were confirmed.

The apparent kinetic parameters were carried assuming a pseudo first-order reaction with respect to the tar model compound and independent of H_2O concentration as the latter was fed in excess. The pseudo first-order assumption to represent the tar model compounds steam reforming reaction have been widely accepted in the literature [154], [169]. Wei and Iglesia [170] used kinetic and isotopic tracer methods on the methane steam reforming reaction on Rh/Al_2O_3 and Rh/ZrO_2 and found that the rate of reaction was independent on H_2O pressure (5-45 kPa) at 873 K. Similarly, Mukai et al. [171] found that the toluene steam reforming reaction rate was almost independent of the partial pressure of H_2O at 873 K using a $Ni/La_{0.7}Sr_{0.3}AlO_{3-\delta}$ catalyst in the steam to carbon range $1.4 \leq S/C \leq 2.3$.

$$-r_{app} = k_{app} \times C_{tar} \quad \textbf{Eq. 3.8}$$

Under conditions very close to plug flow, a mass balance for the tar compound gives:

$$k_{app} = \frac{-\ln(1-X_C)}{\tau} \quad \textbf{Eq. 3.9}$$

where r_{app} is the rate of conversion (kmol m^{-3} h^{-1})), kapp is the apparent kinetic constant (m^3(Tcat. N_2-free) kg^{-1} h^{-1}), C_{tar} is the tar model compound concentration (kmol m^{-3}), X_c is the carbon conversion, and τ is the residence time in the catalyst bed that was calculated as follows:

$$\tau = \frac{W_{cat}}{Q_{in}(T)} \quad \textbf{Eq.3.10}$$

where W_{cat} is the catalyst weight (kg) and $Q_{in}(T)$ is the inlet volume flow rate at the catalyst bed temperature ($m^3\ h^{-1}$) after subtracting the N_2 flow ($m^3\ h^{-1}$), with this units of measurement the obtained. Using this measurement units for the Q_{in} (T) the obtained kapp was thus calculated at the catalyst temperature and without considering the N_2 flow rate. This was done to compare the results with the reported data of Aznar et al. [154].

The apparent kinetic constant (k_{app}) of tar model compounds were calculated using the carbon conversion (**Eq. 3.4**)) and therefore the obtained k_{app} refers to all the reactions involved in the formation of CO, CO_2 and CH_4.

3.3 Effect of H_2S and thiophene on the steam reforming activity of Ni/Al_2O_3, Ni/mayenite and Rh/Al_2O_3.

3.3.1 Experimental set-up and experimental conditions

Experimental set-up

The laboratory-scale tests were conducted in an atmospheric plug-flow reactor (**Figure 3.6**). The detailed description can be found from Tuomi et al. [172] The quartz reactor used in the experiments had an inner diameter of 10 mm equipped with a thermocouple pocket of 4 mm. The temperature was measured from the center of the catalyst bed by a K-type thermocouple. All gases and vapors were mix before entering the reactor and the inlet line was heated to 300 °C. The exit line was also heated to 300 °C to avoid condensation of tar compounds.

A continuous gas analyzer (Sick Maihak S710) was used to determine the CO, CO_2, H_2 and O_2 content in dry gas. All hydrocarbons were analyzed by an online GC Agilent 7890A equipped with two columns and two FID detectors. For the experiments carried out without thiophene a GS-GASPRO column (30 m, 0.32 mm ID, film 20 μm) was used to analyses hydrocarbons from CH_4 to C5, whereas benzene concentration was quantified using a HP-5 column (30 m, 0.32 mm ID, film 25 μm). In the presence of thiophene, all compounds were separated using a HP-5 column (30 m, 0.32 mm ID, film 25 μm). Calibration of the continuous gas analyzer was performed every two weeks with a standard gas bottle supplied by AGA. Calibration of the online GC for thiophene measurements was done once at the beginning of the experiments using a gas bottle supplied by AGA with a C_4H_4S analytical value equal to 188 ppm ± 2 %.

For some selected tests, gas bag samples were collected to measure the thiophene outlet concentration and other sulfur containing compounds. The analysis was made by a GC

(Agilent 7890A) equipped with a flame photometric detector (FPD). The samples were taken after 2 h of run to saturate the stainless-steel lines with H_2S and thus limit the error in the measurement caused by the adsorption of H_2S

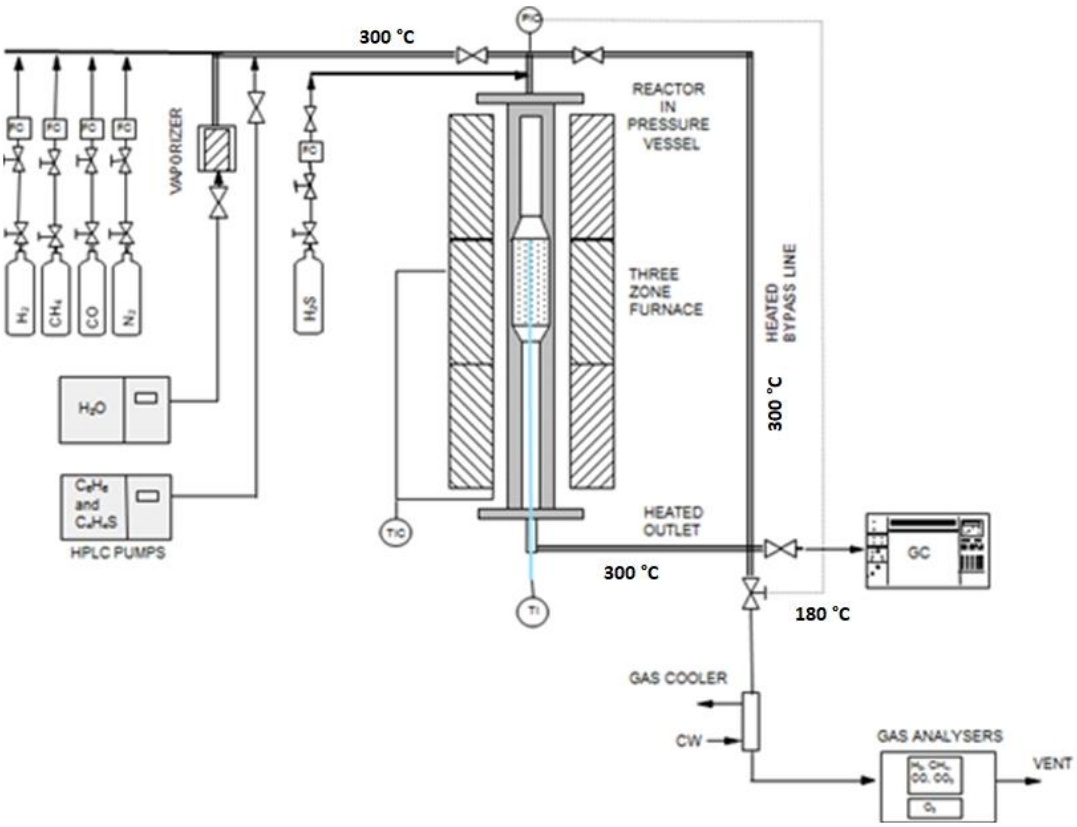

Figure 3.6 Atmospheric plug flow reactor used in the study of the effect of sulfur compound on the steam reforming activity of various catalysts.

Operating conditions

The model COG composition used in the tests is presented in **Table 3.5¡Error! No se encuentra el origen de la referencia.**. Benzene (Merck, >99.7 %) was used as tar model compound. For the study of the impact of thiophene on the steam reforming reaction, a mixture of thiophene 5 wt. % (Merck, >99.0) and benzene 95 wt. % (Merck, >99.7) was used. As sulfur chemisorption has a strong dependence on temperature, benzene and thiophene reforming was studied without methane in the gas to ensure close-to-isothermal catalyst bed conditions. In addition to reforming experiments, the effect of H_2S on the water gas shift (WGS) reaction was studied without hydrocarbons in the feed. The total gas flow rate was

2.1 N l/min in all the experiments. The GHSV calculated considering the effective bed volume inside the quartz reactor was 76 000 h^{-1}.

Steam ageing of the catalysts was not performed before the experiments.

Table 3.5 Inlet composition used in the experiments of the effect of sulfur compounds on the steam reforming activity of various catalysts.

	Dry gas composition					Wet basis		
	CO vol. %	CH_4 vol. %	H_2 Vol. %	N_2 Vol. %	H_2S ppm(v)	C_4H_4S ppm(v)	C_6H_6 ppm(v)	H_2O vol. %
SR CH_4+Bz	5.3	35.9	50.0	8.8	0-200	0	1000	48.7
SR CH_4+Bz+Th	5.3	35.9	50.0	8.8	0	50	950	48.7
SR Bz	5.3	0	50.0	44.7	0-200	0	1000	48.7
SR Bz+Th	5.3	0	50.0	44.7	0	50	950	48.7
WGS	5.3	0	50.0	44.7	0-100	0	0	48.7

The experiments were conducted in the temperature range 650-900 °C. Several experiments were carried out in duplicate and the average value is presented in the figures of the result section.

All experiments were run for at least 2 hours. To evaluate of the time required for the establishment of the sulfur chemisorption equilibrium in the entire catalyst bed, sulfur was added once steady state conditions were reached. The GHSV was kept constant by replacing the corresponding sulfur flow with nitrogen and vice versa.

Thermal decomposition tests of the mixture of benzene and thiophene were carried out with SiC particles. In those experiments the volume of the bed, the total inlet flow rate and the

inlet composition were the same as in the catalytic steam reforming of the mixture benzene-thiophene.

3.3.2 Materials and methodology

Catalysts synthesis and characterization

The catalysts used in the experiments were Ni/Al_2O_3, Rh/Al_2O_3 and Ni/mayenite. The latest was synthesized using the auto-combustion method using glycine as oxidizer, nickel loading was 20 wt. %. The detailed synthesis procedure can be found elsewhere [14]. Ni/Al_2O_3 and Rh/Al_2O_3 were prepared by wet impregnation. The nickel loading was 10 wt. % and the rhodium loading was 1.5 wt. %.

In each test 1.2 g of catalyst were used with particle size of 200-300 μm. To achieve uniform bed temperatures, the catalysts were diluted with SiC to 1:1 volume ratio. The particle size of SiC was 300–355 μm.

The nickel catalysts were characterized by hydrogen chemisorption and XRD. X-ray diffraction analyses were performed with a PANalytical X'Pert PRO MPD Alpha-1 diffractometer using Cu Kα1 radiation (45 kv and 40 mA) in continuous scan mode in the range 10°-70° (2ϑ) and a step size of 0.0131°. The diffractograms were analyzed with the EVA software.

Temperature programmed reduction (TPR) measurements before the H_2 chemisorption analysis were performed under a 5 vol-% H_2/argon flow from room temperature to 800 °C with a 10 °C/min rate. A thermal conductivity detector (TCD) was used to measure the H_2 consumption. Ni/mayenite and Ni/Al_2O_3 showed a unique and pronounced trough at 750 °C and 400 °C respectively, while Rh/Al_2O_3 displayed a small trough at 230 °C with a shoulder at 180 °C. The pulse chemisorption technique was carried out at 25 °C using 0.1 g of catalyst under a 5 vol-% H_2/argon flow.

3.3.3 Data treatment and analysis

Surface coverage

Sulfur coverage on the nickel catalysts was calculated using the equation proposed by Alstrup et al. [122] derived from a Temkin-like isotherm. This equation was further verified and its validity was extended on nickel anodes by Hansen [173]. Alstrup et al. [122] measured sulfur chemisorption isobars for a $Ni/MgAl_2O_4$ catalyst in the temperature range 500-1000 °C and H_2S/H_2 ratio range 7-50 ppm. They concluded that up to 90 % of saturation the results were well described by **Eq. 3.11** with $\Delta H°$=-289 kJ mol^{-1}, $\Delta S°$=-19 J mol^{-1} K^{-1} and α=0.69

$$\frac{P_{H_2S}}{H_2} = \exp\left[\frac{\Delta H^{\circ}(1-\alpha\theta_s)}{RT} - \frac{\Delta S^{\circ}}{R}\right] \qquad \textbf{Eq. 3.11}$$

Thus, resulting in **Eq. 3.12**

$$\theta_s = 1.45 - 9.53\times10^{-5}T + 4.17\times10^{-5}T\ln\left(\frac{P_{H_2S}}{P_{H_2}}\right) \qquad \textbf{Eq. 3.12}$$

where T represents the temperature (k)

Elemental balances and conversion

Atomic balance calculations were performed based on the inlet and outlet stream compositions quantified by the online GC and the continuous gas analyzer. The total and dry flow rate at the reactor outlet were calculated from the carbon and oxygen balances, while the dry gas flow rate at the inlet was determined from the mass flow meters. It should be noted that in the absence of CH_4, the increase in the outlet flow rate was negligible (less than 1 %) and therefore did not have a strong effect in the benzene or thiophene conversions calculations.

Benzene, thiophene and methane conversions were calculated from **Eq. 3.13**.

$$X_i = \frac{\dot{F}_{i,IN} - \dot{F}_{i,OUT}}{\dot{F}_{i,OUT}} 100\% \qquad \textbf{Eq. 3.13}$$

where X_i is the conversion of the hydrocarbon; $\dot{F}_{i,IN}$ and $\dot{F}_{i,OUT}$ are the inlet and outlet molar flor rates of the hydrocarbons, respectively.

3.4 Effect of adding a KCl aerosol on the reforming activity of a pre-sulfided commercial Ni/$MgAl_2O_4$.

3.4.1 Experimental set-up and experimental conditions

Experimental set-up

For the experimental investigation a 5kWth bubbling fluidized bed (ABFB) gasifier was used coupled to a high temperature hot gas ceramic filter. The system was developed at KTH [174]. The reactor consists of a bubbling fluidized bed (inner diameter of 50 mm and a height of 300 mm) and a freeboard (diameter of 100 mm and height of 0.45 m). The freeboard lowers the gas velocity, which allows the bed particles in the gas to fall back into the bed. The total volume of the reactor is 5.1 L. The gasifier is externally heated and has a maximum operating temperature of 950 °C. The fluidization and oxidation media were pre-heated to 650 °C, before entering the reactor. When the system reaches steady conditions, the fuel is fed with a screw feeder directly into the fluidized bed near a gas distribution plate placed at the bottom of the reactor chamber. The fuel hopper is equipped with nitrogen purge gas and a cooling system to prevent heat up of the fuel in the screw feeder by the product gas, which would alter the fuel physical properties and make the feed rate irregular. The outlet of the filter was connected to an electrically heated fixed bed catalytic reactor (reformer). Both the filter and the catalytic fixed bed reactor have a length of 700 mm and an inner diameter of 50 mm. Sampling points for tar indicated as "SPA" (solid phase adsorption) and permanent gas were located before and after the catalytic reactor. At the outlet of the particulate filter the alkali aerosol generator (Constant Output Atomizer model 3076, TSI Inc.) with diffusion dryer was connected. Large droplets are removed by impaction on the wall opposite the jet and excess liquid is drained at the bottom of the Atomizer assembly block. The generated fine aerosol particles were then transported through tubes to the filter vessel where they evaporated into its molecular constituents as they enter the heated reactor. All the piping connections were trace heated and insulated to avoid condensation

of water and tar compounds Biomass is fed into the fluidized bed with a screw feeder. The temperatures and velocity of the rotor that powers the screw-feeder are set in an external control panel. The schematic representation of the used experimental setup is illustrated in **Figure 3.7**.

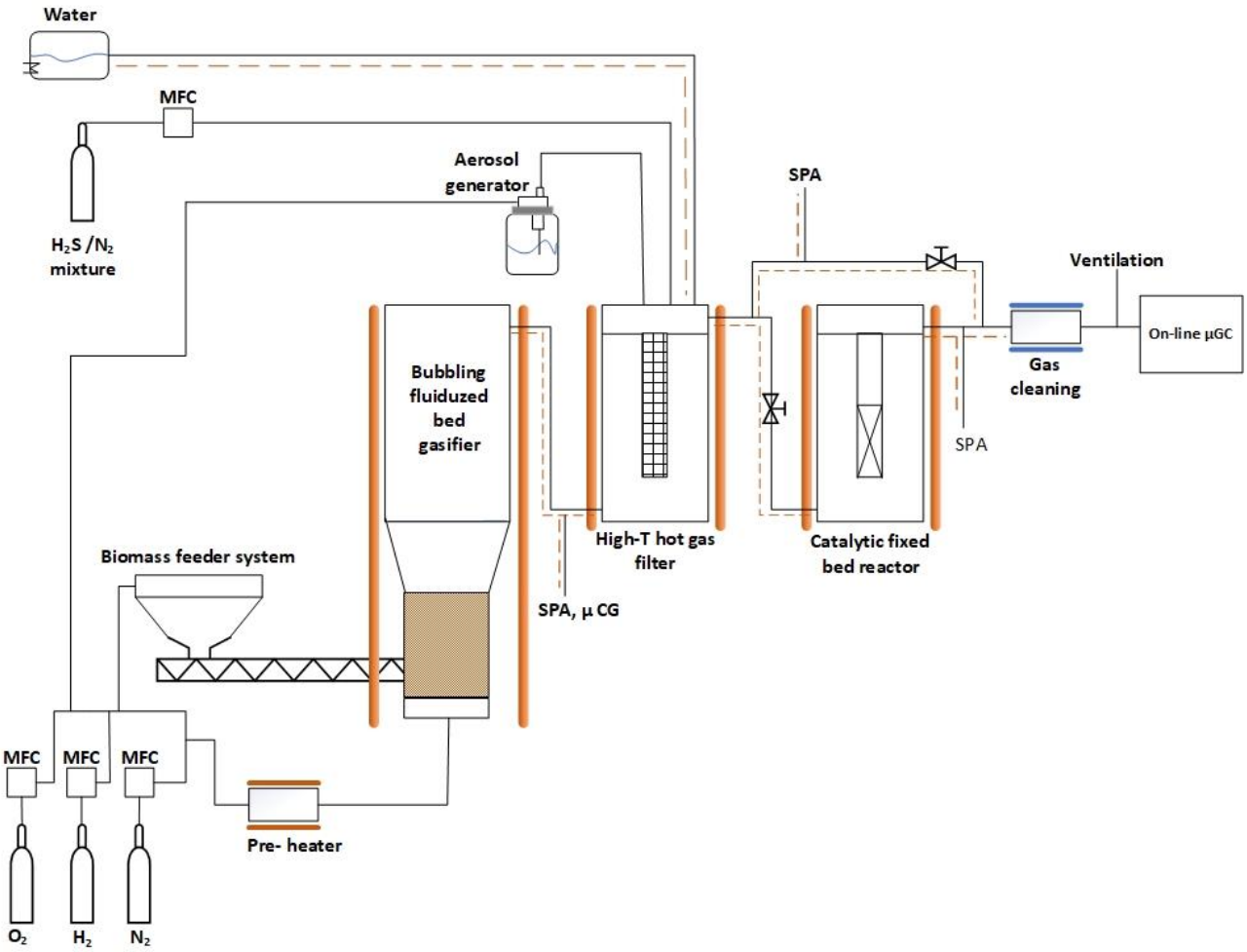

Figure 3.7 Experimental set-up used in the study of the effect of dosing potassium in the gas phase on the reforming activity of a pre-sulfided commercial Ni/$MgAl_2O_4$.

Operating conditions

The detailed experimental conditions are shown in **Table 3.6**.

Table 3.6. Experimental conditions used in the study of the effect of dosing potassium in the gas phase on the reforming activity of a pre-sulfided commercial Ni/$MgAl_2O_4$.

Gasification agent	O_2
Biomass feeding rate (g h^{-1})	208 ±2
λ	0.24-0.25
Average bed temperature (°C)	820 ±6
Average Freeboard temperature (°C)	733 ±5
Filter temperature (°C)	850 ±2
Reformer temperature (°C)	803 ±3

3.4.2 Materials and methodology

Materials

Pine pellets in the size range of 1.5 - 2 mm were used in all experiments and the results of ultimate and proximate analysis are reported in **Table 3.7**. The gasifier bed material was a dense alumina (350 g) with a particle size of 63–125 μm and density of 3960 kg/m^3. This material was replaced each test.

Table 3.7 Proximate and ultimate analysis of the pine pellets.

Proximate analysis	
Moisture (wt. %)	7.4
Ash (wt. % db)	0.52
Volatile matter (wt. % daf)	80.10
Fixed carbon (wt. % daf)	19.38
Ultimate analysis (daf)	
C (wt. %)	47.7
H (wt. %)	6.3
N (wt. %)	0.16
S (wt. %)	≤ 0.01
O (by diff) (wt. %)	45.29
Cl (wt. %)	0.03
K (mg/kg)	639
Na (mg/kg	57.3

Catalyst and inert material

Ni/$MgAl_2O_4$ and magnesium aluminate ($MgAl_2O_4$-spinel) in pellets form were provided by Haldor Tospoe (Haldor Topsøe A/S HT-25934 and HT-80541 respectively). Prior to use, both the catalyst and the support were ground to an average particle size of 3.6mm (3.15< dp <4.0 mm).

Inert nonporous silica free fillers (Vereinigte Füllkörper-Fabriken,Duranit® Inert D99) of 3.175 mm in diameter were used as bed diluent.

Catalyst and support characterization

Nitrogen adsorption measurements were performed (Micromeritics, ASAP 2000). The samples were outgassed by evacuation at 250 °C for 4 h prior to analysis. Data were collected at liquid nitrogen boiling temperature (77 K). The surface area was calculated by the

Brunauer–Emmett–Teller (BET) method with data collected at relative pressures between 0.06 and 0.2.

To determine the total carbon content on the catalyst surface, chemical analysis of the fresh and used catalyst were performed by ELTRA, CS-2000 series instruments. Total sulfur and potassium content were determined by Inductively coupled plasma mass spectrometry (ICP-MS) after acid digestion of the solid samples.

Catalyst pre-treatment

Prior to pre-treatment of the catalyst and support, the experimental setup was cleaned by steaming at 900°C for 12 h to volatilize any residual K located on the walls of the system upstream the reformer and thus minimize the risk of K uptake other than the alkali aerosol generator.

Initially, 25g of catalyst and 25g of support were mixed with 50g of inert diluent and subjected to activation by reduction in H_2 at 550±1 °C for 4h.

After reduction, the bed was subjected to steam ageing at 900 °C for 5 h at a molar Steam/H_2 ratio of 10. Ageing with steam stabilizes the catalyst and minimize any further sintering that would result in erroneous interpretation of activity loss during operation.

In order, to eliminate any transient phenomena due to sulfidation of the catalyst during operation, the catalyst and the support were subjected to sulfidation at 803 ± 2 °C at a H_2S/H_2 ratio of $1{,}88\times10^{-4}$ for 4 h. The actual sulfur coverage, θ_s, at this temperature and sulfidation conditions (H_2S/H_2) would yield a sulfur coverage of ca. 0.97 according to **Eq. 3.12**. The steps comprising the pre-treatment of the catalyst are summarized in **Figure 3.8**.

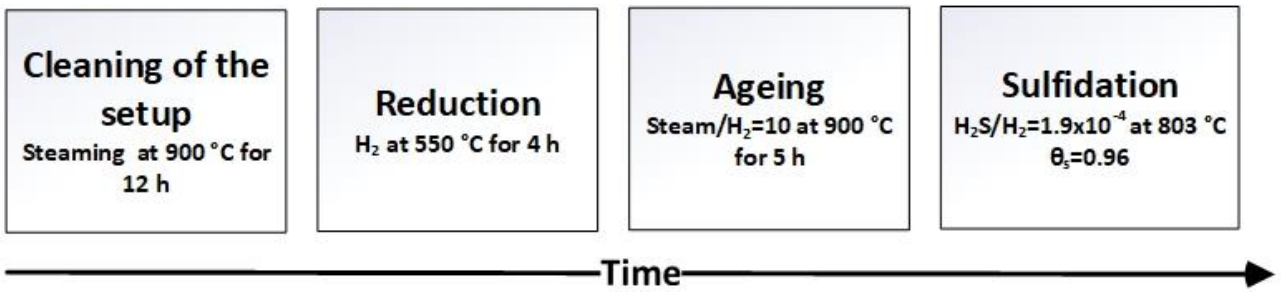

Figure 3.8 Pre-treatment steps applied in the study of the study of the effect of dosing potassium in the gas phase on the reforming activity of a pre-sulfided commercial Ni/$MgAl_2O_4$.

Catalytic experiments

Once the catalyst and the support were sulfided, direct exposure to producer gas from the gasifier with additional KCl dosing from the aerosol generator followed until saturation of the surface. The duration of the saturation phase was determined based on previous results performed at similar conditions were saturation of K uptake of the catalysts was achieved in ca. 20 h on stream [16]. The completion of the saturation phase was also verified by the observed unchanged conversion of CH_4, C_2H_4 and $C_{10}H_8$ [15].

After the saturation phase, the bed was removed and the catalyst and support were separated.

The catalyst and the bed diluent were then mixed with additional inert diluent occupying the same volume as the support to ensure similar hydrodynamic behavior of the bed between the saturation and decay phases.

The bed was then placed in the reactor and was exposed to the producer gas but without KCl aerosol supply (decay phase). Identical space velocities between saturation and decay phases was achieved by substitution of aqueous KCl solution in the aerosol generator by millipore water. The duration of the catalyst activity decay phase was determined by the observed conversion of methane and naphthalene species (chapter 7 section 7.3). The same procedure was followed also for the support.

The reforming activity of the inert material was evaluated during the decay phase by replacing both the support and catalyst with inert material occupying the same volume.

Possible gas phase reactions catalyzed by the addition of KCl aerosol to the system[128] were assessed by dosing the aerosol and using the reforming reactor without either support, catalyst or inert. A schematic representation of the catalytic experiments is illustrated in **Figure 3.9**.

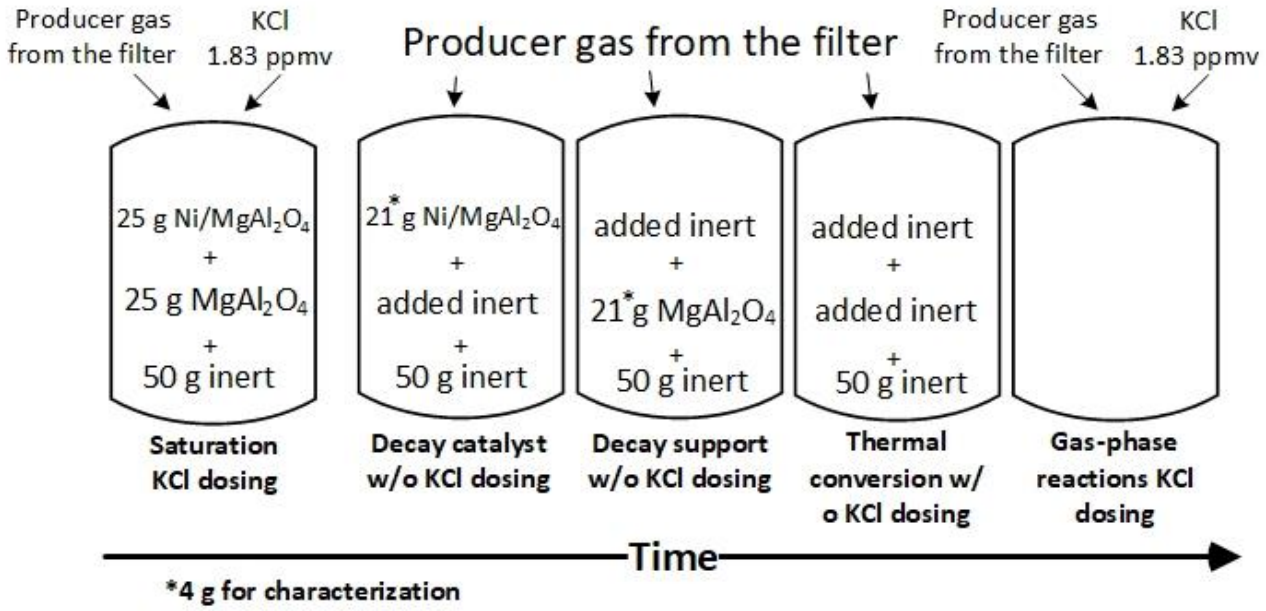

Figure 3.9 Schematic representation of the experiments done during the study of the study of the effect of dosing potassium in the gas phase on the reforming activity of a pre-sulfided commercial $Ni/MgAl_2O_4$.

3.4.3 Data treatment and analysis

Tar and gas analysis

The composition of the dry tar-free gas was determined with a micro-GC (Thermo Scientific, C2V-200). Tar samples were collected and analyzed using the solid phase adsorption couple with a gas chromatograph (SPA-GC) method [175]. A gas sample of 100 ml was manually taken through an amino sorbent. Later the solid phase extraction tube was eluted using dichloromethane and dichloromethane/acetonitrile (1:1) to obtain an aromatic fraction and phenol fraction. The obtained samples were analyzed, using a gas chromatograph (Varian CP 3800).

Catalyst activity

The catalyst activity was evaluated through the conversion of methane, ethylene and naphthalene. The conversion was calculated according to **Eq. 3.14**

$$x_i = 1 - \frac{N_{i,out}}{N_{i,in}} \qquad \textbf{Eq. 3.14}$$

where x_i, $N_{i,out}$ and $N_{i,in}$ are the conversion the exit molar flow and in the inlet molar flow of species i, respectively.

The normalized observed rate of reaction was calculated as follows:

$$R_{obs} = \frac{N_{i,out} - N_{i,in}}{A_{BET}} \qquad \textbf{Eq. 3.15}$$

where R_{obs} is the normalized observed rate of reaction (mol m^{-2} h^{-1}) and A_{BET} is the specific surface area of the catalyst (m^2). Conversion of heavy tar compounds (C_{10+}) was computed but it is not shown due to unacceptable high standard deviation values. The major contribution of the latter obtained values are likely to come from the sample collection[176]. Benzene conversion was also calculated using the results from the SPA measurements although the former reliability and accuracy is disputable due to incomplete adsorption and evaporation during storage[176], [177]

Water content and molar flow calculation

Calculation of the water content is based assuming the water gas shift (WGS) reaction reached equilibrium (WGS) according to **Eq. 3.16**

$$K_{eq} = \frac{[CO_2][H_2]}{[CO][H_2O]} \qquad \textbf{Eq. 3.16}$$

where K_{eq} is the equilibrium constant of the WGS reaction and [CO], [CO_2], [H_2] and [H_2O] are the molar concentration of CO, CO_2, H_2 and H_2O respectively. The temperature dependent equation proposed by [178] was used to calculate K_{eq}. A known flow of N_2 was fed to the system and it was used to obtain the total dry volume flow.

3.4.4 External mass transfer limitations

External mass transfer limitations for CH_4, C_2H_4 and $C_{10}H_8$ were evaluated using the Mears' criterion (**Eq. 3.6**). The concentration of the reactants was estimated using the inlet volumetric flow to the reactor and the molar flow of each reactant. The density value for CH_4 was taken from [179] at 725 °C. In the case of C_2H_4 the critical value [180] combined with the ideal gas law was used to calculate the density value at 803 °C. The $C_{10}H_8$ density value was calculated in the same way as in the C_2H_4, the critical density value was taken from [181]. The estimation of the viscosities at the reactor temperature were done using the equation proposed by Chung et al. [182]. The velocity at the inlet of the reactor was calculated considering the inlet volumetric flow and the reactor diameter (50 mm). The binary (in air) effective diffusion coefficients were obtained from [165] as were also verified (in N_2) using the equation proposed by Fuller at al. [183]–[185]. The equation proposed by Dixon. A. G. [186] was used to estimate the bulk void fraction Ɛ which was used to calculated the bulk density of the catalyst bed. The specific observed rate of reaction ($-r_{A,obs}$) was obtained by subtraction of the observed rate of reaction of the catalyst minus the thermal rate of reaction for each component, the result was then divided by the grams of catalyst used during the decay phase (≈ 21 g). In **Table 3.8** the calculated values for the Mears' criterion are listed for each compound.

Table 3.8 Mears criterion values estimated based on the values obtained at the beginning of the decay phase.

Compound	**CH_4**	**C_2H_4**	**$C_{10}H_8$**
Density (kg m^{-3})	0.193	56.23	218.95
Dynamic viscosity (Pa s) 10^{-5}	2.75	2.87	2.07
Reynolds number R_{ep}	3.44	1003.23	5415.30
Schmidt number Sc 10^{-3}	N/A*	3.43	1.42
Sherwood number Sh	0.24	11.13	24.44
Concentration (mol m^{-3}) 10^{-2}	82.22	18.89	4.78
Effective binary (N_2) diffusion coefficient (m^2 s^{-1}) 10^{-5}	12.34	8.81	3.93
Mass transfer coefficient k (m s^{-1}) 10^{-2}	1.38	27.25	26.67
Mears' criterion	**1.49**	**0.19**	**0.28**

*according to [168]

Results and discussion

In the following chapters the results obtained during the four studies are presented and discussed. A summary of the discussion and results is also reported for each work.

4 Coarse tar removal using readily available low-cost materials

Tar abatement in-situ and also ex-situ, as proposed in the hot gas filtration technology, through the use of low-cost materials with mechanical and chemical features suitable to efficiently handle different biomass feedstocks needing the same syngas cleaning treatment is considered a critical step [187]–[190]. Materials with high surface area and/or with active functional groups, i.e. O-containing groups, have been studied for the in-situ reduction of tar produced during biomass gasification and pyrolysis. The use of carbonaceous materials such as char and activated carbon for tar removal and/or cracking offers several advantages over the traditional Ni-based catalysts [95]. Activated carbon due to its huge surface area is an attractive material for tar abatement. Char offers different advantages to be used in tar abatement process: its in-situ production from the gasification of biomass makes it readily available and cheap, furthermore after deactivation, the spent char can be simply re-gasified or combusted recovering its energy content [58], [59].

In the present study the in-situ tar removal capacity of four materials was investigated and compared in a two-stage reactor with fixed bed configuration at three different temperatures (650°C, 700°C and 750°C). The volatiles were produced in the first stage from the pyrolysis of olive pomace and were forced to flow through the tar abatement bed (second stage). The selection of the bed materials was based on their specific area; hence to cover a wide interval of this parameter, activated carbon, alumina, char produced from the pyrolysis of olive pomace and pumice stone were utilized.

The study was divided in two campaigns. The first campaign comprised the evaluation of the effect of the temperature on the tar removal capacity of the materials. The temperatures chosen covered to range of temperature utilized in the high temperature hot tar filtration technology. The second campaign was dedicated to evaluating the deactivation of the tar removal capacity of the materials exposing the materials for extended period and keeping the temperature constant (700 °C). The method used is described in section 3.1.3 of the Experimental part (chapter 3)

Limitations of the experimental set-up

The main hindrance of the used experimental set-up is the irregular and not uniformly distributed tar feed to the bed materials placed in the tar removal reactor. This problem was caused by the used homemade feeding system and due to presence of nascent char which was deposited progressively during the experiment. Moreover, constant fluid dynamic conditions were not verified and probably were not achieved despite that all the experiments were performed using the same bed height. In addition, the method employed to condense and collect the tar was not comply to the European tar sampling and analysis Protocol [191] and hence comparison with results reported in the literature cannot be done straightforwardly. Another limitation stem from the use of a single fixed thermocouple located perpendicularly in the middle of the bed and thus the later could only track the temperature in one small portion of the bed. Nevertheless, as the goal of the study was the comparison of several materials under similar experimental conditions the results obtained can be used to drawn general conclusions about the tar reforming capacity of the different materials. Moreover, the total amount of tar obtained during the blank experiments using the same experimental set-up was used to quantify the tar removal capacity of the different materials by difference.

4.1 Effect of the temperature on the tar removal capacity of the materials

Table 4.1 shows the amount of bed material used and the tar removed at each of the studied temperatures. As the materials had different apparent densities the corresponding weight ensuring 8 cm bed height in the fixed reactor varied for each material. The highest tar removal percentages at each temperature were observed when the activated carbon was used. In this case, the value was not dependent on the external temperature as already at the lowest tested temperature this material removed 98% of the incoming tar. The high tar removal capacity of activated carbon has been attributed mainly to its high specific area. Mun et al. [69] studied the tar removal capacity of a commercial activated carbon on a two-staged sewage sludge air gasifier and observed a 6-fold reduction in the total amount of tar at 800 °C. The authors [69] measured 6 mg Nm^{-3} of tar at 700 while at 800 the tar concentration was 2 mg Nm^{-3}, blank tests at these temperature were not reported. The promising performance of the tested material was ascribed to its high specific surface area i.e. 950 m^2 g^{-1}. The lower tar concentration measured at 800 °C could be due to enhanced oxidation reaction in the gasifier which modified the amount and structure of the tar fed to the activated carbon fixed bed.

The use of char and pumice yielded similar tar removal results at each temperature studied despite having one-order of magnitude difference in the specific surface area of the materials. This outcome, could be ascribed to a less important role of the specific surface area than the presence of -OH, C-O and C=O groups and alkali/alkaline earth metals in the tar removal capacity of char at high temperatures as pointed out by several researchers [60], [61], [192].

The tar removal capacity of γ-Al_2O_3 was apparently independent of the temperature as in the case of the activated carbon. The tar removal using this material is known to proceed in a sequence of coking and reforming in the presence of steam and/or CO_2 [67], [193], [194]. In the present study, owing to the expected low content of steam in the feed stream to the fixed bed compared to the amount found in the producer gas coming from oxygen/steam

gasification processes, the reforming of the deposited coke is predicted to be limited. Thus, the temperature dependence of the tar removal capacity of γ-Al_2O_3 followed the coking reactions, which are less sensitive to the temperature than the reforming reactions. From **Table 4.1** the tar removal % achieved with γ-Al_2O_3 was greater than in the case of char and pumice.

The tar removal capacity normalized by grams of bed material at each temperature studied is depicted in **Figure 4.1**. It can be noticed that using this parameter the γ-Al_2O_3 exhibited the worst performance whereas at the highest temperature the activated carbon and char showed similar values. The tar removal capacity increment for char and pumice was greater when the temperature was increased from 650 °C to 700 °C.

Table 4.1 Tar removed at different temperatures after 50 g of biomass fed to the pyrolysis reactor.

	Weight of bed material (g)	tar removed (g)			Tar removed (%)		
		650 °C	700 °C	780 °C	650 °C	700 °C	780 °C
Activated carbon	45	7.8	7.8	7.8	98	98	98
γ-Al_2O_3	60	7.0	7.2	7.3	87	90	91
Char	40	5.4	6.3	6.8	67	78	86
Pumice stone	43	5.3	6.2	6.7	67	77	85

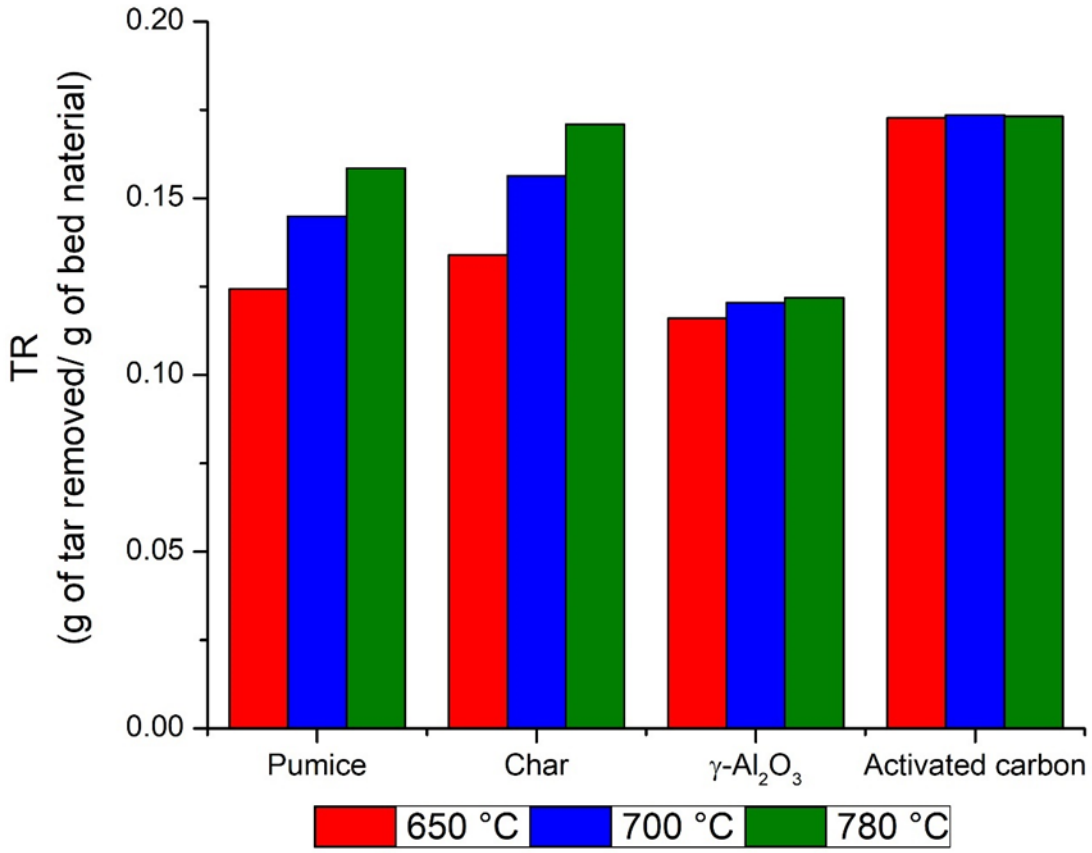

Figure 4.1 tar removal capacity of the bed materials at different temperatures.

Table 4.2 Average CO, CO_2, CH_4 and H_2 volume per gram of biomass obtained during the test carried out at 700 °C

	Non-condensable gas volume per gram of biomass fed (l @ 25 °C g^{-1} biomass)			
	CO_2	CH_4	H_2	CO
Activated carbon	0.07	0.05	0.10	0,07
γ-Al_2O_3	0.07	0.04	0.13	0,08
Char	0.06	0.03	0.06	0,05
Pumice stone	0.05	0.03	0.04	0,04
Blank	0.04	0.03	0.04	0,04

Table 4.2 shows the average gas volume per gram of biomass obtained at 700 °C for the four materials used as well as the values achieved during the blank test. An important increase in the H_2, CO and CO_2 values were observed when activated carbon and γ-Al_2O_3 were utilized. In the case of pumice stone, the attained values were practically unchanged with respect to the blank test, whereas when char was used a slight increment in the H_2 and CO_2 values were achieved. The larger increment observed for H_2 than for CH_4 suggested that coke formation followed by dehydrogenation rather than cracking reactions of higher molecular mass hydrocarbons prevailed in all cases. Similar results were obtained by Kuramoto et al. [193], Matsuoka et al. [67] and Hosokai et al. [194]

4.2 Deactivation of the material with time on stream

Table 4.3 shows the amount of bed material used and the tar removed after each run. The percentage tar removed that included the effect of the char deposited at the bottom of the pyrolysis reactor on the amount of tar fed to the tar removal reactor is more relevant than the amount of tar removed. However, the procedure and set-up adopted in the present work does not allow to use analogous amount of tar in the feed to the tar removal reactor during any of the three runs. In addition, the severity of the process is lessened from one run to the next. In any case the results are useful to compare different materials exposed to the same operating conditions.

The activated carbon showed the best performance exhibiting both the highest tar removal percentage and stability. On the other hand, a pronounced deactivation occurred in the case of char and pumice. Because the amount of tar fed to the tar removal reactor decreased with each run, the tar removal deactivation displayed by char and pumice is underestimated and is likely to be severer in a different set-up that consents constant feeding of tar at each run. According to Shen et al. [63] tar is adsorbed on the char matrix and undergoes polymerization reactions, producing hydrogen and soot, the latter staying over the char surface as solid deposits. This soot blocks the active sites, hindering the interaction of the active sites with the gaseous tar. Moreover, If the carbon deposition rate is higher than the

carbon consumption rate, soot will accumulate on the surface, decreasing the number of active sites available for reaction with tar molecules and then the biochar activity. Along with the same line, the decreased activity of the char observed in the present study could be ascribed to the lower carbon consumption rate than the carbon deposition rate caused by the soot deposited on the surface.

The deactivation behavior of char and pumice followed a similar trend with time on stream i.e. an initial relatively small loss of tar removal activity after run 2 was followed by a larger decrement of the tar removed during run 3. While in the case of γ-Al_2O_3 a less sharp deactivation was noticed, possibly because the larger amount of material used.

The coke deposited on the bed material at the end of the deactivation experiment is reported in **Table 4.4**. It is important to mention that the values are reported in weight percentages, hence depend on the amount of bed material used. Considering the amount of γ-Al_2O_3 used in the experiments the greater quantity of deposited coke after the deactivation was observed on this material. This high value is in line with the proposed tar removal mechanism [67], [193] for this material that was stated above.

Pumice and char showed analogous coke deposited. These values are, however, lower than the one observed using activated carbon despite the higher stability of the latter. The similar coke deposition values and deactivation behavior could be attributed to an analogous main tar removal mechanism while the slightly better performance of char might be due to the presence of alkali/alkaline earth metals on [60], [61], [192].

Comparing the coke deposited value and the activity and stability of char and pumice with that of activated carbon and considering that similar amounts of each bed material was used on the experiments, it appeared that the specific surface area played a major role on the tar removal performance of the activated carbon under the present conditions i.e. absence of oxidizing agent and ca. 700 °C.

Table 4.3 Tar removed after each of the three runs of 50 g of biomass fed to the pyrolysis reactor.

	Weight of bed material (g)	tar removed (g)			Tar removed (%)		
		run 1	run 2	run 3	run 1	run 2	run 3
Activated carbon	45	7.8	6.8	4.3	98	97	96
γ-Al_2O_3	60	7.2	6.1	3.6	90	87	81
Char	40	6.3	5.0	2.1	78	71	48
Pumice stone	43	6.2	4.8	1.6	78	69	36

Table 4.4 Coke deposited on the materials after the deactivation experiments

	Coke deposited (wt. %)
Activated carbon	13
γ-Al_2O_3	14
Char	8
Pumice stone	6

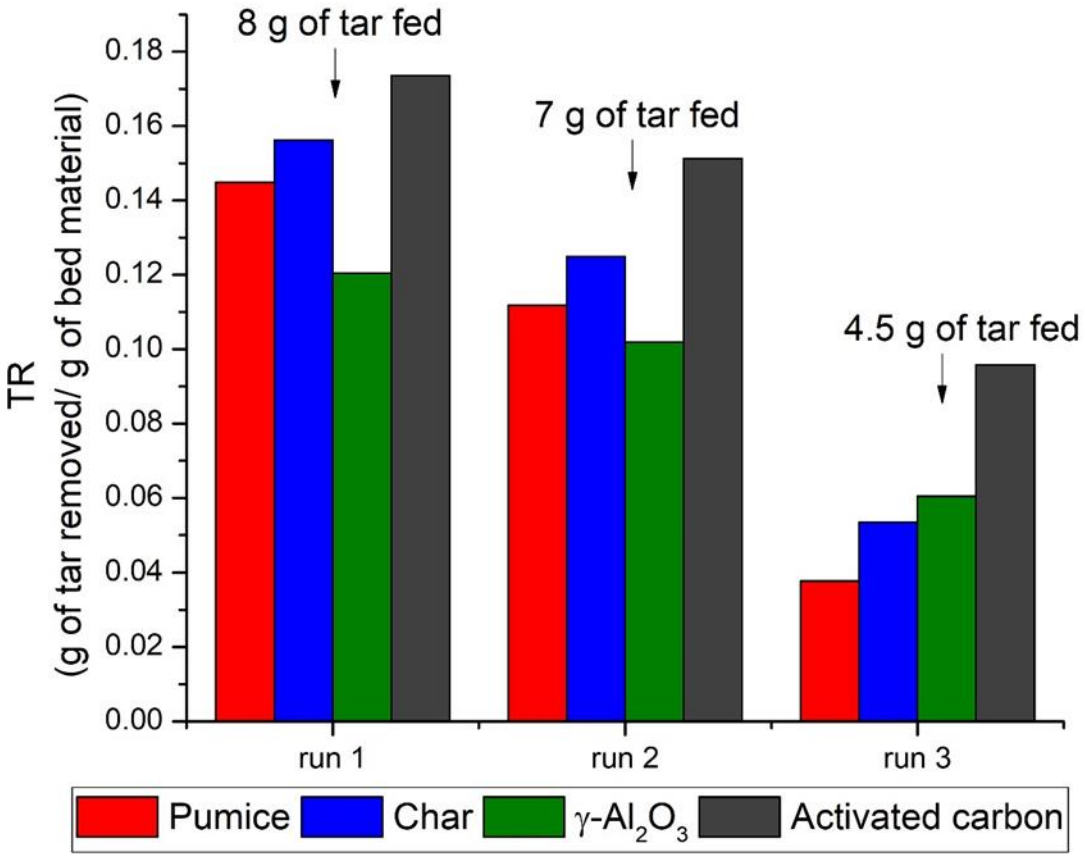

Figure 4.2 Deactivation of the tar removal capacity of the bed materials after 3 runs in series of 50 g of biomass each at 700 °C

The tar removal capacity normalized by grams of bed material after each run is depicted in **Figure 4.2**. Deactivation was significant with char and pumice as can be seen for the decrement of tar capacity from run 2 to run 3, the values obtained at the end of the later run are even lower than the value attained with γ-Al_2O_3.

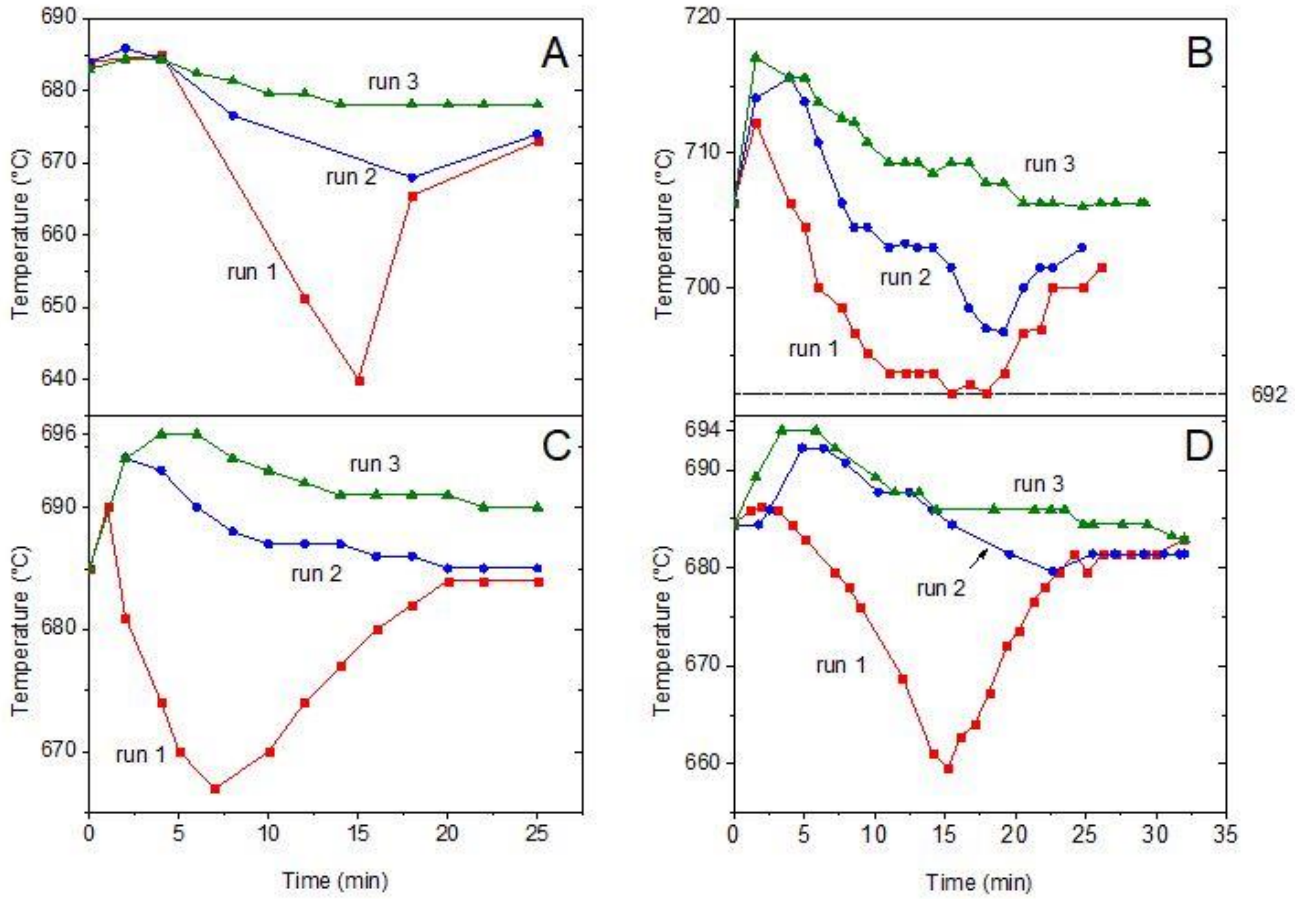

Figure 4.3 Temperature profile of the three runs at an external temperature of 700 °C. A) Char. B) γ-Al_2O_3. C) Pumice. D) Activated carbon.

To have a better understanding of the mechanism of tar removal and deactivation of the used materials, the temperature, average total dry gas flow rates (N_2 free basis) and flow rate of condensable compounds were measured during the deactivation experiments.

Figure 4.3 depicts the temperature profile during each run for the materials tested. Qualitatively the curves representing each run followed similar trends for all the materials. During run 1 a decrease in the bed temperature was observed that started with a delay of 2-5 minutes and had a maximum after 15 minutes except in the case of pumice. A progressively less pronounce decrease of the temperature is observed with each run.

In the present study the temperature decrease is supposed to be associated with cracking reactions of tar species [81] and more likely with the endothermic reduction reactions of coke i.e. water gas reaction, reverse Boudouard [9] and dehydrogenation. Therefore, the

temperature decrement was used as an indirect measure of the extent of cracking and coke endothermic reduction reactions over the materials.

From the temperature profile and considering the tar removal capacity and deactivation results it could be inferred that in the case of the low specific surface area materials i.e. char and pumice, their tar removal capacity depends on the availability of active sites capable of remove the coke deposited on the surface and once this sites are covered by coke, likely due to faster coking rate than gasification rate, these low specific surface area materials deactivated markedly as can be deduced from **Figure 4.3 A and C** and in **Table 4.3.** On the other hand, the activated carbon maintained its tar removal capacity during the three runs despite the evident attenuation in the extent of tar cracking and coke reduction reactions as inferred from **Figure 4.3 D**. After the first run the high tar removal capacity achieved with activated carbon could be ascribed to its high specific surface area capable of removed the tar by adsorption followed probably by coke formation. A similar conclusion can be drawn in the case of γ-Al_2O_3 although in this case, the possible presence of acid sites on its surface capable of enhancing the coking and successive dehydrogenation reactions could be the reason of its optimal tar removal capacity [68], [193].

Interestingly, activated carbon, pumice and γ-Al_2O_3 exhibited an exothermic peak at the beginning of the experiments lasting ca. 5 min, especially evidenced during run 2 and 3. This interesting result is in agreement with several authors [6], [195]–[197] who found that decomposition of cellulose, hemicellulose and especially lignin under inert atmosphere was endothermic at early stages of devolatilization followed by a predominantly exothermic behavior that was attributed to primary char formation. The reasons behind the absence of this exothermic peak during the tests with char were not investigated, more experiments are needed to clarify this behavior.

The average total gas volume on N_2-free basis per gram of biomass and average H_2 volume per gram of biomass are listed in **Table 4.5**. As the materials were exposed to the tar-containing gas for longer periods both the average total gas volume and the average H_2 volume decreased when activated carbon and γ-Al_2O_3 were used. Kuramoto et al. [193]

studied the tar removal performance of mesoporous γ-Al_2O_3 in a two-stage fluidized bed biomass gasifier. Upon long-term tar exposure the H_2 yield (mol mol^{-1} 100 g of C) decreased from ~15 to ~8 whereas the yields of carbon oxides and CH_2 did not vary at all [193]. As evidenced in **Table 4.5** The use of pumice stone did not affect the average total gas volume or the H_2 volume per gram of biomass compared to the blank experiment, while a slight improvement was observed in the experiments carried out with char. Contrarily, a significant improvement was observed in the case of activated carbon and γ-Al_2O_3 despite the fact that the temperature reduction during the first run in all the materials was roughly similar with the larger value found in the case of char. This interesting result warrants additional experiments and the use of additional temperature measurements along the bed.

Table 4.5 Average total gas volume on N_2-free basis per gram of biomass and average H_2 volume per gram of biomass

	Average total gas volume on N_2-free basis (l g $biomass^{-1}$ @ 25 °C)			Average H_2 volume (l g $biomass^{-1}$ at 25 °C)		
	run 1	run 2	run 3	run 1	run 2	run 3
Activated carbon	0.30	0.26	0.22	0.10	0.08	0.06
γ-Al_2O_3	0.35	0.30	0.26	0.13	0.10	0.09
Char	0.22	0.17	0.17	0.06	0.05	0.05
Pumice stone	0.17	0.17	0.17	0.04	0.04	0.04
Blank	0.16	0.16	0.16	0.04	0.04	0.04

4.3 Summary

A preliminary study of the tar removal capacity of activated carbon, in-situ prepared char, pumice stone and γ-Al_2O_3 was conducted. The tar was produced from the pyrolysis of olive pomace without addition of external oxidizing agents. The best performances were obtained with activated carbon and γ-Al_2O_3, in the former case the reason can be attributed to the high specific surface area that in addition to the expected improved adsorption capacity it also (directly and/or indirectly) acted as a catalyst to produce non-condensable gases from the tar. The excellent results observed with γ-Al_2O_3 could be ascribed to the plausible presence of acid sites on its surface capable of enhancing the coking and successive dehydrogenation reactions could be the reason of its optimal tar removal capacity. The pumice stone showed discrete performance, although in this case there were no signs of catalytic reaction enhancing the production of condensable gases. Finally, the tar removal performance of char was promising considering its relatively low specific surface area and mainly is availability and cost. Deactivation of the tar removal capacity of this material was rather fast and this needs to be considered in the design of the guard bed vessel, although the disposal of this material should not present serious problems

5 Steam reforming of toluene as tar model compound on Ni/mayenite synthesized using innovative procedures.

In spite of the extensive effort devoted to reduce the concentration of tar species inside the gasifier itself to the actual stringent values required for downstream applications, the results are still far from satisfactory [23]. Hence the use of cleaning and conditioning technologies downstream the gasifier is crucial to adhere to the requirements of end users. Amid those strategies, the catalytic steam reforming reaction is a promising solution because it can take advantage of the high temperature of the syngas at the gasifier exit, additionally, it has the potential to increase the amount of the most valuable gases i.e. H_2, CO and CH_4 present in the syngas while reducing the waste streams generated using the classic wet cold gas cleaning technologies [198].

The majority of commercial steam reforming plants for tar species from 1950 to 2009 had used nickel-based catalysts [198] and is still the most common active metal used nowadays. This trend can be ascribed to the optimum balance between cost and activity of nickel. However, deactivation by carbon deposition is still an unresolved problem that has negative consequences on the operational costs [86].

Many efforts for suppressing coke formation on Ni catalysts have been undertaken, from those studies it has been showed that the use of thermal-stable supports featuring high amount of "free" oxygen species related to the presence of hydroxide, peroxide and superoxide radicals can enhance the resistance of coke of nickel catalysts [14], [93], [199]. A pioneering work on the production of H_2 from catalytic steam reforming of bio-oil conducted by Wang et al. [98] tested the unique O^- storage and emission behavior of mayenite ($C_{12}Al_{14}O_{33}$). The authors speculated that the high initial activity of the Mg/mayenite catalyst could be attributed to reactions of the bio-oil vapor with the active O^- .

Li et al. [93] demonstrated the excellent performance of Ni/mayenite on the steam reforming of toluene, highlighting the carbon formation resistance and sulfur-tolerant ability of the catalyst. Di Carlo et al. [200] studied the steam reforming activity of a Ni/mayenite catalyst using a microreactor fed by a slipstream coming from a bench-scale fluidized-bed biomass gasifier. The catalyst maintained a high conversion (0.9) of heavy hydrocarbons for 12 h at 800 °C. The above referenced studies prepared the mayenite support using the solid-state reaction method. Li et al. [93] used $Ca(OH)_2$ and $Al(OH)_3$ as precursors whereas Di Carlo et al. [200] employed $CaCO_3$ to obtain $Ca(CH_3COO)_2$ and this compound was mixed Al_2O_3 to obtain the mayenite support.

In this section two different synthetic routes and the use of different precursors to produce mayenite were investigated and compared. The Ni/mayenite catalysts with a Ni loading of 10 wt% were obtained by wet impregnation and using a one-step preparation whereby the nickel was added during the support synthesis. The catalysts were tested in the steam reforming of toluene which is one of the most abundant tar compounds present in the producer gas from fluidized bed gasifiers [201]. Additionally, characterization of the synthesized support and catalysts was conducted to correlate the structural, morphologic and topologic features of the samples with their steam reforming performance. The experimental part of this study was described in section 3.2 of the chapter 3.

5.1 Fresh catalyst characterization

XRD patterns of the synthetized catalysts are shown in **¡Error! No se encuentra el origen de la referencia.**

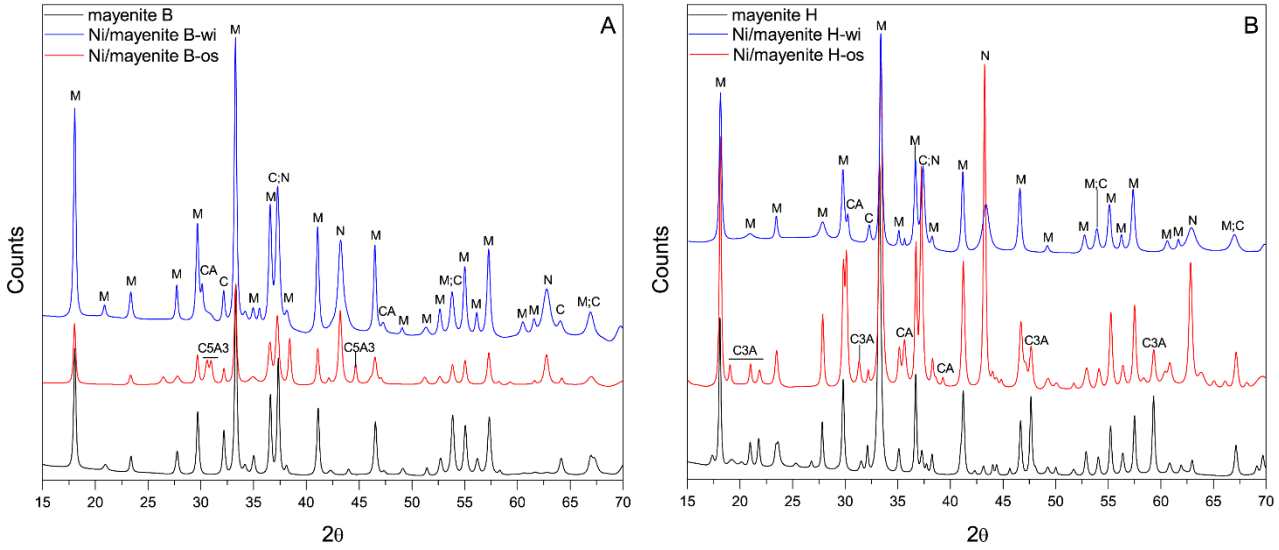

Figure 5.1 XRD patterns of maynetie synthetized by boehmite (**A)** and hydroxides (**B)** precursors. M ($Ca_{12}Al_{14}O_{33}$); C (CaO); N (NiO); CA ($CaAl_2O_4$); C3A ($Ca_3Al_2O_6$); C5A3 ($Ca_5Al_6O_{14}$).

The main crystal structures of both supports are similar despite of the different precursor used. The characteristic {211} and {420} reflections of crystalline $Ca_{12}Al_{14}O_{33}$ (18.1° and 33.3°) [94], [202], [203] and CaO (32.2°, 37.3°, 64.1°) can be distinguished. Furthermore, in the case of mayenite H (

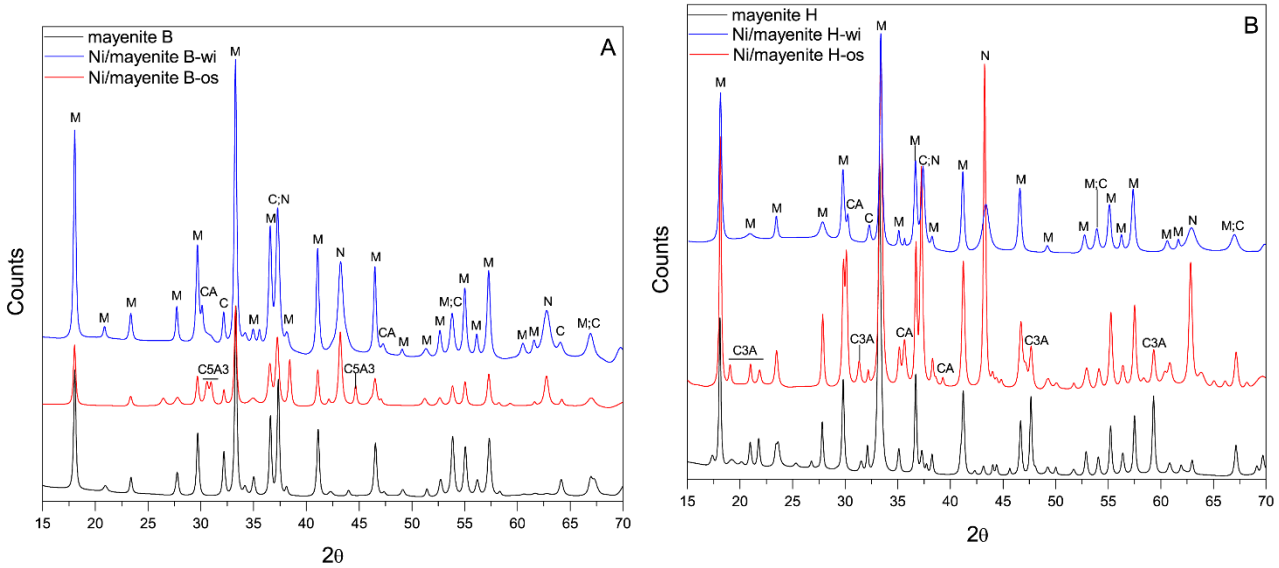

) diffraction rays corresponding to $Ca_3Al_2O_6$ (C3A) at 2θ angles of 20.9°, 21.7°, 47.6° and 45.5° are clearly detected. The presence of CaO was probably due to segregation of the Ca during the preparation [94], [203], whereas the presence of $Ca_3Al_2O_6$ is predicted as is an high temperature intermediates of mayenite formation. This latter exhibits wide crystals that prevent the formation of mayenite. Furthermore, as previously reported, this phase is common when powder reactants that lead to a heterogeneous mixture are used [204]. After Ni nitrate addition and calcination, neither $NiAl_2O_4$ spinel phase nor hydrated structures $Ca(OH)_2$ or formation of solid solution between NiO and CaO were identified. The Ni/mayenite catalysts showed the characteristic reflections of crystalline NiO at 43.2° and 62.8°. The wet impregnation method led in both cases to the formation of a little amount of $CaAl_2O_4$ phase probably due to the hydration and subsequent calcination stages used during the preparation. This phase was detected in larger amount in the Ni/mayenite H-os sample. Instead the Ni/mayenite B-os catalyst exhibited the doublet belonging to $Ca_5Al_6O_{14}$ (C5A3) at 2θ = 30.6 and 31.0°, which is recognized in the literature as the low temperature metastable phase (< 950 °C) in the Ca–Al–O system [204], [205].

Table 5.1 shows the nickel crystal size, BET surface area, pore volume and average pore diameter of the fresh calcined catalysts.

The diffraction patterns of catalysts after the in-situ activation (700 °C for 30 min in 0.5 NL min^{-1} of 16 % H_2/N_2 and then held at 750 °C for 1h) showed well defined diffraction rays of metallic nickel. The average crystallite size of metallic nickel (**Table 5.1**) is about 20–22 nm and 38-71 nm for the samples prepared by wet impregnation and one-step method, respectively.

The surface area of the mayenite B catalysts (mayenite B, Ni/mayenite B-wi and Ni/mayenite B-os) are higher than those of mayenite H (mayenite H, Ni/mayenite H-wi and Ni/mayenite H-os). The decrease in the surface area could be attributed to collapse of the pores in the samples, which occurs with an increase in the temperature (1250 °C compared to 950 °C) that lead to a high compaction of the crystals, as demonstrated by SEM images (**Figure 5.2**) and the lower pore volume values (**Table 5.1**). Furthermore, the catalysts obtained by wet

impregnation method (Ni/mayenite B-wi and Ni/mayenite H-wi) exhibits surface areas relevantly bigger than their respective support (mayenite B and mayenite H). The increase in the surface area after impregnation could be due to the hydration stage used during the preparation. Indeed, as previously reported [206], [207], the addition of the aqueous solution of nickel nitrate may lead to the formation of hexagonal $Ca(OH)_2$ that became porous CaO during the subsequent calcination step at 900 °C. Furthermore, the Ni insertion led to a general small increase of the surface area in all the catalysts, suggesting that the metallic nanoparticles did not fill the support's pore structure.

The obtained BET surface area values are in fair agreement with the reported values in the literature , regardless of the preparation method used, which values ranging from 2.5 to 24.3 $m^2\ g^{-1}$ [93], [94], [207]–[209].

Table 5.1 BET-BJH data for fresh catalysts

Catalyst	Nickel crystal size (nm)[a]	BET Surface Area ($m^2\ g^{-1}$)[b]	Pore Volume ($cm^3\ g^{-1}$)[c]	Average Pore Diameter (nm)[d]
mayenite B	-	4.1	0.015	1.9
Ni/mayenite B-wi	20.7	12.9	0.027	12.6
Ni/mayenite B-os	37.9	4.5	0.009	1.9
mayenite H	-	0.2	0.0007	26.7
Ni/mayenite H-wi	21.7	6.8	0.027	17.9
Ni/mayenite H-os	70.5	0.6	0.0022	20.3

[a] by XRD; [b] by BET equation; [c-d] by BJH desorption.

The morphological study of the obtained samples was accomplished using SEM-EDS (**Figure 5.2**). The mayenite B series consisted of well-defined laminar aggregates with nano-thickness ~50 nm. Ni/mayenite B-wi displayed NiO crystallites, not uniformly distributed on $Ca_{12}Al_{14}O_{33}$, as evidenced in **Figure 5.2**. Ni/mayenite H-wi instead exhibited a microstructure of $Ca_{12}Al_{14}O_{33}$ formed by dendritical aggregates. The lower specific surface area and poorly developed pore structure of Ni/mayenite H-os effectively inhibited the dispersion of Ni active metal, as shown by EDS maps in **Figure 5.2**.

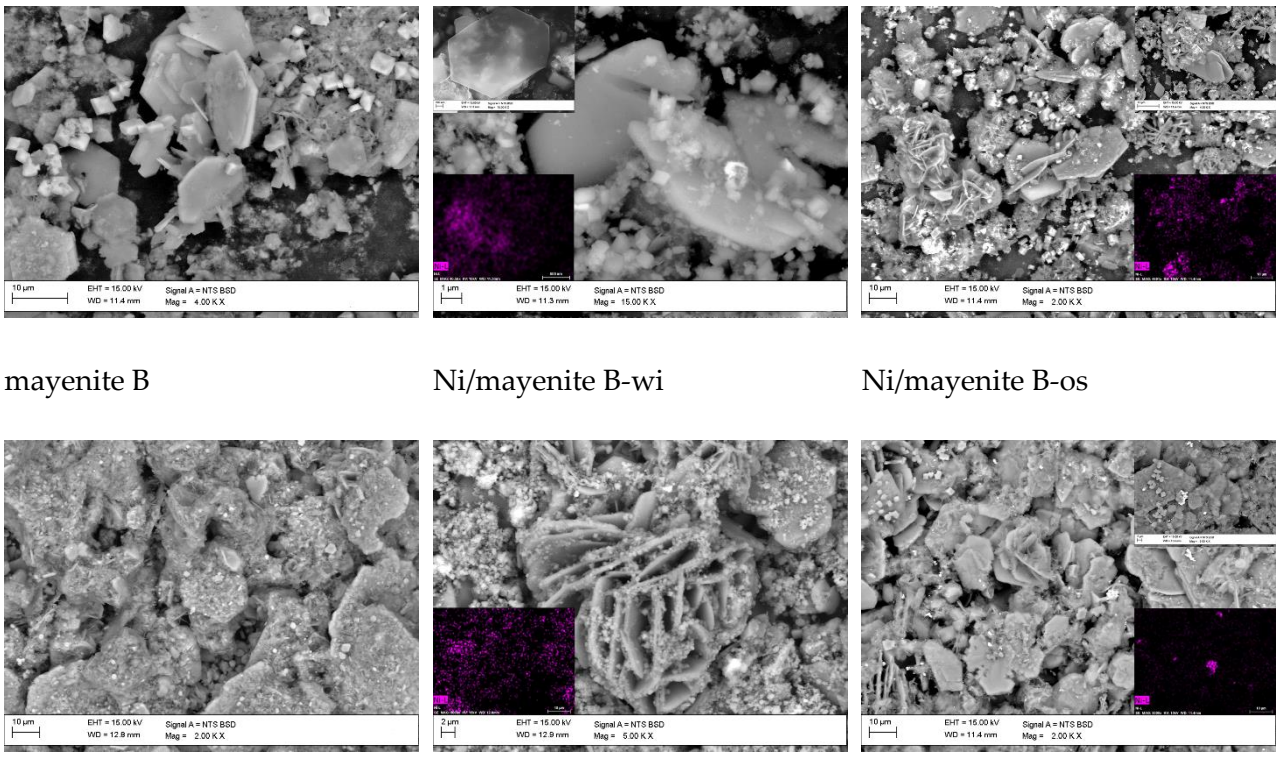

mayenite B | Ni/mayenite B-wi | Ni/mayenite B-os

mayenite H | Ni/mayenite H-wi | Ni/mayenite H-os

Figure 5.2 SEM micrographs showing the Ni dispersion on the synthetized catalysts. EDS maps of Ni are included as insets.

TPR profiles of Ni/mayenite catalysts in **Figure 5.3** were used to estimate the Ni available for reduction. The reduction degree calculated considering the theoretical nickel loading is listed in **Table 5.2**.

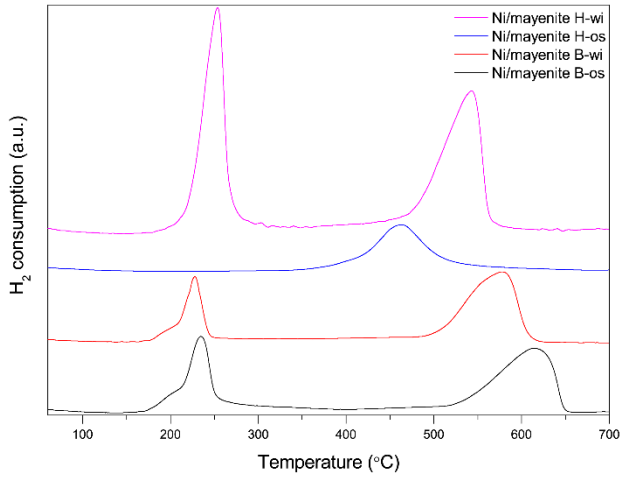

Figure 5.3 Temperature programmed reduction (TPR) profiles of the Ni/mayenite catalysts

On all the catalysts the main H_2 consumption was observed in the temperature range between 150 and 650 °C. On Ni/mayenite B catalysts the main reduction peaks, observed around 230 and 615 °C, lead to a reduction degree of 66 and 63 % for Ni/mayenite B-wi and Ni/mayenite B-os, respectively. The peak at lower temperature could be ascribed to the reduction of isolated NiO particles [210], [211] with smaller size and very finely distributed, which weakly interacted with or were far from the support and then easier to reduce. For higher temperatures, the reduction peak at 615 °C can be ascribed to a stronger interaction state of NiO with the mayenite support and CaO [212], [213]. The area corresponding to the reduction of these latter Ni species is the largest among the peaks detected, denoting that Ni bonded to the mayenite support are the principal Ni species in this catalyst. As previous reported, the strong interaction of Ni^{2+} ions with the mayenite support reduce the mobility and agglomeration with other Ni particles on the surface [94]. The peaks were slightly shifted to lower temperature for the Ni/mayenite B-wi sample. Furthermore, the Ni-based reduction degree (**Table 5.2**) on the B-wi catalysts is higher than that on the B-os catalysts. This behavior can be interpreted as a consequence of the stronger interaction between Ni and mayenite introduced by the one step method. The highest reduction degree was

obtained with the Ni/mayenite H-wi catalyst (83.23%). In this case the area associated with the low and high reduction temperature peaks were identical. From Table 3it is possible to identify on this latter catalyst that the temperature and the H_2 consumption of the low temperature reduction peak were considerably higher than the corresponding values of the Ni/mayenite B catalysts. This result could be ascribed to higher content of isolated NiO particles in this catalyst as reported by Cabello et al. [211]. Furthermore, the high temperature reduction peak was shifted to lower temperatures with respect to the Ni/mayenite B catalysts, this result, as stated above, could suggest a weaker metal-support interaction. It is well documented [214]–[216] that the strong nickel-support interactions are beneficial for the enhancement of the catalysts stability and the carbon deposition tolerance. Considering the obtained TPR it is expected that the catalyst where the strongest Ni-support interactions were present was the Ni/mayenite B-os (**Table 5.2**). On the other hand, the reduction degree of Ni/mayenite H-os was only about 5%, probably due to the high calcination temperatures markedly decreasing the accessibility of nickel and thus its reducibility [169], [217]. From the TPR profiles of the synthetized catalysts, the reduction temperature for catalysts testing was set at 700 °C, in order to reduce an important proportion of the Ni^{2+} species with weak and high interaction with the mayenite support.

Table 5.2 Catalyst properties after H_2 temperature-programmed reduction (TPR) experiments

Catalyst	Content (10^{-3} mol g_{cat}^{-1})	Main consumption peaks (°C)	H_2 consumption (10^{-3} mol g_{cat}^{-1})	Reduction degree[(a)] (%)
Ni/mayenite B-wi	1.7	228; 578	0.31; 0.81	66.0
Ni/mayenite B-os		235; 614	0.44; 0.64	63.31
Ni/mayenite H-wi		253; 543	0.71; 0.71	83.23
Ni/mayenite H-os		460	0.09	5.08

(a) based on H_2 consumption data and the theoretical nickel loading.

5.2 Steam reforming of toluene (STR)

Thermodynamic considerations

From the equilibrium calculations conducted using the Aspen plus V8.8® software the following vol. % dry composition of the gas was obtained: H_2 = 21.2 %, CO = 2.7 %, CO_2 = 6.6 % and CH_4 = 4.0 x 10^{-3}. Carbon conversion at 700 °C was 1 i.e. complete carbon conversion. Moreover, carbon conversion was 0.99 at the lowest temperature used in this study i.e. 620 °C. The influence of the excess of steam on the WGS reaction and hence on the equilibrium H_2 vol. % value that can be obtained considering only the steam reforming (SR) and WGS reactions was explored using the equilibrium reactor of Aspen plus V8.8® with the same thermodynamic method as in the Gibbs reactor case. First the simulation was run setting only the SR reaction. Next a second run was done but this time both the WGS and SR reaction were set. The difference in the H_2 vol. % of the two simulations was due to the WGS reaction induced by the excess of steam. The share of the WGS reaction on the equilibrium H_2 vol. % value decreased from 27 to 25 % when the temperature increased from 620 to 740 °C

Experimental results

Ni/mayenite H-os did not show any steam reforming activity at the experimental conditions used in the present work, thus it was not considered in the figures of the results and discussion section. This outcome could be attributed to its unfavorable structural and morphological features as discussed in the fresh catalyst characterization section. Moreover, the low reduction degree of the nickel present in this catalyst could also contributed to its negligible STR conversion.

The conversion as a function of time-on-stream (ToS) at 700 °C is shown in **Figure 5.4**. In the case of Ni/mayenite B-wi and Ni/mayenite H-wi a similar trend was observed. These catalysts exhibited high conversion values which a slight deactivation towards the end of the test. On the other hand, lower but stable values were obtained using Ni/mayenite B-os. The lower activity of the latter catalyst could be attributed to the higher nickel crystal size and/or due its lower reduction degree which is related to a lower amount of potential

chemically actives sites and hence lower conversions. Contribution to the observed lower conversion by virtue of the degradation of the support and the presence of NiO after the tests as found during the characterization of the spent catalyst cannot be excluded. After 6 h ToS analogous carbon conversion values were observed for the three catalysts.

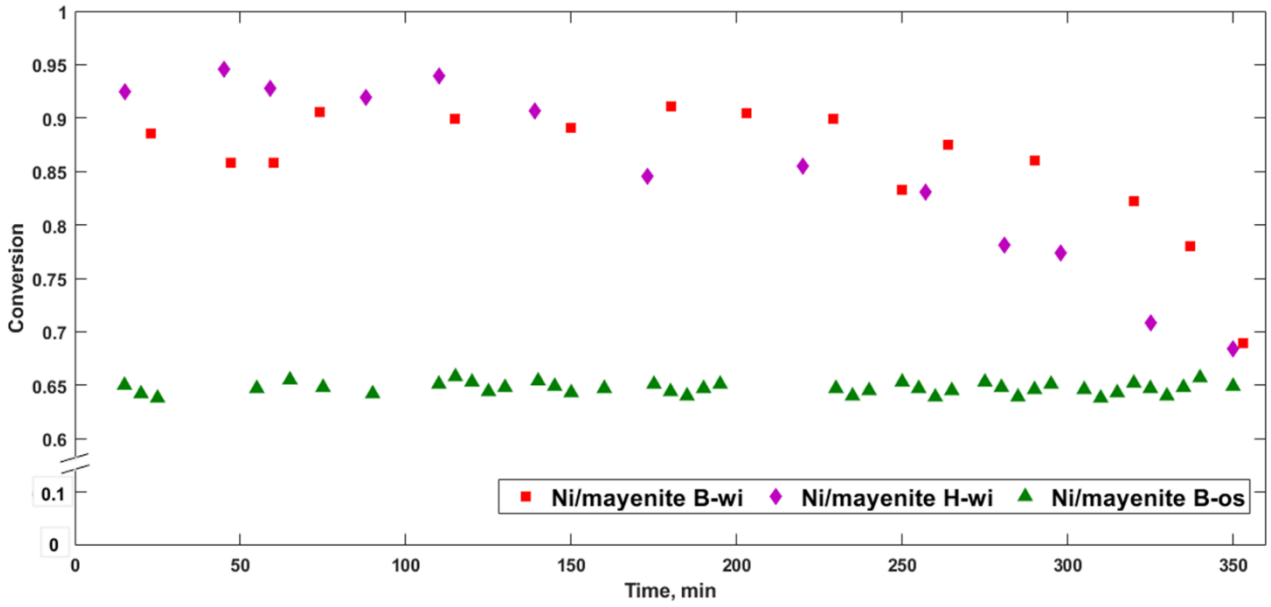

Figure 5.4 Toluene conversion as a function of time-of-stream (ToS) at 700 °C.

The S_{H_2} obtained values illustrated in **Figure 5.5** were proximate to 1 throughout the entire experiment, being slightly lower in the case of Ni/mayenite B-os.

Based on these results it is safe to say that the extent of the reactions other than the complete steam reforming of toluene to carbon oxides and hydrogen was insignificant. Moreover, the activity decrease observed at the end of the test for Ni/mayenite B-wi and Ni/mayenite H-wi did not affect the S_{H_2} achieved with these catalysts.

The conversion as a function of temperature is depicted in **Figure 5.6**. As in the conversion as a function of ToS the Ni/mayenite B-wi and Ni/mayenite H-wi catalysts showed a comparable activity, besides the curves seemed to follow a linear relationship. A lower activity was observed for Ni/mayenite B-os as expected from the results obtained during the six hour-long tests. The latter catalyst needed higher temperature to equal the conversion values achieved with catalysts synthesized by wet impregnation.

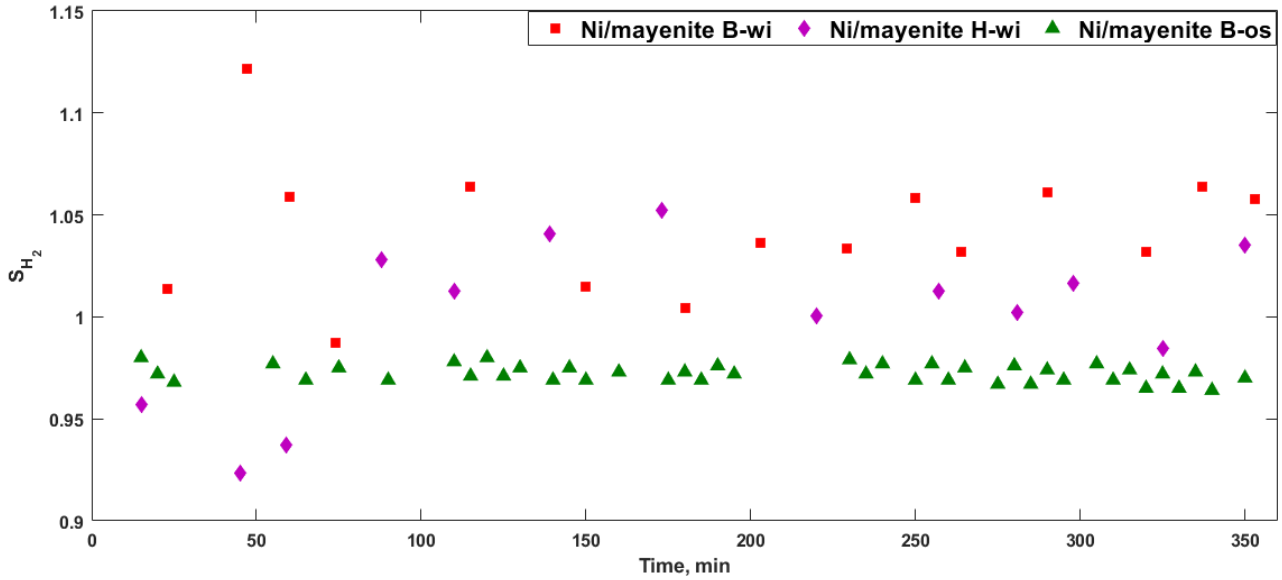

Figure 5.5 S_{H_2} Hydrogen selectivity parameter to identify whether reactions other than those described in the selected reaction network occurred at 700 °C.

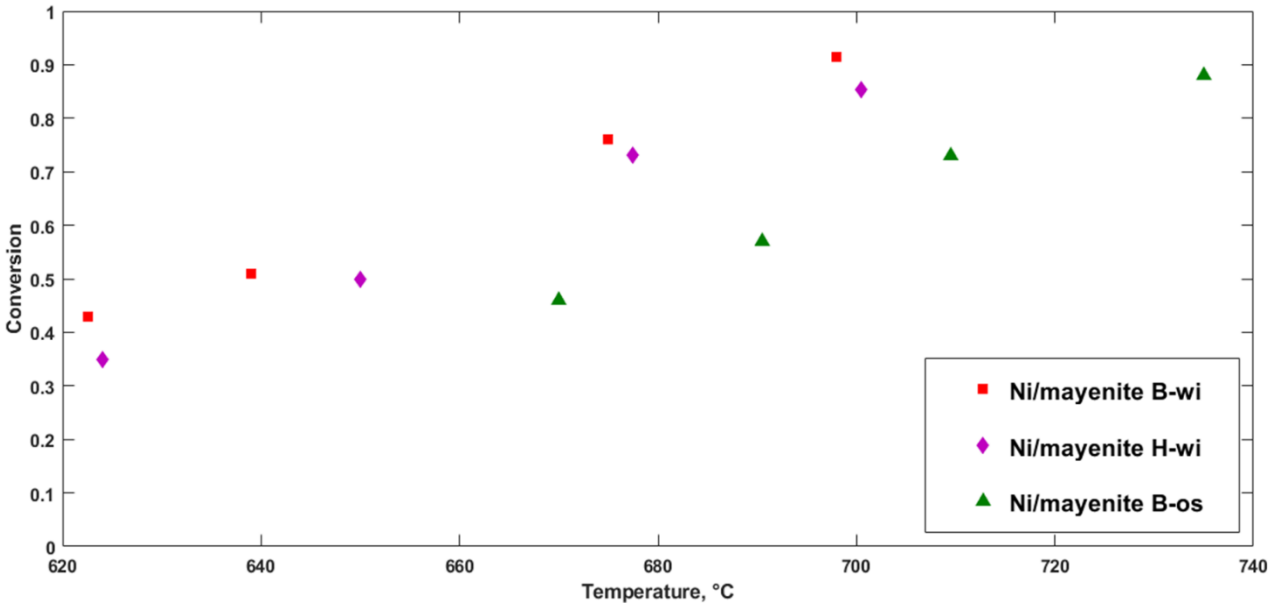

Figure 5.6 Toluene conversion as a function of temperature at S/C=5.

Table 5.3 shows the measured gas volumetric flow rate (N_2-free basis), the concentration of H_2, CO and CO_2 and the calculated hydrogen selectivity S_{H_2} at three different temperatures for the three catalysts considered. As expected, the gas flow rate and the measured concentration of non-condensable gases increased with temperature. The highest CO_2 vol% values were obtained with Ni/mayenite B-os despite the higher temperature applied during the tests with this catalyst. This result could be ascribed to a higher WGS reaction activity

of the catalyst synthesized with the one-step procedure. S_{H_2} values were close to 1 in all cases, hence, it can be assumed that in the studied operating conditions the extent of reactions forming or consuming hydrogen other than the reactions based on **Eq. 3.2** and **Eq. 3.3** were negligible.

As stated above from the equilibrium carbon conversion calculations almost complete carbon conversion was reached already at the lowest applied temperature of this study. From the experimental results showed in **Figure 5.6** is evident that the tests were performed far from the equilibrium, specially the experiments done at temperatures ≤ 650 °C with the catalysts synthesized by the wet impregnation method. Additionally, considering the $S_{H_2}^{II}$ values and the CO_2, CO and H_2 equilibrium values showed in **Table 5.3** it can be concluded that the WGS reaction was far from equilibrium and was controlled by the kinetics of the process for the whole range of temperature applied.

Interestingly, CH_4 was not detected during the steam reforming experiments carried out in the present study. Probably, the methanation reaction did not occur in the present catalytic system. Furthermore, it can be speculated that the extent of reactions forming methane e.g. hydrodealkylation, were negligible and/or the methane formed was converted to CO, CO_2 and H_2. According to Mukai et al. [218] the most abundant intermediate in the steam reforming reaction of toluene at 600 °C on a $Ni/La_{0.7}Sr_{0.3}AlO_{3-\delta}$ was C_2H_4. However, in the present study C_2H_4 was not detected in any of the tests. The results observed in the present study are in agreement with Świerczyński et al. [169] who observed only CO, CO_2 and H_2 when the catalyst temperature was ≥ 650 °C using a Ni/olivine catalyst during the STR with a space-time of 9 kg_{cat} h m^{-3} at 25 °C. Koike et al. [219] did not detect any traces of CH_4 after steam reforming of phenol at 600 °C over a Ni-Fe/Mg/Al catalyst. It is noteworthy to mention that the CH_4 vol % at equilibrium was 0.04 % at 620 °C.

Table 5.3 Total dry gas flow rate (N_2-free basis) and main non-condensable gases measured at the outlet of the reactor at different temperatures.

	Ni/mayenite B-wi			Ni/mayenite H-wi			Ni/mayenite B-os		
Cat. Temperature (°C)	623	639	675	624	650	678	690	710	735
Total dry gas flow rate, N_2-free basis (l min^{-1} at 25 °C)	0.04	0.07	0.09	0.03	0.05	0.09	0.03	0.07	0.09
H_2 (vol. %)	7.5	12.7	17.3	7.2	12.4	17.3	7.1	12.4	17.3
H_2 equilibrium (vol. %)	21.6	21.6	21.4	21.6	21.5	21.4	21.3	21.2	21.0
CO_2 (vol. %)	1.9	2.9	4.0	1.9	2.9	4.4	2.0	3.5	5.0
CO_2 equilibrium (vol. %)	7.1	6.9	6.7	7.1	6.9	6.7	6.6	6.5	6.3
CO (vol. %)	1.8	3.5	4.6	1.6	3.3	4.0	1.4	2.3	3.1
CO equilibrium (vol. %)	2.1	2.3	2.6	2.2	2.4	2.6	2.7	2.9	3.1
$S_{H_2}^{II}$	0.97	0.98	0.99	0.98	0.98	0.98	0.96	0.98	0.98

5.3 Kinetic parameters

The k_{app} as a function of temperature for the STR is showed in **Figure 5.7**. In the case of Ni/mayenite B-os the higher temperature at which the k_{app} values presented a sharp increment could be attributed to a different interaction between the support and the nickel active sites in comparison with Ni/mayenite B-wi and Ni/mayenite H-wi as evidenced by

the TPR results. Although strong metal-support interactions are linked with better stability and higher carbon deposition tolerance, some studies[220], [221] stated that the strong metal-support interactions could led to reduction of the amount of chemically active nickel and as a consequence to lower steam reforming conversions. The k_{app} values observed in the present work are comparable with the values obtained by Aznar et al. [154] who studied the steam reforming of a slip-stream taken from a fluidized bed gasifier on commercial nickel catalysts. It should be stressed that the authors [154] used a guard bed which reduced significantly the inlet tar concentration and likely change the composition of the tar, leaving mainly the most recalcitrant components such as benzene and toluene unaltered [222]. When the k_{app} values are computed considering the total wet gas flowrate instead of the N_2-free flowrate a reasonable agreement is found also with the values obtained by Świerczyński et al. [169] who studied the STR in the temperature range of 560 °C to 800 °C

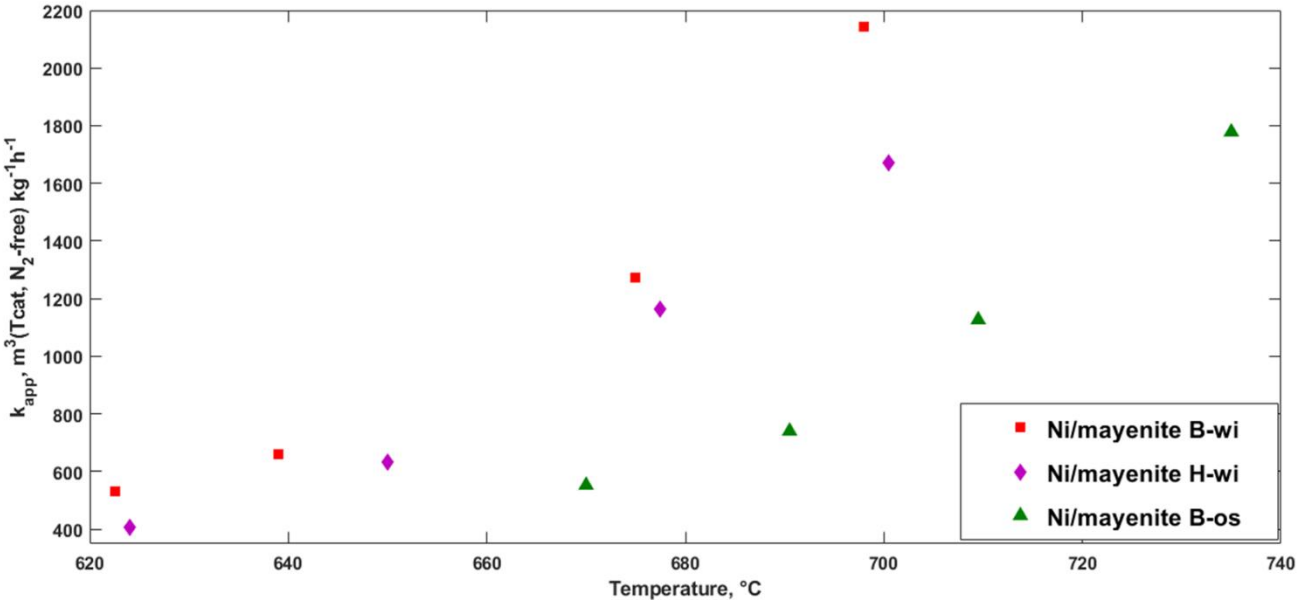

Figure 5.7 k_{app} as a function of temperature for Ni/mayenite B-wi, Ni/mayenite H-wi and Ni/mayenite B-os.

The kinetics parameter for Ni/mayenite B-wi, Ni/mayenite H-wi and Ni/mayenite B-os are listed in **Table 5.4**. Representation of the obtained k_{app} values according to the Arrhenius equation yielded a fair concordance, as shown in **Figure 5.8**, with coefficient of determination values ≥ 0.98 (**Table 5.4**). The Activation energy values obtained for the three catalysts were similar, therefore, analogous chemical nature of nickel active sites is proposed

for all the catalyst. The activation energy values for the steam reforming reaction of toluene and benzene reported in the literature span from 36 to 230 kJ mol^{-1} [93], [161], [223]–[226]. The wide range of values are mainly due to difference in experimental conditions used as well as in the reactor model employed in the various studies. Mukai et al [223] separated the activation energy values in two temperature regions, namely low (≤ 530 °C) and high (≥ 530 °C) temperature. The authors [223] found activation energy values of 113 and 36 kJ mol^{-1} for the low and high temperature region, respectively, using a Ni/$La_{0.7}Sr_{0.3}AlO_{3-\delta}$ calcined at 800 °C. A change in the rate-determining step was thought to be the cause of the change in the activation energy value, the former change was attributed to the lattice oxygen contribution which was found to be important at temperatures ≥ 550 °C. In the present study no distinction was made between low and high temperature regions. Further kinetics studies are required to elucidate this argument. It should be pointed that using the conversion values corresponding to the highest temperature of each sample presented did not comply with the Mears' criterion for absence of external mass transfer

Table 5.4 Kinetic parameter for Ni/mayenite B-wi, Ni/mayenite H-wi and Ni/mayenite B-os.

	Ni/mayenite B-wi	Ni/mayenite H-wi	Ni/mayenite B-os
Ea (kJ mol^{-1})	134	137	145
A (m^3(Tcat) kg^{-1} h^{-1})	3.2 x 10^{10}	3.9 x 10^{10}	5.7 x 10^{10}
R^2	0.98	0.99	0.98

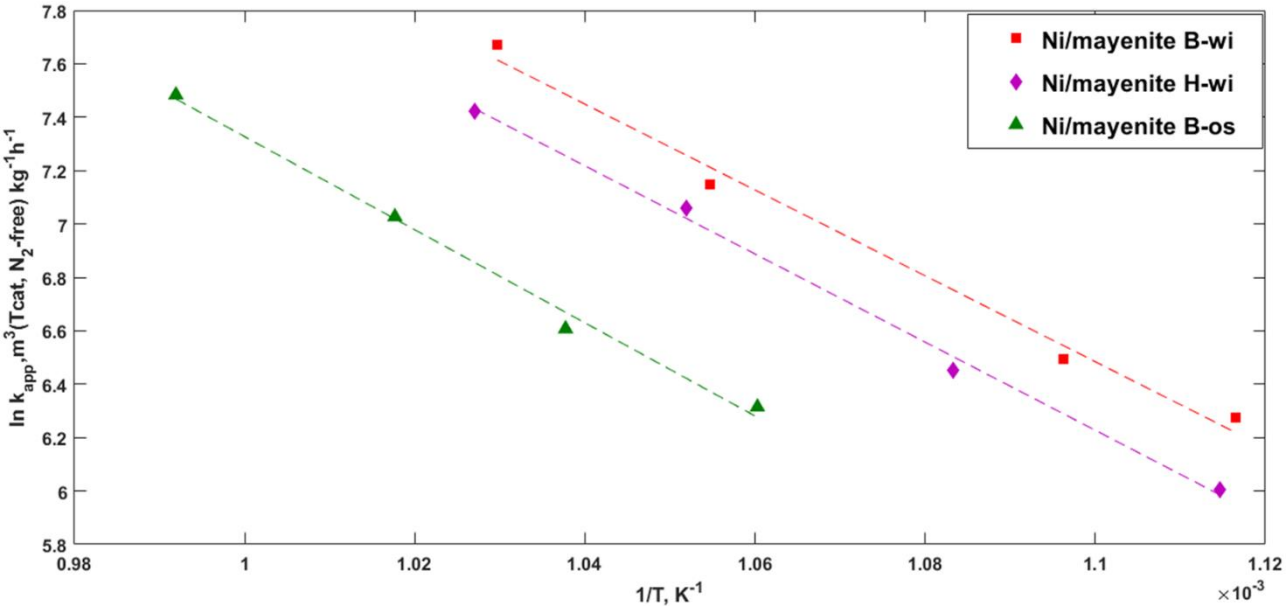

Figure 5.8 Arrhenius representation for the k_{app} values of the steam toluene reforming.

5.4 Characterization of the spent catalysts

The used catalysts were analyzed by means of X-ray diffraction and thermogravimetric oxidation (TPO) analyses to investigate changes in their crystalline structure and to determine the coke content formed during catalytic test.

The XRD profiles of the spent catalysts after 6 h ToS, are presented in **Figure 5.9 A**.

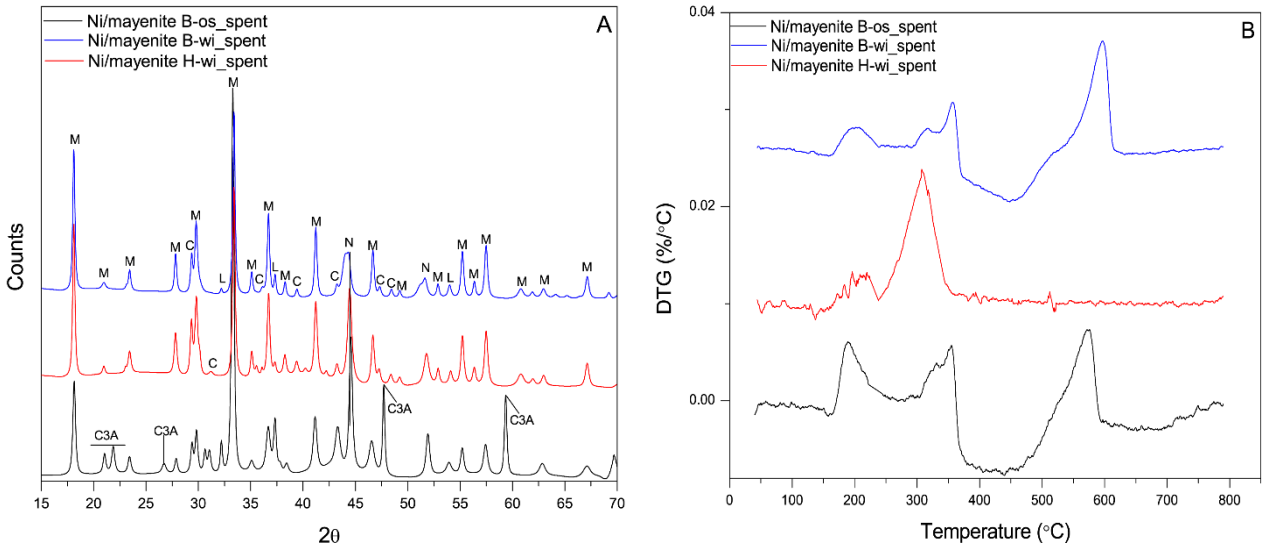

Figure 5.9 (A) XRD patterns of used mayenite. M ($Ca_{12}Al_{14}O_{33}$); L (CaO); N (Ni); C ($CaCO_3$); C3A ($Ca_3Al_2O_6$). **(B)** DTG-TPO profiles of spent catalysts used in the steam reforming of toluene

Diffractograms of spent samples are quite similar to those of the fresh samples. The similarity of the XRD patterns before and after the tests means that the crystalline structure of the Ni and the support did not suffer significant changes during the catalytic tests, irrespective of the composition of the catalyst. Furthermore, no trace of carbon (crystalline phase) was detected on the catalysts after the reforming test. In the XRD pattern in addition to Mayenite, CaO and Ni, also $CaCO_3$ (4.8% for Ni/mayenite B-os, 4.3% for Ni/mayenite B-wi and 11% for Ni/mayenite H-wi) was identified in all the catalysts, which is due to the CO_2 uptake by carbonation reaction on CaO during the steam reforming tests [213]. As previous reported, carbon dioxide removal by adsorption on a solid provide further heat to the reforming reaction that may lead to a higher hydrogen yield. [207]. Additionally, CO_2 sorption by the support could shift the WGS equilibrium reaction to the products side hence promoting the production of H_2 [208]. Furthermore for Ni/mayenite B-os $Ca_3Al_2O_6$ (41.5%) and NiO (7.8%) can be detected, which are a degradation phase of mayenite under humid condition [227] and unreduced Ni, respectively.

From the XRD analysis it is possible to determine the size of the metallic Ni crystallites in the used catalysts by applying the Scherrer equation to the (1 1 1) diffraction line at 2θ = 44.5°. The obtained values after the 6 h long test for the three catalysts are showed in **Table 5.5**

When the fresh and spent catalyst are compared, it is evident that the Ni/mayenite B-wi catalyst showed the largest Ni crystallites increment after use, which could be related to the fact that the isolated NiO species in this sample required the lowest temperature among the studied catalysts and this result is generally linked with high mobility of these species that upon reaction are also the most sensitive to agglomeration phenomenon. In the other cases, after the tests the increase of the Ni crystallite size was notably lower or almost unchanged, therefore it can be deduced that the partial deactivation of the Ni/mayenite H-wi during the 6-hour-long test was not related to the growth or agglomeration of Ni crystallites.

In

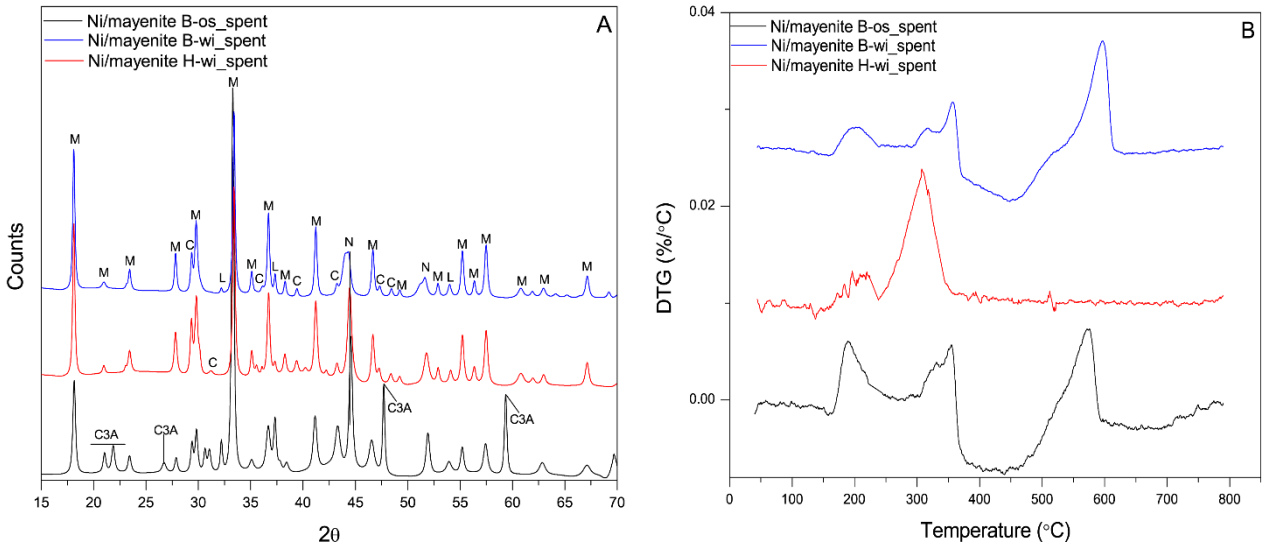

B the DTG-TPO profiles corresponding to the different catalysts used are reported. The DTG profiles of the mayenite obtained by boehmite precursor are similar in the two used catalysts, showing three major peaks at around 200 °C, 350 °C and 600 °C. The percentage of deposited carbon corresponding to each peak is summarized in **Table 5.5**. As widely reported in the literature, the peak at 200 °C can be attributed to the coke deposited on the metal active sites on the surface of the catalyst [228], [229]. The peak at 350 °C, much higher than the previous for Ni/mayenite H-wi, could be related to the oxidation of filamentous carbon species at the metal-support interface and the last high peak appearing at 600 °C could be associated to the oxidation of graphitic carbon species, less reactive and thus oxidized at higher temperatures [83], [94]. No trough related to nickel oxidation was obtained in the case of Ni/mayenite H-wi, probably the oxidation occurred before the measurement, for example during cooling of the catalyst. The oxidation profiles of the used catalysts obtained are similar, but with some differences in the intensity of the oxidation peaks. As shown in **Table 5.5** the Ni/mayenite B-wi catalyst showed peaks with highest percentage at 350 and 600°C compared to the Ni/mayenite B-os counterpart. It is possible that the bigger size of the Ni particles observed on the Ni/mayenite B-os catalysts (**Table 5.5**) aided in the reduction of the the amount of filamentous carbon species, which is typically formed on small Ni particles, as in Ni/mayenite H-wi. Furthermore, in the case of Ni/mayenite B-wi the carbon deposits were mainly graphitic, thus difficult to remove and responsible for catalyst deactivation as noticed at the end of the experiment. The

Ni/mayenite H-wi showed a total amount of coke similar to that of Ni/ mayenite B-wi with an intense peak corresponding to the filamentous carbon species. Therefore, deactivation of the catalysts as observed at the end of the test in **Figure 5.4** could be presumably ascribed to carbon deposition. Interestingly, similar deactivation behavior for Ni/mayenite H-wi and B was observed regardless of the nature of the carbon deposited on the catalysts.

Table 5.5 Average crystallite size of the NiO particles and carbon deposited per unit mass of catalyst.

Catalyst	Crystal size (nm)	Carbon deposited at the three temperatures (%)		
		200 °C	350 °C	600 °C
Ni/mayenite B-wi	31.52	0.19	0.36	0.52
Ni/mayenite B-os	37.86	0.23	0.14	0.10
Ni/mayenite H-wi	27.02	0.10	0.92	0.00

The total (sum) carbon deposited on the catalysts in mg of carbon per g of catalyst (mg of C g of cat.$^{-1}$) after a 6-h-long test at a temperature of 700 °C using toluene as tar model compound is summarized in **Table 5.6**. The peak at 200 °C was considered because this type of carbon can move from the metal to the interface of metal-support where further dehydrogenation and polymerization reactions are likely to occur [228], ultimately developing into filamentous or graphitic carbon. For comparison purposes, the obtained amount of carbon deposited values together with the main experimental conditions as well as the catalysts used and the nickel addition method of several studies taken from the literature are showed in **Table 5.6**.. In general, the values for the carbon deposited on the catalysts are in agreement with the obtained values in this study as the above-

mentioned catalysts were prepared with the aim of reduce the carbon deposition on the catalyst. Notably, the reported carbon deposited on the traditional Ni/α-Al_2O_3 catalyst was one order of magnitude higher than the values measured in the present study.

Table 5.6 Carbon deposited values in addition to the main experimental conditions applied in the corresponding experiment.

Catalyst	Nickel addition (method and loading)	Experimental conditions	Carbon deposited (mg of C g of cat.$^{-1}$)	Reference
$Ni/La_{0.7}Sr_{0.3}AlO_3$	Wet impregnation 5 wt. %	$C_7H_8/H_2O/Ar$ = 3/42/55 vol. % (total 100 ml min^{-1}); GHSV = 12000 h^{-1}; S/C = 2; T= 600 °C; ToS = 180 min.	57	[230]
Ni/α-Al_2O_3			431	
$Ni/LaAlO_3$			800	
Fe_3Ni_8/Palygorskite	Co-precipitation Ni = 8 wt. % Fe = 3 wt. %	C_7H_8 = 3000 ppm; cat. = 0.5 g; ToS = 100 min; T = 700 °C; S/C = 1.	12.2	[226]

		S/C = 1.5	10.9	
		S/C = 2	11.1	
Ni-Fe/Mg/Al	Co-precipitation during the support synthesis (one step) Ni = 12 wt. % Fe = 3.1 wt. %	$C_7H_8/H_2O/Ar$ = 0.75/8.9/26.8 mmol min^{-1}; T = 600 °C; ToS = 80 min; W/F = 0.014 g h mol^{-1}; S/C = 1.7	6.7	[219]
Ni/Mg/Al	Co-precipitation during the support synthesis (one step) Ni = 12 wt. %		79.4	
Ni/mayenite B-wi			10.7	
Ni/mayenite H-wi	Wet impregnation 10 wt. %	C_7H_8 = 47 g Nm^{-3}; GHSV = 73750 h^{-1}; W/F = 0.33 g h mol^{-1}; S/C = 5; ToS = 360 min; T = 700 °C	10.2	The present study
Ni/mayenite B-os	During the support synthesis (one-step) 10 wt. %		4.7	

5.5 Summary

Mayenite and Ni/mayenite catalysts were prepared using two new procedures. Mayenite was synthetized starting from a slurry of the precursors in hydroxide form or alternatively from a gel of boehmite and calcium nitrate, each calcinated at the suitable temperature determined by TGA-DSC. The hydroxides slurry route appears of particular interest for the lower cost of the precursors and the easier and faster preparation, however its calcination temperature was higher (ΔT= 300 °C) than in the case of gel route. A trade-off between the cost of precursor and severity of the synthesis conditions needs to be searched to maximise the efficiency. Both procedures yielded materials with similar crystal structure but differed in their morphological structure. Ni addition was then performed both by wet impregnation or by direct inclusion of the precursors during the mayenite preparation. Neither $NiAl_2O_4$ spinel phase nor formation of solid solution between NiO and CaO were identified on the obtained Ni catalysts. The Ni/mayenite catalysts were then tested on the steam reforming of toluene and pyrocatechol as tar model compounds. The sample obtained by direct inclusion of Ni precursor in the slurry route led to a poor dispersion of nickel and very low specific surface area values, resulting therefore in the absence of catalytic activity. Addition of nickel through the wet impregnation method led to analogous performances in all the conditions studied, despite the morphological and structural differences. The lower activity observed with Ni/mayenite obtained by direct inclusion of Ni precursor in the gel route was attributed to its lower reduction degree, calculated after TPR characterization on the fresh catalyst. Degradation of the support during the experiments evidenced by the presence of $Ca_3Al_2O_6$ and/or the higher initial nickel crystal size calculated for this catalyst could also have contributed to the observed lower conversion values. Deactivation during toluene steam reforming of the Ni/mayenite catalysts produced by wet impregnation was attributed to filamentous and graphitic carbon deposition for mayenite produced by the slurry route and the gel route respectively. Ni/mayenite obtained by direct inclusion of Ni precursor in the gel route showed slightly lower conversion values with respect to the other two catalysts but exhibited promising carbon deposition tolerance in long duration test i.e. no deactivation signs were detected and the amount of coke deposited measured was the lowest among the catalysts studied. Similar activation energies values (≈135 kJ mol^{-1}) were

obtained with catalysts synthesized using the wet impregnation method despite their structural, morphologic and topologic differences and therefore analogous chemical nature of nickel active sites is expected for all the catalyst. Whereas a slightly higher value (147 kJ mol^{-1}) was observed for the Ni/mayenite obtained by direct addition of Ni precursor in the gel route. .

6 Effect of H_2S and thiophene on the steam reforming activity of Ni/Al_2O_3, Ni/mayenite and Rh/Al_2O_3.

Concerns over the poisoning of active nickel sites from sulfur have encouraged decades of research about the adsorption of sulfur on alumina or magnesium supported nickel and noble metal catalysts due to the detrimental economic consequences during its industrial application [231]. Despite the vast H_2S removal technologies available [232], none of them are economically attractive for the cleaning of the producer gas from small-to-medium scale biomass gasifiers due to their operating temperature range (≤ 500 °C) as well as the need for tailored O_2 and/or steam concentration [233]–[236].

Due to the reducing conditions in the gasifier, most of the sulfur is present as H_2S accompanied by low concentrations of COS, CS_2 and various thiophenes [31]. Typical thiophene concentration in biomass gasification gas is less than 10 ppm(v), usually in the range 1-100ppb(v) [237]. However, the study of the impact of this aromatic sulfur compound on the steam reforming activity of nickel and rhodium supported catalysts is helpful as transient periods of impairment operation of the gasifier could led to higher concentrations of thiophene compounds in the producer gas [238]

Lakhapatri et al. [239] used TEM-EDS to study the deactivation mechanism caused by thiophene under steam reforming conditions using a $Ni\text{-}Rh/Al_2O_3$ catalyst and suggested that thiophene decomposition occurs primarily on the surface of Ni crystallites, leading to the deactivation of these sites. Moreover, no bulk sulfide formation (neither on Ni nor on Rh) was found on the used catalyst. The common assumption that organic sulfur compounds are fully converted to H_2S under reforming conditions finds support in thermodynamics studies [238] as well as in the study conducted by Lu et al. [10]. However Lakhapatri et al. [240] in their study of steam reforming of Jet A spiked with thiophene using a Ni/Al_2O_3 catalyst at 800 °C found unreacted thiophene in the condensate after the first few minutes of the reaction. From the results of Rhyner et al.[241] and Mayne et al. [242], it seems

more adequate to state that depending on the reaction conditions, organic sulfur compounds can attain different degrees of conversion and desulfurization.

In this section the impact of H_2S and thiophene on the performance of the steam reforming of benzene as a tar model compound in a simulated COG stream using two typical steam reforming catalysts namely nickel and rhodium supported on alumina was studied. Regeneration of benzene reforming activity of the poisoned Ni/Al_2O_3 was examined changing the temperature and H_2S concentration. In addition, it was also tested a novel mayenite-supported nickel catalyst in the reforming of benzene. The effect of sulfur on the water gas shift reaction activity was investigated with the nickel catalysts. The experimental part of this study was described in section 3.3 of the chapter 3.

6.1 Fresh catalyst characterization

The XRD analysis of the nickel catalysts is presented in **Figure 6.1**. The identification of the chemical species was done correlating the data to powder diffraction file (PDF) numbers. The Ni/Al_2O_3 showed narrow peaks for nickel and alumina phases (**Figure 6.1 B**). The Ni/mayenite spectra displayed the characteristic peaks of mayenite and metallic nickel in addition peaks corresponding to CaO were also present (**Figure 6.1 A**). XRD characterization for the Rh/Al_2O_3 was not performed.

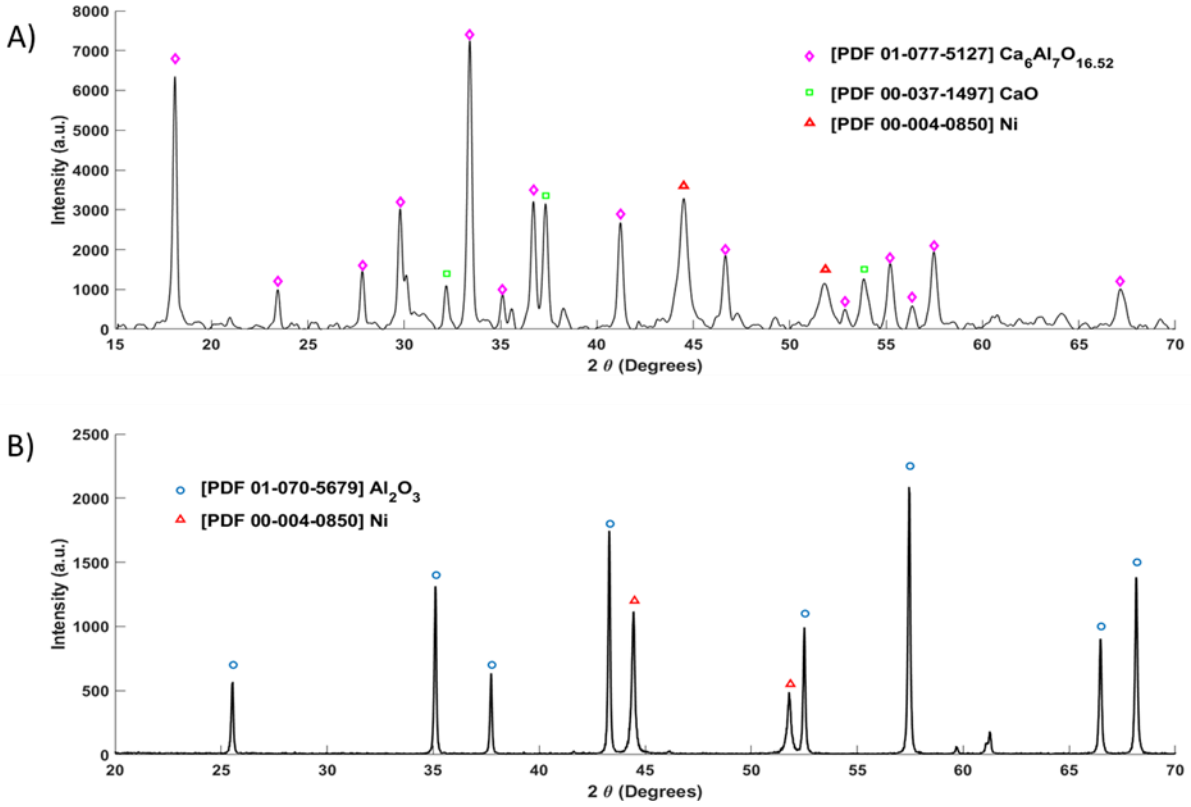

Figure 6.1 Diffractograms of the reduced catalyst. **A)** Ni/mayenite. **B)** Ni/Al_2O_3.

The catalyst properties based on the hydrogen chemisorption analysis are presented in **Table 6.1**. The metal surface area was computed assuming a H/metal=1:1 stoichiometry. The Rh/Al_2O_3 showed the highest dispersion of active metal as well as the largest metal surface area. The sulfur capacity at the saturation (S_0) of the catalysts is also listed in **Table 6.1**. The calculation was done assuming that 440 μg S/m^2 Ni is equivalent to 1 m^2/g Ni as proposed by Rostrup-Nielsen [243] and the metal surface area. The sulfur capacity was calculated to have an approximate value of the maximum sulfur uptake of the catalyst bed used in the experiments. It should be kept in mind that S_0 calculation for the Rh/Al_2O_3 may be less accurate because the equivalence was obtained using a nickel catalyst [243]. The total sulfur capacity of the catalyst bed was calculated from the sulfur capacity at saturation, the theoretical mass content of the metal in the catalyst and the total mass of catalyst in the bed, i.e. 1.2 g.

Table 6.1 Catalysts properties estimated from the H_2 chemisorption characterization

	Metal dispersion (%)	Metal surface area (m^2 g metal^{-1})	Active particle diameter (nm)	Sulfur capacity at saturation (μg g metal^{-1})	Total sulfur capacity of the catalyst bed (μg)
Ni/Al_2O_3	0.4	2.6	255	1144	137
Ni/Mayenite	0.7	4.5	148	1980	475
Rh/Al_2O_3	9.3	41.0	12	18040	324

The sulfur capacity of the catalyst bed can be used to estimate the timeframe for the establishment of a new steady state after poisoning of the fixed bed of powder form catalysts in the presence of H_2S. The sulfur mass flow was 15-294 μg/min when the H_2S concentration was 10-200 ppm(v). When comparing the inlet sulfur mass flow to the sulfur capacity of the catalyst bed (**Table 6.1**), it can be noticed that the catalyst bed is saturated with sulfur in 0.5-9 min, if all the sulfur is adsorbed on the catalyst. The time frame is in line with the observed deactivation time. Similar results are obtained with Ni/mayenite and Rh/Al_2O_3. Further calculations with the same method but using the data of Ashrafi et al [111] who used 110 g of a commercial nickel-based catalyst in pellet form (diameter=2-7 mm) did not yield coherent values compared to the timeframe of deactivation observed by the authors [111]. Underestimation of one order of magnitude of the poisoning response using the estimated total sulfur capacity of the fixed used by Ashrafi et al [111] was likely due to mass transfer limitations. In the present study the benzene reforming activity of Ni/Al_2O_3 did not drop once the initial decay was observed. This outcome evidenced the difference between the sulfur coverage which considers the equilibrium of sulfur chemisorption and the total surface sulfur capacity of the catalyst bed which does not change with temperature or H_2S concentration.

6.2 Sulfur coverage calculations (θ_s)

The calculated sulfur coverage along with the corresponding benzene conversion are displayed in **Table 6.2**. The sulfur coverage was calculated only for the experiments performed without methane using the Ni/Al_2O_3 catalyst. The outlet H_2 concentration was used to calculate the H_2S/ H_2 ratio. The H_2S/H_2 partial pressure ratio stayed well below the bulk sulfide formation at the working temperatures studied [243].The sulfur coverages spanned from 0.86 to 1 and hence all values are relatively close to one. It is important to mention that during the benzene steam reforming reaction carried out with the fresh catalysts i.e. before feeding H_2S, the conversion values were always higher than 94% and the temperature of the catalyst was very close to the set oven temperature. Thus, in all the experiments conducted at the same oven temperature, the catalyst temperature was nearly similar regardless the different H_2S concentration used as can be seen from **Table 6.2**.

Table 6.2 Sulfur coverage and the corresponding benzene conversion on Ni/Al_2O_3 catalyst at different H_2S concentrations at oven temperatures of 700 °C, 800 °C and 900 °C

Oven T. (°C)	H_2S (ppm(v))	Cat T (°C)	θs	X_{C6H6} %	H_2S/H_2 ($x10^{-6}$)
900	25	887	0.86	94	50
	50	888	0.89	89	100
	75	888	0.91	82	150
	100	888	0.93	76	200
	200	889	0.96	52	400
800	10	785	0.87	53	20
	25	786	0.91	26	50
	50	787	0.94	14	100
	75	787	0.96	9	150
	100	788	0.97	6	200
	200	787	1.00	3	400
700	10	683	0.93	4	20
	25	683	0.96	3	50

Sulfur coverage of nickel catalyst was calculated by **Eq. 3.12**. Its use is very popular at typical steam reforming temperatures, mainly because it is easy to apply and have a relatively broad temperature and H_2S/H_2 range of validity. Compared to the conditions of this study, the sulfur chemisorption carried out by Alstrup et al. [122] were done using a 13 wt. % nickel supported on a magnesium-aluminum spinel (4.4 x 4.4 mm cylinders) catalyst with a nickel surface area of 0.3 m^2/g catalyst. Moreover, at high sulfur coverage the subsurface sulfur atoms become stable relative to surface sulfur [244]–[246] and this effect is not taken into account by using **Eq. 3.12**.

The effect of temperature on benzene conversion can be compared at similar surface coverages of sulfur. (**Table 6.2**). For example, at θ_s=0.91 the benzene conversion was 26% and 82% at 800 °C and 900 °C, respectively. Without sulfur in the feed the benzene conversion was close to 100% at both temperatures. In contrast when H_2S was fed to the reactor, even though the sulfur coverage was similar, the activity of the catalyst at 800 °C is clearly lower than at 900 °C. It should be noted that this high sulfur coverage is at the upper limit of the applicability range of **Eq. 3.12**. It is possible that some nickel ensembles with high activation energy become active only at 900 °C. Likewise, the reconstruction of the nickel surface caused by sulfur chemisorption at high temperature could have triggered the formation of new sites for benzene reforming [106]. The hypothesis of reconstruction of the nickel surface by adsorbed sulfur finds considerable support in the literature [119], [121], [247]. According to Maurice et al [121] with increasing sulfur coverage the sulfur phase forms islands, which preferentially develop at step edges on the upper terraces and eventually completely cover the terraces. The Ni atoms then diffuse from the terrace sites to the step edges to reduce the surface stress caused by the sulfur chemisorption thus allowing the formation of a less dense Ni plane [121] and probably this diffusion triggers the formation of new active sites for the reforming reaction..

6.3 Effect of H_2S on steam reforming performance of Ni/Al_2O_3

The impact of the H_2S concentration on the methane and benzene steam reforming activity of Ni/Al_2O_3 is shown in **Figure 6.2 A**. Complete conversion of methane was not achieved at any of the temperatures studied. Considering the results of thermodynamic calculations, it can be concluded that the system did not reach the equilibrium when methane was present in the feed. Moreover, when the oven temperature was 900 °C, the effect of the H_2S concentration seemed to be stronger on the methane conversion than on the benzene conversion. Nevertheless, at 900 °C the moles of carbon converted in the case of methane where higher than for benzene, for all the H_2S concentrations studied. Almost complete deactivation i.e. conversion of methane close 1%, of the catalyst towards methane steam

reforming was observed with 10 ppm(v) H_2S working at oven temperatures ≤ 800 °C. It is important to mention that in the experiments carried out without H_2S, the catalyst bed temperature dropped considerably with respect to the set oven temperature, which can be seen from **Figure 6.2** B. This was particularly evident when the oven temperature was 900 °C and it can be attributed to the endothermic nature of the steam reforming of methane.

For the whole range of operating conditions studied, the chemisorption of H_2S on the catalysts and thus their deactivation was very fast (few seconds), observed from the instantaneous temperature increase of the catalyst bed during the experiments with methane. After a rapid drop in conversion and fast temperature increment, a steady state was reached, and the conversions of methane and benzene remained stable during the rest of the test without signs of further deactivation or activity loss.

Furthermore, formation of any light hydrocarbons during the experiments was not observed, except for a small amount of methane c.a. 240 ppm(v) that was formed at 700 °C in the absence of both H_2S and CH_4 in the feed.

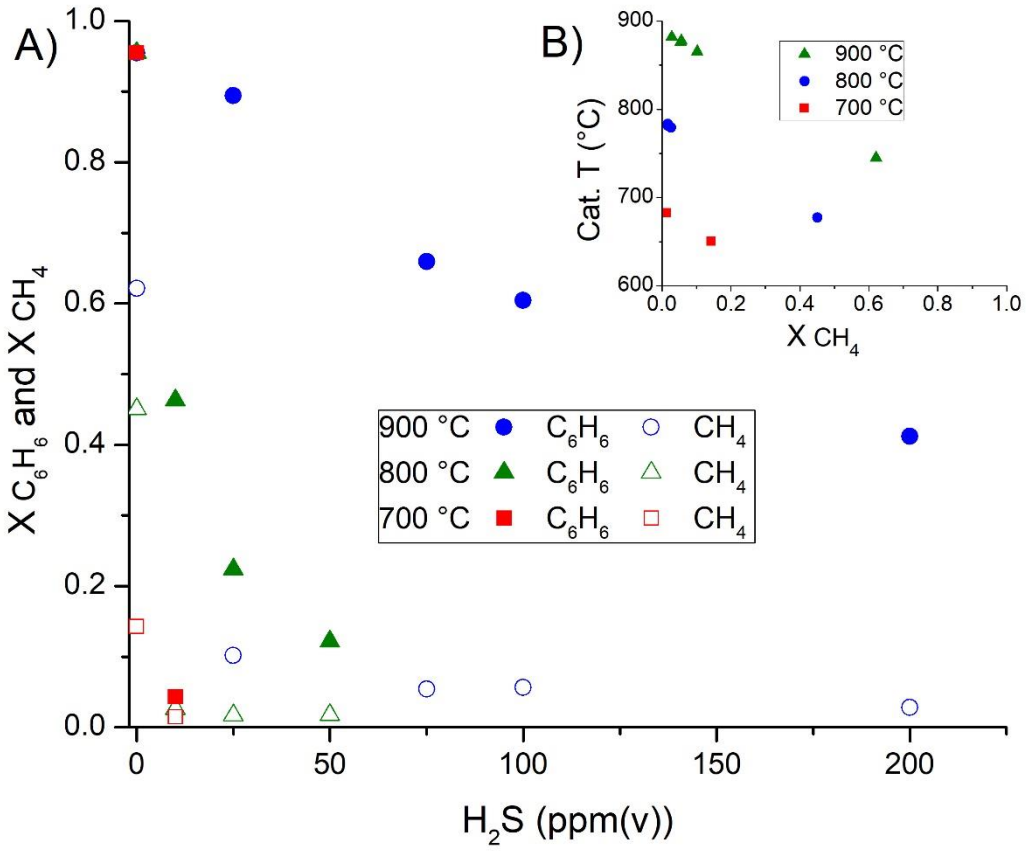

Figure 6.2 A) Impact of the H_2S concentration on the benzene and methane steam reforming activity of Ni/Al_2O_3 at the oven temperatures of 700 °C, 800 °C and 900 °C. **B)** Temperature measured from the center of the catalyst bed as a function of methane conversion. The zero value on the x and y axis were shifted forward for the sake of readability.

The tests conducted without methane in the feed (**Figure 6.3 A**) resulted in a similar benzene conversion versus H_2S concentration curves as the ones reported in **Figure 6.2 A**. During those experiments, the catalyst bed temperature was close to the set oven temperature, only 2 °C-5 °C higher than without H_2S. Compared to the results with methane, the most noticeable differences were found in the experiments carried out at the oven temperature of 900 °C when the H_2S concentration was ≥ 75 ppm(v). At these conditions, the benzene conversion was c.a. 15% points higher in the absence of methane. It should be mentioned that during the benzene steam reforming experiments the catalyst bed temperature was 888 °C i.e. 10 °C higher than the temperature measured during the tests conducted when methane was also present

The CO_2 concentration measured at the outlet of the reactor was around 2-3 vol. % during the benzene steam reforming without H_2S in all the temperatures. However, when H_2S was present, the CO_2 concentration dropped to zero very fast i.e. less than 5 minutes after the introduction of H_2S. This behavior was observed for all the temperatures and H_2S concentrations studied, even when benzene conversion was high.

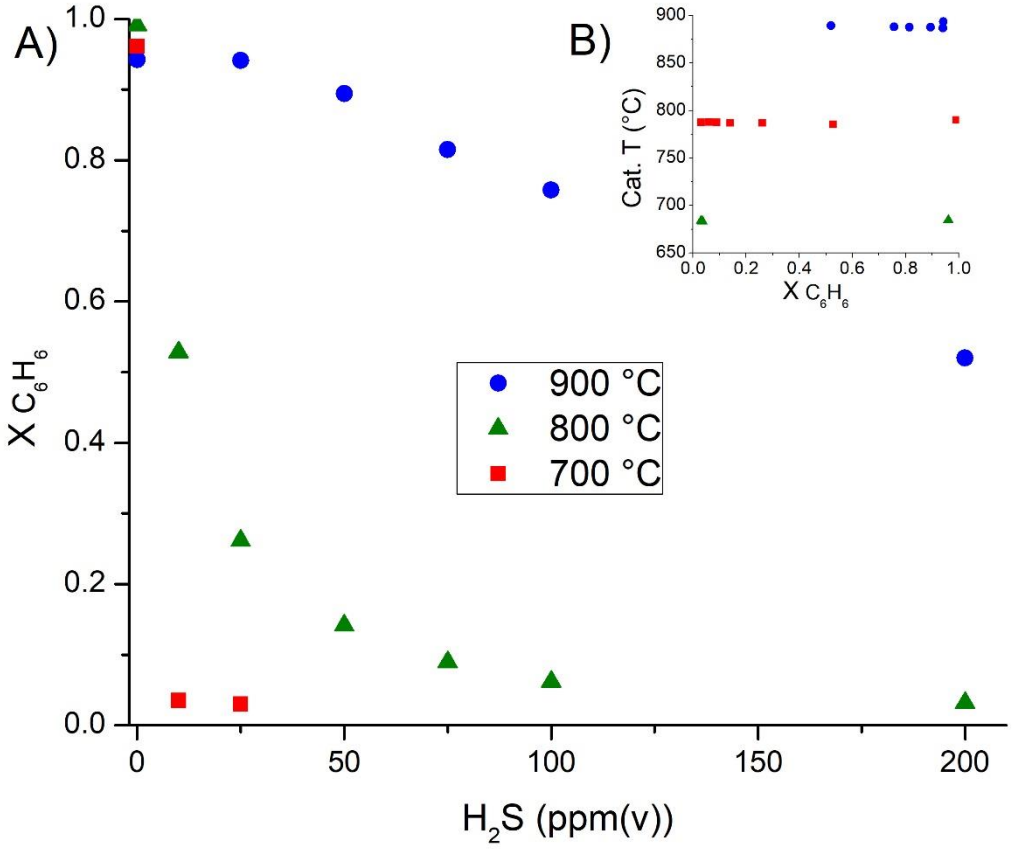

Figure 6.3 A) Impact of H_2S on the benzene steam reforming activity of Ni/Al_2O_3 in the absence of methane at set oven temperatures of 700 °C, 800 °C and 900 °C. **B)** Temperature measured from the centre of the catalyst bed as a function of benzene conversion. The zero value on the x and y axis were shifted forward for the sake of readability.

The effect of H_2S on the steam reforming activity was studied with the Ni/Al_2O_3 catalyst. **Figure 6.2 A** shows that benzene conversion was less affected by the presence of sulfur than methane conversion. This was particularly evident when the oven temperature was ≥ 800 °C. Several researchers have obtained similar results [16], [113].

When comparing benzene conversion when methane was fed to the reactor (**Figure 6.2 A**) to the conversion values when methane was not present in the feed (**Figure 6.3 A**), it is interesting to note how the benzene conversion at 700 °C and 800 °C is almost identical with increasing H_2S concentration i.e. the presence of methane had no effect on the benzene conversion. On the contrary, differences between the benzene conversion versus H_2S concentration curves were observed at 900 °C, particularly when the H_2S concentration was ≥75 ppm(v).

A possible explanation for the observed results can be that at high catalyst temperature (≥870 °C) and when the active sites for steam reforming conversion are exiguous due to high sulfur coverage, competitive reactions between methane and benzene for the scant active sites could take place, hence reducing the benzene conversion with respect to the tests carried out in the absence of methane. However, Jess [248] did not observe any competitive reactions between benzene and methane during steam reforming of simulated COG using a commercial nickel catalyst. Unlike in the present study, he did not add sulfur in the feed. As a possible explanation for the absence of competitive reactions he proposed that methane and benzene are adsorbed weakly and hence do not influence the catalytic conversion of each other. Nonetheless, it must be borne in mind that in the present work the content of methane in the gas was an order of magnitude higher than that of benzene. Therefore, the nickel active sites requirement for methane decomposition must likely be higher than the nickel sites needed for benzene decomposition, if the same types of site are required [249].

On the other hand, when the temperature was ≤ 800 °C, it can be argued that differences in thermal stability of C_6H_6 and CH_4 (benzene being thermally less stable [250]) and also possible differences in activation energy required to reform those compounds, contributed to the absence of competitive reactions i.e. methane steam reforming is much slower than the benzene reforming and hence did not affect the steam reforming rate of the aromatic compound.

6.4 Poisoning and regeneration of Ni/Al_2O_3 catalyst

The ability of the catalyst to regenerate its C_6H_6 and CH_4 steam reforming activity from the sulfur poisoning was studied with Ni/Al_2O_3, the results are showed in **Figure 6.4**. The regeneration experiments consisted of three phases: initial activity, poisoning phase and regeneration. All the phases were done at the same temperature. The regeneration from H_2S poisoning was done by setting the H_2S in the inlet stream to zero. The catalyst regained rapidly (ca. 5 min) its initial benzene steam reforming activity for the whole range of H_2S concentrations studied. When the catalyst had been exposed to H_2S concentrations of ≤ 100 ppm(v), the methane conversion increased from zero to 37% in the first 5 minutes of regeneration and after this first increment the methane conversion continued to rise steadily, although at a slower rate. On the other hand, regeneration of the methane steam reforming activity of the catalyst after exposure to 200 ppm(v) of H_2S was slower at the beginning of the experiment although it reached the same level of conversion as in the 100 ppm(v) test after 60 minutes time on stream. Complete regeneration of the methane steam reforming activity of the catalyst was not achieved at any of the H_2S concentrations studied as can be seen on **Figure 6.4**.

Figure 6.5 depicts the results of the experiments carried out at 800 °C and 700 °C using 25 ppm(v) and 10 ppm(v) H_2S in the feed, respectively. The used H_2S concentrations were chosen to have similar sulfur coverages as in the tests carried out at 900 °C and 75 ppm(v) H_2S (**Table 6.2¡Error! No se encuentra el origen de la referencia.**). At 800 °C, the benzene steam reforming activity was recovered completely, and the recovery was only slightly slower than in the regeneration experiments at 900 °C. In contrast, at 700 °C the observed regeneration of benzene reforming activity was much slower reaching similar conversion values as in the fresh catalyst after 255 min. The methane conversion, on the other hand, reached only 36% of the initial conversion at both temperatures at the end of the tests. The catalyst temperature at the end of the regeneration experiments was 746 °C and 667 °C when

the oven temperature was 800 °C and 700 °C, respectively, these values were higher than the initial ones, which were 680 °C and 650 at 800 °C and 700 °C respectively.

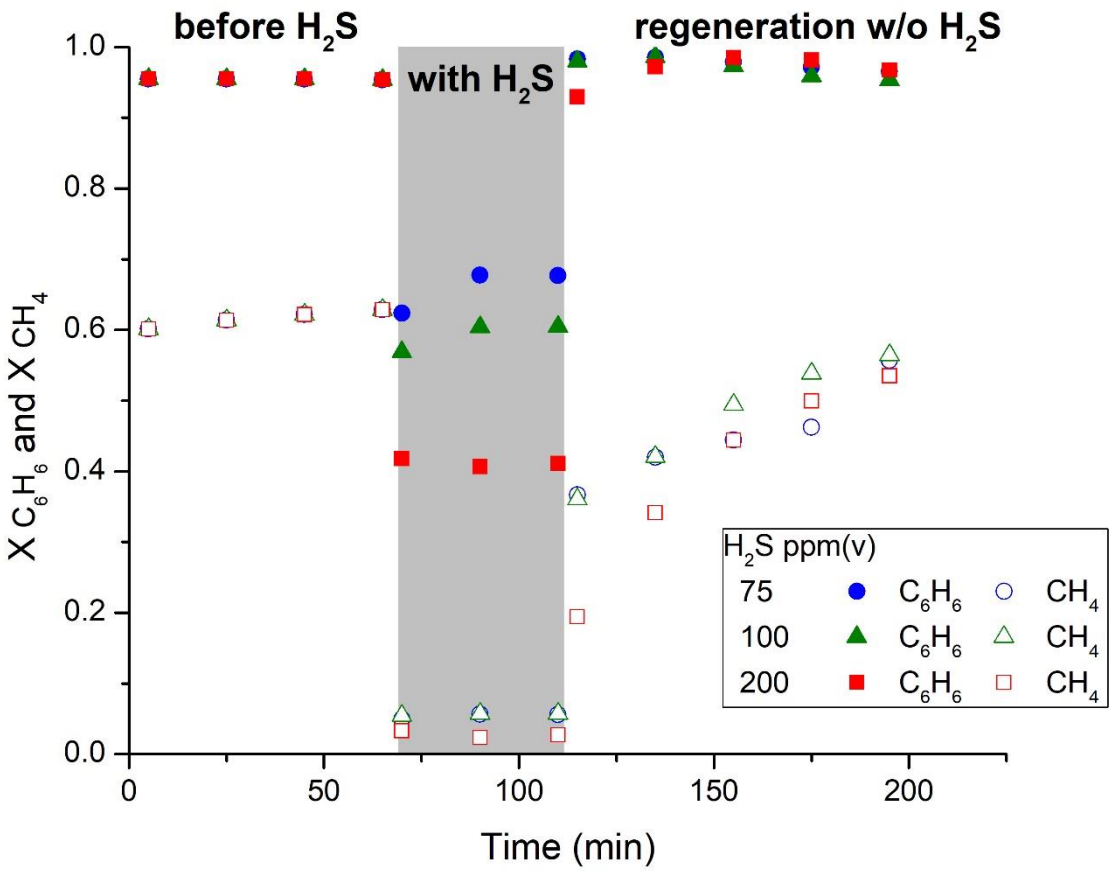

Figure 6.4 Regeneration of the benzene and methane steam reforming activity of Ni/Al_2O_3 after exposure to H_2S at 900 °C. The zero value on the x and y axis were shifted forward for the sake of readability.

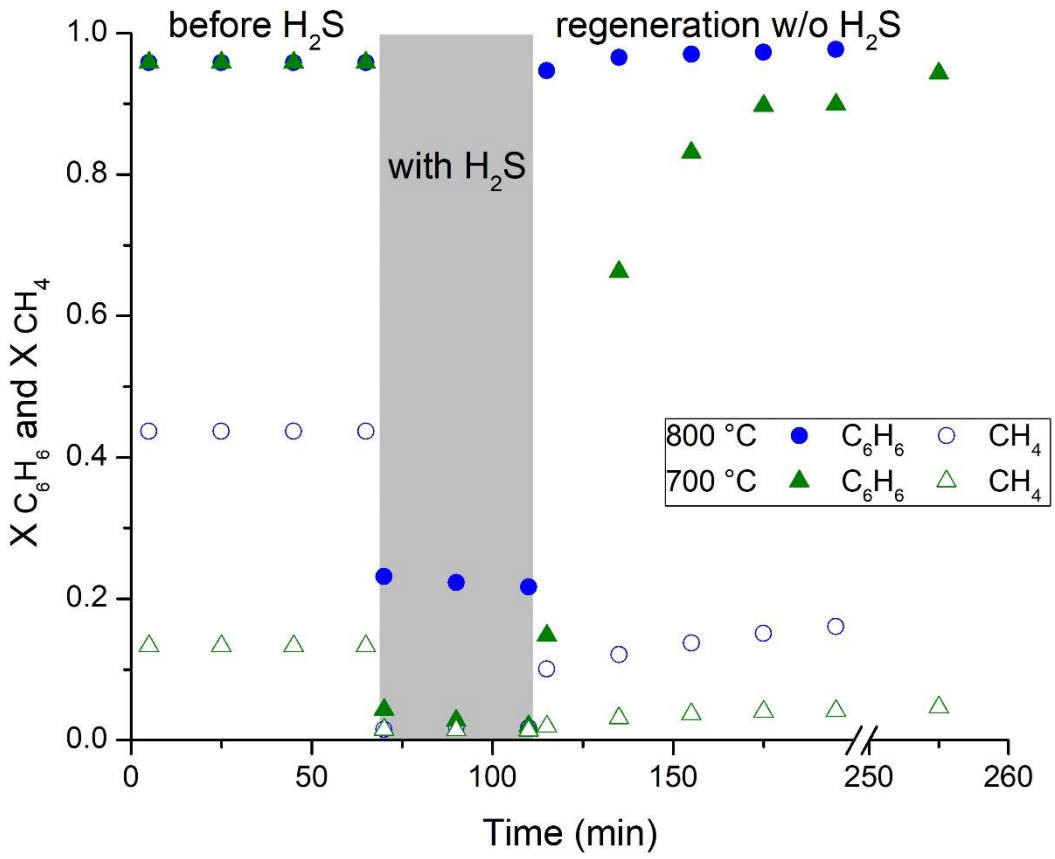

Figure 6.5 Regeneration of the benzene and methane reforming activity of Ni/Al_2O_3 at 800 °C and 700 °C after exposure to 25 ppm(v) and 10 ppm(v), respectively. The zero value on the x and y axis were shifted forward for the sake of readability.

The observed fast deactivation times observed, regardless of the H_2S concentration, detected by the rapid increase in the catalyst bed temperature could be ascribed to the fact that sulfur binds strongly and preferably to the nickel surface sites with the highest activity for steam reforming, namely edges and steps [83], [121], [251]. Therefore, even the lowest concentration of H_2S i.e. lowest sulfur coverage, can deactivate the sites responsible for the major share of activity of the catalyst and consequently it will cause an immediate effect on the catalyst temperature. The remained steam reforming activity could be due to the sulfur-free terrace sites [83] and/or due to formation of new sites for the steam reforming [106].

The regeneration experiments showed that benzene steam reforming activity is more easily recovered than methane. As stated in the result section complete regeneration of the steam methane reforming activity of the catalyst was not achieved at any of the H_2S concentrations

studied. This was especially the case at the temperatures of 700 and 800 °C (**Figure 6.5**). Ashrafi et al [111] studied the regeneration of a Ni-based catalyst at 700 °C after poisoning the catalyst with 108 ppm(v) H_2S. They attained 45% methane steam reforming recovery of the initial activity after 6 hours ToS, whereas in our study the methane conversion reached 36% of initial conversion during the regeneration time of around 2 hours.

The low recovery of the methane steam reforming activity at lower temperatures can be ascribed to the inability to remove enough sulfur from the surface of the catalyst due to the high binding energy of the sulfur chemisorbed on nickel, which requires higher temperatures for the break of the nickel-sulfur bond. However, it is also possible that the catalyst structure may have undergone an irreversible change during the poisoning experiments [252]. Even though the regeneration of the catalyst activity in benzene steam reforming was fast in the present study extrapolation of the obtained results to industrial-scale application cannot be done straightforwardly. On the industrial-scale steam reformers both, the equilibration time and the regeneration time of the catalysts even at high temperatures is difficult and slow because the elution process is subject to diffusion restrictions and even without diffusion restrictions, the sulfur leaving the reactor in a hydrogen stream will decrease exponentially with time [12].

6.5 Steam reforming of a thiophene-containing simulated COG stream

To evaluate and compare the activity of the catalysts on the conversion of thiophene, Ni/mayenite, Ni/Al_2O_3 and Rh/Al_2O_3 catalysts were tested at different temperatures. In addition, thermal conversion of benzene and thiophene was studied with SiC. The results are presented in **Table 6.3**. With SiC, the conversion of benzene was negligible even when the SiC bed temperature was 895 °C. However, thiophene conversion reached 72% at 895 °C, whereas at the lowest temperature, i.e. 686 °C, 16% conversion was attained. With the Rh/Al_2O_3, complete conversion of thiophene was attained at all the temperatures, whereas with the nickel catalysts incomplete conversion of thiophene was observed at temperatures ≤. 680 °C.

Table 6.3 Conversion of thiophene and benzene and CO_2 volume fraction in outlet gas for the catalysts studied.

Bed material	T oven (°C)	T cat (°C)	X C_6H_6 (%)	X C_4H_4S (%)	CO_2 before feeding C_4H_4S (dry vol. %)	CO_2 during C_4H_4S exposure (dry vol. %)
SiC	900	895	1	72	0.0	0.0
	800	790	0	41	0.0	0.0
	700	686	0	16	0.0	0.0
Rh/Al_2O_3	900	873	97	100	3.0	0.2
	800	775	43	100	2.7	0.0
	700	673	6	100	2.3	0.0
Ni/Al_2O_3	900	875	85	100	2.2	0.2
	800	780	9	100	2.3	0.0
	700	675	0	83	2.4	0.0
Ni/mayenite	900	885	81	100	3.0	2.4
	800	784	11	100	3.3	1.8
	700	679	4	86	2.7	0.4

Figure 6.6 shows the effect of the catalyst bed temperature on the benzene steam reforming conversion in the presence of thiophene for the three catalysts studied. Both nickel catalysts exhibited similar trends, whereas the rhodium catalyst shows higher activity values at temperatures ≥ 775 °C. Moreover, a similar decrease in the activity was noticed for the three catalysts at temperatures ≤ 725 °C. Every point in the curve represents the steady state observed conversion at every temperature and hence different sulfur coverages are expected along the curve. Nevertheless, as the thiophene concentration was kept constant

and the H_2 concentration at the outlet was similar for all the experiments conducted, the sulfur coverage should be also similar for the three catalysts at a fixed temperature.

The presence of thiophene in the feed affected CO_2 formation on the catalysts as can be seen from **Table 6.3¡Error! No se encuentra el origen de la referencia.**. It is important to mention that with Ni/Al_2O_3 and Rh/Al_2O_3, except for a small amount of CO_2 observed when the oven temperature was 900 °C, the CO_2 formation was inhibited in the presence of thiophene at all the temperatures studied, the same occurred in the experiments with H_2S. With Ni/mayenite significant amounts of CO_2 were measured at all the temperatures, reaching the highest concentration at the highest temperature.

The sulfur compounds formed in the thermal decomposition experiments were analyzed at an oven temperature of 800 °C. The analysis confirmed that almost all the converted thiophene was found as H_2S with a small amount of carbonyl sulfide, i.e. 1 ppm(v). The sulfur containing compounds were analyzed also in the experiments with Ni/Al_2O_3 and Rh/Al_2O_3 in similar conditions as the thermal decomposition experiment. In both cases complete thiophene conversion was observed. As in the thermal experiment, COS (1 ppm(v)) was the only other sulfur compound found, the rest was converted to H_2S. Since no hydrocarbons were detected at the exit of the reactor except benzene which was fed along with thiophene, it was concluded that the catalysts converted the hydrocarbon part of thiophene into CO, CO_2, H_2.

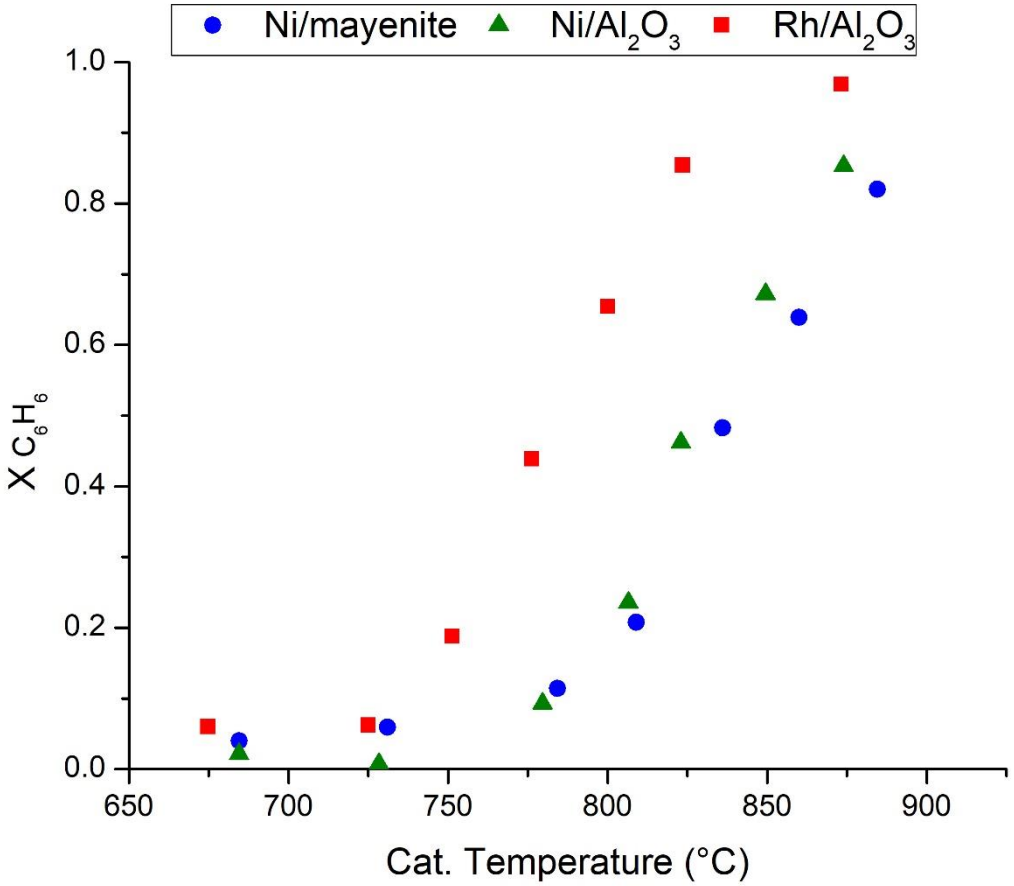

312

313 **Figure 6.6** Benzene conversion as function of the catalyst temperature for the Ni/Al_2O_3, Ni/mayenite and Rh/Al_2O_3 catalysts
314 in the presence of thiophene. The zero value on the y axis were shifted forward for the sake of readability.

315 Thiophene conversion was complete or ≥ 80% with all the three catalysts tested as shown in
316 **Table 6.3¡Error! No se encuentra el origen de la referencia.**. The thermal conversion of
317 thiophene ranged from 17% at the lowest temperature of 675 °C to 72% at 895 °C. Therefore,
318 the catalytic activity had the biggest share in the total conversion of thiophene. Poisoning of
319 the catalyst by sulfur was evidenced by the low benzene conversion at low temperatures.

320 **Figure 6.6** shows that Rh/Al_2O_3 has a higher sulfur tolerance than the Ni catalysts and this
321 difference was most noticeable when the bed catalyst temperature was c.a.780 °C. In the
322 presence of sulfur, the activity of the alumina supported catalysts can be directly related to
323 the active metal as alumina do not interact with sulfur under reducing conditions at
324 temperatures ≥700 °C [113]. Moreover, since the sulfur content in the inlet feed is not enough
325 to form the bulk metal sulfide at the used temperature range [253], the obtained results

cannot be explained by the higher stability of the bulk Ni-sulfide than the bulk Rh-sulfide. An X-ray absorption near edge structure spectroscopy (XANES) study conducted by Chen et al. [254] showed that there are different sulfur species present on Rh and Ni catalysts after the steam reforming of normal paraffins doped with 3-methylbenzothiophene at 800 °C. According to Chen et al. [254] metal sulfide and organic sulfide are the dominant sulfur species on the Ni catalyst, whereas sulfonate and sulphate predominate on the Rh catalyst. Therefore, they postulated that different sulfur chemistry on Ni and Rh catalysts can likely be the reason for their different sulfur tolerance. Along the same line, the results obtained in the present study could be ascribed to different sulfur chemistry. In that case, the sulfur species predominant on the Rh catalyst, seems to be less poisoning for the steam reforming reactions than the species present on the nickel catalyst as was presented by Maxted [255]. The observed similar benzene conversion values for the three catalysts tested at ≤725 °C do not agree with the hypothesis of different sulfur species present on the rhodium catalyst, probably, at this low temperature both rhodium and nickel active sites formed surface sulfides or the poisoning effect of the sulphate species on the rhodium catalyst is as strong as the sulfide species on the nickel catalysts at ≤725 °C. The hypothesis of formation of sulfides rather than sulfates on the Rh clusters supported on CeO_2 under reforming conditions is not supported by the findings of Lee et al [256]. The authors [256] concluded that a simple thermodynamic driving force cannot explained the formation of sulfates on Rh_4/CeO_2 (111) catalysts after conducting a density functional theory (DFT) study.

Moreover, a previous study by Rodriguez and Hrbek [257] using well-defined structures pointed out that the tendency of Rh to lose its electrons upon sulfur adsorption is lower than most transition metals, this feature translates to less changes in the d population of Rh which remains available to interact with reactants and intermediates species [109], [257]. Therefore, it is also reasonable to relate the strong sulfur tolerance of Rh/Al_2O_3 at temperatures ≥ 775 °C with the strong resistance of Rh to the sulfur-induced electron withdrawal.

As shown in **Figure 6.6¡Error! No se encuentra el origen de la referencia.**, similar benzene steam reforming activity in the presence of thiophene was obtained for both nickel catalysts

in spite of the differences in nickel loading, active particle diameter, support, metal surface area, sulfur capacity (**Table 6.1**) and interaction with the support which was deduced from the TPR analysis. Hence, in the case of nickel catalysts, the benzene steam reforming activity in the presence of thiophene was probably determined solely by the uncovered, non-poisoned, active sites in the catalysts i.e. the sulfur surface coverage was similar despite the differences in total surface sulfur capacity. It is conceivable that after the establishment of sulfur equilibrium, comparable number and type of active nickel sites were present on both catalysts.

The regeneration of Ni/Al_2O_3 after exposure to 50 ppm(v) of thiophene was tested with CH_4 but without benzene in the feed since benzene and thiophene were fed together. The catalyst regeneration was followed by CH_4 conversion. The regeneration experiment was conducted at 900 °C. The results are shown in **Figure 6.7**. The regeneration behavior was similar as in the experiments with ≤100 ppm(v) of H_2S, i.e. a fast recovery of the activity in the first five minutes followed by a steady increase at a slower rate. Moreover, benzene conversion (68%) during 50 ppm thiophene poisoning was identical to the conversion obtained in with the 75 ppm(v) of H_2S. The catalyst temperature before and during the exposure to the thiophene-benzene mixture was 773 °C and 871 °C respectively and the end of the regeneration it returned to 773 °C

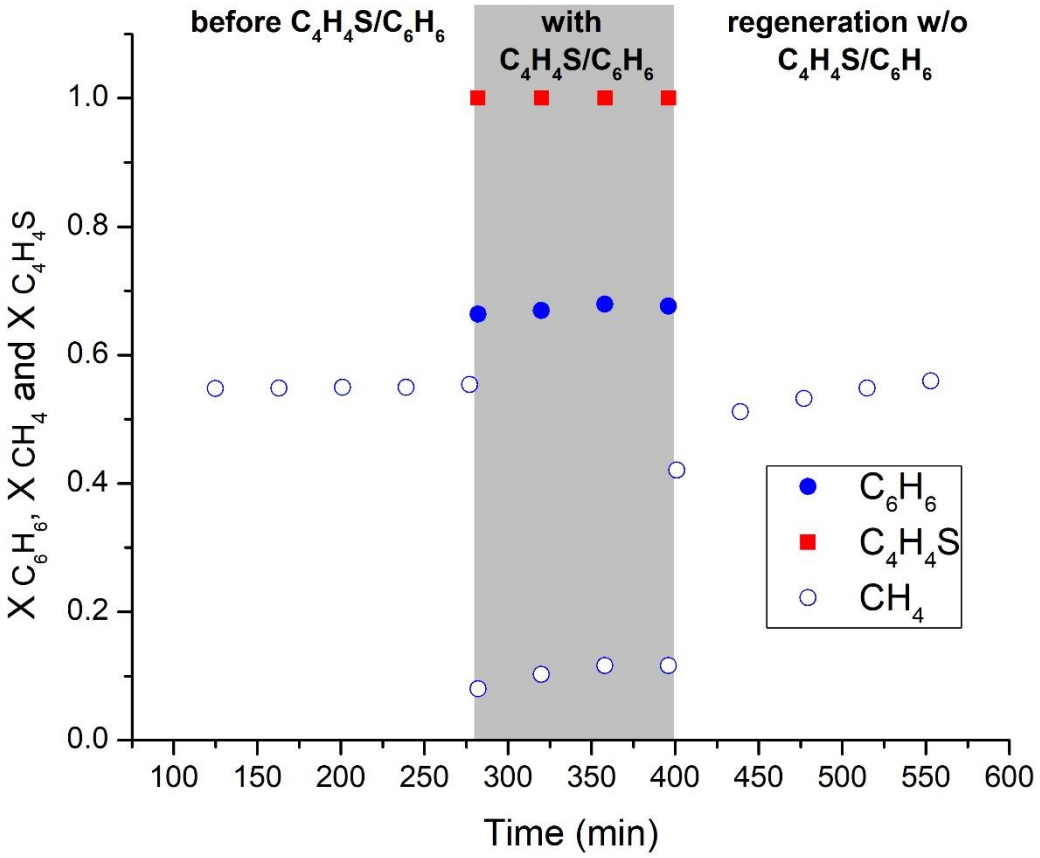

Figure 6.7 Regeneration of the methane steam reforming activity of Ni/Al_2O_3 after exposure to benzene-thiophene mixture at 900 °C.

Regeneration after exposure to thiophene showed similar trends as those found in the regeneration tests after exposure to H_2S. This result was foreseen as it was observed that almost complete conversion of thiophene to H_2S was achieved at temperatures ≥ 730 °C.

6.6 Effect of H_2S on the Water gas shift reaction (WGS)

To have a better understanding of the effect of H_2S on the water gas shift activity of the nickel catalysts, a series of experiments were conducted with only H_2, CO, H_2S and steam. The Ni/mayenite catalyst is clearly more active in WGS reaction than Ni/Al_2O_3 as can be seen from the higher CO_2 concentrations in **Figure 6.8**. The same could be also observed during the experiments with thiophene, in **Table 6.3¡Error! No se encuentra el origen de la referencia.**.

The WGS regeneration tests were carried out at three different temperatures. A H_2S concentration of 100 ppm(v) was used during the poisoning period. As can be seen from **Figure 6.8**., the Ni/mayenite catalyst exhibited an enhanced sulfur poisoning resistance towards the WGS reaction with respect to the Ni/Al_2O_3 catalyst and this feature becomes more evident as the temperature was increased. When the oven temperature was set to 700 °C both catalysts showed negligible regeneration, whereas at 900 °C fast and complete recovery of the WGS activity was achieved with both nickel catalyst. Equilibrium CO_2 vol. % (dry) values calculated using the Gibbs reactor on Aspen Plus® were 4.9 vol. %(db), 4.6 vol. %(db) and 4.4 vol. %(db) at 700 °C, 800 °C and 900 °C respectively. Hence, the WGS reaction did not reach equilibrium at any temperature and with any of the catalyst used. Moreover, during tests with the inert material at similar operating conditions the WGS did not take place at any temperature.

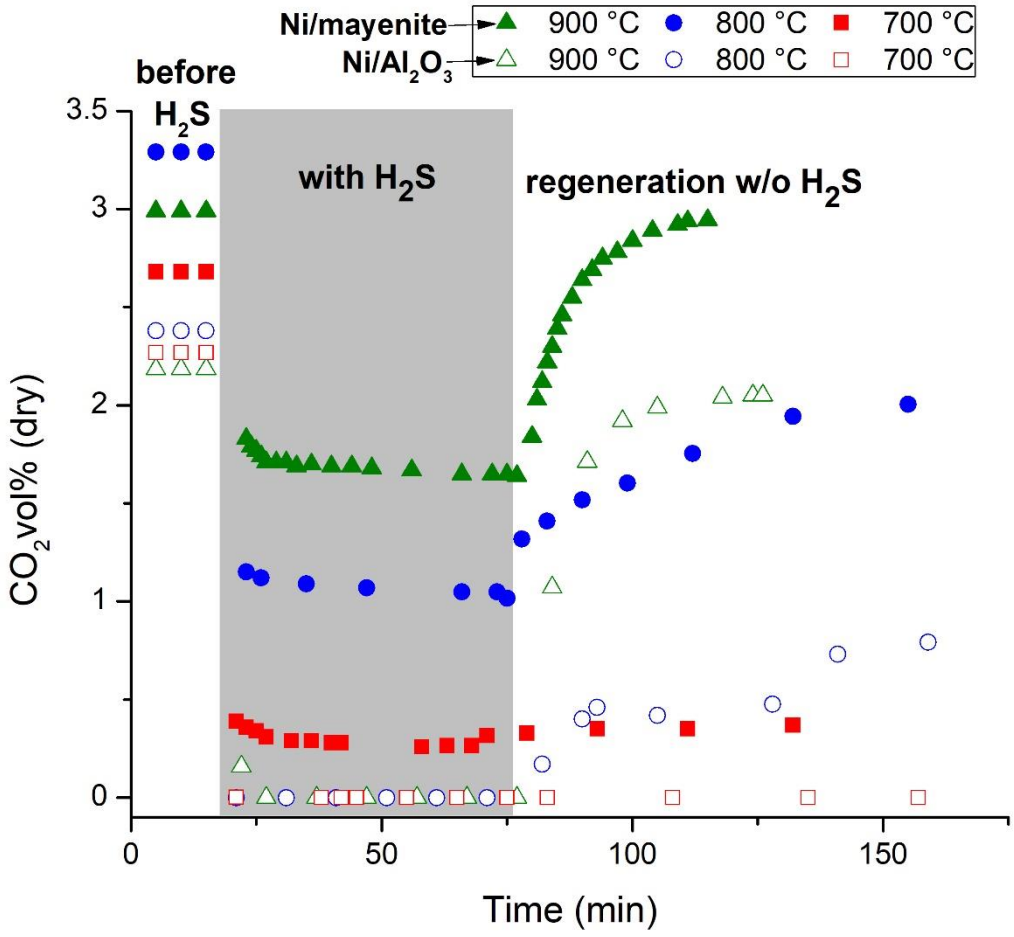

398

399 **Figure 6.8** Regeneration of the water gas shift activity of Ni/Al_2O_3 and Ni/mayenite after exposure to 100 ppm(v) of H_2S at
400 oven temperatures of 700 °C, 800 °C and 900 °C. The zero value on the x and y axis were shifted forward for the sake of
401 readability.

402 The water gas shift activity of the catalysts was evaluated based on CO_2 formation. **Table**
403 **6.3¡Error! No se encuentra el origen de la referencia.**. shows that when thiophene was
404 present in the feed, the WGS activity of Ni/Al_2O_3 and Rh/Al_2O_3 was negligible compared to
405 the activity of Ni/mayenite. In the case of Ni/Al_2O_3 and Rh/Al_2O_3 catalysts CO_2 formation
406 was completely inhibited in the presence of thiophene, except at the highest temperatures
407 close to 900 °C. In the case of Ni/mayenite the decrease in the WGS activity in the presence
408 of thiophene was less pronounced. This result is unexpected considering the similar
409 benzene steam reforming activity showed by both nickel catalysts in the presence of
410 thiophene and the even higher activity of the Rh/Al_2O_3 (**Figure 6.6¡Error! No se encuentra**
411 **el origen de la referencia.**).

Therefore, if the higher obtained benzene conversion (in the presence of thiophene) in the case of Rh/Al_2O_3 was due to the presence of more shielded sulfur species, it can be concluded that the sulfonate and sulphate species are as toxic as the sulfide species for the WGS reaction. Furthermore, according to Karayaka et al [258], the favored WGS path at high temperatures (≥ 800 °C) is the direct oxidation of adsorbed CO and O species. Both CO adsorption on the active metal sites and oxygen migration from the support-metal interface are suppressed by the presence of sulfur species [259]–[262]. Accordingly, it is surmise that the WGS activity at the high temperatures studied is more sulfur-sensitive than the steam reforming of benzene on the Rh/Al_2O_3.

The difference between nickel catalysts towards sulfur poisoning was further studied with WGS experiments. The sulfur-resistance of the Ni/mayenite catalyst compared to the Ni/Al_2O_3 is clearly pictured in **Figure 6.8**. One reason behind the higher sulfur tolerance of Ni/mayenite catalyst could be the ability of mayenite to adsorb sulfur and protect the active nickel sites as was presented by Li et al. [93]. However, in the study of Li et al. [93] the Ni/mayenite showed higher activity than Ni/Al_2O_3 only until the saturation of mayenite.

Another explanation for the WGS activity of the Ni/mayenite catalyst in presence of H_2S is the existence of residual CaO in the catalyst as confirmed by XRD analyses (**Figure 6.1 A**). Muller et al. [263] found that at 800 °C CaO had similar water gas shift activity than the Fe_3O_4, a known catalyst for this reaction. Therefore, it is reasonable to correlate the water gas shift activity of the Ni/mayenite to the presence of active CaO sites on the surface of the catalyst. In addition to the WGS catalytic activity of CaO, the sulfur adsorption capacity of CaO is known from the literature [264]–[266]. However, sulfur binds more strongly to nickel than CaO; the heat of adsorption of sulfur on CaO is 3 times lower than on nickel [267]. Thus, it is possible that the nickel in this case served as a sulfur guard for the active sites of CaO. Moreover, Heesink and Swaaij [268] found that CaO reaction with H_2S was hindered by the presence of CO_2, H_2 and CO in the temperature range of 500 and 700 °C. Hence, the presence of CO_2, CO and H_2 could have inhibited the adsorption of sulfur on the CaO active sites leaving them free to catalyze the WGS reaction. The increasing trend of CO_2 formation

with temperature suggests that in the studied conditions the WGS reaction was far from the equilibrium and therefore was limited by kinetics. In the present study, the activity of the mayenite in water gas shift reaction was not verified.

6.7 Summary

The effect of sulfur compounds on the steam reforming activity of CH_4 and C_6H_6 on Ni/Al_2O_3, Ni/mayenite and Rh/Al_2O_3 catalysts in a simulated COG stream was studied. It was shown that temperature significantly influenced the poisoning effect of H_2S. As the temperature was decreased the poisoning effect increased in agreement with the exothermic nature of the sulfur chemisorption equilibrium.

After the initial poisoning the catalyst activity stayed stable. Moreover, the poisoning of the catalyst was fast in all the conditions studied and the timeframe for the establishment of a new steady state after poisoning was close to the calculated time needed to reach the total sulfur capacity of the catalyst bed. During the regeneration tests the initial benzene conversion was restored in less than 5 minutes. On the other hand, the methane reforming regeneration process was slower

Above 800 °C, thiophene was completely converted with all the catalysts. Thermal conversion of thiophene was appreciable i.e. 42% at 800 °C. In all the experiments, the sulfur containing products from thiophene were mainly H_2S with traces of COS. Ni/Al_2O_3 and Ni/mayenite showed similar benzene steam reforming activity versus temperature in the presence of thiophene despite the differences in the catalyst properties. Rh/Al_2O_3, on the other hand, outperformed both nickel catalysts especially at temperatures ≥ 775 °C in the presence of thiophene. Interestingly, both Ni/Al_2O_3 and Rh/Al_2O_3 catalysts lost completely their WGS activity in the presence of thiophene, even when the C_6H_6 conversion was high.

Fast (≤ 5 min) and complete WGS activity deactivation was observed for Ni/Al_2O_3. Regeneration of the catalyst activity was possible only at 900 °C. Ni/mayenite, on the other hand, exhibited a remarkable sulfur WGS activity tolerance and this feature was enhanced

as the temperature was increased. This result was ascribed to the presence of CaO in the surface of the Ni/mayenite catalyst.

From the results obtained it can be concluded that to achieve moderate-to-high conversion values in the presence of ≈75 ppm(v) of H_2S of the tar compounds present in a H_2-rich syngas with the used catalysts, the operating temperature of the reformer should be close to 900 °C in the case of the nickel catalysts and ca. 850 °C for the rhodium catalyst.

A simplified scheme of the sulfur-passivated catalyst on the benzene steam reforming in the presence of H_2S or thiophene and its regeneration in a sulfur-free H_2-rich feed stream is depicted in **Figure 6.9**

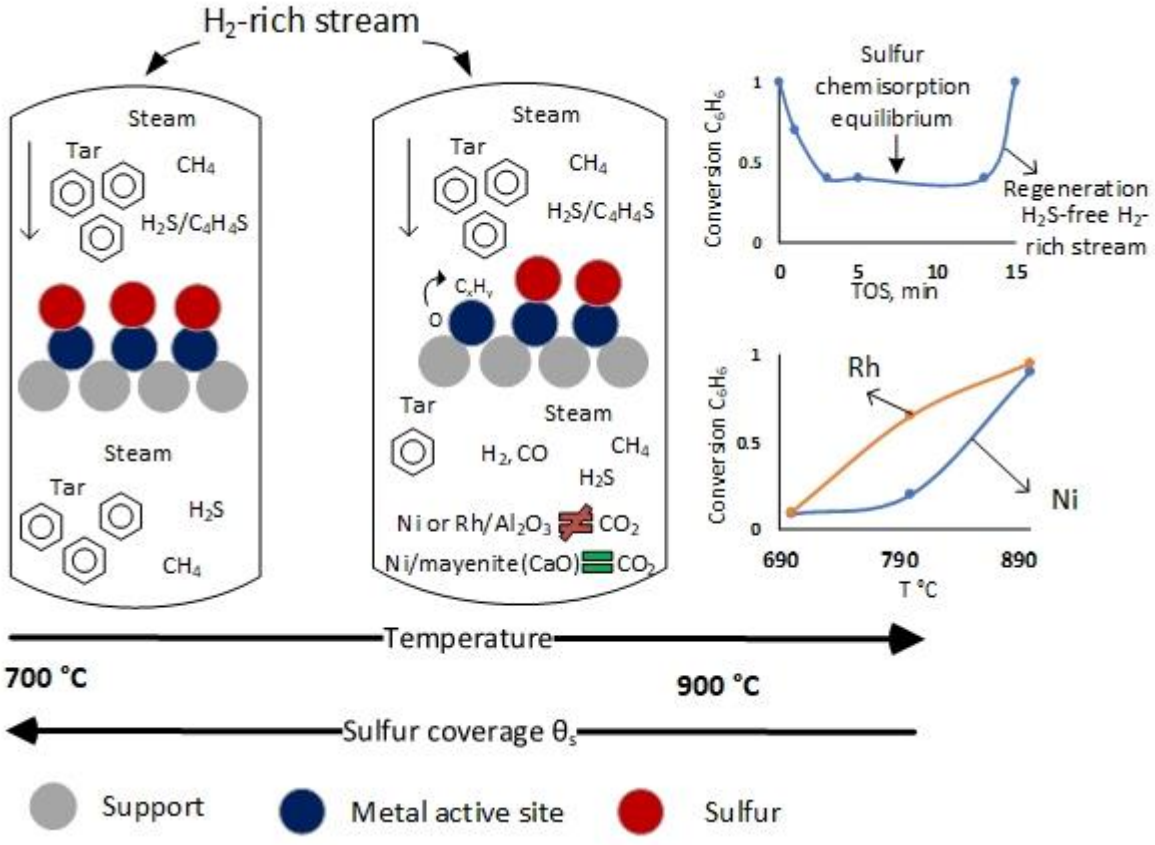

Figure 6.9 A simplified scheme of the sulfur-passivated catalyst on the benzene steam reforming in the presence of H_2S or thiophene and its regeneration in a sulfur-free H_2-rich feed stream.

7 Effect of adding a KCl aerosol on the reforming activity of a pre-sulfided commercial Ni/$MgAl_2O_4$.

Comprehension of the interactions and effects of K and S compounds present in the biomass derived producer gas on the performance of reforming catalysts is crucial. Most of the studies dealing with this topic have used impregnation of K and K salts onto the catalysts to investigate the alkali's effects on the steam reforming of biomass derived producer gas [131], [132]. This method is different from the actual transport and deposition of potassium on the surface of the catalyst used in industrial applications[269]. Moreover, at the high temperatures generally utilized for steam reformers desorption and volatilization of potassium from the K-impregnated catalysts is still an unresolved problem which not only causes loss of the desired promoting effects but can negatively affect downstream processes [137]

An interesting and yet little-known argument regarding the catalytic steam reforming of biomass derived syngas is the influence of potassium on the sulfur tolerance and activity of the catalysts. the above argument has been dealt mainly with K-impregnated catalysts. Promising results were obtained by Díaz et al.[148] using Ni/SiO_2 and by Ferrandon et al. [149] on a $Rh/La\text{-}Al_2O_3$, both research groups attributed the observed increased sulfur tolerance to the presence of potassium decoration that blocked part of the active metal surface hindering sulfur adsorption. Furthermore, the improved sulfur tolerance of the potassium-impregnated Ni/ Al_2O_3 for the hydrodesulfurization reaction of thiophene observed by Chen and Shiue [150] was related to the weakening of the nickel sulfide bond caused by release and transfer of electrons from the potassium to the nickel crystallite. [147] studied the K and S coadsorption on Ni(100) surfaces by means of Auger electron spectroscopy (AES), thermal desorption spectroscopy (TDS) and WF (work-function) measurements in UHV and found that the K overlayer on S-covered Ni(100) weakens the S–Ni bond, and forms a compound with S. Additionally, at S coverages higher than 0.5 ML a KS peak was observed in the AES spectra. Praliud at al. [270] determined by means of XPS,

infrared spectroscopy and magnetic methods that potassium was mainly present as K^+ and speculated that a K-O-Ni surface complex was probably formed. Potassium was deemed to be distributed both in the support decorating the nickel surface into patches or islands but without occupying all the nickel surface. Transfers of electrons from the adsorbed K to the nickel sites was evidenced through CO chemisorption analyses [270].

Few research works [271]–[273] have focused on the effect of addition of alkali salt in vapor phase on the catalyst steam reforming performance. Nevertheless, in those studies, simultaneous addition of the salt and evaluation of the catalyst activity was not performed. Albertazzi et al [272] evaluated the effect of K_2SO_4, KCl, $ZnCl_2$ and a solution derived from biomass fly ash on the steam reforming activity of a Ni/MgAl(O) catalyst. The salt exposure was done using a pneumatic atomizer. After 2 h exposure of 50 g KCl per liter of deionized water the catalyst the dispersion, metallic surface area and BET surface area decreased. The authors [272] attributed this result to pore clogging by the growth of sintered metallic particles and stated that the support remained stable after the test. In addition, cleaning of the K adsorbed on the surface of the catalyst was observed during a subsequent steam methane reforming experiment. Einvall et al. [273] used the same method as in Albertazzi et al [272] to examined the extent of potassium deposition on two catalysts, a Pt/Rh supported on a spinel (Al/Mg) and a commercial $Ni/MgAl_2O_4$ catalyst. A lower alkali deposition was found on the Pt/Rh catalyst, a slightly larger size of the particles of the former catalyst together with differences in surface area, density and particles shape were assumed to be the reasons behind the lower K deposition [273]. Moreover, diminution of the metallic surface area was observed for both catalysts, however, their crystallite size was unaffected. Thus, it was inferred that metallic surface area reduction was due pore blockage by the aerosol particles [273]. According to thermodynamics at 800 °C K_2SO_4 should be in the phase whereas KCl is present in the vapor phase as their melting points are 1067 °C and 773 °C [274]. Furthermore, while K_2SO_4 is predicted to be one of the most abundant compounds present in biomass combustion gases under the reducing conditions of the

gasifier KCl is the predominant potassium alkali salt depending on HCl and steam concentration [35], [274]

Evidently a study of the influence of gas-phase potassium on a sulfur-passivated nickel catalyst is desirable as a deep understanding of this topic can lead to a significant impact on commercial applications, considering that both sulfur and potassium are present in most of the producer gases derived from biomass gasification [31], [33]. In this study the effect of gaseous K adsorption on the surface of sulfur passivated catalyst is investigated under realistic high temperatures reforming conditions. Moreover, the role of the support, the envisage S and K interactions and the overall catalytic activity are discussed. The experimental part of this study was described in section 3.4 of the chapter 3.

7.1 Fresh and spent catalyst characterization

The changes in BET surface area of the catalyst and support after the pretreatment and after the saturation and decay phases with respect to the fresh samples are shown in **Figure 7.1**. It can be appreciated that accelerated ageing resulted in a stabilized support and catalyst and thus sintering is not expected to influence activity changes during the saturation and decay phases. Sehested et al.[275] indicated that K deposition accelerates sintering of the Ni particles at high pressure i.e. 31 bar. However, in the present study the alkali dosing does not affect the surface area of the stabilized catalyst (**Figure 7.1**). Deposition of K on the surface didn't result in reduction of the BET surface area of the support also indicating that the deposition was done in the gas phase and no melted KCl was deposited, thus blocking the pores, as has been reported in other studies[271]–[273].

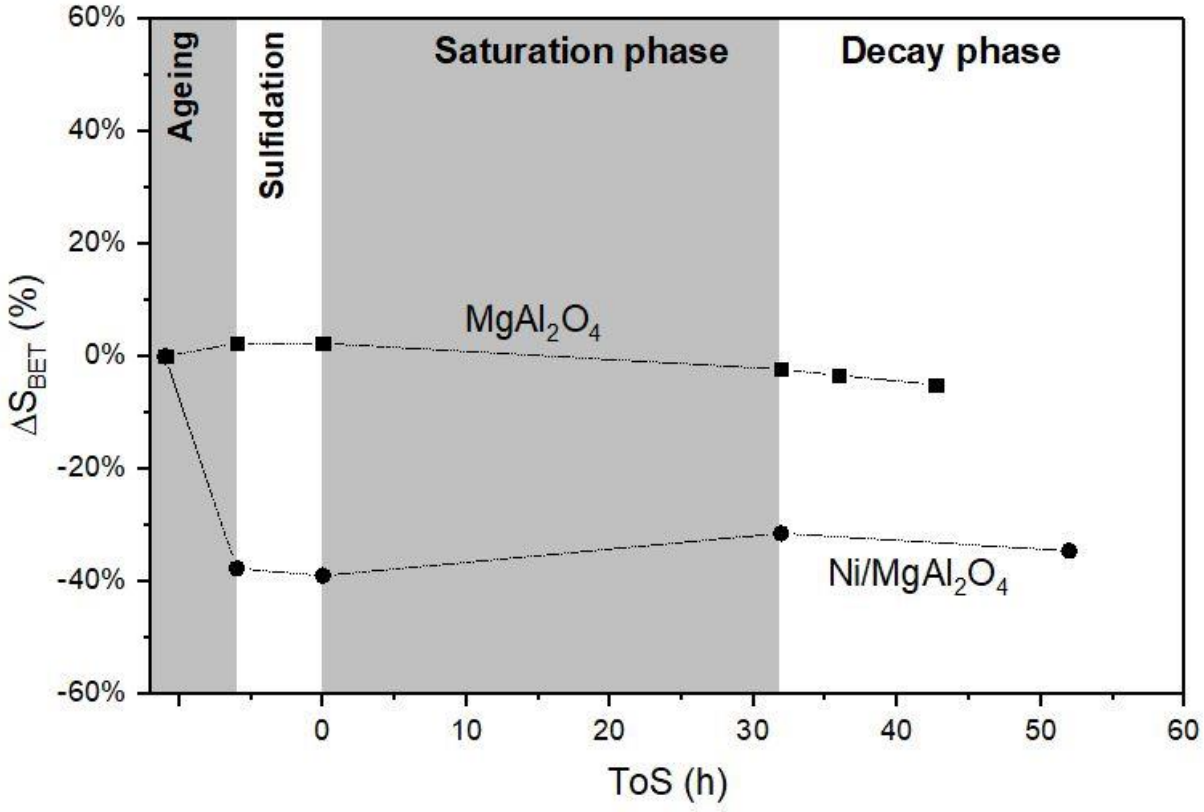

Figure 7.1 The changes in BET surface area of the catalyst and support after the pretreatment and after the saturation and decay phases with respect to the fresh.

7.2 Preferential adsorption site for K and S

Figure 7.2 shows the normalized sulfur and potassium content of the fresh catalyst and the support and after the pretreatment and the studied phases. S chemisorption took place only on the $Ni/MgAl_2O_4$, therefore, spillover of S from the Ni sites to the support can be considered negligible during all the phases of the study i.e. saturation and decay, contrary to what has been suggested by Moud. P [15]. Hence, it can be argued that the interaction, if any, between K and S should occurred mainly in the proximity of the nickel actives sites. This result has a substantial implication on the location and mechanism of the possible K-S interaction. Hepola et al [106], [113] used temperature programmed hydrogenation to evaluate the sulfur adsorption and desorption on α-Al_2O_3 and $LaAl_{11}O_{18}$ after exposure up to 2000 ppm(w) H_2S/Ar at 1 bar and 900 °C and found that the presence of La caused a significant improvement in the sulfur adsorption ability of the support and that α-Al_2O_3

adsorbed negligible amounts of sulfur (≤ 10 ppm(w)). Xie et al. [276] reported sulfur content of 0.29 and 0.18 mg $gcat^{-1}$ for Al_2O_3 and CeO_2-Al_2O_3, respectively, after exposure of 350 ppm(w) of sulfur at 800 °C for 55 h under steam reforming conditions, the sulfur content was measured with a LECO SC 144DR Sulfur Analyzer. Jablonski. W.S. [231] measured 83 and 148 μmol of S on Al_2O_3 and Yttria Stabilized Zirconia (YSZ), respectively upon exposure to 1000 ppm(v) H_2S at 500 °C for 1 h using a flow-through FTIR. Nevertheless, in the above studies it was observed that in the presence of the active metal e.g. nickel, the sulfur adsorption was markedly higher than the value adsorbed by the support. Therefore, it is conceivable that during the saturation phase K-S interactions took place accounting for the decline of the sulfur adsorbed on the nickel sites of the catalyst. The fact that the K content on the catalyst dropped considerably but was not completely removed could indicate the existence of weak and strong K-support bonds and K-Ni-support bonds [277]. Additionally, Kotarba et al. [278] found that the presence of sulfur, on a commercial fused iron catalyst, influenced the desorption of potassium species (atoms, ions and highly excited species) differently, thus giving rise to a higher activation energy for the K ions and highly excited species while lowering the desorption energy of K atoms.

The normalized K content in the support increased during the Saturation phase to a value slightly higher than the one obtained with the catalyst and then decreased at the end of the decay phase. Thus, indicating readily adsorption/desorption on the $MgAl_2O_4$ support of the alkali compound fed in the gas phase under the present conditions. Considering the high s content remaining on the catalyst it can be inferred that the preferential adsorption site for K is on the support surface, likely bonded by the OH-groups therein [133], [279]. This hypothesis does not discard that potassium could be concentrated into islands in the vicinity of the nickel particles or even forming a K-O-Ni complex [270]. Bailey et al. [131]. After K_2CO_3 incipient wetness impregnation of a Ni/Al_2O_3 the authors[131] found that much of the potassium was on the Al_2O_3 surface. Juan-Juan et al. [132] investigated the effect of potassium in a K-promoted Ni/ Al_2O_3 catalyst, prepared using the incipient wet impregnation, on the dry reforming of methane. The results showed that potassium

migrates from the support to the Ni surface, neutralizes a fraction of the active sites and suppressed the coke formation on the catalyst.

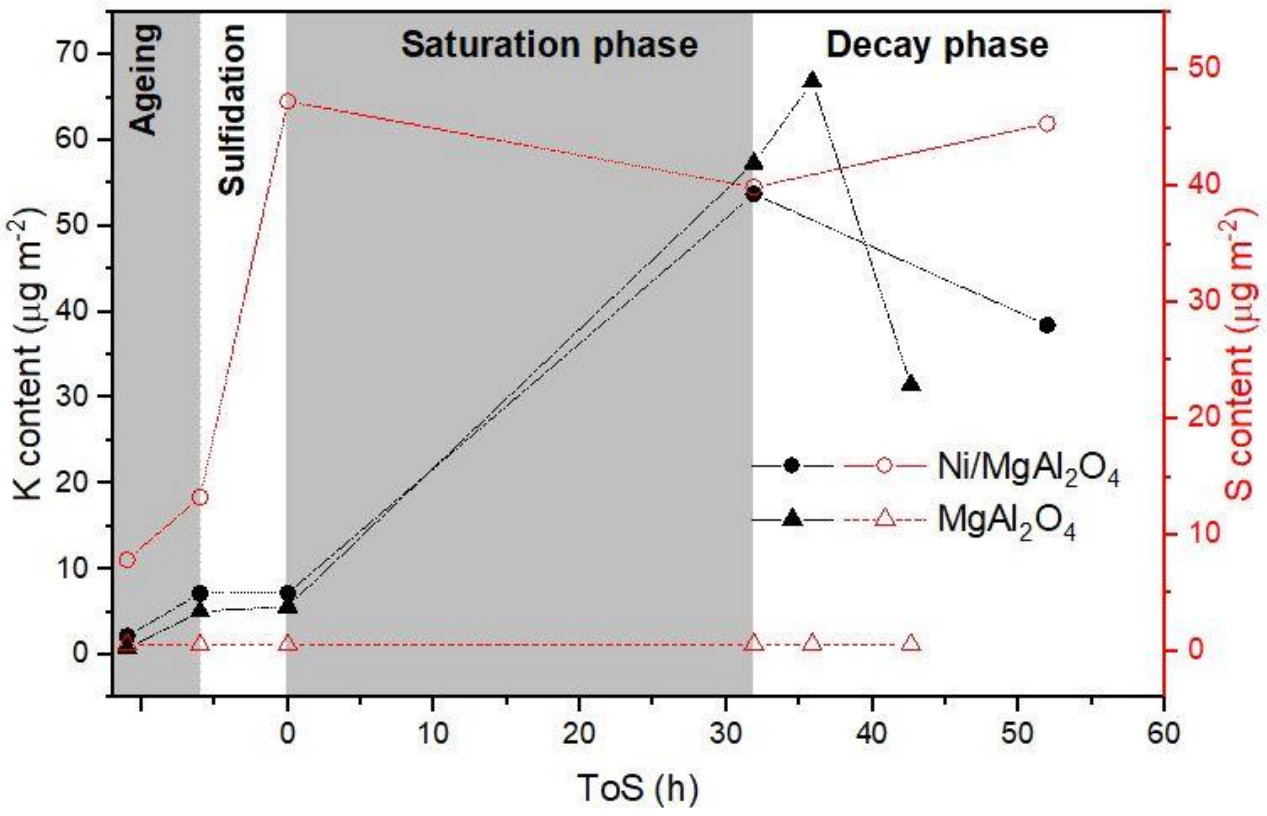

Figure 7.2 normalized sulfur and potassium content of the fresh catalyst and the support and after the pretreatment, saturation and decay phases

7.3 Influence of K aerosol addition to the steam reforming performance of the sulfur-passivated Ni/$MgAl_2O_4$ and role of the support on the total conversion of CH_4, C_2H_4 and $C_{10}H_8$

The CH_4 conversion as a function of ToS along with two horizontal lines representing the thermal conversion (short-dotted line) and the conversion due to gas-phase reactions (dash-dotted line) enhanced by KCl aerosol are depicted in **Figure 7.3**. A positive effect on the conversion is observed during the saturation phase using the nickel catalyst. Conversely, during the decay phase the observed conversion decreased steadily and reached values close to the initial values of the saturation phase. Thus, it can be surmise that the initial

617 sulfur coverage was reestablished this conjecture is supported from the S content value as
618 shown in **Figure 7.2**. Furthermore, the conversion obtained with the support during the
619 decay phase was slightly higher than the thermal conversion and the conversion caused by
620 gas-phase reactions, moreover, the values corresponded to half of the conversion observed
621 with the catalysts during the first 5 h ToS of the decay phase. Thus, the role of the K-
622 impregnated support in the observed CH_4 conversion was non-negligible. Additionally,
623 analogous conversion values were achieved with the catalyst and the support at the end of
624 the decay phase, similar values were also observed during the first 5 h of the saturation
625 phase. Conversion of CH_4 caused by gas phase reactions during KCl dosing was lower than
626 the conversion observed with the catalyst and support during both phases in agreement
627 with Elliott and Baker[128] but similar to the thermal conversion. Therefore, the effect of the
628 gas-phase reactions enhanced by the presence of KCl on the CH_4 conversion was
629 insignificant.

630

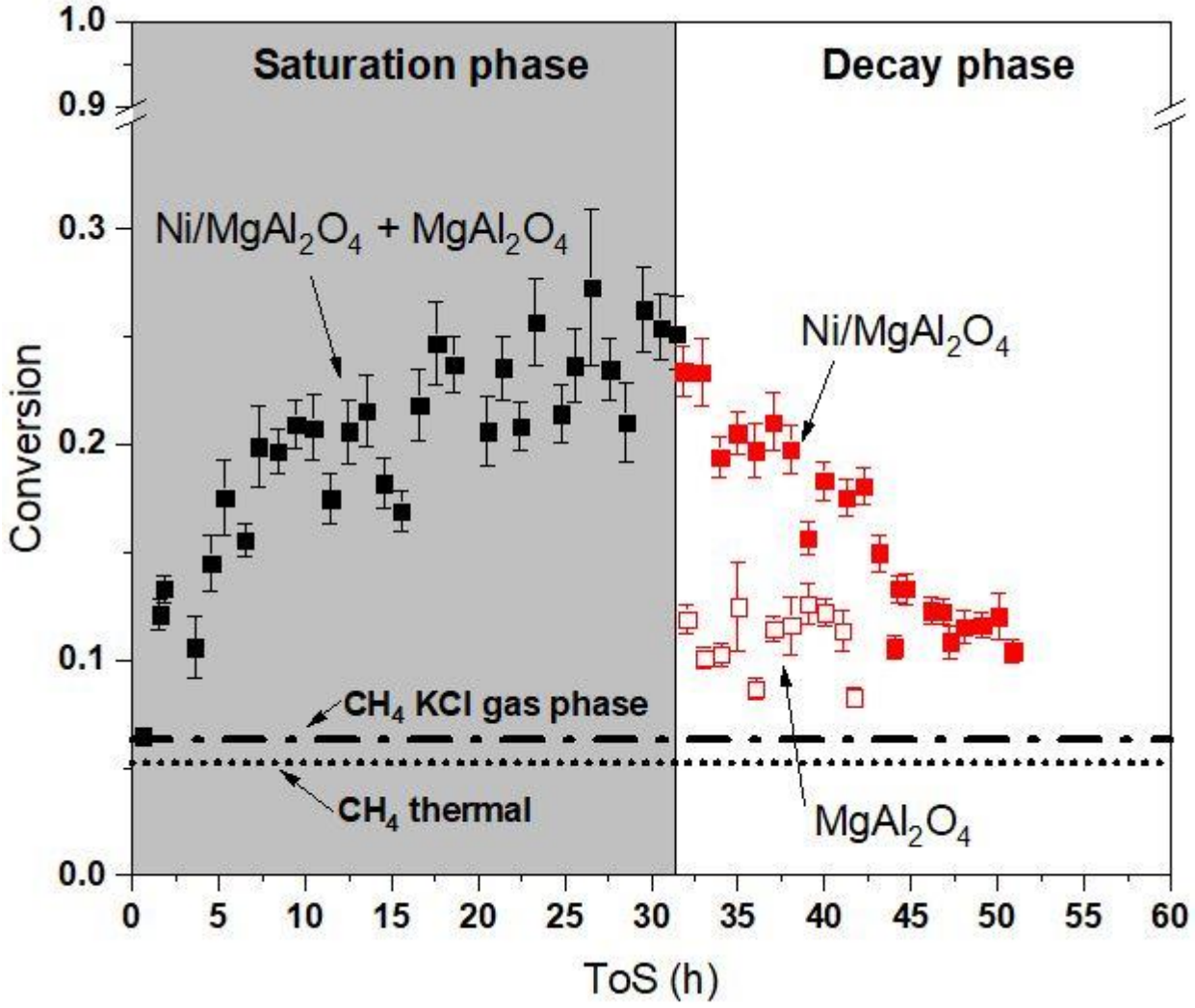

Figure 7.3 CH_4 conversion as a function of ToS during the saturation and decay phases.

The conversion of C_2H_4 as function of ToS during the Saturation phase and decay phase is illustrated in **Figure 7.4**. As can be seen the conversion of C_2H_4 displayed similar trends during the saturation and decay phases as in the case CH_4 when the catalyst was use, although, C_2H_4 conversion values were higher during the saturation phase. At the beginning of the decay phase the conversion attained with the catalyst was significantly higher than the conversion observed with the support, contrarily to what was observed with CH_4. On the other hand, the conversion attained with the support at the end of the decay phase was just slightly lower that the values observed with the catalyst in the closing stages of the decay phase and also analogous to the thermal conversion. This result supported the assumption that at the end of the decay phase the catalyst restored its initial sulfur coverage

643 value i.e. $\theta_S \approx 0.97$. Moreover, C_2H_4 conversion caused by gas phase reactions during KCl
644 dosing was almost identical to the conversion values observed with the support at the end
645 of the decay phase and also analogous to the thermal conversion value. Hence, the effect of
646 the gas-phase reactions enhanced by the presence of KCl on the CH_4 conversion was
647 imperceptible as in the case of CH_4. It is likely that in the experiments carried out with the
648 support and inert material a balance between the formation and consumption of C_2H_4 was
649 established. This premise is reasonable as the formation of olefins from the steam cracking
650 of higher hydrocarbons it is well-known [280]. Formation of C_2H_4 caused by gas phase
651 reactions of tar compounds during KCl dosing could it is also anticipated due to the
652 promoting cracking and dehydrogenating effect of K under tar reforming conditions [128],
653 [131]. Dun at al. [281] found an increased olefin selectivity after K promotion of a charcoal-
654 supported molybdenum Fischer-Tropsch catalyst upon increasing K loading the decrease
655 in activity levels off while the olefin selectivity continued to increase.

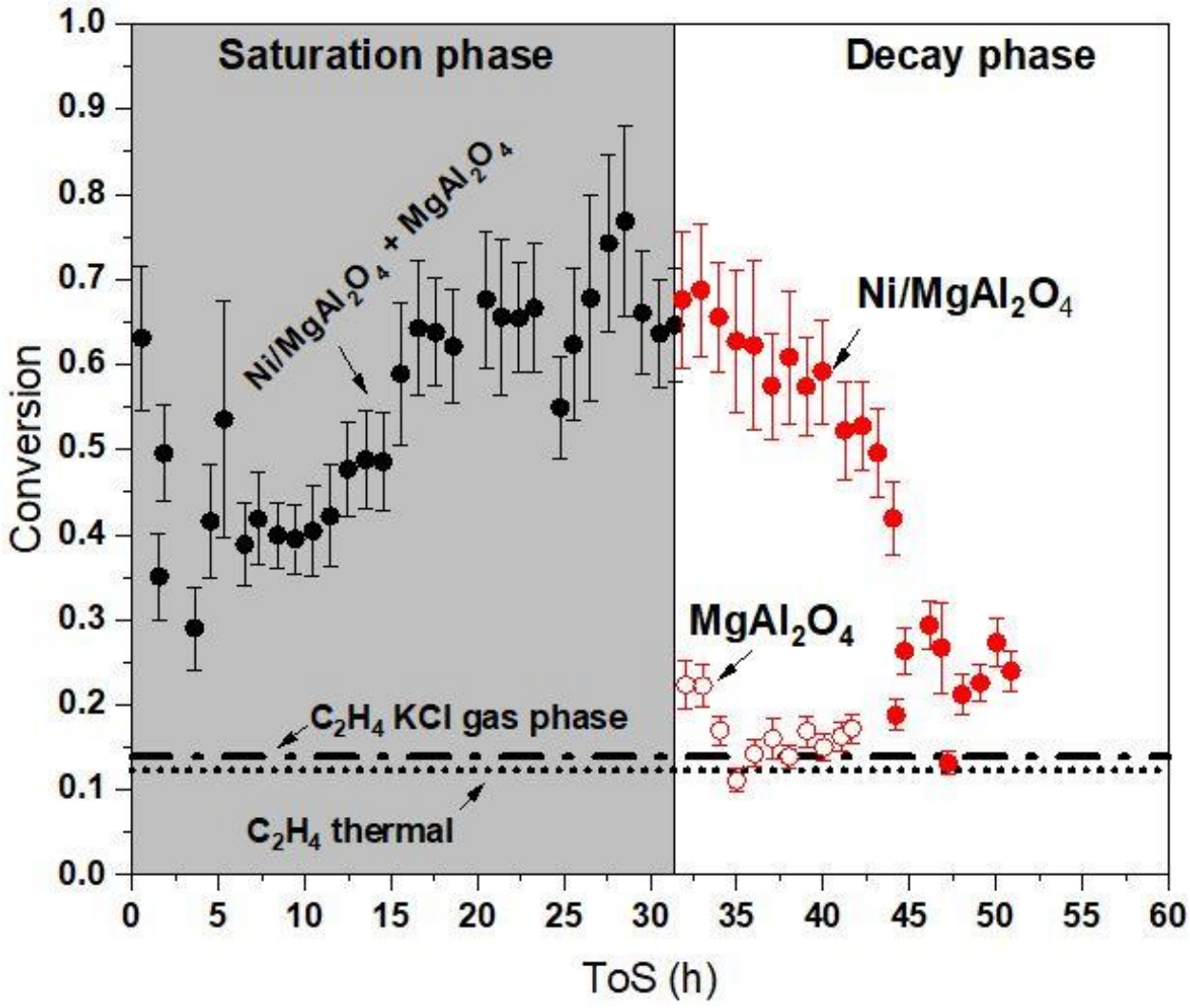

Figure 7.4 Conversion of C_2H_4 as function of ToS during the saturation phase and decay phase

Figure 7.5¡Error! No se encuentra el origen de la referencia. depicts the conversion of $C_{10}H_8$ during the saturation and decay phases. In addition, the thermal conversion of $C_{10}H_8$ (short dashed line) and the conversion of caused by gas-phase reactions in the presence of K aerosol (dash dot), respectively are shown. The total error of each point is considerably higher than in the case of the lighter hydrocarbons due to the greater error sources and uncertainties during the sampling, extraction, identification and quantification steps associated with the SPA-CG method [282]. Nevertheless, a positive effect on the $C_{10}H_8$ conversion during the saturation phase is observed, particularly after 15 h ToS. In the case of the catalyst during the decay phase, after an initial period (ca. 15 h) of seemingly constant values similar to the values obtained at the end of the saturation phase a steady decrement in the conversion values occurred. As with the lighter hydrocarbons, it was assumed that at

669 the end of the decay phase the catalyst restored its initial sulfur coverage. The conversion
670 values found in the case of the support from the period 35 to 37 h ToS were roughly half the
671 values observed with the catalyst. Thence, the K-promoted support showed a notable effect
672 on the overall conversion. Interestingly, a decreasing trend for the conversion values was
673 observed also in the case of the support. From this result and from the decrease in the K
674 content of the support at the end of the decay phase as shown in **Figure 7.2** it can be
675 conjectured that the presence of K in the support enhanced the transformation reactions of
676 $C_{10}H_8$. Furthermore, the conversion value caused by the gas-phase reactions during KCl
677 dosing was higher than the thermal conversion. This result is supported by the findings of
678 Elliott and Baker [128] who studied the pyrolysis of wood at 700 °C in a fluidized bed
679 reactor. After K impregnation of the wood before pyrolysis (8 wt. %) the authors [128]
680 obtained a 90 % $C_{10}H_8$ reduction compared to the experiment with the unpromoted biomass.
681 Although, solid K-carbon reactions are expected to play a major role in the tar compounds
682 conversion [283] ,gas phase reactions aided by formation of radicals at high temperatures (≥
683 750 °C) were observed to enhance the interaction between hydrocarbon compounds formed
684 during the pyrolysis of white oak [48] and could be also important in the conditions used in
685 the present study.

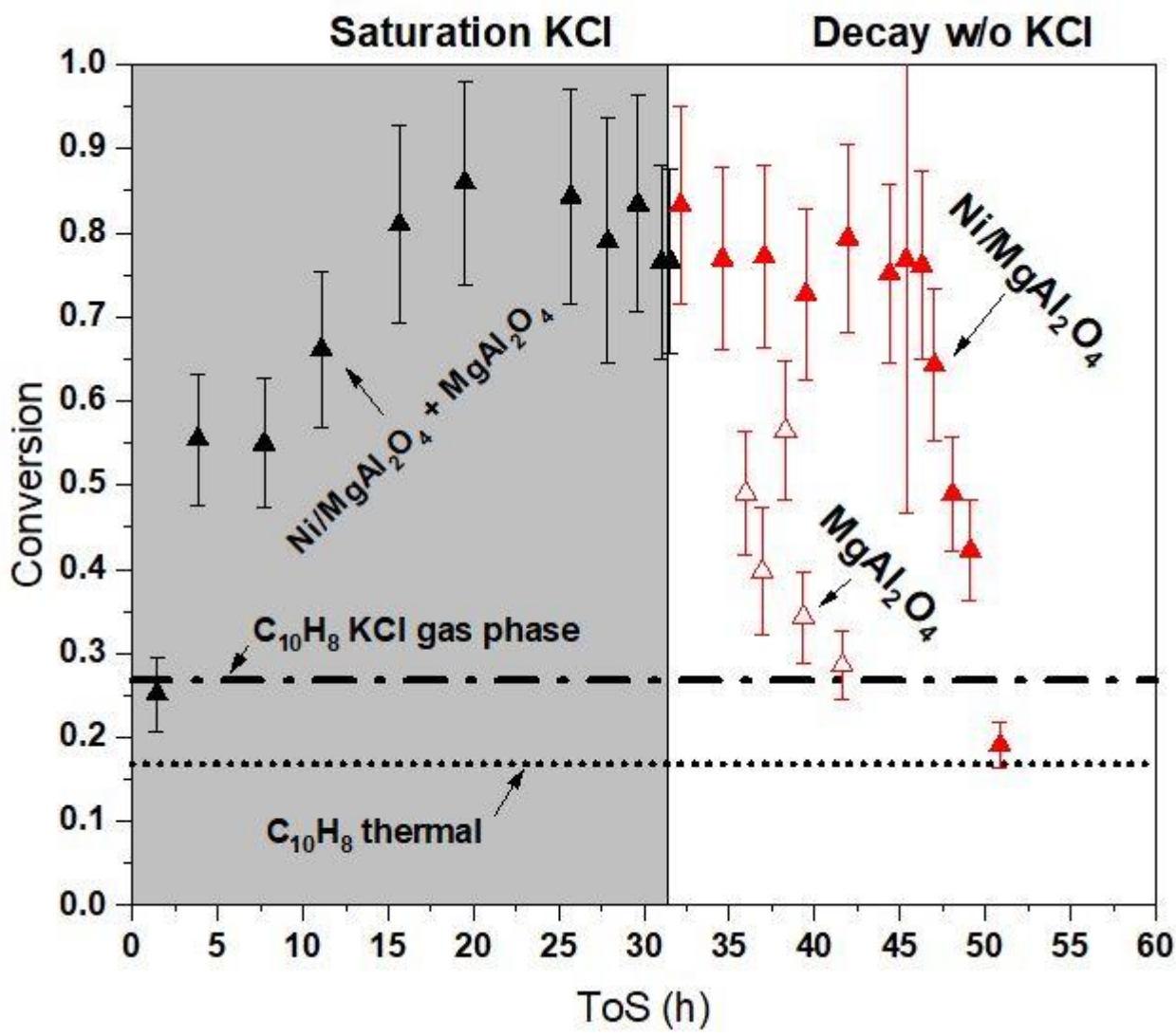

Figure 7.5 Conversion of $C_{10}H_8$ during the saturation and decay phases

Conversion of light and heavy hydrocarbons present in the producer gas through steam reforming and cracking reactions is predicted to increase the molar flow rate of H_2. **Figure 7.6** displays the H_2 molar flow formation as a function of ToS, calculated as the difference between the measured H_2 molar flow rate at the outlet and inlet of the reforming reactor. A constant value around 1.5 mol h^{-1} was observed during the saturation phase with an increasing trend towards the end of the experiment. This increasing behavior towards the end of the saturation phase cannot be explained by a higher conversion of CH_4, C_2H_4 or $C_{10}H_8$ as it can be appreciated in **Figure 7.3**, **Figure 7.4** and **Figure 7.5**, respectively. Although an increasing trend in the C_{10+} conversion was obtained during the end of the saturation phase its contribution to the H_2 formation was negligible compared to the observed H_2

increment in **Figure 7.6**. Despite the uncertainties in the C_6H_6 conversion values a clear increment was noticed after 28 h ToS (**Table 7.1**), the contribution on the H_2 production was 0.44 mol h^{-1} assuming complete steam reforming reaction to CO and H_2, therefore, the observed H_2 increment at the end of the saturation phase could be ascribed to the increased C_6H_6 conversion during the same period. The H_2 molar flow formation showed a decreasing behavior during the decay phase in the case of the catalyst. This result is in accordance with the observed CH_4, C_2H_4 and $C_{10}H_8$ conversion decrement during the decay phase. In the case of the support the values were close to zero and similar to the H_2 molar flow formation achieved during the thermal conversion of the producer gas. Considering this result as well as the observed CH_4, C_2H_4 and $C_{10}H_8$ conversion values in the case of the support (**Figure 7.3**, **Figure 7.4** and **Figure 7.5**) it can be surmise that the observed conversion in the case of the support cannot be ascribed to steam reforming reactions, hence, probably coke formation reactions were the reason behind the observed $C_{10}H_8$ conversion with the support [193]. Interestingly, the H_2 molar flow formation caused by gas-phase reactions enhanced by KCl aerosol addition where clearly higher than the increment observed by the thermal reactions and in the case of the support. A possible contribution to the H_2 increment due to gas-phase reactions during KCl dosing could be ascribed to the carbothermic reduction reaction whereby metal K is formed. The latter can further react with steam to produce KOH and H_2 as proposed by McKee [283]. Its noteworthy to point out that according to the Mears' criterion, calculated based on the values observed at the beginning of the decay phase, in the case of CH_4 the experiments were run under external mass transfer limitations whereas for C_2H_4 and $C_{10}H_8$ external mass transfer limitations are likely less severe but cannot be excluded, see **Table 3.8**. Thence the observed impact of K aerosol addition on the conversion of CH_4, C_2H_4 and $C_{10}H_8$ is also a function of the mass transfer coefficient at the experimental conditions used in the reactor.

725 **Table 7.1** C_6H_6 conversion the corresponding H_2 formation assuming complete steam reforming reaction to CO and H_2

Time (h)	1.4	3.8	7.7	11.0	15.6	19.4	25.7	27.8	29.6	31.0	31.5
C_6H_6 conversion	-1.6	-0.8	-0.4	-0.7	-0.4	-0.2	0.1	0.4	0.5	0.6	0.6
SD	0.47	0.18	0.09	0.14	0.08	0.04	0.03	0.10	0.12	0.19	0.14
H_2 formation (mol h^{-1})	-1.21	-0.61	-0.30	-0.48	-0.27	-0.13	0.09	0.31	0.39	0.47	0.46
SD	0.43	0.19	0.09	0.15	0.08	0.04	0.03	0.10	0.12	0.17	0.14

726 a H_2 formation considering complete C_6H_6 steam reforming to CO and H_2

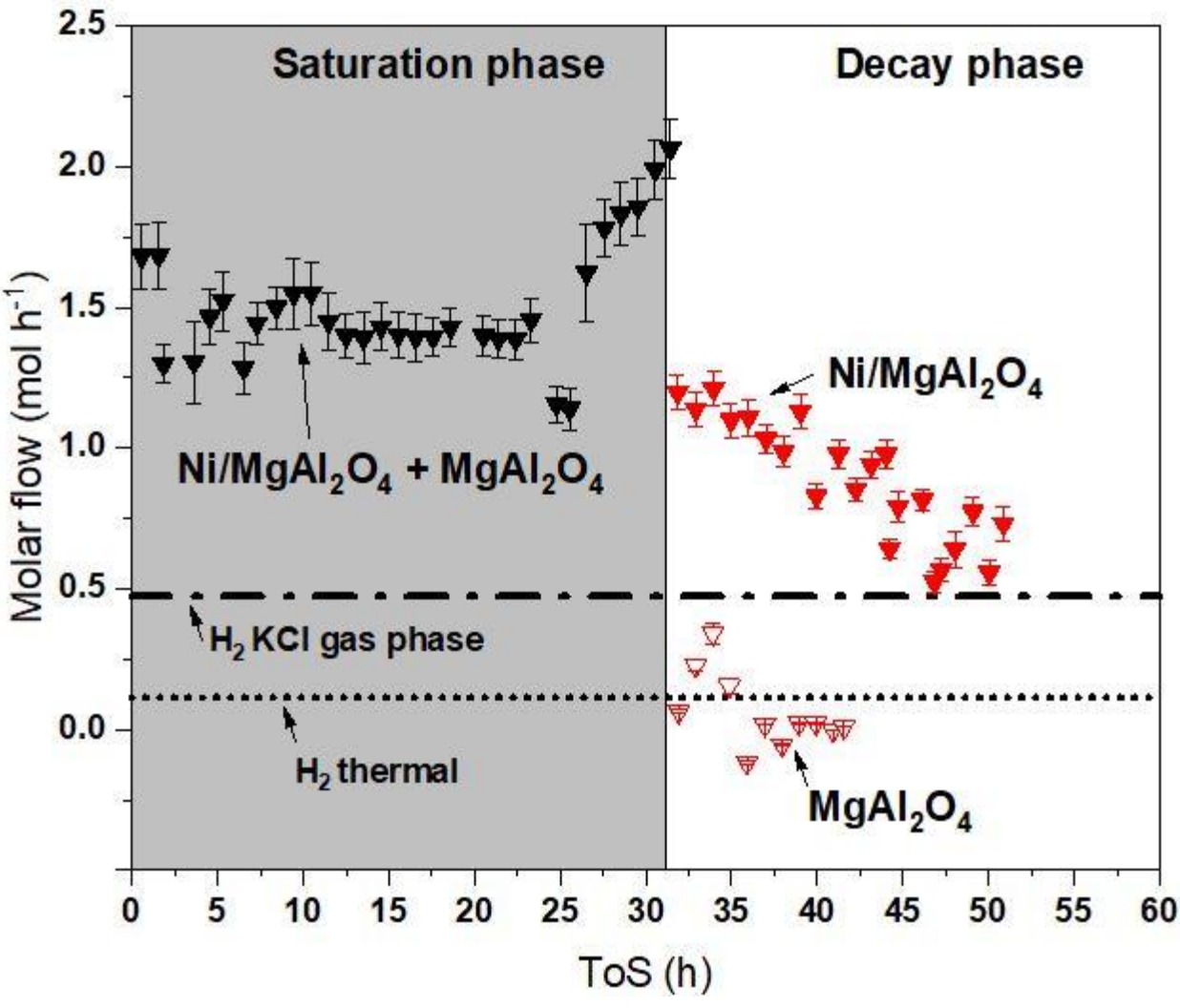

727

728 **Figure 7.6** H_2 molar flow formation as a function of ToS. Calculated as the difference between the measured H_2 molar flow
729 rate at the outlet and inlet of the reforming reactor

7.4 Proposed mechanism for the K interaction with the S-passivated Ni/$MgAl_2O_4$ under realistic steam reforming conditions.

Based on the obtained results of CH_4, C_2H_4 and $C_{10}H_8$ conversion, H_2 molar flow increment and K and S content on the catalyst before and after the different phases studied i.e. saturation and decay, a proposed mechanism for the interaction of K species on the S-passivated catalysts was proposed and is illustrated in **Figure 7.7.** In the proposed mechanism the positive effect of K addition to the reforming reactor is associated with changes in the sulfur coverage of the catalyst[16], for example by weakening of the nickel sulfide bond[147], [150] . In the absence of gas-phase K, the θ_s of the catalyst is expected to be around 0.97 with small fluctuations depending on the gasification and filtration conditions. The steam reforming activity of the catalyst at this high S-coverage is limited and close to the values found at the end of the decay phase[15]. Therefore, lowering of the θ_s by means of K and adsorbed S interaction and consequently increment in the catalyst steam reforming activity is predicted. Three plausible locations for the potassium species that are involved during the interaction with sulfur chemisorbed on the catalyst surface were contemplate; 1) potassium species adsorbed on the support relatively far from the nickel active sites. On this position it is predicted a high concentration of K species but also a strong bonding with the support and thereby less mobility is anticipated for this K species. 2) gas-phase potassium species. The probability in this case is lower although its contribution cannot be excluded. 3) K-species in close proximity to the nickel active site e.g. Ni-support interface. The third proposed location it is the most likely scenario based on the results obtained in the present study and previous studies[15]. This hypothesis is supported by the findings of Pitchon et al.[284], who observed the presence of K at the interface between the particle and the support of a Ni/SiO_2 catalysts impregnated by KNO_3. Strong interaction of potassium and sulfur was evinced from the results of Rostrup-Nielsen [266]. Comparing the sulfur poisoning regenerability of a K-impregnated Ni/$MgAl_2O_4$ with the unpromoted catalyst the author [266] obtained significant differences. The regeneration experiments were carried out raising the temperature from 500 to 800 °C in a 75 mol. %

steam/argon stream and it was evaluated by measuring the sulfur content in the outlet stream. Whereas complete regeneration was obtained for the unpromoted catalysts, negligible sulfur removal was observed for the K promoted one. During parallel chemisorption studies Rostrup-Nielsen [266] proved that H_2S was not retained by KOH at the low H_2S partial pressure used in the experiments (10^{-6}). Therefore it was suggested that a multistep process involving the formation of K_2SO_4 was the cause of the nearly complete sulfur retention [266]. Whether the K-S interaction will result in the formation of a gaseous/vapor potassium-sulfur compound as observed by Arabczyk et al [151] cannot be concluded with the results obtained. Formation of H_2S enhanced by weakening of sulfur-nickel bond is envisaged due to the high temperature and relatively high H_2 concentration [238].

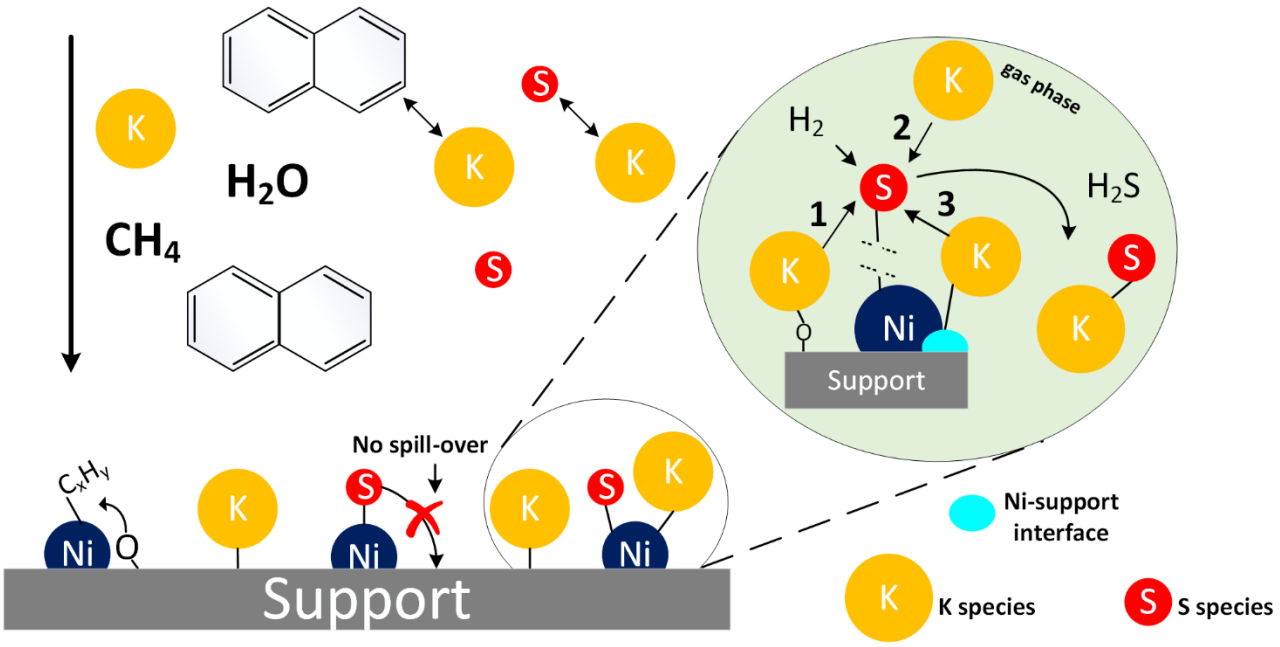

Figure 7.7 Proposed mechanism for the interaction and impact of K on the S-passivated $Ni/MgAl_2O_4$ under steam reforming conditions.

7.5 Carbon deposition on the catalyst and support

Under high temperatures steam reforming conditions (≥ 750 °C) methane and higher hydrocarbon compounds decomposition are the main pathway for the carbon formation [285]. The presence of olefins and aromatic compounds in the feed to the reformer are known to accelerate the coke deposition on the catalyst [87], [243]. Moreover, the addition of small quantities of sulfur ($0.7 \leq \theta_S \leq 0.9$) has been shown to control the filamentous carbon deposition on nickel supported catalysts [285], [286].

The specific carbon content measured on the catalyst and support after the pretreatment steps, the saturation phase and the decay phase are listed in **Table 7.2**. A significant increment in the carbon content on the support is obtained after the saturation and decay phases. On the other hand, the carbon content on the catalyst is 2-fold and 50-fold lower, respectively, after the saturation phase and decay phase. Moud et al. [16] working under similar conditions and using the same setup and catalyst as in the present study showed that the measured carbon content on the catalyst was 3.7 mg $gcat^{-1}$ after 36 h ToS. This value is comparable with the value obtained in the present study. Xie et al. [287] observed significantly lower carbon deposition on a Ni/CeO_2-Al_2O_3 compared to the support alone upon steam reforming of Norpar13 without and with sulfur at 800 °C for 55 h ToS. This result was attributed to the possible migration of carbon deposit precursors on the support to the active metal sites along with enhancing steam adsorption and activation due to support-metal interactions [287]. The large carbon deposition measured on the support was ascribed to fuel thermal cracking reaction. Li et al. [229] used Thermogravimetry-Differential Thermal Gravimetry/Analysis (TG-DTG and DTA) techniques to study the coke formation on an industrial reforming Pt-Sn/γ-Al_2O_3 catalysts. The catalyst sample was discharged from an industrial reformer unit. On the DTA curve of the coked catalyst it was obtained a sharp peak at 511 °C and a small shoulder-like peak at 245 °C. the former was attributed to the combustion of coke deposited on the support while the latter was ascribed to the carbon deposited on the metal catalyst. In the present study, however, the carbon

content was distinctly low in the catalyst (Ni metallic and support) than in the support alone after the reforming experiments.

Considering the carbon content results obtained with the catalyst it is safe to say that the positive influence on the S-passivated catalyst activity during the saturation phase with respect to the decay phase was not masked by differences in carbon accumulation on the catalysts during the experiments. The high coke content measured on the support after the saturation and decay phases in is accordance with the lower H_2 molar flow formation (**Figure 7.6**) during the decay phase with the support compared to the catalyst i.e. the steam reforming activity of the support was negligible compared to the activity of the catalyst.

Table 7.2 Specific carbon content after the different pretreatments and phases (saturation and decay) of the study.

	Specific carbon content (mg $gcat^{-1}$)			
	Ageing	Sulfidation	Saturation phase	Decay phase
$Ni/MgAl_2O_4$	≤ 0.5	0.6	2.2	0.7
$MgAl_2O_4$	≤ 0.7	0.6	19.4	35.7

7.6 Summary

It was shown that sulfur compounds were adsorbed only on the $Ni/MgAl_2O_4$ while its presence was not found on the support ($MgAl_2O_4$). On the other hand, similar amounts of K were obtained on the catalyst and support after addition of KCl in the vapor phase to the reformer. Considering the high S content remaining on the catalyst, it was deemed that the preferential adsorption site for K was on the support. Conversion obtained with the aged and sulfur-passivated catalyst was ≤ 0.2 for all the hydrocarbon compounds examined. Significant increment in the activity of the catalyst was observed during KCl aerosol addition reaching conversion values ≥ 0.6 in the case of C_2H_4 and $C_{10}H_8$. This result was ascribed to K-S interactions causing reduction in the sulfur coverage of the catalyst. When feeding of KCl was stopped the conversion obtained with the catalyst decreased steadily in the case of CH_4 and C_2H_4 while more ToS was required to observed a diminution in the

$C_{10}H_8$ conversion. Conversion of the K-promoted support in the absence of KCl dosing was similar to the sulfur-passivated catalyst except for $C_{10}H_8$ which was higher although it showed decreasing trend with ToS. The increment in the H_2 molar flow at the outlet with respect to the inlet of the reactor was pronounce during KCl addition, whereas after stopping the aerosol dosing a steady decreasing behavior was observed. Conversion due to gas-phase reactions during KCl addition was ≤ 0.1 for CH_4 and C_2H_4 These values were close to the values achieved with the inert material. Therefore, the effect of the gas-phase reactions enhanced by the presence of KCl were limited for these light hydrocarbons. In the case of $C_{10}H_8$ conversion, the observed conversion caused by gas-phase reactions enhance by the presence of KCl was notably higher than the thermal conversion. The surface area of the catalyst was not affected by the KCl addition, exposure to the producer gas for 50 h ToS or the sulfidation period. Consequently, the ageing method used was effective and ensured stable BET surface area throughout the length of the tests. Based on the results it was proposed a mechanism where K present in the Ni-support interface interacts with the sulfur adsorbed on the nickel active site thereby enabling the later to catalyze the steam reforming reaction. Carbon deposition was found to be markedly higher in the case of the support compared to the catalyst.

8 Conclusions and recommendations

As stated at the beginning of the present work the gasification of biomass to produce biofuels and for fuel cell applications still needs better techno-economic assessments and deeper understanding of the phenomena behind the conversion of the feedstock to the final products. Synergistic collaboration between academia and industry its necessary to overcome the present knowledge gap. Removal of tar remains the main hurdle to realize efficient and profitable processes. Search and test of low-cost readily available and preferably environmental-friendly materials seems to be a viable way to tackle the tar removal subject. The use of catalytic hot tar removal methods will play an important role in the development of the technology and intensify efforts should be devoted to the comprehension of this secondary methods.

The use of char as guard bed in the catalytic hot tar removal configuration appears as a promising solution, which will increase the lifetime of the steam reformer catalysts. The guard bed configuration as well as operation parameters warrant more and detailed studies. The fixed bed design used in the tar removal experiments will create unsustainable pressure drop values on commercial applications systems and thus alternatives configurations must be employed, such as fluidized bed reactors and/or splitting of the gas stream.

The main contribution to the research literature from chapter 5 is the new synthesis routes for mayenite preparation together with the comparison of the impact of the Ni addition method to the obtained supports in the steam reforming reaction of model tar compounds. Different preparation methods will result in different interaction of the active sites with the support and this information is lacking in the existing literature where no distinction have been made between different synthesis routes for mayenite-supported nickel catalysts (although for the Ni-CaO-mayenite catalysts there is one study that have reported on the different interaction mechanisms caused by differences in the nickel addition method [208]). Different nickel-support interactions due to the applied nickel addition method were verified by TPR analysis. Longer ToS and severer conditions, closer to that found in real

874 producer gas from biomass gasifiers, are warranted to assess the steam reforming activity
875 and stability of the Ni/mayenite catalysts in order to draw further conclusions and give a
876 relevant contribution to the research community.

877 The use of **Eq. 3.12** developed by Alstrup et al. [122] for the calculation of the sulfur coverage
878 θs ,although its popular acceptance, must be done with care due to its inherent limitations
879 at high sulfur coverages values. As was shown on the sulfur poisoning studies on chapters
880 6 and 7, typical temperatures and H_2S concentration values present in the syngas produced
881 from biomass gasification correspond to $\theta s \geq 0.9$ thus in the range of significant inaccuracy
882 of the equation. Moreover with the increasing utilization of fuel cells systems in
883 transportation and portable applications with in-situ hydrogen production [288] the effects
884 of diffusion restrictions on the sulfur elution will be less severe and the study of the intrinsic
885 sulfur tolerance and regeneration behavior of the catalysts will have greater relevance. The
886 unexpected sulfur tolerance on the WGS activity of the Ni/mayenite (synthesized by the
887 auto-combustion method) is a promising result which needs a deeper understanding of the
888 reasons behind its improved sulfur tolerance. More characterization techniques (preferably
889 in-situ e.g. the conductivity sensor proposed by Fremerey et al. [289], [290]) to study the
890 structure, morphology and chemical composition of the fresh and spent catalyst should give
891 the information missing such as the number of poisoned active sites at each sulfur
892 concentration and temperature used in order to correlate it with the observed catalysts
893 activity and therefore be able to propose exhaustive conclusions. This later information
894 could be used to elaborate an empirical correlation which allow the calculation of the sulfur
895 coverage of the catalyst. From the results obtained it can be concluded that to achieve
896 moderate-to-high conversion values in the presence of ≈75 ppm(v) of H_2S of the tar
897 compounds present in a H_2-rich syngas with the used catalysts, the operating temperature
898 of the reformer should be close to 900 °C in the case of the nickel catalysts and ca. 850 °C for
899 the rhodium catalyst.

900 It was demonstrated in chapter 7 that adsorption of sulfur on the support at the
901 experimental conditions used did not occurred. Its adsorption took place only on the nickel

902 sites of the catalysts. On the other hand, the preferable adsorption site for potassium was
903 determined to be on the support. These results are essential to gain insight on the observed
904 beneficial effect of adding an aerosol of an aqueous KCl solution in the reformer reactor to
905 the performance of a sulfur-passivated commercial Ni/$MgAl_2O_4$ on the steam reforming of
906 CH_4, C_2H_4 and $C_{10}H_8$.The promising results obtained during the study of the effect of K
907 addition require in-depth understanding, especially the conjecture of the decreased sulfur
908 coverage caused by interaction of K species with the sulfur adsorbed on the nickel sites. The
909 source of K should not add corrosive or poisoning compounds to the producer gas stream.
910 The use of simulated producer gas streams with known and limited concentration of tar
911 compounds as well as non-condensable gases could help to elucidate the complex
912 interaction between K and the sulfur passivated Ni/$MgAl_2O_4$ catalyst. As suggested by
913 Pouya Moud [15], in-situ determination of the K adsorption energy on sulfur passivated
914 nickel-based catalysts will contribute to enlighten the reasons behind the positive effect of
915 K addition in the steam reforming performance of the catalyst. In addition as already
916 proposed by Pouya Moud [15] the use of surface science studies together with
917 computational aided investigations such as DFT modelling are require to clarify the
918 thermodynamic speciation of the K and S species and it will give an atom-resolved picture
919 of the mechanisms of interaction. A technoeconomic study regarding the design of the
920 gasifier and producer gas cleaning systems aiming the addition of K before the tar reforming
921 reactor is needed to make a contribution of industrial relevance. Further experiments are
922 required to gain insight on the nature (ions, atoms and excited potassium species [278]) and
923 activation energy of the interaction between k and the sulfur-passivated catalyst.

9 Acknowledgments

I am grateful to my supervisor prof. Marco Scarsella for his support throughout my career. His encouragements helped me brought this work to conclusion. My gratitude goes also for prof. Paolo De Filippis for his availability and fruitful discussions. It was a pleasure to work with Benedetta de Caprariis, Paola Bracciale and Titta, I admire you and wish the best for each of you. My journey as a PhD student started thanks to prof. Luca di Palma and prof. Elizabetta Petrucci and I am always grateful for this opportunity.

I have spent many days working along with different master's students. It has been a leaning path and all of the students are part of it. Hope all of you find your way to success and joy.

A special dedication goes to my colleagues and supervisors in VTT and KTH. I have met talented, laborious and humble people. I only have good memories from you. I am deeply grateful to Noora Kaisalo for her co-supervisor role when I was in VTT.

Interesting conversations about life and work have made my time at DICMA more pleasurable and for that I am grateful to Irene Bavasso and Giorgio Vilardi.

I want to give my sincere gratitude to my family. Your support and love have always been present.

Claudia Strambo has contributed to the realization of this work in many ways and I truly appreciate what you have done.

10 References

[1] IEA, "Key world energy statistics," 2017.

[2] I. Dincer, A. Midilli, and H. Kucuk, *Progress in Exergy, Energy, and the Environment | Ibrahim Dincer | Springer*. .

[3] B. V. Mathiesen *et al.*, "Smart Energy Systems for coherent 100% renewable energy and transport solutions," *Appl. Energy*, vol. 145, pp. 139–154, 2015.

[4] The Royal Society, "Sustainable biofuels: prospects and challenges," *Sustain. biofuels*, no. January, pp. 1–79, 2008.

[5] L. Zhang, C. (Charles) Xu, and P. Champagne, "Overview of recent advances in thermo-chemical conversion of biomass," *Energy Convers. Manag.*, vol. 51, no. 5, pp. 969–982, 2010.

[6] V. Strezov, B. Moghtaderi, and J. A. Lucas, "Thermal Study of Decomposition of Selected Biomass Samples," *J. Therm. Anal. Calorim.*, vol. 72, pp. 1041–1048, 2003.

[7] S. Heidenreich and P. U. Foscolo, "New concepts in biomass gasification," *Prog. Energy Combust. Sci.*, vol. 46, pp. 72–95, 2015.

[8] I. Hannula and E. Kurkela, "Liquid transportation fuels bed gasification of lignocellulosic biomass," 2013.

[9] K. Engvall, H. Kusar, K. Sjöström, and L. J. Pettersson, "Upgrading of raw gas from biomass and waste gasification: Challenges and opportunities," *Top. Catal.*, vol. 54, no. 13–15, pp. 949–959, 2011.

[10] Y. Lu, J. Chen, Y. Liu, Q. Xue, and M. He, "Highly sulfur-tolerant Pt/$Ce_{0.8}Gd_{0.2}O_{1.9}$ catalyst for steam reforming of liquid hydrocarbons in fuel cell applications," *J. Catal.*, vol. 254, no. 1, pp. 39–48, 2008.

[11] A. C. McCoy, M. J. Duran, A. M. Azad, S. Chattopadhyay, and M. A. Abraham, "Performance of sulfur tolerant reforming catalysts for production of hydrogen from jet fuel simulants," *Energy and Fuels*, vol. 21, no. 6, pp. 3513–3519, 2007.

[12] J. R. Rostrup-Nielsen and L. . Christiansen, *Concepts in syngas manufacture*, Vol. 10. London:

Imperial College Press, 2011.

[13] J. Sehested, "Four challenges for nickel steam-reforming catalysts," *Catal. Today*, vol. 111, no. 1–2, pp. 103–110, 2006.

[14] B. de Caprariis, M. P. Bracciale, P. De Filippis, A. D. Hernandez, A. Petrullo, and M. Scarsella, "Steam reforming of tar model compounds over ni supported on CeO 2 and mayenite," *Can. J. Chem. Eng.*, vol. 95, no. 9, pp. 1745–1751, 2017.

[15] P. H. Moud, *Catalytic Conversion of Undesired Organic Compounds to Syngas in Biomass Gasification and Pyrolysis Applications*. 2017.

[16] P. H. Moud, K. J. Andersson, R. Lanza, and K. Engvall, "Equilibrium potassium coverage and its effect on a Ni tar reforming catalyst in alkali- and sulfur-laden biomass gasification gases," *Appl. Catal. B Environ.*, vol. 190, pp. 137–146, 2016.

[17] S. V. Vassilev, D. Baxter, L. K. Andersen, and C. G. Vassileva, "An overview of the chemical composition of biomass," *Fuel*, vol. 89, no. 5, pp. 913–933, 2010.

[18] A. E. Farrell and A. R. Gopal, "Bioenergy research needs for heat, electricity, and liquid fuels," *MRS Bull.*, vol. 33, no. 4, pp. 373–380, 2008.

[19] F. X. Collard and J. Blin, "A review on pyrolysis of biomass constituents: Mechanisms and composition of the products obtained from the conversion of cellulose, hemicelluloses and lignin," *Renew. Sustain. Energy Rev.*, vol. 38, pp. 594–608, 2014.

[20] M. Van de Velden, J. Baeyens, A. Brems, B. Janssens, and R. Dewil, "Fundamentals, kinetics and endothermicity of the biomass pyrolysis reaction," *Renew. Energy*, vol. 35, no. 1, pp. 232–242, 2010.

[21] M. Van de Velden, J. Baeyens, A. Brems, B. Janssens, and R. Dewil, "Fundamentals, kinetics and endothermicity of the biomass pyrolysis reaction," *Renew. Energy*, vol. 35, no. 1, pp. 232–242, 2010.

[22] T. A. Milne, R. J. Evans, and N. Abatzaglou, "Biomass Gasifier '"Tars"': Their Nature, Formation, and Conversion," no. November, 1998.

[23] W. Torres, S. S. Pansare, and J. G. Goodwin, "Hot gas removal of tars, ammonia, and hydrogen sulfide from biomass gasification gas," *Catal. Rev. - Sci. Eng.*, vol. 49, no. 4, pp.

407–456, 2007.

[24] N. Couto, A. Rouboa, V. Silva, E. Monteiro, and K. Bouziane, "Influence of the biomass gasification processes on the final composition of syngas," *Energy Procedia*, vol. 36, pp. 596–606, 2013.

[25] L. Devi, K. J. Ptasinski, and F. J. J. G. Janssen, "A review of the primary measures for tar elimination in biomass gasification processes," *Biomass and Bioenergy*, vol. 24, no. 2, pp. 125–140, 2002.

[26] V. Nemanova, "Biomass Gasification in Abfb : Tar Mitigation," KTH Royal Institute of Technology, 2014.

[27] A. Van der Drift and H. Boerrigter, "Synthesis gas from biomass for fuels and chemicals," *SYNBIOS Conf. Stock. Sweden. May*, no. January, pp. 1–31, 2005.

[28] K. J. Andersson, M. Skov-Skjøth Rasmussen, and P. E. Højlund Nielsen, "Industrial-scale gas conditioning including Topsoe tar reforming and purification downstream biomass gasifiers: An overview and recent examples," *Fuel*, vol. 203, pp. 1026–1030, 2017.

[29] D. Dayton, "Review of the Literature on Catalytic Biomass Tar Destruction: Milestone Completion Report," no. December, 2002.

[30] E. Baker, M. Brown, D. C. Elliott, and L. Mudge, "Characterization and treatment of tars from biomass gasifiers," *AIChE 1988 Summer Natl. Meet.*, p. 11, 1988.

[31] X. Meng, W. De Jong, R. Pal, and A. H. M. Verkooijen, "In bed and downstream hot gas desulphurization during solid fuel gasification: A review," *Fuel Process. Technol.*, vol. 91, no. 8, pp. 964–981, 2010.

[32] P. J. Woolcock and R. C. Brown, "A review of cleaning technologies for biomass-derived syngas," *Biomass and Bioenergy*, vol. 52, pp. 54–84, 2013.

[33] K. Salo and W. Mojtahedi, "Fate of alkali and trace metals in biomass gasification," *Biomass and Bioenergy*, vol. 15, no. 3, pp. 263–267, 1998.

[34] S. Q. Turn, C. M. Kinoshita, D. M. Ishimura, and J. Zhou, "The fate of inorganic constituents of biomass in fluidized bed gasification," *Fuel*, vol. 77, no. 3, pp. 135–146, 1998.

[35] A. Norheim, D. Lindberg, J. E. Hustad, and R. Backman, "Equilibrium calculations of the composition of trace compounds from biomass gasification in the solid oxide fuel cell operating temperature interval," *Energy and Fuels*, vol. 23, no. 2, pp. 920–925, 2009.

[36] K. Froment, F. Defoort, C. Bertrand, J. M. Seiler, J. Berjonneau, and J. Poirier, "Thermodynamic equilibrium calculations of the volatilization and condensation of inorganics during wood gasification," *Fuel*, vol. 107, pp. 269–281, 2013.

[37] H. Hofbauer, G. Veronik, T. Fleck, R. Rauch, H. Mackinger, and E. Fercher, "The FICFB - Gasification Process," in *Bridgwater A.V., Boocock D.G.B. (eds) Developments in Thermochemical Biomass Conversion. Springer, Dordrecht*, vol. 2, 1997, pp. 1016–1025.

[38] A. Larsson, M. Seemann, D. Neves, and H. Thunman, "Evaluation of performance of industrial-scale dual fluidized bed gasifiers using the chalmers 2-4-MWth gasifier," *Energy and Fuels*, vol. 27, no. 11, pp. 6665–6680, 2013.

[39] C. Pfeifer, S. Koppatz, and H. Hofbauer, "Steam gasification of various feedstocks at a dual fluidised bed gasifier: Impacts of operation conditions and bed materials," *Biomass Convers. Biorefinery*, vol. 1, no. 1, pp. 39–53, 2011.

[40] T. Murakami, G. Xu, T. Suda, Y. Matsuzawa, H. Tani, and T. Fujimori, "Some process fundamentals of biomass gasification in dual fluidized bed," *Fuel*, vol. 86, no. 1–2, pp. 244–255, 2007.

[41] G. Xu, T. Murakami, T. Suda, and Y. Matsuzawa, "Reactor siphon and its control of particle flow rate when integrated into a circulating fluidized bed," *Ind. Eng. Chem. Res.*, vol. 44, no. 24, pp. 9347–9354, 2005.

[42] M. L. Mastellone and U. Arena, "Olivine as a Tar Removal Catalyst During Fluidized Bed Gasification of Plastic Waste," *VTT Publ.*, vol. 54, no. 504, pp. 3–194, 2003.

[43] J. Marinkovic, H. Thunman, P. Knutsson, and M. Seemann, "Characteristics of olivine as a bed material in an indirect biomass gasifier," *Chem. Eng. J.*, vol. 279, pp. 555–566, 2015.

[44] K. Göransson, U. Söderlind, J. He, and W. Zhang, "Review of syngas production via biomass DFBGs," *Renew. Sustain. Energy Rev.*, vol. 15, no. 1, pp. 482–492, 2011.

[45] J. Corella, J. M. Toledo, and G. Molina, "A Review on Dual Fluidized-Bed Biomass

Gasifiers," *Ind. Eng. Chem. Res.*, vol. 46, pp. 6831–6839, 2007.

[46] R. Warnecke, "Gasification of biomass: comparison of fixed bed and fluidized bed gasifier," *Biomass and Bioenergy*, vol. 18, pp. 489–497, 2000.

[47] J. A. Ruiz, M. C. Juárez, M. P. Morales, P. Muñoz, and M. A. Mendívil, "Biomass gasification for electricity generation: Review of current technology barriers," *Renew. Sustain. Energy Rev.*, vol. 18, pp. 174–183, 2013.

[48] M. W. Jarvis *et al.*, "Elucidation of biomass pyrolysis products using a laminar entrained flow reactor and char particle imaging," *Energy and Fuels*, vol. 25, no. 1, pp. 324–336, 2011.

[49] B. Shukla and M. Koshi, "Comparative study on the growth mechanisms of PAHs," *Combust. Flame*, vol. 158, no. 2, pp. 369–375, 2011.

[50] B. Shukla and M. Koshi, "A novel route for PAH growth in HACA based mechanisms," *Combust. Flame*, vol. 159, no. 12, pp. 3589–3596, 2012.

[51] M. L. Valderrama Rios, A. M. González, E. E. S. Lora, and O. A. Almazán del Olmo, "Reduction of tar generated during biomass gasification: A review," *Biomass and Bioenergy*, vol. 108, no. November 2017, pp. 345–370, 2018.

[52] M. Kurkela, "Biomass gasification fundamentals to support the development of BTL in forest industry Publishable fi Biomass gasifi cation fundamentals to support the development of BTL in forest industry Publishable fi nal scientifi c report of Nordsyngas project Edit," Finland, 2015.

[53] P. Simell *et al.*, "Clean syngas from biomass. Process development and concept assessment," *Biomass Convers. Biorefinery*, vol. 4, no. 4, pp. 357–370, 2014.

[54] E. Kurkela, M. Kurkela, and I. Hiltunen, "Steam-oxygen gasification of forest residues and bark followed by hot gas filtration and catalytic reforming of tars: Results of an extended time test," *Fuel Process. Technol.*, vol. 141, pp. 148–158, 2016.

[55] S. Tuomi, E. Kurkela, P. Simell, and M. Reinikainen, "Behaviour of tars on the filter in high temperature filtration of biomass-based gasification gas," *Fuel*, vol. 139, pp. 220–231, 2015.

[56] E. Simeone, M. Siedlecki, M. Nacken, S. Heidenreich, and W. De Jong, "High temperature gas filtration with ceramic candles and ashes characterisation during steam-oxygen blown

gasification of biomass," *Fuel*, vol. 108, pp. 99–111, 2013.

[57] Z. Min, P. Yimsiri, M. Asadullah, S. Zhang, and C. Z. Li, "Catalytic reforming of tar during gasification. Part II. Char as a catalyst or as a catalyst support for tar reforming," *Fuel*, vol. 90, no. 7, pp. 2545–2552, 2011.

[58] Z. Min, S. Zhang, P. Yimsiri, Y. Wang, M. Asadullah, and C. Z. Li, "Catalytic reforming of tar during gasification. Part IV. Changes in the structure of char in the char-supported iron catalyst during reforming," *Fuel*, vol. 106, pp. 858–863, 2013.

[59] P. Gilbert, C. Ryu, V. Sharifi, and J. Swithenbank, "Tar reduction in pyrolysis vapours from biomass over a hot char bed," *Bioresour. Technol.*, vol. 100, no. 23, pp. 6045–6051, 2009.

[60] T. Matsuhara, S. Hosokai, K. Norinaga, K. Matsuoka, C. Z. Li, and J. I. Hayashi, "In-situ reforming of tar from the rapid pyrolysis of a brown coal over char," *Energy and Fuels*, vol. 24, no. 1, pp. 76–83, 2010.

[61] D. Fuentes-Cano, A. Gómez-Barea, S. Nilsson, and P. Ollero, "Decomposition kinetics of model tar compounds over chars with different internal structure to model hot tar removal in biomass gasification," *Chem. Eng. J.*, vol. 228, pp. 1223–1233, 2013.

[62] Y. Shen and K. Yoshikawa, "Recent progresses in catalytic tar elimination during biomass gasification or pyrolysis - A review," *Renew. Sustain. Energy Rev.*, vol. 21, pp. 371–392, 2013.

[63] Y. Shen, "Chars as carbonaceous adsorbents/catalysts for tar elimination during biomass pyrolysis or gasification," *Renew. Sustain. Energy Rev.*, vol. 43, pp. 281–295, 2015.

[64] Y. Zeng, S. Ju, W. Xing, and C. Chen, "Computer simulation of the adsorption of thiophene/benzene mixtures on MFI and MOR," *Sep. Purif. Technol.*, vol. 55, no. 1, pp. 82–90, 2007.

[65] T. Sueyasu, T. Oike, A. Mori, S. Kudo, K. Norinaga, and J. I. Hayashi, "Simultaneous steam reforming of tar and steam gasification of char from the pyrolysis of potassium-loaded woody biomass," *Energy and Fuels*, vol. 26, no. 1, pp. 199–208, 2012.

[66] I. Narváez, J. Corella, and A. Orío, "Fresh Tar (from a Biomass Gasifier) Elimination over a Commercial Steam-Reforming Catalyst. Kinetics and Effect of Different Variables of Operation," *Ind. Eng. Chem. Res.*, vol. 36, no. 2, pp. 317–327, 1997.

[67] K. Matsuoka *et al.*, "Mechanism of woody biomass pyrolysis and gasification in a fluidized bed of porous alumina particles," *Energy and Fuels*, vol. 20, no. 3, pp. 1315–1320, 2006.

[68] A. Erkiaga, G. Lopez, M. Amutio, J. Bilbao, and M. Olazar, "Steam gasification of biomass in a conical spouted bed reactor with olivine and γ-alumina as primary catalysts," *Fuel Process. Technol.*, vol. 116, pp. 292–299, 2013.

[69] T. Y. Mun, B. S. Kang, and J. S. Kim, "Production of a producer gas with high heating values and less tar from dried sewage sludge through air gasification using a two-stage gasifier and activated carbon," *Energy and Fuels*, vol. 23, no. 6, pp. 3268–3276, 2009.

[70] G. Asgari, B. Roshani, and G. Ghanizadeh, "The investigation of kinetic and isotherm of fluoride adsorption onto functionalize pumice stone," *J. Hazard. Mater.*, vol. 217–218, pp. 123–132, 2012.

[71] M. Kitis, S. S. Kaplan, E. Karakaya, N. O. Yigit, and G. Civelekoglu, "Adsorption of natural organic matter from waters by iron coated pumice," *Chemosphere*, vol. 66, no. 1, pp. 130–138, 2007.

[72] M. Kitis, E. Karakaya, N. O. Yigit, G. Civelekoglu, and A. Akcil, "Heterogeneous catalytic degradation of cyanide using copper-impregnated pumice and hydrogen peroxide," *Water Res.*, vol. 39, no. 8, pp. 1652–1662, 2005.

[73] U. A. Guler and M. Sarioglu, "Removal of tetracycline from wastewater using pumice stone: Equilibrium, kinetic and thermodynamic studies," *J. Environ. Heal. Sci. Eng.*, vol. 12, no. 1, pp. 1–11, 2014.

[74] F. Akbal, "Adsorption of basic dyes from aqueous solution onto pumice powder," *J. Colloid Interface Sci.*, vol. 286, no. 2, pp. 455–458, 2005.

[75] F. Öztürk Akbal, N. Akdemir, and A. Nur Onar, "FT-IR spectroscopic detection of pesticide after sorption onto modified pumice," *Talanta*, vol. 53, no. 1, pp. 131–135, 2000.

[76] A. Rachel, B. Lavedrine, M. Subrahmanyam, and P. Boule, "Use of porous lavas as supports of photocatalysts," *Catal. Commun.*, vol. 3, no. 4, pp. 165–171, 2002.

[77] R. Coll, J. Salvado, X. Farriol, and D. Montane, "Steam reforming model compounds of biomass gasification tars : conversion at different operating conditions and tendency

towards coke formation," *Fuel Process. Technol.*, vol. 74, pp. 19–31, 2001.

[78] J. Rostrup-Nielsen, *Catalysis science and technology*, 5th ed., no. c. Springer-Verlag Berlin Hiedelberg, 1984.

[79] C. H. Bartholomew and R. J. Farrauto, *Fundamentals of Industrial Catalytic Processes*, Second Edi. 2006.

[80] J. R. Rostrup-Nielsen, J. Sehested, and J. K. Nørskov, "Hydrogen and synthesis gas by steam- and C02 reforming," vol. 47, pp. 65–139, 2002.

[81] M. M. Yung, W. S. Jablonski, and K. A. Magrini-Bair, "Review of catalytic conditioning of biomass-derived syngas," *Energy and Fuels*, vol. 23, no. 4, pp. 1874–1887, 2009.

[82] S. Anis and Z. A. Zainal, "Tar reduction in biomass producer gas via mechanical, catalytic and thermal methods: A review," *Renew. Sustain. Energy Rev.*, vol. 15, no. 5, pp. 2355–2377, 2011.

[83] H. S. Bengaard *et al.*, "Steam Reforming and Graphite Formation on Ni Catalysts," *J. Catal.*, vol. 209, no. 2, pp. 365–384, 2002.

[84] I. Chorkendorff and J. W. Niemantsverdriet, *Concepts of Modern Catalysis and Kinetics*. 2003.

[85] J. Sehested, "Four challenges for nickel steam-reforming catalysts," *Catal. Today*, vol. 111, no. 1–2, pp. 103–110, 2006.

[86] P. V. Aravind and W. De Jong, "Evaluation of high temperature gas cleaning options for biomass gasification product gas for Solid Oxide Fuel Cells," *Prog. Energy Combust. Sci.*, vol. 38, no. 6, pp. 737–764, 2012.

[87] M. Argyle and C. Bartholomew, "Heterogeneous Catalyst Deactivation and Regeneration: A Review," *Catalysts*, vol. 5, no. 1, pp. 145–269, 2015.

[88] P. G. Menon, "Coke on catalysts-harmful, harmless, invisible and beneficial types," *J. Mol. Catal.*, vol. 59, no. 2, pp. 207–220, 1990.

[89] S. Helveg, J. Sehested, and J. R. Rostrup-Nielsen, "Whisker carbon in perspective," *Catal. Today*, vol. 178, no. 1, pp. 42–46, 2011.

[90] J. R. Rostrup-nielsen, "Steam Reforming," *Handb. Heterog. Catal.*, pp. 2882–2905, 2004.

[91] J. R. Rostrup-Nielsen, "Industrial relevance of coking," *Catal. Today*, vol. 37, no. 3, pp. 225–232, 1997.

[92] P. R. S. Jackson, D. J. Young, and D. L. Trimm, "Coke deposition on and removal from metals and heat-resistant alloys under steam-cracking conditions," *J. Mater. Sci.*, vol. 21, no. 12, pp. 4376–4384, 1986.

[93] C. Li, D. Hirabayashi, and K. Suzuki, "A crucial role of O^{2-} and O_2^{2-} on mayenite structure for biomass tar steam reforming over Ni/$Ca_{12}Al_{14}O_{33}$," *Appl. Catal. B Environ.*, vol. 88, no. 3–4, pp. 351–360, 2009.

[94] E. Savuto *et al.*, "Steam reforming of tar model compounds over Ni/Mayenite catalysts: effect of Ce addition," *Fuel*, vol. 224, no. October 2017, pp. 676–686, 2018.

[95] B. de Caprariis, M. P. Bracciale, P. De Filippis, A. D. Hernandez, A. Petrullo, and M. Scarsella, "Steam reforming of tar model compounds over ni supported on CeO2 and mayenite," *Can. J. Chem. Eng.*, vol. 95, no. 9, pp. 1745–1751, 2017.

[96] Q. Zhuang, Y. Qin, and L. Chang, "Promoting effect of cerium oxide in supported nickel catalyst for hydrocarbon steam-reforming," *Appl. Catal.*, vol. 70, no. 1, pp. 1–8, 1991.

[97] A. Cao, R. Lu, and G. Veser, "Stabilizing metal nanoparticles for heterogeneous catalysis," *Phys. Chem. Chem. Phys.*, vol. 12, no. 41, pp. 13499–13510, 2010.

[98] Z. Wang *et al.*, "Production of hydrogen from catalytic steam reforming of bio-oil using C12A7-O--based catalysts," *Appl. Catal. A Gen.*, vol. 320, pp. 24–34, 2007.

[99] H. Hosono, K. Hayashi, K. Kajihara, P. V. Sushko, and A. L. Shluger, "Oxygen ion conduction in $12CaO{\cdot}7Al_2O_3$: O^{2-}conduction mechanism and possibility of O-fast conduction," *Solid State Ionics*, vol. 180, no. 6–8, pp. 550–555, 2009.

[100] P. V. Sushko, A. L. Shluger, K. Hayashi, M. Hirano, and H. Hosono, "Mechanisms of oxygen ion diffusion in a nanoporous complex oxide 12CaO7 Al_2O_3," *Phys. Rev. B - Condens. Matter Mater. Phys.*, vol. 73, no. 1, pp. 1–10, 2006.

[101] H. Boysen, M. Lerch, A. Stys, and A. Senyshyn, "Structure and oxygen mobility in mayenite (Ca12Al 14O33): A high-temperature neutron powder diffraction study," *Acta Crystallogr. Sect. B Struct. Sci.*, vol. 63, no. 5, pp. 675–682, 2007.

[102] H. Hosono, K. Hayashi, K. Kajihara, P. V. Sushko, and A. L. Shluger, "Oxygen ion conduction in $12CaO{\cdot}7Al_2O_3$: O^{2-} conduction mechanism and possibility of O-fast conduction," *Solid State Ionics*, vol. 180, no. 6–8, pp. 550–555, 2009.

[103] D.-K. Lee *et al.*, "Defect chemistry of the cage compound, Ca12Al14O33-δ - understanding the route from a solid electrolyte to a semiconductor and electride _," *Phys. Chem. Chem. Phys.*, vol. 11, no. 30, pp. 3105–3114, 2009.

[104] K. Hayashi, M. Hirano, and H. Hosono, "Thermodynamics and kinetics of hydroxide ion formation in $12CaO{\cdot}7Al_2O_3$," *J. Phys. Chem. B*, vol. 109, no. 24, pp. 11900–11906, 2005.

[105] J. R. Rostrup-Nielsen, "Sulphur Poisoning (Steam Reforming and Methanation)," *Chem. Eng. Sci.*, vol. 39, no. 1, p. 209, 1984.

[106] J. Hepola, J. McCarty, G. Krishnan, and V. Wong, "Elucidation of behavior of sulfur on nickel-based hot gas cleaning catalysts," *Appl. Catal. B Environ.*, vol. 20, no. 3, pp. 191–203, 1999.

[107] E. Wimmer, C. L. Fu, and A. J. Freeman, "Catalytic promotion and poisoning: All-electron local-density-functional theory of CO on Ni(001) surfaces coadsorbed with K or S," *Phys. Rev. Lett.*, vol. 55, no. 23, pp. 2618–2621, 1985.

[108] H. Wise, "Mechanisms of catalyst poisoning by sulfur species," *Stud. Surf. Sci. Catal.*, vol. 68, no. C, pp. 497–504, 1991.

[109] F. Abild-Pedersen, O. Lytken, J. Engbæk, G. Nielsen, I. Chorkendorff, and J. K. Nørskov, "Methane activation on Ni(1 1 1): Effects of poisons and step defects," *Surf. Sci.*, vol. 590, no. 2–3, pp. 127–137, 2005.

[110] P. W. Wentrcek, J. G. McCarty, C. M. Ablow, and H. Wise, "Deactivation of alumina-supported nickel and ruthenium catalysts by sulfur compounds," *J. Catal.*, vol. 61, no. 1, pp. 232–241, 1980.

[111] M. Ashrafi, T. Pröll, C. Pfeifer, and H. Hofbauer, "Experimental study of model biogas catalytic steam reforming: 2. Impact of sulfur on the deactivation and regeneration of Ni-based catalysts," *Energy and Fuels*, vol. 22, no. 6, pp. 4190–4195, 2008.

[112] S. Appari, V. M. Janardhanan, R. Bauri, and S. Jayanti, "Deactivation and regeneration of Ni

catalyst during steam reforming of model biogas: An experimental investigation," *Int. J. Hydrogen Energy*, vol. 39, no. 1, pp. 297–304, 2014.

[113] J. Hepola and P. Simell, "Sulphur poisoning of nickel-based hot gas cleaning catalysts in synthetic gasification gas II. Chemisorption of hydrogen sulphide," *Appl. Catal. B Environ.*, vol. 14, no. 3–4, pp. 305–321, 1997.

[114] J. R. Rostrup-Nielsen, "Sulfur passivated nickel catalysts for carbon-free steam reforming of methane," *J. Catal.*, vol. 85, pp. 31–43, 1984.

[115] J. Biswas, G. M. Bickle, P. G. Gray, and D. D. Do, *The role of crystallite structure on mechanisms of coke and sulphur poisoning in catalytic reforming*, vol. 34, no. C. Elsevier Science Publishers B.V., 1987.

[116] H. S. Bengaard *et al.*, "Steam reforming and graphite formation on Ni catalysts," *J. Catal.*, vol. 209, no. 2, pp. 365–384, 2002.

[117] C. H. Bartholomew, *Mechanisms of nickel catalyst poisoning*, vol. 34, no. C. Elsevier Science Publishers B.V., 1987.

[118] D. R. Mullins, D. R. Huntley, and S. H. Overbury, "Nature of the sulfur induced surface reconstruction on Ni(111)," *Surf. Sci.*, vol. 323, no. 1–2, 1995.

[119] A. Grossmann, W. Erley, and H. Ibach, "Adsorbate-induced surface stress and surface reconstruction: oxygen, sulfur and carbon on Ni(111)," *Surf. Sci.*, vol. 337, no. 3, pp. 183–189, 1995.

[120] J. A. Rodriguez, J. file:///D:/papers/THIOPHENE/Adsorptio. of thiophene on surfaces of clean and N. molybdenum sulfide. pd. Dvorak, A. T. Capitano, A. M. Gabelnick, and J. L. Gland, "Adsorption of thiophene on surfaces of clean and Ni-promoted molybdenum sulfide," *Surf. Sci.*, vol. 429, no. 1, 1999.

[121] V. Maurice, N. Kitakatsu, M. Siegers, and P. Marcus, "Low-coverage sulfur induced reconstruction of Ni(111)," *Surf. Sci.*, vol. 373, pp. 307–317, 1997.

[122] I. Alstrup, J. R. Rostrup-Nielsen, and S. Røen, "High Temperature Hydrogen Sulfide Chemisorption on Nickel Catalysts," *Appl. Catal.*, vol. 1, no. 5, pp. 303–314, 1981.

[123] R. W. Fowler and C. H. Bartholomew, "Activity, Adsorption, and Sulfur Tolerance Studies

of Fluidized Bed Methanation Catalysts," *Ind. Eng. Chem. Prod. Res. Dev.*, vol. 18, no. 4, pp. 339–347, 1979.

[124] E. J. Erekson and C. H. Bartholomrw, "Sulfur poisoning of nickel methanation catalysts. II. In situ deactivation by H_2S of nickel and nickel bimetallics," *Appl. Catal.*, vol. 5, no. 3, pp. 323–336, 1983.

[125] I. Alstrup, B. S. Clausen, C. Olsen, R. H. H. Smits, and J. R. Rostrup-Nielsen, *Promotion of Steam Reforming Catalysts*, vol. 119. Elsevier Masson SAS, 1998.

[126] A. . González.A, "RhPt and Ni Based Catalysts for Fuel Reforming in Energy Conversion," KTH, 2015.

[127] R. Hadden, J. Howe, and K. Waugh, "Hydrocarbon steam reforming catalysts- alkali induced resistance to carbon formation," *Catal. Deactiv.*, no. i, pp. 177–184, 1991.

[128] D. C. Elliott and E. G. Baker, "The effect of catalysis on wood-gasification tar composition," *Biomass*, vol. 9, no. 3, pp. 195–203, 1986.

[129] E. G. Baker, M. D. Brown, and R. J. Robertus, "Catalytic Gasification of Bagasse for the Production of Methanol," 1985.

[130] L. Znak and J. Zieliński, "The effect of potassium on Ni/Al_2O_3catalyst in relation to CO/H_2reaction," *Appl. Catal. A Gen.*, vol. 413–414, pp. 132–139, 2012.

[131] K. M. Bailey, T. K. Campbell, and J. L. Falconer, "Potassium Promotion of Ni/Al_20_3 Catalysts," vol. 54, pp. 159–175, 1989.

[132] J. Juan-Juan, M. C. Román-Martínez, and M. J. Illán-Gómez, "Effect of potassium content in the activity of K-promoted Ni/Al2O3catalysts for the dry reforming of methane," *Appl. Catal. A Gen.*, vol. 301, no. 1, pp. 9–15, 2006.

[133] M.-R. Li, Z. Lu, and G.-C. Wang, "The effect of potassium on steam-methane reforming on the Ni_4/Al_2O_3 surface: a DFT study," *Catal. Sci. Technol.*, vol. 7, no. 16, pp. 3613–3625, 2017.

[134] A. Kotarba, M. Hagström, K. Engvall, and J. B. C. Pettersson, "High pressure desorption of K+from iron ammonia catalyst migration of the promoter towards Fe active planes," *Catal. Letters*, vol. 95, no. 1–2, pp. 93–97, 2004.

[135] K. Engvall, L. Holmlid, and P. G. Menon, "Comparative loss of alkali promoter by desorption from two catalysts for the dehydrogenation of ethyl benzene to styrene," *Appl. Catal.*, vol. 77, no. 2, pp. 235–241, 1991.

[136] K. Engvall, L. Holmlid, A. Kotarba, J. B. C. Pettersson, P. G. Menon, and P. Skaugset, "Potassium promoter in industrial ammonia synthesis catalyst: Studies by surface ionization," *Appl. Catal. A Gen.*, vol. 134, no. 2, pp. 239–246, 1996.

[137] E. V. Albano, "On the oxygen induced stabilization of adsorbed alkali atoms," *Surf. Sci.*, vol. 215, no. 3, pp. 333–347, 1989.

[138] E. L. Garfunkel and G. A. Somorjai, "POTASSIUM AND POTASSIUM OXIDE MONOLAYERS ON THE PLATINUM (111) AND STEPPED (755) CRYSTAL SURFACES: A LEED, AES AND TDS STUDY," *Surf. Sci.*, vol. 115, pp. 441–454, 1982.

[139] H. Kassman, J. Pettersson, B. M. Steenari, and L. E. Åmand, "Two strategies to reduce gaseous KCl and chlorine in deposits during biomass combustion - Injection of ammonium sulphate and co-combustion with peat," *Fuel Process. Technol.*, vol. 105, pp. 170–180, 2013.

[140] K. O. Davidsson, L. E. Åmand, B. M. Steenari, A. L. Elled, D. Eskilsson, and B. Leckner, "Countermeasures against alkali-related problems during combustion of biomass in a circulating fluidized bed boiler," *Chem. Eng. Sci.*, vol. 63, no. 21, pp. 5314–5329, 2008.

[141] K. O. Davidsson *et al.*, "Potassium, chlorine, and sulfur in ash, particles, deposits, and corrosion during wood combustion in a circulating fluidized-bed boiler," *Energy and Fuels*, vol. 21, no. 1, pp. 71–81, 2007.

[142] S. Jiménez and J. Ballester, "Effect of co-firing on the properties of submicron aerosols from biomass combustion," *Proc. Combust. Inst.*, vol. 30 II, pp. 2965–2972, 2005.

[143] S. Jiménez and J. Ballester, "Influence of operating conditions and the role of sulfur in the formation of aerosols from biomass combustion," *Combust. Flame*, vol. 140, no. 4, pp. 346–358, 2005.

[144] K. A. Christensen, M. Stenholm, and H. Livbjerg, "The formation of submicron aerosol particles, HCl and SO2in straw-fired boilers," *J. Aerosol Sci.*, vol. 29, no. 4, pp. 421–444, 1998.

[145] P. Henderson, P. Szakálos, R. Pettersson, C. Andersson, and J. Högberg, "Reducing

superheater corrosion in wood-fired boilers," *Mater. Corros.*, vol. 57, no. 2, pp. 128–134, 2006.

[146] P. Glarborg and P. Marshall, "Mechanism and modeling of the formation of gaseous alkali sulfates," *Combust. Flame*, vol. 141, no. 1–2, pp. 22–39, 2005.

[147] A. C. Papageorgopoulos and M. Kamaratos, "K and S coadsorption on Ni (100) surfaces," *J. Phys. Condens. Matter*, vol. 12, no. 44, 2000.

[148] A. Díaz, J. A. Odriozola, and M. Montes, "Influence of alkali additives on activity and toxicity of H 2S and thiophene over a Ni/SiO 2 catalyst," *Appl. Catal. A-general*, vol. 166, no. 1, pp. 163–172, 1998.

[149] M. Ferrandon, J. Mawdsley, and T. Krause, "Effect of temperature, steam-to-carbon ratio, and alkali metal additives on improving the sulfur tolerance of a Rh/La-Al2O3 catalyst reforming gasoline for fuel cell applications," *Appl. Catal. A Gen.*, vol. 342, no. 1–2, pp. 69–77, 2008.

[150] I. Chen and D. W. Shiue, "Resistivity to Sulfur Poisoning of Nickel-Alumina Catalysts," *Ind. Eng. Chem. Res.*, vol. 27, no. 8, pp. 1391–1396, 1988.

[151] W. Arabczyk, D. Moszyński, U. Narkiewicz, R. Pelka, and M. Podsiadły, "Poisoning of iron catalyst by sulfur," *Catal. Today*, vol. 124, no. 1–2, pp. 43–48, 2007.

[152] R. B. Anderson, F. S. Karn, and J. F. Shultz, "Factors in sulfur poisoning of iron catalysts in Fischer-Tropsch synthesis," *J. Catal.*, vol. 4, no. 1, pp. 56–63, 1965.

[153] V. Pallozzi, A. Di Carlo, E. Bocci, and M. Carlini, "Combined gas conditioning and cleaning for reduction of tars in biomass gasification," *Biomass and Bioenergy*, vol. 109, no. July 2017, pp. 85–90, 2018.

[154] M. P. Aznar, M. A. Caballero, J. Gil, J. A. Martín, and J. Corella, "Commercial steam reforming catalysts to improve biomass gasification with steam-oxygen mixtures. 2. Catalytic tar removal," *Ind. Eng. Chem. Res.*, vol. 37, no. 7, pp. 2668–2680, 1998.

[155] H. McLaughlin, F. Shields, J. Jagiello, and G. Thiele, "Analytical Options for Biochar Adsorption and Surface Area," in *Char Characterization*, 2012, pp. 1–19.

[156] J. Gil, J. Corella, M. P. Aznar, and M. A. Caballero, "Biomass gasification in atmospheric and bubbling fluidized bed: Effect of the type of gasifying agent on the product distribution,"

Biomass and Bioenergy, vol. 17, no. 5, pp. 389–403, 1999.

[157] J. Corella, A. Orío, and P. Aznar, "Biomass gasification with air in fluidized bed: Reforming of the gas composition with commercial steam reforming catalysts," *Ind. Eng. Chem. Res.*, vol. 37, no. 12, pp. 4617–4624, 1998.

[158] M. Valentini, G. Groppi, C. Cristiani, M. Levi, E. Tronconi, and P. Forzatti, "The deposition of γ-Al2O3 layers on ceramic and metallic supports for the preparation of structured catalysts," *Catal. Today*, vol. 69, no. 1–4, pp. 307–314, Sep. 2001.

[159] S. Gražulis *et al.*, "Crystallography Open Database - An open-access collection of crystal structures," *J. Appl. Crystallogr.*, vol. 42, no. 4, pp. 726–729, 2009.

[160] A. W. Burton, K. Ong, T. Rea, and I. Y. Chan, "On the estimation of average crystallite size of zeolites from the Scherrer equation: A critical evaluation of its application to zeolites with one-dimensional pore systems," *Microporous Mesoporous Mater.*, vol. 117, no. 1–2, pp. 75–90, 2009.

[161] D. Swierczynski, C. Courson, and A. Kiennemann, "Study of steam reforming of toluene used as model compound of tar produced by biomass gasification," *Chem. Eng. Process. Process Intensif.*, vol. 47, no. 3, pp. 508–513, 2008.

[162] K. Polychronopoulou, J. L. G. Fierro, and A. M. Efstathiou, "The phenol steam reforming reaction over MgO-based supported Rh catalysts," *J. Catal.*, vol. 228, no. 2, pp. 417–432, 2004.

[163] G. F. Froment, "Fixed Bed Catalytic Reactors. Technological and Fundamental Design Aspects," *Chemie Ing. Tech.*, vol. 46, no. 9, pp. 374–386, 1974.

[164] H. S. FOGLER, *Elements of Chemical Reaction Engineering*, Fourth ed. Upper Saddle River, N.J.: Prentice Hall PTR, 2006.

[165] O. E. R. US EPA, "EPA On-line Tools for Site Assessment Calculation."

[166] G. F. Froment, K. B. Bischoff, and J. De Wilde, *Chemical Reactor Analysis and Design*, Third. John Wiley & Sons, Inc., 2011.

[167] U. Oemar, M. A. Li, K. Hidajat, and S. Kawi, "Mechanism and Kinetic Modeling for Steam Reforming of Toluene on $La_{0.8}Sr_{0.2}Ni_{0.8}Fe_{0.2}O_3$ Catalyst," *ALChE*, vol. 60, no. 4, pp. 4190–4198, 2014.

[168] C. Testing, F. Kapteijn, and J. A. Moulijn, "9 Laboratory Reactors 9.1," 1997.

[169] D. Świerczyński, S. Libs, C. Courson, and A. Kiennemann, "Steam reforming of tar from a biomass gasification process over Ni/olivine catalyst using toluene as a model compound," *Appl. Catal. B Environ.*, vol. 74, no. 3–4, pp. 211–222, 2007.

[170] J. Wei and E. Iglesia, "Structural requirements and reaction pathways in methane activation and chemical conversion catalysed by rhodium," *Journal of Catalysis*, vol. 225. pp. 116–127, 2004.

[171] D. Mukai *et al.*, "Role of support lattice oxygen on steam reforming of toluene for hydrogen production over Ni/La0.7Sr0.3AlO3-δ catalyst," *Appl. Catal. A Gen.*, vol. 453, pp. 60–70, 2013.

[172] S. Tuomi, N. Kaisalo, P. Simell, and E. Kurkela, "Effect of pressure on tar decomposition activity of different bed materials in biomass gasification conditions," *Fuel*, vol. 158, pp. 293–305, 2015.

[173] J. B. Hansen, "Correlating Sulfur Poisoning of SOFC Nickel Anodes by a Temkin Isotherm," *Electrochem. Solid-State Lett.*, vol. 11, p. B178, 2008.

[174] E. Heginuz, B. Gregertsen, V. Sorvari, P. Vriesman, and K. Sjöström, "Studies on solid fuel pyrolysis and fluidization in a laboratory-scale, atmospheric, fluidized bed reactor," in *Finnish-Swedish flame days*, 1996.

[175] C. Brage, Q. Yu, G. Chen, and K. Sjöström, "Use of amino phase adsorbent for biomass tar sampling and separation," *Fuel*, vol. 76, no. 2, pp. 137–142, Jan. 1997.

[176] M. Israelsson, M. Seemann, and H. Thunman, "Assessment of the solid-phase adsorption method for sampling biomass-derived tar in industrial environments," *Energy and Fuels*, vol. 27, no. 12, pp. 7569–7578, 2013.

[177] A. J. Grootjes, "Tar measurement by the Solid Phase Adsorption (SPA) method," in *19th European Biomass Conference and Exhibition*, 2011, p. 13.

[178] C. A. Callaghan, "Kinetics and Catalysis of the Water-Gas-Shift Reaction: A Microkinetic and Graph Theoretic Approach," *Dep. Chem. Eng.*, vol. Ph. D. The, p. 400, 2006.

[179] "Methane - Density and Specific Weight." [Online]. Available: https://www.engineeringtoolbox.com/methane-density-specific-weight-temperature-

pressure-d_2020.html. [Accessed: 03-Dec-2018].

[180] V. Vesovic, "ETHYLENE," in *A-to-Z Guide to Thermodynamics, Heat and Mass Transfer, and Fluids Engineering*, Begellhouse, 2011.

[181] C. Tsonopoulos and D. Ambrose, "Vapor-Liquid Critical Properties of Elements and Compounds. 3. Aromatic Hydrocarbons," *J. Chem. Eng. Data*, vol. 40, no. 3, pp. 547–558, 1995.

[182] T. C. Horng, M. Ajlan, L. L. Lee, K. E. Starling, and M. Ajlan, "Generalized Multiparameter Correlation for Nonpolar and Polar Fluid Transport Properties," *Ind. Eng. Chem. Res.*, vol. 27, no. 4, pp. 671–679, 1988.

[183] E. N. Fuller, P. D. Schettler, and J. C. Giddings, "A new method for prediction of binary gas-phase diffusion coefficients," *Ind. Eng. Chem.*, vol. 58, no. 5, pp. 18–27, 1966.

[184] E. N. Fuller, K. Ensley, and J. C. Giddings, "Diffusion of halogenated hydrocarbons in helium. The effect of structure on collision cross sections," *J. Phys. Chem.*, vol. 73, no. 11, pp. 3679–3685, 1969.

[185] J. P. Polling, B. E.; Prausnitz, J. M.; O'Connell, *The properties of gases and liquids*. 2001.

[186] A. G. Dixon, "Correlations for wall and particle shape effects on fixed bed bulk voidage," *Can. J. Chem. Eng.*, vol. 66, no. 5, pp. 705–708, 1988.

[187] C. Pfeifer, R. Rauch, and H. Hofbauer, "In-Bed Catalytic Tar Reduction in a Dual Fluidized Bed Biomass Steam Gasifier," *Ind. Eng. Chem. Res.*, vol. 43, no. 7, pp. 1634–1640, 2004.

[188] P. A. Simell, J. K. Leppälahti, and J. B. son Bredenberg, "Catalytic purification of tarry fuel gas with carbonate rocks and ferrous materials," *Fuel*, vol. 71, no. 2, pp. 211–218, 1992.

[189] U. Arena, L. Zaccariello, and M. L. Mastellone, "Tar removal during the fluidized bed gasification of plastic waste," *Waste Manag.*, vol. 29, no. 2, pp. 783–791, 2009.

[190] D. Li, M. Tamura, Y. Nakagawa, and K. Tomishige, "Metal catalysts for steam reforming of tar derived from the gasification of lignocellulosic biomass," *Bioresour. Technol.*, vol. 178, pp. 53–64, 2015.

[191] W. van de Kamp, P. de Wild, H. A. M. Knoef, J. P. A. Neeft, and J. H. A. Kiel, "Tar

measurement in biomass gasification , standardisation and supporting R&D," 2006.

[192] Y. Song *et al.*, "Effects of volatile-char interactions on in situ destruction of nascent tar during the pyrolysis and gasification of biomass. Part I. Roles of nascent char," *Fuel*, vol. 122, pp. 60–66, 2014.

[193] K. Kuramoto *et al.*, "Cracking and coking behaviors of nascent volatiles derived from flash pyrolysis of woody biomass over mesoporous fluidized-bed material," *Ind. Eng. Chem. Res.*, vol. 48, no. 6, pp. 2851–2860, 2009.

[194] S. Hosokai *et al.*, "Spontaneous generation of tar decomposition promoter in a biomass steam reformer," *Chem. Eng. Res. Des.*, vol. 83, no. 9 A, pp. 1093–1102, 2005.

[195] I. Milosavljevic, V. Oja, and E. M. Suuberg, "Thermal effects in cellulose pyrolysis: Relationship to char formation processes," *Ind. Eng. Chem. Res.*, vol. 35, no. 3, pp. 653–662, 1996.

[196] C. Di Blasi, "Modeling chemical and physical processes of wood and biomass pyrolysis," *Prog. Energy Combust. Sci.*, vol. 34, no. 1, pp. 47–90, 2008.

[197] A. Demirbaş, "Mechanisms of liquefaction and pyrolysis reactions of biomass," *Energy Convers. Manag.*, vol. 41, no. 6, pp. 633–646, 2000.

[198] J. Kopyscinski, T. J. Schildhauer, and S. M. A. Biollaz, "Production of synthetic natural gas (SNG) from coal and dry biomass - A technology review from 1950 to 2009," *Fuel*, vol. 89, no. 8, pp. 1763–1783, 2010.

[199] E. Savuto, A. Di Carlo, K. Gallucci, S. Natali, and E. Bocci, "Characterization and performance analysis of an innovative Ni/Mayenite catalyst for the steam reforming of raw syngas," *Fuel*, vol. 194, pp. 348–356, 2017.

[200] A. Di Carlo *et al.*, "Reforming of tar contained in a raw fuel gas from biomass gasification using nickel-mayenite catalyst," *Int. J. Hydrogen Energy*, vol. 40, no. 30, pp. 9088–9095, 2015.

[201] S. Mani, J. R. Kastner, and A. Juneja, "Catalytic decomposition of toluene using a biomass derived catalyst," *Fuel Process. Technol.*, vol. 114, pp. 118–125, 2013.

[202] A. S. Tolkacheva *et al.*, "Synthesis of dense ceramics of single-phase mayenite (Ca12Al14O32)O," *Russ. J. Appl. Chem.*, vol. 84, no. 6, pp. 907–911, Jun. 2011.

[203] M. P. Bracciale *et al.*, "Influence of the catalyst support on the steam reforming performance of toluene as tar model compound," *Chem. Eng. Trans.*, vol. 65, 2018.

[204] M. Ruszak, S. Witkowski, P. Pietrzyk, A. Kotarba, and Z. Sojka, "The Role of Intermediate Calcium Aluminate Phases in Solid State Synthesis of Mayenite (Ca12Al14 O33)," *Funct. Mater. Lett.*, vol. 04, no. 02, pp. 183–186, 2011.

[205] M. G. Vincent and J. W. Jeffery, "The crystal structure of pentacalcium trialuminate, 5CaO.3Al $_2$ O $_3$," *Acta Crystallogr. Sect. B Struct. Crystallogr. Cryst. Chem.*, vol. 34, no. 5, pp. 1422–1428, May 1978.

[206] C. S. Martavaltzi and A. A. Lemonidou, "Parametric Study of the CaO–Ca $_{12}$ Al $_{14}$ O $_{33}$ Synthesis with Respect to High CO $_2$ Sorption Capacity and Stability on Multicycle Operation," *Ind. Eng. Chem. Res.*, vol. 47, no. 23, pp. 9537–9543, Dec. 2008.

[207] M. R. Cesário, B. S. Barros, C. Courson, D. M. A. Melo, and A. Kiennemann, "Catalytic performances of Ni-CaO-mayenite in CO2sorption enhanced steam methane reforming," *Fuel Process. Technol.*, vol. 131, pp. 247–253, 2015.

[208] J. Phromprasit, J. Powell, S. Wongsakulphasatch, W. Kiatkittipong, P. Bumroongsakulsawat, and S. Assabumrungrat, "Activity and stability performance of multifunctional catalyst (Ni/CaO and Ni/$Ca_{12}Al_{14}O_{33}$-CaO) for bio-hydrogen production from sorption enhanced biogas steam reforming," *Int. J. Hydrogen Energy*, vol. 41, no. 18, pp. 7318–7331, 2016.

[209] J. N. Kim, C. H. Ko, and K. B. Yi, "Sorption enhanced hydrogen production using one-body CaO-$Ca_{12}Al_{14}O_{33}$-Ni composite as catalytic absorbent," *Int. J. Hydrogen Energy*, vol. 38, no. 14, pp. 6072–6078, 2013.

[210] K. V. Manukyan *et al.*, "Nickel Oxide Reduction by Hydrogen: Kinetics and Structural Transformations," *J. Phys. Chem. C*, vol. 119, no. 28, pp. 16131–16138, 2015.

[211] A. Cabello, P. Gayán, L. F. De Diego, A. Abad, M. T. Izquierdo, and J. Adánez, "Relevance of the catalytic activity on the performance of a NiO / CaAl2O4 oxygen carrier in a CLC process," *Appl. Catal. B Environ.*, vol. 147, pp. 980–987, 2014.

[212] J. Zhang, H. Xu, X. Jin, Q. Ge, and W. Li, "Characterizations and activities of the nano-sized Ni/Al2O 3 and Ni/La-Al2O3 catalysts for NH3 decomposition," *Appl. Catal. A Gen.*, vol. 290,

no. 1–2, pp. 87–96, 2005.

[213] A. Di Giuliano, F. Giancaterino, C. Courson, P. U. Foscolo, and K. Gallucci, "Development of a Ni-CaO-mayenite combined sorbent-catalyst material for multicycle sorption enhanced steam methane reforming," *Fuel*, vol. 234, no. June, pp. 687–699, 2018.

[214] B. Abdullah, N. A. Abd Ghani, and D. V. N. Vo, "Recent advances in dry reforming of methane over Ni-based catalysts," *J. Clean. Prod.*, vol. 162, pp. 170–185, 2017.

[215] S. Sokolov, E. V. Kondratenko, M. M. Pohl, A. Barkschat, and U. Rodemerck, "Stable low-temperature dry reforming of methane over mesoporous La_2O_3-ZrO_2 supported Ni catalyst," *Appl. Catal. B Environ.*, vol. 113–114, pp. 19–30, 2012.

[216] L. Zhang, X. Wang, B. Tan, and U. S. Ozkan, "Effect of preparation method on structural characteristics and propane steam reforming performance of Ni-Al_2O_3 catalysts," *J. Mol. Catal. A Chem.*, vol. 297, no. 1–2, pp. 26–34, 2009.

[217] F. Arena, B. A. Horrell, D. L. Cocke, A. Parmaliana, and N. Giordano, "Magnesia-supported nickel catalysts I. Factors affecting the structure and morphological properties," *J. Catal.*, vol. 132, no. 1, pp. 58–67, 1991.

[218] D. Mukai *et al.*, "In situ IR study for elucidating reaction mechanism of toluene steam reforming over Ni/La0.7Sr0.3AlO3-δcatalyst," *Appl. Catal. A Gen.*, vol. 466, pp. 190–197, 2013.

[219] M. Koike, D. Li, H. Watanabe, Y. Nakagawa, and K. Tomishige, "Comparative study on steam reforming of model aromatic compounds of biomass tar over Ni and Ni-Fe alloy nanoparticles," *Appl. Catal. A Gen.*, vol. 506, pp. 151–162, 2015.

[220] M. A. Goula, N. D. Charisiou, K. N. Papageridis, A. Delimitis, E. Pachatouridou, and E. F. Iliopoulou, "Nickel on alumina catalysts for the production of hydrogen rich mixtures via the biogas dry reforming reaction: Influence of the synthesis method," *Int. J. Hydrogen Energy*, vol. 40, no. 30, pp. 9183–9200, 2015.

[221] L. Pelletier and D. D. S. Liu, "Stable nickel catalysts with alumina-aluminum phosphate supports for partial oxidation and carbon dioxide reforming of methane," *Appl. Catal. A Gen.*, vol. 317, no. 2, pp. 293–298, 2007.

[222] A. M. Steele, S. Poulston, K. Magrini-Bair, and W. Jablonski, "Catalytic syngas purification from model biomass gasification streams," *Catal. Today*, vol. 214, pp. 74–81, 2013.

[223] D. Mukai, S. Tochiya, Y. Murai, M. Imori, Y. Sugiura, and Y. Sekine, "Structure and activity of Ni/La0.7Sr0.3AlO 3-δ catalyst for hydrogen production by steam reforming of toluene," *Appl. Catal. A Gen.*, vol. 464–465, pp. 78–86, 2013.

[224] N. Kaisalo, P. Simell, and J. Lehtonen, "Benzene steam reforming kinetics in biomass gasification gas cleaning," *Fuel*, vol. 182, pp. 696–703, 2016.

[225] H. Depner and A. Jess, "Kinetics of nickel-catalyzed purification of tarry fuel gases from gasification and pyrolysis of solid fuels," *Fuel*, vol. 78, no. 12, pp. 1369–1377, 1999.

[226] X. Zou *et al.*, "High catalytic performance of Fe-Ni/Palygorskite in the steam reforming of toluene for hydrogen production," *Appl. Energy*, vol. 226, no. July, pp. 827–837, 2018.

[227] J.-P. Eufinger, A. Schmidt, M. Lerch, and J. Janek, "Novel anion conductors – conductivity, thermodynamic stability and hydration of anion-substituted mayenite-type cage compounds $C_{12}A_7$:X (X = O, OH, Cl, F, CN, S, N)," *Phys. Chem. Chem. Phys.*, vol. 17, no. 10, pp. 6844–6857, Feb. 2015.

[228] J. Ruixia, X. Zaiku, Z. Chengfang, and C. Qingling, "Characterization and performance of Pd-La/spinel catalyst for preparation of 2,6-diisopropylaniline," *Appl. Catal. A Gen.*, vol. 250, no. 2, pp. 209–220, 2003.

[229] C. L. Li *et al.*, "Coke formation on an industrial reforming Pt–Sn/ γ-Al_2O_3 catalyst," *Catal. Letters*, vol. 65, pp. 209–216, 2000.

[230] D. Mukai *et al.*, "Role of support lattice oxygen on steam reforming of toluene for hydrogen production over Ni/$La_{0.7}Sr_{0.3}AlO_{3-\delta}$ catalyst," *Appl. Catal. A Gen.*, vol. 453, pp. 60–70, 2013.

[231] W. Jablonski, "Investigation of sulfur interactions on a conventional nickel-based solid oxide fuel cell anode during methane steam and dry reforming," Colorado School of Mines, 2015.

[232] A. Lanzini *et al.*, "Dealing with fuel contaminants in biogas-fed solid oxide fuel cell (SOFC) and molten carbonate fuel cell (MCFC) plants: Degradation of catalytic and electro-catalytic active surfaces and related gas purification methods," *Prog. Energy Combust. Sci.*, vol. 61, pp. 150–188, 2017.

[233] C. Petit, B. Mendoza, and T. J. Bandosz, "Hydrogen sulfide adsorption on MOFs and MOF/Graphite oxide composites," *ChemPhysChem*, vol. 11, no. 17, pp. 3678–3684, 2010.

[234] L. V. A. Truong and N. Abatzoglou, "A H2S reactive adsorption process for the purification of biogas prior to its use as a bioenergy vector," *Biomass and Bioenergy*, vol. 29, no. 2, pp. 142–151, 2005.

[235] Y. Xiao, S. Wang, D. Wu, and Q. Yuan, "Experimental and simulation study of hydrogen sulfide adsorption on impregnated activated carbon under anaerobic conditions," *J. Hazard. Mater.*, vol. 153, no. 3, pp. 1193–1200, 2008.

[236] A. M. Ebrahim, J. Jagiello, and T. J. Bandosz, "Enhanced reactive adsorption of H2S on Cu-BTC/S- and N-doped GO composites," *J. Mater. Chem. A*, vol. 3, no. 15, pp. 8194–8204, 2015.

[237] P. E. J. Abbott, N. Macleod, and G. E. Wilson, "Process For Generating a Synthetic Natural Gas," US2013/0317126 A1, 2013.

[238] A. Attar, "Chemistry, thermodynamics and kinetics of reactions of sulphur in coal-gas reactions: A review," *Fuel*, vol. 57, no. 4, pp. 201–212, 1978.

[239] S. L. Lakhapatri and M. A. Abraham, "Deactivation due to sulfur poisoning and carbon deposition on Rh-Ni/Al_2O_3 catalyst during steam reforming of sulfur-doped n-hexadecane," *Appl. Catal. A Gen.*, vol. 364, no. 1–2, pp. 113–121, 2009.

[240] S. L. Lakhapatri and M. A. Abraham, "Analysis of catalyst deactivation during steam reforming of jet fuel on Ni-(PdRh)/γ-Al2O3 catalyst," *Appl. Catal. A Gen.*, vol. 405, no. 1–2, pp. 149–159, 2011.

[241] U. Rhyner, P. Edinger, T. J. Schildhauer, and S. M. A. Biollaz, "Experimental study on high temperature catalytic conversion of tars and organic sulfur compounds," *Int. J. Hydrogen Energy*, vol. 39, no. 10, pp. 4926–4937, 2014.

[242] J. M. Mayne, A. R. Tadd, K. A. Dahlberg, and J. W. Schwank, "Influence of thiophene on the isooctane reforming activity of Ni-based catalysts," *J. Catal.*, vol. 271, no. 1, pp. 140–152, 2010.

[243] J. Rostrup-Nielsen, "Catalytic Steam Reforming," in *Catalysis Science and Technology*, Vol. 5., vol. 5, J. R. Anderson and M. Boudart, Eds. Berlin: Springer, 1984, pp. 1–117.

[244] T. Ogura, T. Ishimoto, and M. Koyama, "Density functional theory study of sulfur poisoning on nickel anode in solid oxide fuel cells: Effects of surface and subsurface sulfur atoms," *J. Chem. Eng. Japan*, vol. 47, no. 11, pp. 793–800, 2014.

[245] C. . Ng and G. . Martin, "Poisoning of Ni/SiO_2 catalysts with H_2S: chemisorption of H_2, CO, C_6H_6, and C_2H_2 studied by magnetic methods," *J. Catal.*, vol. 54, no. 3, pp. 384–396, 1978.

[246] S. . Weeks and E. . Plummer, "New evidence for multiple binding sites for sulfur at the Ni(100)-vacuum interface," *Chem. Phys. Lett.*, vol. 48, no. 3, pp. 601–603, 1977.

[247] L. Ruan, I. Stensgaard, F. Besenbacher, and E. Laegsgaard, "Observation of a Missing-Row Structure on an fcc (111) Surface : The (5√3 X 2) S Phase on Ni (111) Studied by Scanning Tunneling Microscopy," vol. 71, no. 18, 1993.

[248] A. Jess, "Catalytic upgrading of tarry fuel gases: A kinetic study with model components," *Chem. Eng. Process. Process Intensif.*, vol. 35, no. 6, pp. 487–494, 1996.

[249] J. Hepola and P. Simell, "Sulphur poisoning of nickel-based hot gas cleaning catalysts in synthetic gasification gas I. Effect of different process parameters," *Appl. Catal. B Environ.*, vol. 14, no. 3–4, pp. 287–303, 1997.

[250] A. Jess, "Mechanisms and kinetics of thermal reactions of aromatic hydrocarbons from pyrolysis of solid fuels," *Fuel*, vol. 75, no. 12, pp. 1441–1448, 1996.

[251] M. P. Andersson *et al.*, "Structure sensitivity of the methanation reaction: H2-induced CO dissociation on nickel surfaces," *J. Catal.*, vol. 255, no. 1, pp. 6–19, 2008.

[252] J. Hepola, "Sulfur transformations in catalytic hot-gas cleaning of gasification gas," *VTT Publ.*, no. 425, pp. 1–54, 2000.

[253] J. R. Rostrup-nielsen, "Chemisorption of hydrogen sulfide on a supported nickel catalyst," *J. Catal.*, vol. 11, no. 3, pp. 220–227, 1968.

[254] Y. Chen, C. Xie, Y. Li, C. Song, and T. B. Bolin, "Sulfur poisoning mechanism of steam reforming catalysts: an X-ray absorption near edge structure (XANES) spectroscopy study," *Phys. Chem. Chem. Phys.*, vol. 12, no. 21, pp. 5503–5513, 2010.

[255] E. B. Maxted, "The poisoning of metallic catalysts," *Adv. Catal.*, vol. 3, pp. 129–178, 1951.

[256] K. Lee, E. Lee, C. Song, and M. J. Janik, "Density functional theory study of propane steam reforming on Rh-Ni bimetallic surface: Sulfur tolerance and scaling/Br??nsted-Evans-Polanyi relations," *J. Catal.*, vol. 309, pp. 248–259, 2014.

[257] J. A. Rodriguez and J. Hrbek, "Interaction of sulfur with well-defined metal and oxide surfaces: Unraveling the mysteries behind catalyst poisoning and desulfurization," *Acc. Chem. Res.*, vol. 32, no. 9, pp. 719–728, 1999.

[258] C. Karakaya, R. Otterstätter, L. Maier, and O. Deutschmann, "Kinetics of the water-gas shift reaction over Rh/Al_2O_3catalysts," *Appl. Catal. A Gen.*, vol. 470, pp. 31–44, 2014.

[259] C. H. Bartholomew, P. K. Agrawal, and J. R. Katzer, "Sulfur Poisoning of Metals," *Adv. Catal.*, vol. 31, no. C, pp. 135–242, 1982.

[260] R. Chakrabarti, J. L. Colby, and L. D. Schmidt, "Effects of biomass inorganics on rhodium catalysts: I. Steam methane reforming," *Appl. Catal. B Environ.*, vol. 107, no. 1–2, pp. 88–94, 2011.

[261] S. Peucheret, M. Feaviour, and S. Golunski, "Exhaust-gas reforming using precious metal catalysts," *Appl. Catal. B Environ.*, vol. 65, no. 3–4, pp. 201–206, 2006.

[262] M. P. Andersson *et al.*, "Structure sensitivity of the methanation reaction: H2-induced CO dissociation on nickel surfaces," *J. Catal.*, vol. 255, no. 1, pp. 6–19, 2008.

[263] C. R. Müller, R. Pacciani, C. D. Bohn, S. A. Scott, and J. S. Dennis, "Investigation of the Enhanced Water Gas Shift Reaction Using Natural and Synthetic Sorbents for the Capture of CO_2," *Ind. Eng. Chem. Res.*, vol. 48, no. 23, pp. 10284–10291, 2009.

[264] P. Yrjas, K. Iisa, and M. Hupa, "Limestone and dolomite as sulfur absorbents under pressurized gasification conditions," *Fuel*, vol. 75, no. 1, pp. 89–95, 1996.

[265] C. A. P. Zevenhoven, K. P. Yrjas, and M. M. Hupa, "Hydrogen sulfide capture by limestone and dolomite at elevated pressure. 2. Sorbent particle conversion modeling," *Ind. Eng. Chem. Res.*, vol. 35, no. 3, pp. 943–949, 1996.

[266] J. R. Rostrup-nielsen, "Some principles relating to the regeneration of sulfur-poisoned nickel catalysts," *J. Catal.*, vol. 21, no. 2, pp. 171–178, 1971.

[267] M. Hartman, K. Svoboda, O. Trnka, and J. Čermák, "Reaction between hydrogen sulfide and

limestone calcines," *Ind. Eng. Chem. Res.*, vol. 41, no. 10, pp. 2392–2398, 2002.

[268] A. B. M. Heesink and W. P. M. Van Swaaij, "The sulphidation of calcined limestone with hydrogen sulphide and carbonyl sulphide," *Chem. Eng. Sci.*, vol. 50, no. 18, pp. 2983–2996, 1995.

[269] E. S. Wangen, A. Osatiashtiani, and E. A. Blekkan, "Reforming of syngas from biomass gasification: Deactivation by tar and potassium species," *Top. Catal.*, vol. 54, no. 13–15, pp. 960–966, 2011.

[270] H. Praliaud, M. Primet, and G. A. Martin, "Physico-chemical properties of potassium-promoted Ni/SiO_2catalysts," *Appl. Surf. Sci.*, vol. 17, no. 1, pp. 107–123, 1983.

[271] Y. P. Li *et al.*, "Effect of Alkali Vapor Exposure on Ni-MgO/γ-Al_2O_3 Cordierite Monolithic Catalyst for Biomass Fuel Gas Reforming," *Ind. Eng. Chem. Res.*, vol. 49, no. 7, pp. 3176–3183, Apr. 2010.

[272] S. Albertazzi *et al.*, "Effect of fly ash and H2S on a Ni-based catalyst for the upgrading of a biomass-generated gas," *Biomass and Bioenergy*, vol. 32, no. 4, pp. 345–353, 2008.

[273] J. Einvall *et al.*, "Investigation of reforming catalyst deactivation by exposure to fly ash from biomass gasification in laboratory scale," *Energy and Fuels*, vol. 21, no. 5, pp. 2481–2488, 2007.

[274] S. Albertazzi *et al.*, "Pt-Rh/MgAl(O) catalyst for the upgrading of biomass-generated synthesis gases," *Energy and Fuels*, vol. 23, no. 1, pp. 573–579, 2009.

[275] J. Sehested, J. A. P. Gelten, and S. Helveg, "Sintering of nickel catalysts: Effects of time, atmosphere, temperature, nickel-carrier interactions, and dopants," *Appl. Catal. A Gen.*, vol. 309, no. 2, pp. 237–246, 2006.

[276] C. Xie, Y. Chen, Y. Li, X. Wang, and C. Song, "Sulfur poisoning of CeO2-Al2O3-supported mono- and bi-metallic Ni and Rh catalysts in steam reforming of liquid hydrocarbons at low and high temperatures," *Appl. Catal. A Gen.*, vol. 390, no. 1–2, pp. 210–218, 2010.

[277] T. Borowiecki *et al.*, "Studies of potassium-promoted nickel catalysts for methane steam reforming: Effect of surface potassium location," *Appl. Surf. Sci.*, vol. 300, pp. 191–200, 2014.

[278] A. Kotarba, J. Dmytrzyk, U. Narkiewicz, and A. Baranski, "Sulfur poisoning of iron

ammonia catalyst probed by potassium desorption," *React. Kinet. Catal. Lett.*, vol. 74, no. 1, pp. 143–149, 2001.

[279] C. Pedrero, T. Waku, and E. Iglesia, "Oxidation of CO in H2-CO mixtures catalyzed by platinum: Alkali effects on rates and selectivity," *J. Catal.*, vol. 233, no. 1, pp. 242–255, 2005.

[280] G. Taralas, "Modeling the Influence of Mineral Rocks , Active in Different Hot Gas Conditioning Systems and Technologies , on the Production of Light α-Olefins," *Can. J. Chem. Eng.*, vol. 77, pp. 1205–1214, 1999.

[281] J. W. Dun, E. Gulari, and K. Y. S. Ng, "Fischer-Tropsch synthesis on charcoal-supported molybdenum: The effect of preparation conditions and promotion on activity and selectivity," *Appl. Catal.*, vol. 15, pp. 247–263, 1985.

[282] A. Horvat, M. Kwapinska, G. Xue, S. Dooley, W. Kwapinski, and J. J. Leahy, "Detailed Measurement Uncertainty Analysis of Solid-Phase Adsorption-Total Gas Chromatography (GC)-Detectable Tar from Biomass Gasification," *Energy and Fuels*, vol. 30, no. 3, pp. 2187–2197, 2016.

[283] D. W. McKee, "Mechanisms of the alkali metal catalysed gasification of carbon," *Fuel*, vol. 62, no. 2, pp. 170–175, 1983.

[284] V. Pitchon, P. Gallezot, C. Nicot, and H. Praliaud, "Study by Analytical Electron Microscopy of the Potassium Distribution on Silica-Supported Nickel and Palladium Catalysts," *Appl. Catal.*, vol. 47, no. 2, pp. 357–365, 1989.

[285] D. . Trimm, "Catalysts for the control of coking during steam reforming," *Catal. Today*, vol. 49, no. 1–3, pp. 3–10, 1999.

[286] J. R. Rostrup-Nielsen, "Promotion by poisoning," 1991.

[287] C. Xie, Y. Chen, Y. Li, X. Wang, and C. Song, "Influence of sulfur on the carbon deposition in steam reforming of liquid hydrocarbons over CeO2-Al2O3 supported Ni and Rh catalysts," *Appl. Catal. A Gen.*, vol. 394, no. 1–2, pp. 32–40, 2011.

[288] M. Krumpelt, T. R. Krause, J. D. Carter, J. P. Kopasz, and S. Ahmed, "Fuel processing for fuel cell systems in transportation and portable power applications," *Catal. Today*, vol. 77, no. 1–2, pp. 3–16, 2002.

[289] P. Fremerey, A. Jess, and R. Moos, "Why does the conductivity of a nickel catalyst increase during sulfidation? An exemplary study using an in operando sensor device," *Sensors*, vol. 15, no. 10, pp. 27021–27034, 2015.

[290] P. Fremerey, A. Jess, and R. Moos, "Is it possible to detect in situ the sulfur loading of a fixed bed catalysts with a sensor?," *J. Sensors Sens. Syst.*, vol. 4, no. 1, pp. 143–149, 2015.